Consequences of Fault Currents Contributed by Distributed Generation

Supplemental Project Report

Power Systems Engineering Research Center

A National Science Foundation
Industry/University Cooperative Research Center
since 1996

Power Systems Engineering Research Center

Consequences of Fault Currents Contributed by Distributed Generation

Natthaphob Nimpitiwan
Gerald Heydt

Research Project Team

Gerald T. Heydt
Natthaphob Nimpitiwan
Arizona State University

Anjan Bose
Washington State University

A. P. Sakis Meliopoulos
Georgia Tech

PSERC Publication 06-21

June 2006

Information about this project

For information about this project contact:

Gerald T. Heydt, Ph.D.
Arizona State University
Department of Electrical Engineering
Tempe, AZ 85287
Phone: 480-965-8307
Fax: 480-965-0745
Email: heydt@asu.edu

Power Systems Engineering Research Center

This is a project report from the Power Systems Engineering Research Center (PSERC). PSERC is a multi-university Center conducting research on challenges facing a restructuring electric power industry and educating the next generation of power engineers. More information about PSERC can be found at the Center's website: http://www.pserc.org.

For additional information, contact:

Power Systems Engineering Research Center
Arizona State University
509 Engineering Research Center
Tempe, Arizona 85287-5706
Phone: 480 965 8307
Fax: 480 965 0745

Notice Concerning Copyright Material

Acknowledgements

The Power Systems Engineering Research Center (PSERC) sponsored the research project "New Implications of Power System Fault Current Limits." The project began in 2002 and a final report was issued in 2005. This is a supplementary project report. This particular report is the Ph.D. thesis of Natthaphob Nimpitiwan.

We express our appreciation for the support provided by the PSERC industrial members and by the National Science Foundation under grant NSF EEC-0001880 received from the Industry / University Cooperative Research Center program.

We extend special thanks to Prof. George G. Karady, Prof. Richard G. Farmer, Prof. Raja Ayyanar and Prof. Stephen M. Phillips at Arizona State University and Jamnarn Hokierti, Kasetsart University. The authors acknowledge Mr. A. B. Cummings, Dr. Rao S. Thallam and Mr. John D. Blevins at Salt River Project, Prof. Anjan Bose, Washington State University, and Prof. A. P. Sakis Meliopoulos, Georgia Institute of Technology. Special thanks to Dr. Siddharth Suryanarayanan for his technical and editorial advice.

Executive Summary

New generation capacity from distributed generation (DG) is growing in the overall generation mix due in part to state and national initiatives to address global-warming concerns. Of concern in power system design and operation are the implications of high penetration of DG on fault currents and protection system coordination. Installation of DGs in the distribution system increases the fault current throughout the system. Depending on the penetration level, locations, and type of DGs, the protection system may lose coordination with high numbers of DG units when the protection system is designed with conventional techniques. Circuit breaker capabilities and settings of protective relays that were previously designed for a system without DGs may not safely and appropriately coordinate to manage faults in a system with DGs. And accurate fault analysis in systems with inverter-based generation may not be possible with conventional fault analysis tools and techniques. At low inverter-based DG penetration levels (e.g., below five percent of system capacity), conventional protection analysis methods may be quite adequate. However, at high penetration levels (e.g., ten percent or higher), new methods may be necessary.

Fault calculations in power systems are used to determine the interrupting capability of circuit breakers. The calculation of fault current at the system buses is done conventionally by applying the system Z_{bus} matrix. A modification of the Z_{bus} method for fault current calculation is suitable for analysis of synchronous machine DG implementation, even at high penetration levels.

The equivalent impedance seen by the system in the case of synchronous machine DGs is higher than that of the inverter-based DGs. Hence, inverter-based generation sources appear to be 'softer' in the sense that their fault currents are not as severe as synchronous machine sources. However, in the presence of inverter-based DG, the calculation of fault current by applying the Z_{bus} matrix may not be practical due to the complexity in estimating the transient impedance of the inverter-based DGs.

Inverters are also nonlinear, so to analyze system dynamics and changes in the fault response of the system with inverter-based DGs, a simulation technique was developed to incorporate an inverter-based DG model. This inverter-based DG model was used in illustrative examples of systems with added DGs.

The fault current estimation is done using statistical analysis of voltage and current variations. The estimation technique is applied to a test bed system. This estimation technique could be used as an *on-line assessment* of fault current to help an operator avoid undesired operating conditions.

To quantify the increase in fault current system-wide, an index called the "average change of fault current" (ACF) was created. A least squares statistical estimation-method was used to estimate coefficients of the ACF model. One of the possible applications of the ACF is to assign the cost of protection system upgrades due to the commissioning of DGs.

Operating costs can be increased when operators consider the effects of increased fault currents from DG additions because operators may need to alter unit commitment schedules. To assess this possibility, the unit commitment problem with fault level constraints was modeled by applying dynamic programming. For an illustrative case, the

generation of DG units under a fault current level constraint resulted in higher operating costs than operation without the constraint.

The increase in fault currents resulting from installing DG in a distribution system might result in the need for protection system redesign. In this project, it was found that this coordination problem could be solved using various optimization techniques, such as linear programming and a genetic algorithm. The main disadvantage of the linear programming methodology is the large dimensionality of the problem. The problem is more complicated when two or more relays with different operating principles are required to coordinate in the protection system. For efficiency of fault analysis, it would be helpful to have tools that could be used in systems with and without DGs.

To that end, an artificial ant colony optimization (ACO) technique was developed and demonstrated for the coordination of protective relay settings (including time dial settings, multiple of pickup, delay time, and current and potential transformer ratio taps). The ACO technique can solve a discrete optimization problem with large dimensionality. The main advantage of using the ACO technique is its ability to solve the mixed scheme coordination problem with distance relays and ITDOC relays, and with large dimension (i.e., number of relays in the system). Illustrative analyses showed that installation of DG resulted in a larger objective function, so new calculations were needed to assure a well-coordinated protection system. Both the formulation of protection coordination and typical results are shown using ACO technique. Case studies were used to illustrate the technique. The ACO algorithm performs well in an off-line, discrete, constrained optimization.

It is expected that the next step toward application of the fault current calculation and use in protection strategies would be to work with established software vendors to implement the substantial capability of Matlab-Simulink in their protection analysis software.

The following are potential research areas related to increased power system fault current due to DGs:

Estimation and allocation of costs due to the need to consider protection

For specific applications of DG, the cost of upgrading protection and interruption devices should be considered. This dollar cost should be allocated properly.

Simplified model of inverter-based DG

The developed model of the inverter based DG requires a large amount computation effort and memory. It would be useful to simplify this model. This is an important issue for analyzing a larger system without losing accuracy. An alternative is to integrate PSpice analysis with Matlab models.

Optimal siting of DGs

A technique is needed for optimal siting of DGs. The objective of this optimization would be to minimize the operating costs and system upgrades. The possible technical approaches are Lagrangian relaxation and evolutionary algorithms (i.e., genetic algorithms, ant colony, and tabu search).

TABLE OF CONTENTS

Page

LIST OF TABLES

Table Page

LIST OF FIGURES

NOMENCLATURE

A	Coefficient indicates the contribution of operation time primary protections
AC	Alternating current
ACF	Average change of fault current
$ACF_{(bus)}$	Bus ACF
ACO	Ant colony algorithm
AVR	Automatic voltage regulator
B	Coefficient indicates the contribution of the coordination time
C	Coefficient indicates the contribution of number of constraint violation
C_{bs}	Best objective value
CAAA	Clean air act amendments
CB	Electric circuit breaker
CHP	Combined heat and power
CI	Coordination interval
CIGRE	International Council on Large Electricity Systems
CT	Current transformer
CV	Number of constraint violation
DC	Direct current
DG	Distributed generation
DG_{imp}	Impedance of distributed generator
DOE	Department of Energy
DR	Distributed resource
E	Pre-fault voltage
EA	Evolutionary algorithm
ECED	Environmentally constrained economic dispatch
ED	Economic dispatch
EIC	Equal incremental cost method
EMI	Electromagnetic interference
EP	Evolutionary programming
EPRI	Electric Power Research Institute
EPS	Electric power system
ES	Evolutionary strategy
E/X	Ratio of system voltage and equivalent reactance
f_j	Function applied in the least squares estimator
f_s	Switching frequency
F	Relationship matrix
F^+	Pseudoinverse of the relationship matrix
FCL	Fault current limiter
FFT	Fast Fourier transforms
FLC	Fault level constraint
FT	Fourier transforms

GA	Genetic algorithm
G_i	power output of generator at bus i
$G_{it}^{\min}$	Minimum power output of generator at bus i at time t
$G_{it}^{\max}$	Maximum power output of generator at bus i at time t
GP	Genetic programming
HGA	Hierarchical genetic algorithm
i	Complex number $\sqrt{-1}$
IC	Current interrupting capability
IPP	Independent power producer
I_{fj}	Fault current at bus j
$I_{f,n}$	Fault current at bus n before installing new DG
$I_{fDG,n}$	Fault current at bus n after installing new DGs
I_p	Injected current at bus p
ITDOC	Inverse time directional overcurrent relay
j	Complex number $\sqrt{-1}$
J	Random setting selected by using the roulette wheel technique
k	Order of the function applied in the least squares estimator
ℓ_{qr}	Primitive line impedance from bus q to bus r
m	Number of the bus with DG
m_a	Modulation index
M	Multiple of pick up current
MCFC	Molten carbonate fuel cells
MM	Minimum melting time of fuse
MTG	Microturbine generators
n	Number of all historical data
nDG	Number of bus with DG
$nbus$	Total buses in the system
N_i^k	Feasible neighborhood of relay i for ant k
NUG	Non-utility generator
OC	Operating cost
OPF	Optimal power flow
p	Number of the coefficient of the least squares estimator
$p_{i\ell}^k$	Probability of feasible neighbor
PAFC	Phosphoric acid fuel cells
PCC	Point of common coupling
P_{cost}	Production cost
PEM	Proton exchange membrane
P_{DG}	Critical power rating of distributed generation
P_{ref}	Reference power output value
PI	Proportional integral controller
PSB	Power system block sets
PV	Photovoltaic

q	Number of historical data cases
Q_i	reactive power generated by DG at bus i
r	Residual of the least squares estimator
R_t	spinning reserved at time period t
R_{xy}	Covariance of two variables, x and y
$Rmin$	Minimum operation time of primary protection relay
$Rmax$	Maximum operation time of primary protection relay
S_{cost}	Transition cost
SLG	Single line to ground fault
SOFC	Solid oxide fuel cell
SRP	Salt River Project
SS_{Res}	Residual or error sum of squares
$t_{\alpha/2,n-p}$	Value from t-distribution
t_{zone2}	time delay of back up protection
$TDown_i$	Minimum down time constrains of for unit i
TD	Time dial setting
Ton_i	Minimum up time for unit i
$Toff_i$	Minimum down time for unit i
T_{upi}	Minimum up time of generator unit i
T_s	Simulation time step
TC	Total clearing time of fuse
TD	Time dial setting
THD_I	Total harmonic distortion of current
THD_V	Total harmonic distortion of voltage
U_{it}	Status of unit i at time period t
UC	Unit commitment
UF	Fraction of the total cost paid by utility company
V_{abc}	Line-neutral voltage in abc variables
V_{dq0}	Line-neutral voltage in the $dq0$ reference frame
V_i^0	Voltage at bus i before installing DG
$V_i^{\min}$	Minimum voltage magnitude at bus i
$V_i^{\max}$	Maximum voltage magnitude at bus i
$v_{an}(t)$, $v_{bn}(t)$, $v_{cn}(t)$	Line to neutral voltage in time domain variables
V_f	Pre-fault voltage
V_j	Voltage at bus j during fault
w	Coefficient vector
$\hat{w}$	Estimated value of w
X_0	Zero sequence equivalent reactance of the system
X_1	Positive sequence equivalent reactance of the system
X	System reactance
X_d , X_q	Synchronous reactance
X_d', X_q'	Transient reactance
X_d'', X_q''	Subtransient reactance

X/R	Ratio of system equivalent reactance to system equivalent resistance
y	Output vector of the least square estimation technique
Z_{bus}	Bus impedance matrix
Z_{bus}^{+}	Positive sequence bus impedance matrix
Z_{bus}^{-}	Negative sequence bus impedance matrix
Z_{bus}^{0}	Zero sequence bus impedance matrix
z_{gen}	Generator transient impedance
$z_{DG,\ell}^{(b)}$	Transient impedance of DG at bus ℓ case b
Z_{orig}	Bus impedance matrix of original system
z_f	Fault impedance
$Z_{ij,orig}$	Diagonal element of bus impedance matrix of the system before installing a new DG
$Z_{ij,new}$	Diagonal element of bus impedance matrix of the system after installing a new DG
Z_L	Load impedance
Z_s	Equivalent impedance seen at the source side
$\Delta\lvert I_f \rvert$	Change of fault current due to installing new DGs
$\Delta\lvert V \rvert$	Change in voltage
α	Parameter determine the impact of pheromone
β	Parameter determines the impact of objective value
σ_r^2	Variance of residual
$\hat{\sigma}_r^2$	Estimation of variance of residual
δ_{diff}	Difference of phase angle between V_1 and V_2
μ_x	Mean value of x
ρ	Discount factor
$\tau_{i\ell}^{bs}$	Amount of pheromone laid on path ℓ
$\eta_{i\ell}$	Inverse of objective function on path ℓ

CHAPTER 1

INTRODUCTION: DISTRIBUTED GENERATION AND FAULT CURRENT ANALYSIS

1.1 Motivation

Deregulation, utility restructuring, technology evolution, environmental policies and increasing electric demand are stimuli for deploying new distributed generation (DG). In state of the union 2006, President George W. Bush announced a 22 percent increase in clean energy research at the Department of Energy. Since 2001, the U.S. government has spent nearly 10 billion dollars on clean energy research [1].

According to the U.S. Department of Energy (DOE), DG is defined as [2] "the modular electric generation or storage located near the point of use. Distributed generation systems include biomass-based generators, combustion turbines, thermal solar power and photovoltaic systems, fuel cells, wind turbines, microturbines, engines/generator sets and storage and control technologies. Distributed resources can either be grid connected or independent of the grid. Those connected to the grid are typically interfaced at the distribution system".

According to the IEEE Standard 1547-2003, DG is defined as "Electric generation facilities connected to an area Electric Power System (EPS) operator through a Point of Common Coupling (PCC); a subset of Distributed Resource (DR)" [3]. Reduction of investment in transmission and distribution system upgrades and fast installation are the major benefits to the power utilities. Many applications, such as upgrading the reliability of the power supply, peak shaving, grid support and combined heat and power (CHP), are the major benefits to distributed generation owners.

However, the appearance of co-generation, DG, and unconventional generation may result in unwanted (and often unexpected) consequences. This thesis focuses on one such unwanted consequence: increased fault current. In this thesis, focus is given to operation during faulted conditions. Circuit breaker capability and configuration of protective relays that were previously designed for the system without DGs may not safely manage faults. There may be some operating and planning conditions that are imposed by the fault current interrupting capability of the existing circuit breakers and the protective relay configurations. These situations can result in the safety degradation of the electric power system. At present, there is a very low penetration of DG in the United States. However, many indicators imply that DG penetration is increasing. The cited fault current concerns are expected to occur at a significant level of DG penetration. Also, *locally* DG penetration could be high in some circumstances. The study in [4] shows that the significant penetration level of the Western Electricity Coordinating Council (WECC) during the peak load in summer is between 10 – 20 percent. The identification and alleviation of degraded operation of power systems during fault conditions is the main objective of this work.

A protection system consists of many components to accommodate the fault in a system (i.e., distance relay, overcurrent relay and directional overcurrent relay). The coordination of these protective relays is set up during the process of system design based on the fault current calculation. To clear faults properly with in a specific time, each protective relay has to coordinate with the other protective relays which are located at all adjacent buses. However, installation of DGs in the distribution system increases the fault

current throughout the system. After the installation of DGs, there may be some protective relays in the system need to be readjusted. A potential research area is to investigate the other types of algorithms (e.g., artificial ant algorithm, simulated annealing) to optimize the coordination setting of protective relays in the distribution system with new DGs.

Assessment of the ability of power systems to manage the increase of fault currents due to DGs should be investigated. The assessment of fault can be separated to two types: assessment prior to DGs installation and online assessment.

Assessment prior to DGs installation

Fault currents in power systems determine the ratings of the circuit interruption devices and the settings of power system protective relays. Once the circuit breakers are in place and relay settings have been implemented, there may be some operating and planning implications imposed by the changing fault current. Fault analysis should be done prior to the installation of a new DG. A protection system and associated circuit interruptions may need to be upgraded or replaced. A method for assigning the costs of upgrading to the customers that have installed DG should be developed. In some cases, entirely new protective relay settings and upgraded circuit breakers may be needed. This is a complicated issue which depends on the type of the customer, the size and the type of the DG equipment, and the operating intention of the DG system. All approaches to allocate the responsibility and the cost of these changes should be on the basis of simple and fair market for every customer and utility. The identification of what is fair and what is simple has not been done for the case of fault currents due to added DGs. These issues

are needed to guarantee safety and reliability of the system which should be covered by the owner of the DG.

Online assessment

The main variables that affect fault currents are the installation of DGs and the change of system topology. An online assessment of fault current should be developed to assure the safe operation of the system. The online assessment of fault may take the operating data from the supervisory control and data acquisition system (SCADA) and estimate the system wide fault currents. The estimation of fault current from the operating data may be used to estimate the fault current based on the statistical analysis. This online assessment may necessary to help the operator to avoid unsafe operating conditions.

1.2 Objectives

The main objective of this research is to establish an algorithm for the identification of operating limits imposed by the system fault current interruption capability. Another objective is to identify the locations and techniques which would improve the fault interruption capability and relay settings where the protection system must be upgraded. The technical approaches for these objectives are:

- Modeling different types of DG
- AC fault analysis
- Identification of the operating conditions and hardware
- Analysis of the economic impact on the increased fault current

- Online assessment of fault currents
- Optimal coordination of the power system protection in the presence of DGs.

The overview and objectives of this work are shown in depicted. 1.1. Consequences of fault currents contributed by DGs are one of the important aspects which electric utility companies have to consider before installing a new DG into their systems.

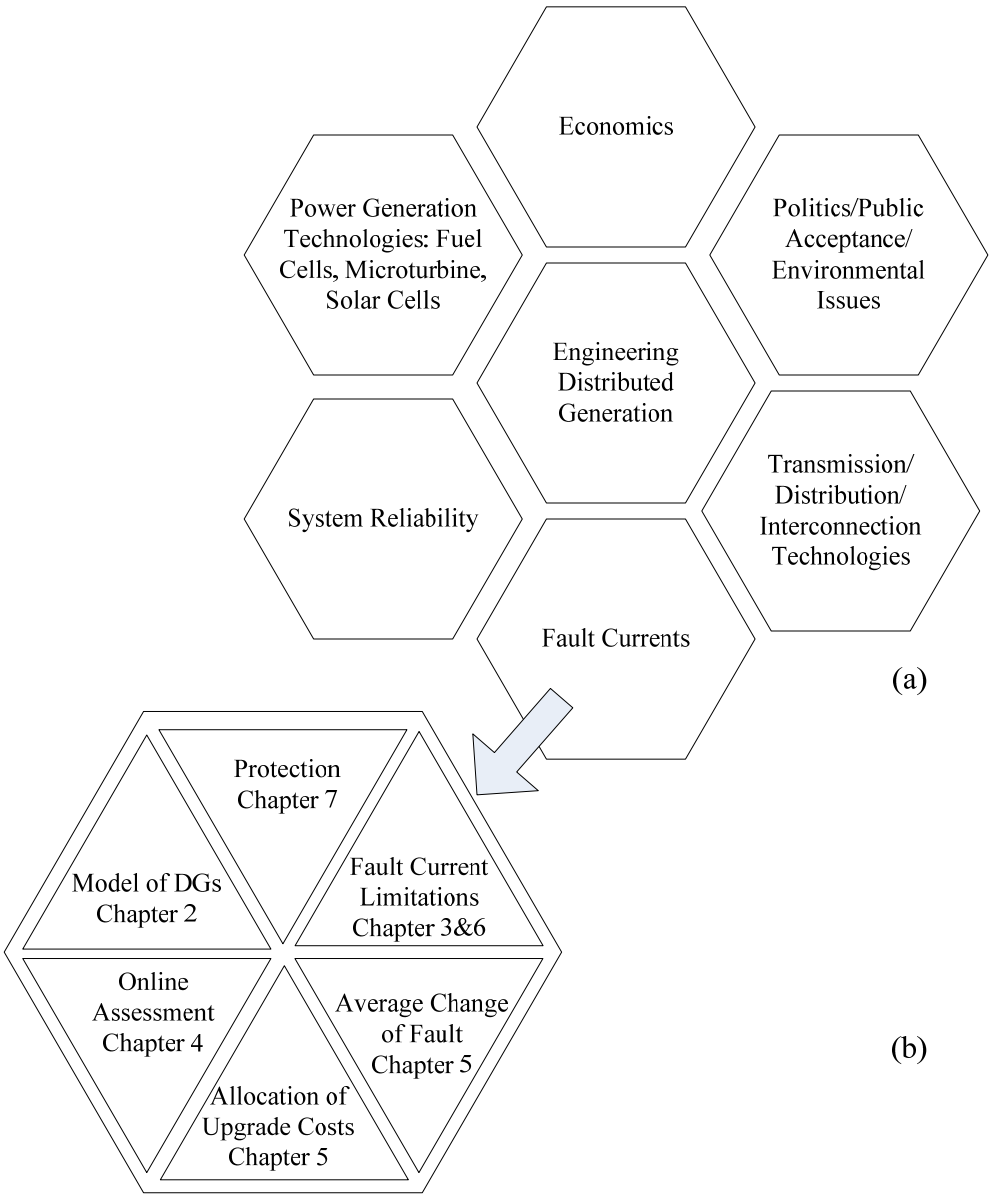

Figure 1.1 (a) Overview and (b) Objectives of this work

1.3 Literature review

In the subsequent six sections, a brief overview of pertinent literature is given. The overview is organized into five parts:

In Section 1.4, distributed generation

- Distributed generation
- Non-utility generators
- Installing DG
- U.S. national policies on DG (in Section 1.5)

In Section 1.6, the application standards

- The IEEE Standard 1547
- The IEEE Standard C37.04-1999

In Section 1.7, control strategy and design of inverter based DG

In Section 1.8, system considerations

- Online assessment of fault current
- Economic impact on the installation of DGs

In Section 1.9, coordination of relays

- Impact of DGs on fault current and system protection.

1.4 Literature review: distributed generation

The definitions of size and type of DGs vary over a wide range. Some examples of the definitions are shown as the follows:

- DOE considers the DG range to be from less than a kW to tens of MW [3]

- The Electric Power Research Institute (EPRI) considers DGs from a few kW to 50 MW as well as energy storage devices sited near customer loads [5]
- Gas Research Institute considers DGs between 25 kW to 25 MW [6]
- The International Council on Large Electricity Systems (CIGRE) considers DGs as a generation unit that is not centrally planned, not centrally dispatched and smaller than 100 MW [7].

Since the 1990s, reciprocating engines and gas turbines have been rapidly placed into service. Perhaps this deployment is a result of problems in dealing with transmission issues, and problems in siting conventional generation – but, for whatever reason, protection engineers as well as transmission and distribution engineers have to increasingly deal with problems related to the added DG in the power systems.

The emergence of small and medium size DG arises from two major necessities: inadequacy of efficient power production (both economy and environment friendly) and requirement of high reliability from industrial or commercial customers with a very high value product. Table 1.1 shows approximate data for the cost of DGs per kW [8].

Distributed generation can appear in different forms, both renewable and nonrenewable. Renewable technologies include fuel cells, wind turbine, solar cell, and geothermal. Nonrenewable technologies include combined cycles, cogeneration, combustion turbine and microturbines. References [10, 11] briefly discuss on DG technologies which are available in the market.

Table 1.1 Approximate price of DG per kilowatt [8, 9]

Technology	Size Range (kW)	Approximate Installed Cost ($/kW)
Diesel engine	20 - 10,000	125 - 300
Turbine generator	500 - 25,000	450 - 870
Wind turbine	10 - 1,000	~ 1,000
Microturbine	30 - 200	350 - 750
Fuel cell	50 - 2,000	1,500 - 3,000
Photovoltaic	< 1 - 100	~ 3,000

Non-utility generators

Increasing of non-utility generators (NUGs) rapidly increases consideration of effects of distributed generations to the grid. Statistics show that, the proportion of total capacity and DG capacity will grow up to 20 percent or approximately from 40 GW to more than 150 GW by the end of the decade [12].

Installing DG

Installing DG at a customer site enhances certain aspects of the power quality of the owners significantly by mitigating the voltage sag during a fault. Most faults on a power system are temporary, like arcing from overhead line to ground or between phase conductors. These temporary faults on a distribution system should be detected and cleared by protection relays and reclosers. During the period of the fault, the voltage in the distribution system drops. This phenomenon is called “voltage sag”. The magnitude

of the sag depends on the line impedance from substation to the fault location. Locally installed distributed generation at a customer site can provide voltage support during fault in the utility transmission system and improve the voltage sag performance. Moreover, DG improves the owner reliability markedly as a typical back up generator can be started up within 2 minutes. Gomez and Morcos in [13] propose a methodology for coordinating the ride through capability of sensitive equipment and overcurrent protection in the presence of DGs. The proposed methodology is accomplished by comparing the Computer Business Equipment Manufacturing Association (CBEMA) curve of the sensitive equipment with the time/voltage characteristics of protective equipment.

Although there are many advantages of installing DGs, a few operating conflicts cannot be ignored. If there is a high penetration of DGs, the conventional utility supply may not be able to serve the load when the DGs drop off-line [14]. Installing a small or medium DG may not have a significant impact on the power quality indices at the feeder-level. The main reason for this observation is that IEEE Standard 1547 requires that the load be disconnected from the supply feeder after a specified period of time (a rather short time, measured in cycles). The DG, after the cited disconnection, will have no impact on the supply feeder. The DG has a local impact. That is, the local load may be served properly, but others on the common feeder will not experience improvement in voltage regulation.

Installation of DGs has been discussed in many research papers, such as those dealing with the reliability of the distribution system, coordination of protective devices, ferroresonance, frequency control, and consequences of increased fault current [13, 15,

16].

1.5 Literature review: U.S. national policy on DG

Due to many reasons, such as the demand of clean energy, the congestion of transmission system and the volatility fuel price, the department of energy (DOE) by distributed energy office (DE) has a strategic plan that the twenty percent of new installed generation capacity should be from DG by the year 2020 [17]. In the year 2001, the total generating capacity of the United States was approximately 800 GW [18]. DOE forecasts that the demand of electric power would be increased by twenty five percent in the next ten years. Also, the electricity demand is expected to grow sharply over the next twenty years. This means that the United States will need about 393 GW of new installed capacity by 2020 [18]. According to the DOE strategic plan, Berkley Lab interprets that approximately 28 GW of new DG capacity will be installed by 2020 [17]. The energy demand in the United States for the recent past (1970) projected to 2020 can be found in [18].

In California, with legislation passed in 2002, the utilities are required to purchase renewable energy in order to meet the renewable portfolio standard (RPS). This requires retail sellers to increase their sales of electricity from renewable sources to achieve 20 percent by 2017 [19]. The legislature has created a new ten-year investment fund for sustainable energy technologies more than $5.5 billion [20]. Since the RPS legislation was passed in 2002, three state energy agencies have adopted the Energy Action Plan. (The three agencies are the California Energy Commission, California Public Utilities Commission, and the California Power Authority.). The Energy Action Plan establishes a

more aggressive goal for renewable energy development, with a target of 20 percent by 2010 [21].

This information indicates that the DGs will be a significant portion of electrical generation for serving the electricity demand in the United States. Consequences of installing these DGs are needed to be investigated before the installations. This analysis should be accomplished to avoid the results from the increased of fault current throughout the system.

1.6 Literature review: IEEE Standards

In this section, the IEEE Standards 1547 [3] and C37.04-1999 [22] are discussed. Standard 1547 relates to DGs and C37.04 relates to fault current interruptions.

The IEEE Standard 1547

This standard provides the specifications and requirements for interconnection of DR with area EPS. According to this standard, DR is defined as sources of electric power including both generators and energy storage technologies. DG is the electric generation facility which is a subset of DR. The requirements for interconnection of DR under normal conditions specified in the IEEE Standard 1547 are:

- the voltage regulation of the system after installing DG is ± 5 % on a 120 volt base at the service entrance (billing meter) [23]
- the DR unit should not cause the voltage fluctuation at the PCC higher than ± 5 % of the prevailing voltage level of the local EPS
- the network equipment loading and IC of protection equipment, such as fuse and CB should not be exceeded

- the grounding of the DR should not cause overvoltages that exceed the rating of the equipment in local EPS.

The requirements for interconnection of DR under abnormal conditions are:

- the DR unit should not energize to the area EPS when the area EPS is out of service
- the DR unit should not cause the misoperation of the interconnection system due to Electromagnetic Interference (EMI)
- the interconnection system should be able to withstand the voltage and current surges
- the DR unit should cease to energize the area EPS within the specific clearing time due to abnormal voltage and frequency
- the DR unit should not cause power quality problems higher than specified tolerable limits, such as DG harmonic current injection, flicker and resulting harmonic voltages.

In case the system frequency is lower than 57 Hz, the DR unit should cease to energize to the area EPS within 16 ms. When a fault is detected, the DGs must be disconnected from the electric utility company supply and the DG should pick up the local load. The disconnection is needed because: (1) a fault close to the DG in the supply system must be interrupted and (2) the local DG can not support the power demands of the distribution system (apart from the local load). The disconnection of the DG from the network must occur rapidly. Table 1.3 shows the IEEE 1547 requirement [3] for disconnection times.

Table 1.2 Required clearing times for DGs higher than 30 kW

(from IEEE Standard 1547 [3])

Voltage range % of (base voltage)	Clearing time (s)[b]
$V < 50$	0.16
$50 \leq V < 0.88$	2.00
$110 < V < 120$	1.00
$V \geq 120$	0.16

[b] DR ≤ 30 kW, maximum clearing times; DR > 30 kW, default clearing times.

Note that the foregoing remarks related to the cost of added equipment and upgrades due to fault currents are separated from the issues related to commonality of technical conditions at DG sites. Most utilities utilize a common set of rules to interconnect the DG to power system, for example:

- Exchange the project information between utility and customer
- Technical analysis by the utility to evaluate the impact of DGs
- Inspection of interconnection and protective equipment by the utility.

These issues are needed to guarantee safety and reliability of the system which should be covered by the owner of the DG.

The IEEE Standard C37.04-1999

The requirement of sizing the current interrupting capability (IC) of circuit breakers (CBs) is discussed in the IEEE Standard C37.04-1999 [22], "IEEE application guide for AC high voltage circuit breakers rated at symmetrical current basis". Two methods for calculating system short circuit current are proposed: the simplified *E/X* method and

the *E/X* method with adjustment for AC and DC decrements. Examples of choosing the IC of a circuit breaker are given in [24, 25].

1.7 Literature review: control strategy and design of inverter based DGs

This section discusses the literature review of models of the inverter based DGs. There are many distributed resources that naturally generate DC voltage such as fuel cells, solar cells, and wind turbine. These distributed resources require three phases inverter to interconnect with the grid system.

The theory of the stand-alone three phase PWM controller can be found in [26]. The authors discuss the design and control of PWM inverter as a standalone unit. Various types of controller performed in *abc* variables are discussed.

M. Prodanovic and T. C. Green in [27, 28] discuss a control strategy of an inverter based DGs and filter design consideration. The proposed control strategy is separated to three parts: internal inductor current control loop, external power control loop, and phase-locked loop. The current control loop is performed in *dq0* reference frame because of the advantages for instantaneous active and reactive power calculation. The authors claim that applying the proposed control technique offer high quality of output power.

T. Takeshita, T. Masuda and N. Matsui in [29] propose a control strategy for a PWM inverter based DGs. The proposed strategy is performed in the *dq0* reference frame and including a harmonic suppression loop. The harmonic suppression loop creates the opposite phase voltage to reduce the harmonic voltage and current outputs. The effectiveness of the proposed method is verified by the simulation and experimental re-

sults.

M. Marwali and A. Keyhani in [30] propose a control strategy of a three phase inverters by applying the internal mode principle. The internal mode principle states that the output voltage and current disturbances can be eliminated by using an adjusted reference signal which composes of the original reference signal and the frequency mode of output disturbances to be eliminated. The simulation and experimental results are shown in this paper. The experimental results presented in the paper verified that the proposed control strategy provides a high power quality output. The control strategy is achieved by using the average power control method. The benefit of the average control method is the ability to reduce the sensitivity of errors from voltage and current measurements.

M. Marwali and A. Keyhani in [31] discuss the load sharing method of the parallel operation of DGs in a stand alone power system. The load sharing is done by exchanging the power information among the DGs (e.g., voltage magnitude and voltage/current phase angle difference). The harmonic control loop is added to guarantee harmonic power sharing under nonlinear loads.

M. E. Baran amd I. El-Markaby in [32] propose the analysis of fault current from inverter based DG by extending the conventional fault analysis. The authors observed that P, Q and I of inverter based DGs vary in exponential fashion. This characteristic is augmented in the dynamic set of equations and in the interaction between coupling variables (i.e., internal voltage (E_f), angle (δ), real (P) and reactive power (Q) output of inverter based DGs). The simulation in this paper is done in ElectroMagnetic Transients including DC (EMTDC). Simulation time step is chosen such that E_f does not change

much during each time step.

1.8 Literature review: system considerations

In this section, selected aspects of operating limits and hardware to accommodate fault current are reviewed. Increased system fault currents resulting from the installation of merchant plants which affects the operating economics should be investigated. There may be the circumstances in which a security constrained OPF and unit commitment (UC) needs to include constraints imposed by the IC of circuit breakers or the setting of protective relays. Distributed and alternative generation may impact these constraints. The potential economic impact of fault current contributed by DGs and merchant plants should be analyzed.

Optimal power flow

Optimal power flow (OPF) studies have been discussed since its introduction in the early 1960s [33]. References [33, 34] have a literature survey in this topic. Classical optimization methods in general can be classified into two groups: direct search methods and gradient-based methods. In direct search methods, the objective function and the constraints are used to guide the search strategy. Since the direct search methods do not require the derivative information, they are often slow and require many function evaluations for convergence. In the gradient based methods, the first (and possibly the second) derivative of the objective and the constraints guide the search strategy. Usually, the gradient based methods converge to the optimal solution faster than the direct search methods. However, gradient based methods may not be capable of solving the non-differentiable or discrete problems.

The majority of the classical techniques to solve non-linear programming problems discussed in the OPF literature are:

- lamda iteration method, also called the equal incremental cost rule (EIC)
- gradient method
- Newton's method
- linear programming method
- interior point method.

References [35-37] have introductions to these topics. Typical objectives of the OPF are minimization of fuel cost, losses and added VARs while maintaining the system constraints. The control variables of the OPF are generator bus voltages, transformer and phase shifter settings and real power at the generator bus. The constraints of the OPF may include generator bus voltages, line flows, transformer capacities and phase angle regulator settings, security constraints, stability constraints, environmental constraints and reliability constraints.

References [38, 39] discuss some difficulties of using classical techniques to solve the optimization problems, such as:

- The convergence to an optimal solution depends on the chosen initial condition. Inappropriate initial condition makes search direction converge into a local optimal solution.
- The classical techniques are inefficient in handling problem with discrete variables.

The following section illustrates the performance and applicability of the OPF with vari-

ous constraints.

Stability constrained OPF

Stability is an important constraint in power system operation. The cost of losing synchronism through a transient instability is high in power systems. A large number of transient stability studies may be needed to avoid this problem. Transient stability may be considered as an additional constraint to the normal OPF with voltage and thermal constraints. In the normal OPF, it is well-understood that the voltage and thermal constraints can be modeled by a set of algebraic equations. However, the stability constrained OPF contains a set of both differential and algebraic equations. The dependence on time is an added level of complexity.

Gan and Thomas in [40] propose a technique to solve this problem by converting the differential- algebraic equations to numerically equivalent algebraic equations. The stability constraints are expressed by the generator rotor angle and the swing equations. LP method with relaxation technique is implemented to solve the OPF problem.

Environmental constraints

According to the requirements of the Clean Air Act Amendment (CAAA) [41], the electric utility industry has to limit the emission of SO_2 to 8.9 million tons per year and multiple NO_2 to 2 million tons per year [42, 43]. The emission rate of each unit can be expressed as a quadratic function of generation active power output (MW) and heat rate (MBtu/h). Emission control can be included in the conventional ED problem by adding the environmental cost to the normal dispatch.

Several authors [44-47] apply an Evolutionary Algorithm (EAs) to solve the ED

problem. The EAs are computer-based problem solving systems. These methods mathematically replicate the mechanisms of natural evolution as the key elements in their design and implementation. Four different EAs are genetic algorithms (GAs), evolutionary strategy (ES), evolutionary programming (EP) and genetic programming (GP). Deb in [44] describes the theory of the multi-objective optimization by applying the EA.

Wong and Yuryevich in [46] apply the EP technique to solve the environmentally constrained economic dispatch (ECED) problem. The EP technique is based on the mechanics of natural selection. Basically, EP searches for the optimal solution by evolving population candidate solutions over a number of generations or iterations. A new population or *individual* is produced from an existing population through a process called "mutation". Individuals in each generation and the mutate population compete with each other through a competition scheme. The winning individuals from the competition scheme form a next generation. The process of evolution may be terminated by two stopping criteria: stop after a specified number of iterations or stop when there is no significant change in the best solution.

Yalcinoz and Altun in [47] and Ma, El-Keib and Smith in [42] propose a solution for ECED problem using modified genetic algorithm. The objective function consists of three terms which are the production cost, emission functions of SO_2 and NO_2. The authors conclude that the proposed GA algorithm is appropriate to be applied to solve the ECED problem.

The foregoing advanced intelligent based algorithms are reasonably well documented in the literature, but there are no known actual applications in operational power

system dispatch.

Unit commitment for system with DGs

Unit commitment (UC) is the problem of determining the optimal schedule of committing (i.e., making available for dispatch) generation subject to operating constraints. The UC problem has been studied extensively. Various mathematical approaches to solve the UC problem have been proposed, such as priority listing, dynamic programming (DP), Lagrangian relaxation (LR), evolutionary programming and integrated algorithm. In general, the constraints that must be satisfied of the unit commitment are system power balance, unit generation limits, minimum/maximum up and down time, spinning reserve and constraint on voltage magnitude. Padhy in [48] gives an overview concept and a bibliographical survey on UC problem.

Siu, Nash and Shawash in [49] propose a real time scheduling of ten hydro units by applying an expert system and DP. The expert system is used to eliminate the infeasible and undesirable solutions. The DP is used to solve the optimal unit commitment problem.

The application of the genetic algorithm (GA) is demonstrated to solve the UC problem in many papers. The feasibility of GA to solve the UC problem in real scale power system has been examined in [50-52]. GA is an adaptive search technique based on the principles and mechanisms from natural evolution (i.e., fitness evaluation, selection, crossover and mutation). However, the major limitation of the GA technique is the large computational time requirement.

Reference [53, 54] solve the short term UC problem by applying a hybrid genetic algorithm and tabu search method (TS). In the first step, the GA which has a good global optima search is applied to give the initial solutions. Then, in the second step, the TS is applied to give the solution near a local optimum. The authors utilize the TS to solve the UC problem because it has a better performance for a local optimum search.

Ma and Shahidehpour in [31] discuss the unit commitment with the transmission security and voltage constraints. The problem is decomposed into two parts: unit commitment problem and transient security / voltage constraint. The UC problem is solved by applying the augmented Lagrangian relaxation method. The dynamic programming algorithm is used to search optimal commitment for generating units.

Online assessment of fault current

Srinivasan and Lanfond [55] propose a short circuit current estimation technique. The fault current estimation technique is based on the statistical analysis of the voltage and current variations during system disturbances. However, the proposed equations are limited to some system configurations. The general equations for estimating various bus types in the system need to be developed.

1.9 Literature review: coordinating of protective relays

Impact of DGs on fault current and system protection

Protection system planning is an indispensable part of an electric power system design. Analysis of fault level, pre-fault condition, and post-fault condition are required for the selection of interruption devices, protective relays, and their coordination. Sys-

tems must be able to withstand a certain limit of faults that also affect reliability indices. Many classical references are found on this topic, such as [36, 56, 57]. This research relates to a new aspect of fault analysis of power systems: the appearance of DG, perhaps at high levels of penetration, and the effect of DG on fault currents.

In general, the addition of generation capacity causes fault currents to increase. The severity of the fault current increasing in the system depends on many factors including penetration level, impedance of DG, the use of Automatic Voltage Regulators (AVR), power system configuration, and the location of DG – approximately in order decreasing importance. This is a simple consequence of the reduction of the Thevenin equivalent impedance seen at the system buses when generation is added to the system. The theory and details of the fault current analysis are discussed in Chapter 3. The consequences of the increased fault current due to the proliferation of distributed generation are briefly discussed as follows:

- *Change in coordination of protective devices:* Figure 1.2 shows a sample distribution system. This system is a primary distribution system that is offered as an example of a distribution system with three DGs. The system is purely radial, three-phase, 4160 V, and is served from a 69 kV subtransmission system at a substation. In the depicted configuration, the protection system may lose coordination upon installation of a DG. This point is illustrated as follows: before installing distributed generation DG1, if a fault to ground occurs at point 1, fuse FA should operate before fuse FB. This is due to the upstream fault on the sub-feeder. When DG1 is included on sub-feeder, the fault current flows from DG1 to fault point 1 and fuse B might open before fuse A if

the difference between I_{FA} and I_{FB} is less than the margin shown in Fig. 1.3. The difference between I_{FA} and I_{FB} is proportional to characteristics of DG1 (e.g., transient impedances and prefault voltages). Thus, these fuses lose coordination in the case of installed DG1 [15, 16].

- *Nuisance trip:* An increase in the fault current in the grid changes the way that the protection system manages faults (relay settings, reclosers, interrupting capability of circuit breakers and fuses). Fig. 1.2 shows a relatively large DG3 installed near the substation. In case a fault occurs on feeders other than where DG3 is located, breaker BB might also trip due to the fault current flowing from DG3 to the fault point. This problem can be solved by implementing a directional relay instead of an overcurrent relay. This is a total reconfiguration of the protective relaying.
- *Recloser settings:* Installing a DG on the feeder normally requires the utility to readjust their recloser settings. In general, a DG must detect the fault and disconnect from the system within the recloser interval and leave some duration to clear the fault. Failure to follow this step might cause a persistent fault rather than a temporary one. Reference [58] recommends a recloser interval of 1 second or more. The IEEE Standard 1547 [3] requires a much shorter time for the recloser.

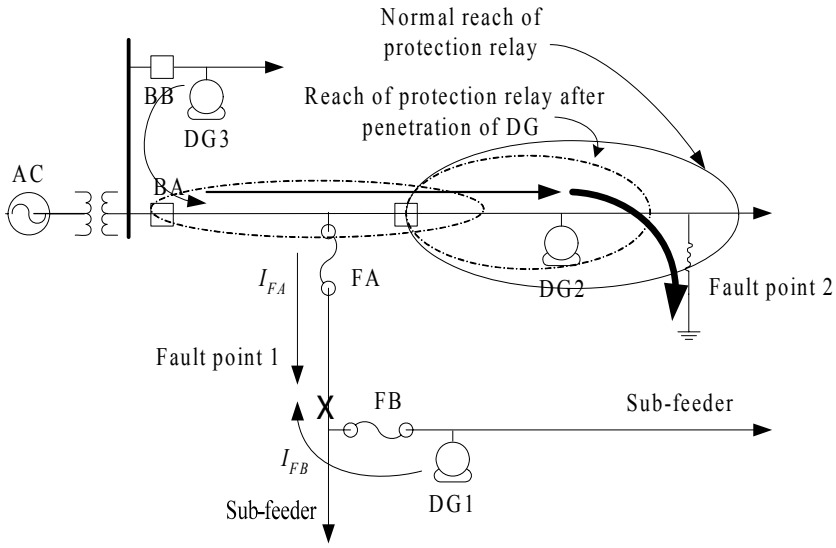

Figure 1.2 The reach of a protective relay for a small sample distribution system with DGs, from Nimpitiwan and Heydt [25].

- *Safety:* Safety degradation from the failure of the protection system may occur because a new DG increases the fault current. If the fault current is higher than the previous level and exceeds the interrupting capability of circuit breaker, the fault current might persist and cause damage to personnel and equipment.

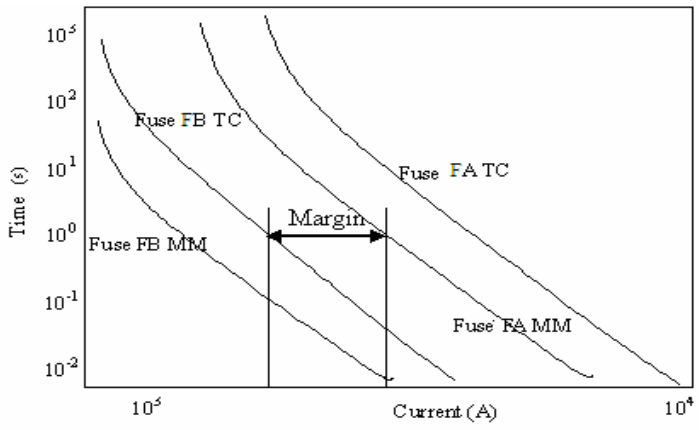

MM: Minimum melting TC: Total clearing

Figure 1.3 Time-current characteristic of the fuse in the sample system of Fig. 1.2 from Nimpitiwan and Heydt [25]

- *Changing the reach of protective relays:* A DG may reduce the reach of power system protective relaying under certain circumstances. Consider a resistive fault occurring at fault point 2 during the peak load as shown in Fig. 1.2. The presence of DG2 in between the fault point and a protective relay might cause a lower fault current to be seen by the protective relay. The DG effectively reduces the reach (i.e., zone) of the relay. This increases the risk of high resistive faults to go undetected. In such a case, backup protection may operate to interrupt a fault. So and Li in [59] apply an evolutionary algorithm to set the time coordination of overcurrent relays for a ring fed distribution system with the presences of DGs. The objective of the optimization is to maximize the satisfaction of coordination constraints.

Coordination of protective devices is a problem to enable proper selection of the protective devices and appropriate sequence of operations. Protection system of a typical industrial network may consist of several types of relay and hundreds of relay units. Directional overcurrent relays (DOCR) and distance relays remain as good technical and economical alternatives for the industrial practices. In general, the databases that are required for the coordination of protective devices are the short circuit data base and protective devices data base.

The problem associated with the application of DOCR is the difficulty in setting the coordination of relays. In practical industrial networks, the settings of overall protection coordination are complicated and are relatively harder to obtain. The working group of the IEEE Power System Relaying Committee in [60] provides the review for the development of computer aided coordination of line protection.

The IEEE working group G-7 of the relay standards committee in [61] introduces the mathematical model of inverse time over current relays. This paper provides an analytical representation of operating characteristics of typical electromechanical relays. Two equations are applied to define the reset time and the pick up time. Constants in these equations (i.e., *A*, *B*, *p* and *tr*) refer to the average of the two main series of induction disk overcurrent relays found in North America. Three sets of the standard constants are provided to represent the characteristics of moderately inverse, very inverse and extremely inverse over current relays. Practically, the performance characteristics of digital overcurrent relays can be prescribed with 15 % accuracy by the standard inverse time characteristics proposed in [61].

Urdaneta, Restrepom Márquez and Sánchez in [62] solve the problem of optimal coordination of DOCR by applying linear programming methodology. The optimization problem is configured to minimize the weighted operating time of the relays in the system. These relays are subject to the constraints associated with the coordination criteria and relay operating characteristics. However, the main disadvantage of the linear programming methodology is the large dimensionality. That is, the problem is more complicated when two or more relays with different operating principles are required to coordinate in the protection system.

Pérez and Urdaneta in [63] discuss a technique to determine the optimal coordination time of distance relays in a mixed protection scheme with DOCR by applying linear programming methodology. The distance relays are included in the protection system known as backup definite time relays (BDTRs). The setting of BDTRs must be calcu-

lated using the consideration of both DOCRs and BDTRs to avoid the loss of selectivity. The authors propose two additional constraints associated with the coordination between DOCRs and distance relays.

Evolutionary algorithms (EA) can be applied to optimize the protective relay settings. One of the main advantages of EA is the outstanding ability to solve combinatorial optimization problems and discrete solution space problems. So and Li in [59, 64] propose the time coordination method to set up the coordination of the protective relays by the application of a genetic algorithm (GA). The main objective of the time coordination method is to minimize the relay operating time within coordination constraints, such as the operation time margin between the upstream and downstream relays. However, the major disadvantages of GA are the computation time which is relatively slow. The GA computation time is more intensive compared to the other methods (e.g., an ant colony algorithm [65, 66]).

Artificial ant colony optimization (ACO) is a novel optimization technique to solve the traveling salesman problem (TSP) [65]. Reference [65] provides a brief discussion on the main idea of the ACO technique. The algorithm of the ACO has been inspired by real behavior of ants. Several aspects of the ant behavior are mimicked in the process of calculation, such as foraging, pheromone deposition, pheromone evaporation and local search. As the essence of the ACO technique, pheromone deposition is a form of indirect communication by dropping a chemical on ground which increases the probability that the ants will follow the same path. The basic principle and applications of the ACO can be found in [65, 66].

Since the initial introduction in 1997 by M. Dorigo [65] , the ACO algorithm has been applied to solve several optimization problems in power systems, such as the unit commitment problem [67], distribution system planning [68] and large capacitor placement in distribution systems [69]. Application of the ACO algorithm for coordinating relays in power systems can be found in [70].

CHAPTER 2

MODEL OF INVERTER BASED DISTRIBUTED GENERATORS

2.1 Inverter based generation sources

Generation resources are traditionally synchronous generators, and modeling of these machines is well known and applied. Unlike conventional sources, power generated in fuel cells, solar sources and some microturbines, are DC. In the case of these resources, an inverter is needed to interface with the AC system network. Also, recent developments in the operation of power systems have suggested that inverter based generation sources may be used for synchronous machines. That is, the synchronous generator is isolated from the AC system through an AC / AC converter in order to isolate the dynamics of the network from the local synchronous generator. Whatever the motivation, it is appropriate to examine inverter based generation sources and their impact on fault response in power systems. The inverter and its controls are described in this chapter. Pulse Width Modulation (PWM) is used as the base technology for the inverters described here. The models are programmed in Simulink.

The model of the inverter based DG presented in this chapter is accomplished under the assumption that the input voltage from DC sources to the PWM inverter are regulated by using DC/DC converters and chopper circuits. The analysis and design of the voltage regulator circuits are discussed in [71].

2.2 Control of inverter based distributed generations

Inverter based DGs operate as controlled voltage sources connected to the grid system through a step up transformer. The step up transformer with delta – delta connec-

tion (4 kV/12.47 kV) eliminates the zero sequence components from inverter to the grid. Figure 2.1 shows the connection of inverter based DG to the grid system.

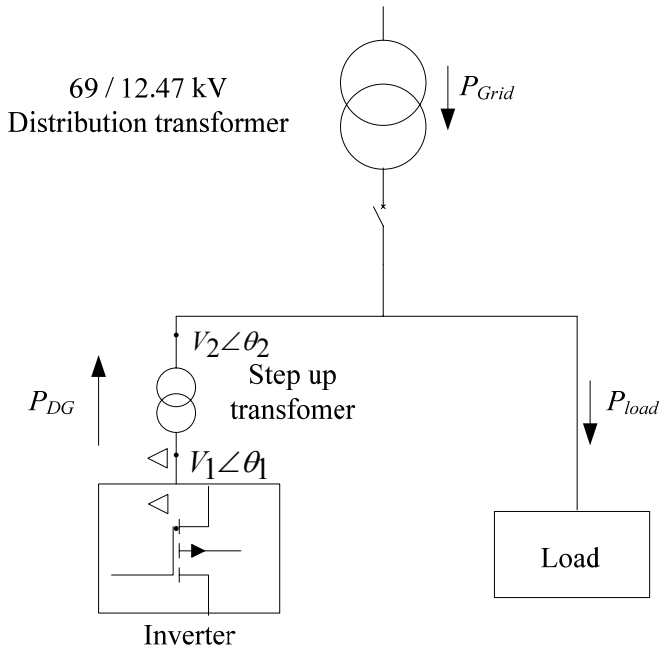

Figure 2.1 Inverter based DG connecting to a grid system

Consider the active power of an inverter based DG, denominated as P_{DG}. Let P_{DG} be at the output of the inverter. The active power P_{DG} is an average of the instantaneous power $p_{DG}(t)$. The average is taken over at least one cycle – but, more likely, taken over a time period measured in seconds if mechanical dynamics are to be studied. The active power output of the inverter based DG could be estimated as,

$$P_{DG} = \frac{|V_1||V_2|}{X}\sin(\delta) \tag{2.1}$$

where $|V_1|$, $|V_2|$ are the voltage magnitudes at the primary and secondary sides of the step up transformer and δ is the difference of phase angle between V_1 and V_2. Equation (2.1) is a simplistic representation of P_{DG} because:

- Inverter losses are ignored
- Inverter dynamics are ignored
- Equation (2.1) is an elementary model based on lossless AC circuit theory, and no source dynamics are modeled. For example, in a fuel cell, the DG source at the fuel cell terminals may not be constant.

In this development, (2.1) is not used. Instead, a full calculation of the real part of VI^* is used. It is expected that the relatively long time dynamics of $\delta(t)$ are well modeled using $\mathrm{Re}\{VI^*\}$ because V and I are rms values averaged over at least one cycle. Figure 2.2 shows the control model for the inverter based DG. The control strategies are to generate the balanced three phase voltage and to control the power output of the inverter. The controller consists of two control loops:

- the amplitude controller
- the angle difference controller.

The amplitude and angle difference controller provide the modulating signal to the pulse width modulation signal generator. The harmonics from the PWM inverter is filtered out by an LC low pass filter. The cutoff frequency, f_c, should be set low enough to block harmonics but high enough provide the attenuation of harmonics of the inverter voltage.

Amplitude controller

There is no standard design for an inverter for the application described here. However, the following is a generic discussion of a PWM based design. In a PWM inverter, the key control elements are the amplitude controller and the phase controller. The amplitude controller provides the balanced three phase output voltage to the grid at

the desired voltage amplitude. As shown in Fig. 2.3, the amplitude controller consists of a phase locked loop (PLL) and a PI controller.

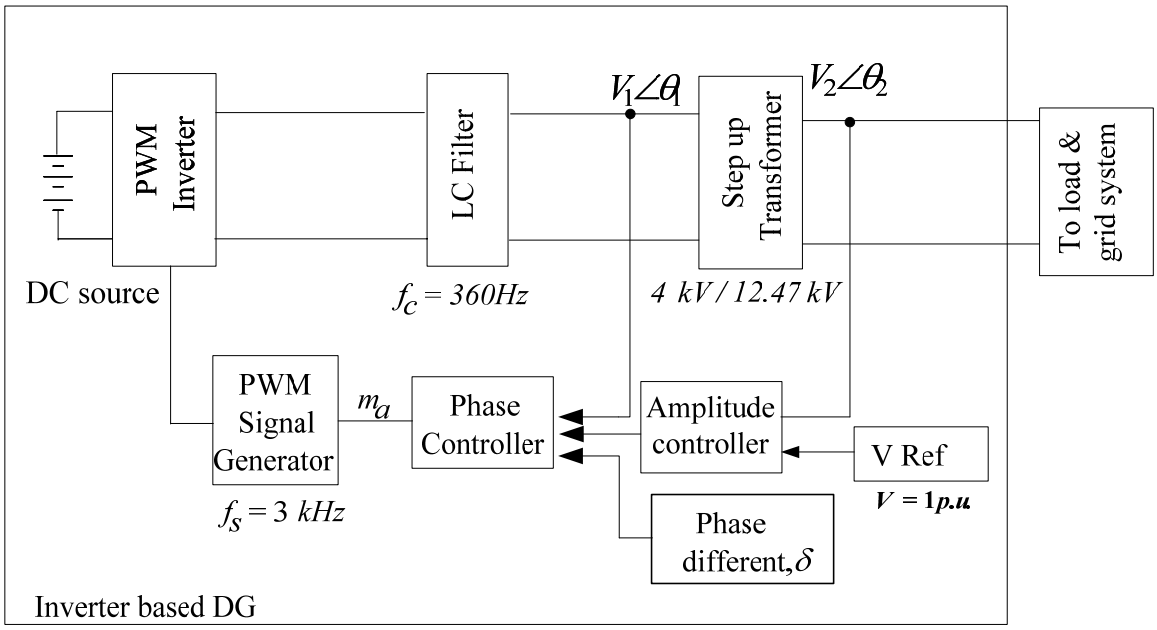

Figure 2.2 Control model for an inverter based DG, taken from Nimpitiwan, Heydt, Ayyanar and Suryanarayanan [72]

The output voltage of the DG, V_2, is transformed via a time dependent transformation. The transform used is the *dq0* transformation. This transformation has the property of frequency domain shifting the input phase voltages to a low frequency voltage. Also, high frequency terms occur. In this discussion, it is assumed that the high frequency terms that occur in the *dq0* transformed variables are filtered out. The control is performed in *dq0* reference frame because of the advantage for the instantaneous voltage angle calculation. Details of the *dq0* transformation are discussed in Appendix B. The transform equations from v_{abc} to $v_{dq0}(t)$ is

$$\begin{bmatrix} v_d(t) \\ v_q(t) \\ v_0(t) \end{bmatrix} = \frac{2}{3} \begin{bmatrix} \cos(\omega_e t) & \cos(\omega_e t - \frac{2\pi}{3}) & \cos(\omega_e t + \frac{2\pi}{3}) \\ -\sin(\omega_e t) & -\sin(\omega_e t - \frac{2\pi}{3}) & -\sin(\omega_e t + \frac{2\pi}{3}) \\ \frac{1}{2} & \frac{1}{2} & \frac{1}{2} \end{bmatrix} \begin{bmatrix} v_{an}(t) \\ v_{bn}(t) \\ v_{cn}(t) \end{bmatrix} \tag{2.2}$$

and the inverse transform from V_{dq0} to V_{abc} is

$$\begin{bmatrix} v_a(t) \\ v_b(t) \\ v_c(t) \end{bmatrix} = \begin{bmatrix} \cos(\omega_e t) & -\sin(\omega_e t) & 1 \\ \cos(\omega_e t - \frac{2\pi}{3}) & -\sin(\omega_e t - \frac{2\pi}{3}) & 1 \\ \cos(\omega_e t + \frac{2\pi}{3}) & -\sin(\omega_e t + \frac{2\pi}{3}) & 1 \end{bmatrix} \begin{bmatrix} v_d(t) \\ v_q(t) \\ v_0(t) \end{bmatrix}$$

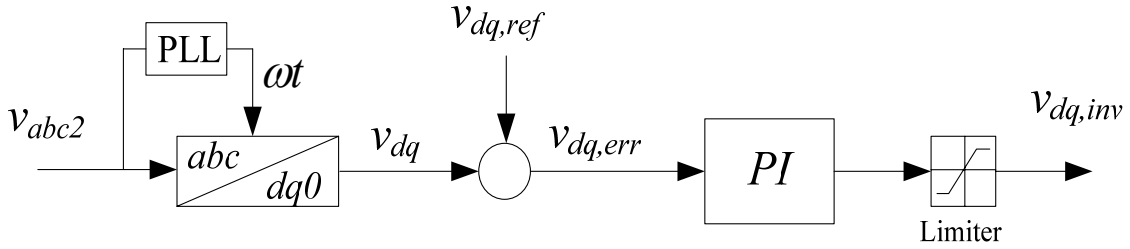

Figure 2.3 Amplitude controller, taken from Nimpitiwan, Heydt, Ayyanar and Suryanarayanan [72]

Note that the matrix coefficient in the transform equation, (2.2), can be chosen arbitrarily. This is related to the inverse of transformation. For example, in (2.2), the coefficient is 2/3 and the coefficient of inverse transform is 1.

The time domain variables $v_{an}(t)$, $v_{bn}(t)$ and $v_{cn}(t)$ mainly consist of "power frequency" components (i.e., 60 Hz components). The *dq0* transformation is time varying with DC and power frequency components. Therefore, $v_d(t)$, $v_q(t)$ and $v_0(t)$ generally contain DC, 60 Hz, and 120 Hz components. This is a consequence of the property that the

Fourier transform (FT) of a product is the convolution of the FTs of the component multipliers. If a low pass filter is applied to the vector $\begin{bmatrix} v_d(t) & v_q(t) & v_0(t) \end{bmatrix}'$, then $\begin{bmatrix} v_d & v_q & v_0 \end{bmatrix}'$ results. The latter vector is nearly DC, under near balanced sinusoidal steady state conditions. The $[]'$ signal is often well suited for control purposes. More discussion of the *dq0* transformation for this application appears in Appendix B. For purposes of designing and modeling a controller rms voltage of $v_{an}(t)$, $v_{bn}(t)$, $v_{cn}(t)$, $v_d(t)$, $v_q(t)$, and $v_o(t)$ are used. These rms values are denoted as V_{an}, V_{bn}, V_{cn}, V_d, V_q, and V_0. The same notation is used for current.

A proportional plus integral (PI) controller minimizes the error signal, that is, the difference between the reference signal and the instantaneous voltages $v_d(t)$ and $v_q(t)$.

Phase controller

The phase controller provides a phase difference, δ_{diff}, between V_1 and V_2 (see Fig. 2.1). The value of the phase difference, δ_{diff} and approximate power flow can be calculated from (2.1). A model of the phase controller is shown in Fig. 2.4. Inputs to the phase controller, V_1 and V_2, are transformed to *dq0* reference frame. The phase of V_1 and V_2 can be calculated as,

$$\theta = \tan^{-1}\left(\frac{v_d}{v_q}\right)$$

In the phase controller, a PI controller is applied to minimize the error of specified power output value, P_{ref}. The output average power of the inverter based DG is measured as the output from a low pass filter.

The cut-off frequency of the low pass filter has to be set at the appropriate value to attenuate the disturbance from measurement, but high enough to provide a good transient response of the phase controller. The output of the PI controller is added to the phase of V_1 and used to calculate the required amplitude and phase of the modulating signal. The last step in the phase difference controller is to transform the modulating signal back to the *abc* reference frame. The complete model of inverter based DG in Matlab Simulink is shown in Fig. 2.5. A single tuned filter is installed at the output terminal of the inverter based DG to attenuate the third harmonic current.

2.3 Illustration of inverter based distributed generation

In this section, the dynamic performance of the model of the inverter based DG as discussed in Section 2.2 is examined. Although a specific design is shown here for illustrative purposes, experience in working with inverter based DG models indicates that the approach taken here may be valid in the 10 kVA – 20 MVA class. Output voltage and current at the terminal of an inverter based DG from the simulation are recorded for the analysis in the frequency domain. The illustrative cases are separated into two parts:

- stand alone operation (disconnected from the grid), Case 2.1
- DG connected to the grid, Case 2.2.

Note that all case studies are listed and described in Appendix C.

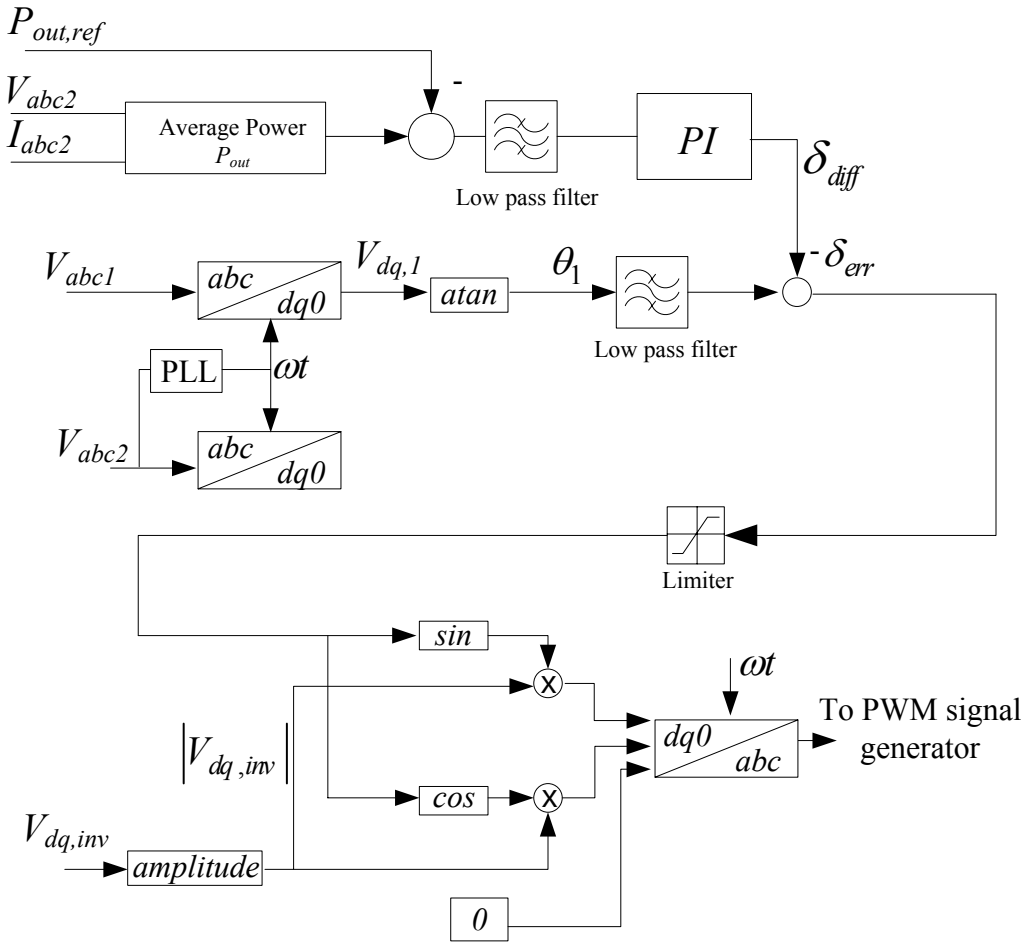

Figure 2.4 Phase controller, taken from Nimpitiwan, Heydt, Ayyanar and Suryanarayanan [72]

Stand alone operation (disconnected from the grid), Case 2.1

In Case 2.1, the simulation is built with a local load and an inverter based DG which is disconnected from the grid system. The purpose of the simulation in Case 2.1 is to show the transient response of the inverter based DG due to the change of load. In the case of the stand alone operation, the inverter requires only the amplitude controller to set the voltage at the reference point. The output power varies depending on the load. The inverter based DG parameters used in the simulation are shown in Table 2.1.

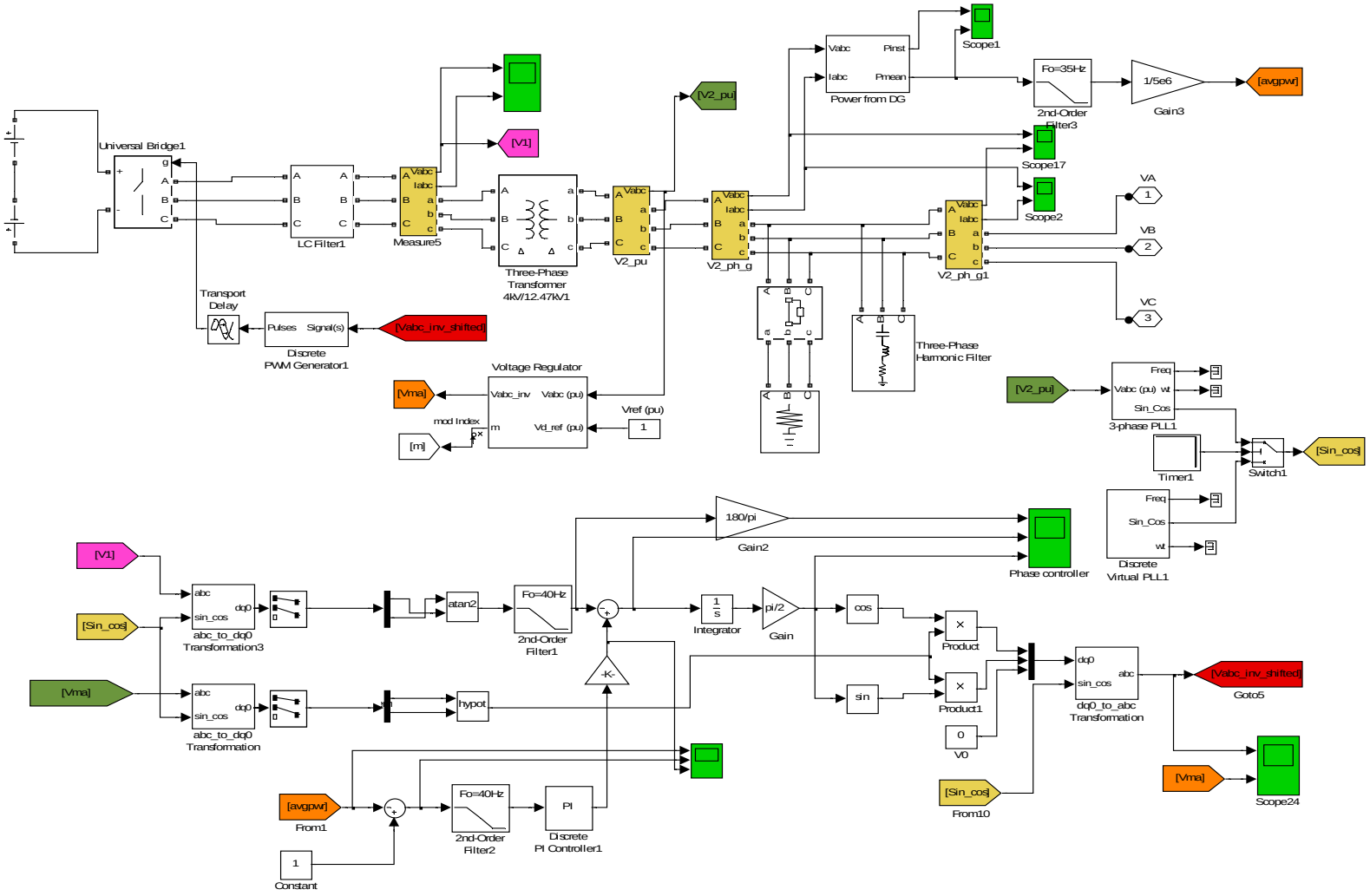

Figure 2.5 Model of inverter based distributed generation in Matlab Simulink

Table 2.1 Characteristics of an inverter based distributed generation for simulations; Cases 2.1 and 2.2

DG characteristics	Parameter
Switching frequency, f_s	3 kHz
Three phase output voltage, V_o	12.47 kV
Rated frequency	60 Hz
Short circuit impedance of the step up transformer (7 MW)	0.1 p.u.
Active power output	2-6 MW
Reactive power output	0-3 MVAr
Power factor	0.8-1 lagging
Simulation time step	50 μs
DC input voltage to the inverter	5 kV

The simulation time is from t = 0.0 to 0.3 s with simulation time step, T_s = 50 μs. The three phase output voltage is set at 1.0 p.u. or 12.47 kV. To demonstrate the dynamic performance of the inverter based DG, after reaching the steady state, the load is changed from 3 MW / 0.1 MVAR to 5 MW / 0.1 MVAR at t = 0.15 s. Figures 2.6 and 2.7 show the output line to neutral voltage and current of the inverter based DG, respectively. Note that, in Fig. 2.6, a voltage swell occurs during the change of the load. In this case, the voltage swell is approximately 5 percent of the nominal operating voltage. Figure 2.8 depicts the modulation index (m_a) in the amplitude controller which is used to control the switching of PWM generator.

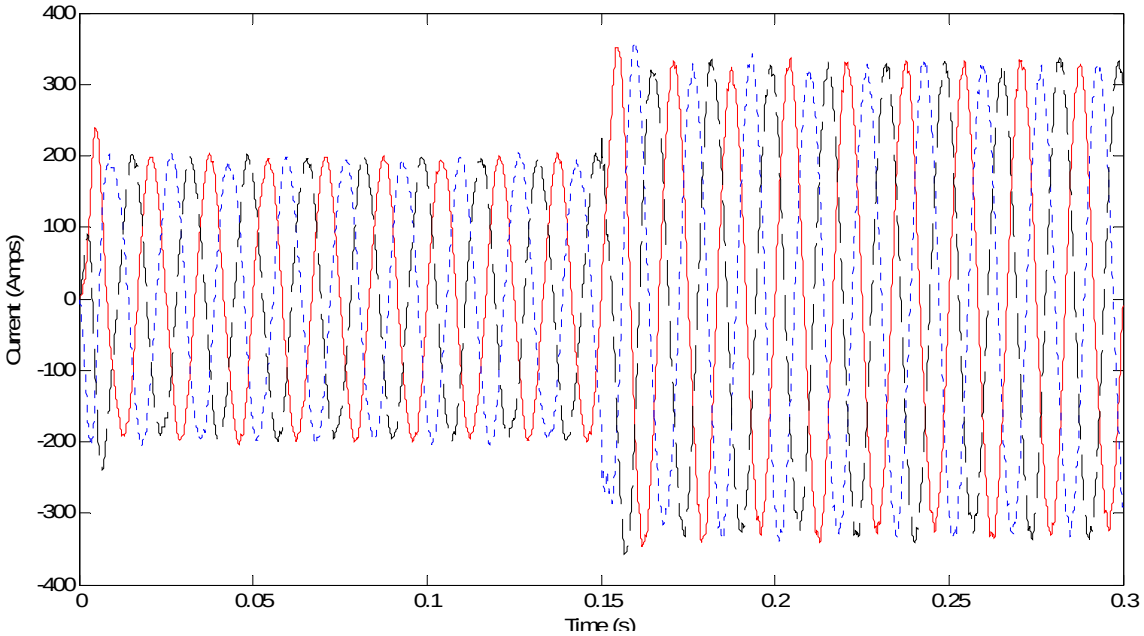

Figure 2.6 Output current of the inverter based DG (stand alone) with load change at t = 0.15 s, Case 2.1

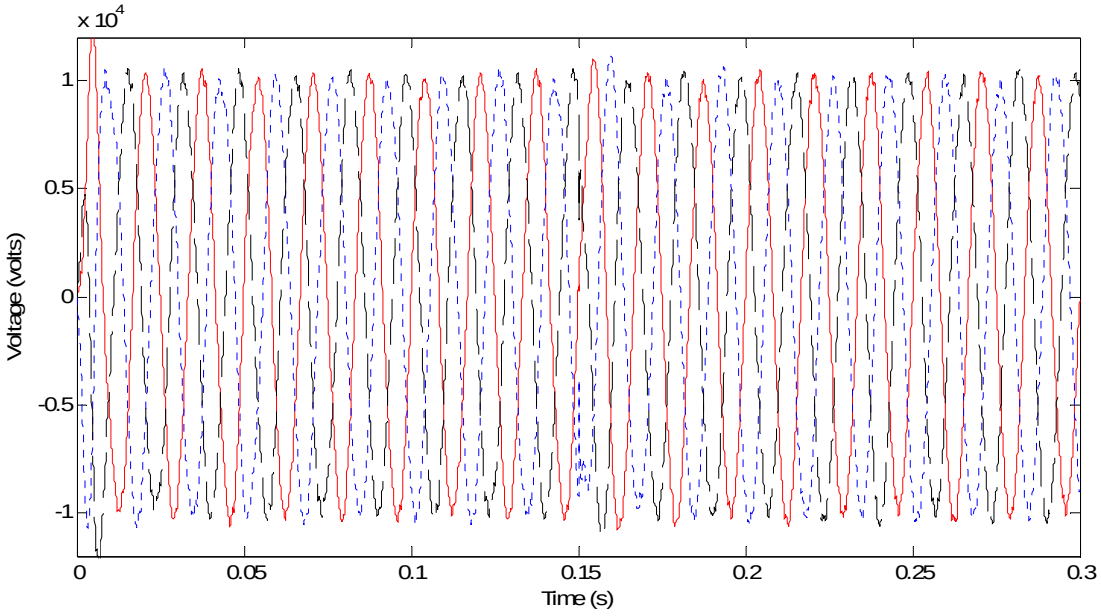

Figure 2.7 Output voltage of the inverter based DG (stand alone) with load change at t = 0.15 s, Case 2.1

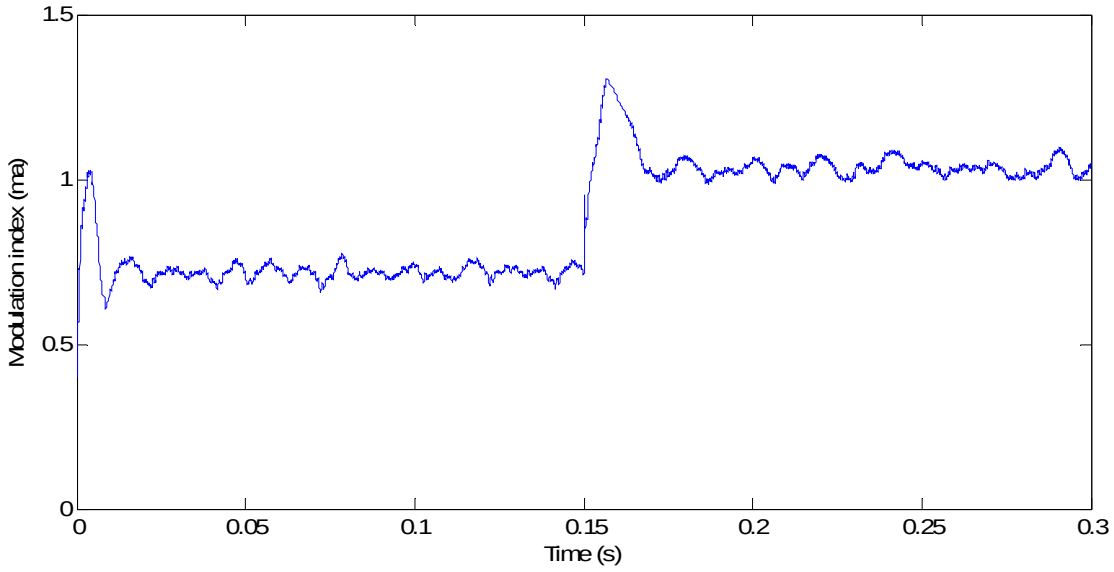

Figure 2.8 Modulation index (m_a) of the inverter based DG (stand alone) with load change at t = 0.15 s, Case 2.1

According to the specific design and the indicated operating condition, after reaching the steady state, the total harmonic distortion (THD_I and THD_V) are 1.36 and 0.66 percent, respectively. Figures 2.9 and 2.10 depict the harmonic content of the output voltage and current of inverter based DG in Case 2.1. Note that the plots are shown in semi logarithmic scale.

The average active and reactive power output (average over one cycle) is shown in Figs. 2.11-12. The active power changed from 3 MW to 5 MW at t = 0.15 s. Note that the inverter output follows the load demands and the transient response time is in the range of 20-30 ms.

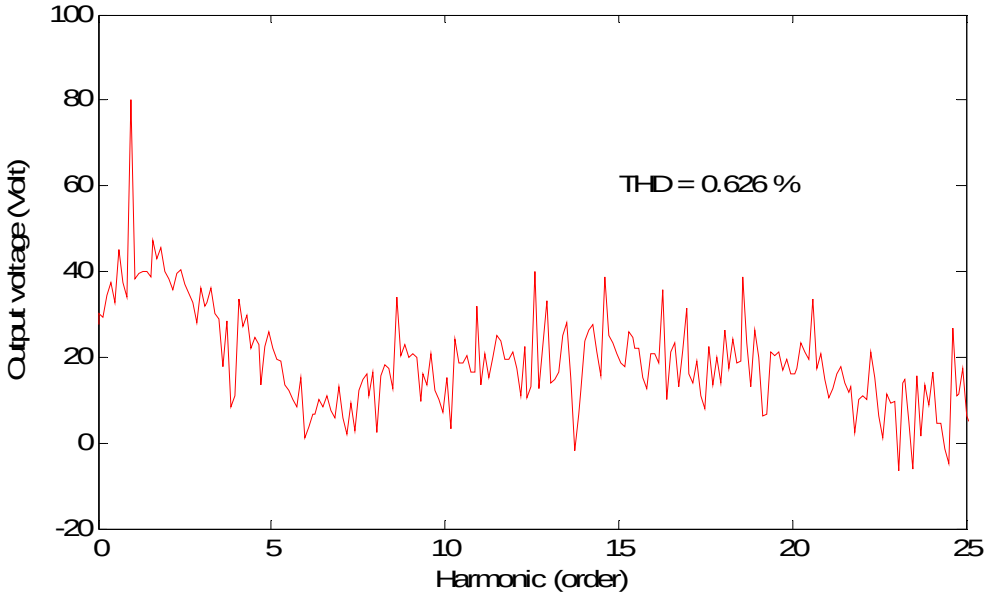

Figure 2.9 Harmonic content of the output line-neutral voltage from inverter based DG with a stand alone operation, Case 2.1

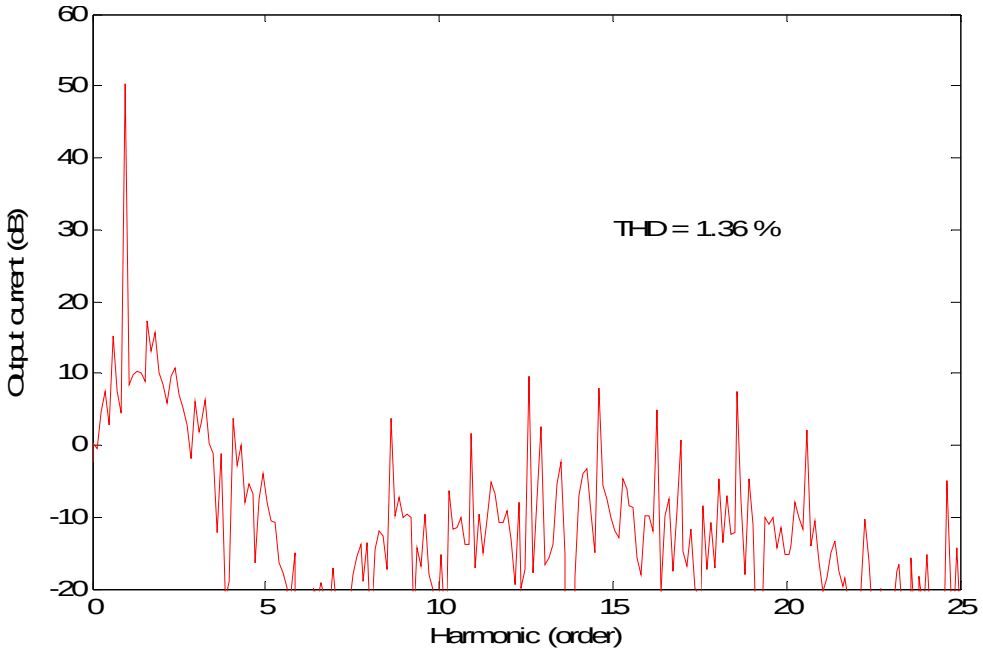

Figure 2.10 Harmonic content of the output current from inverter based DG with a stand alone operation, Case 2.1

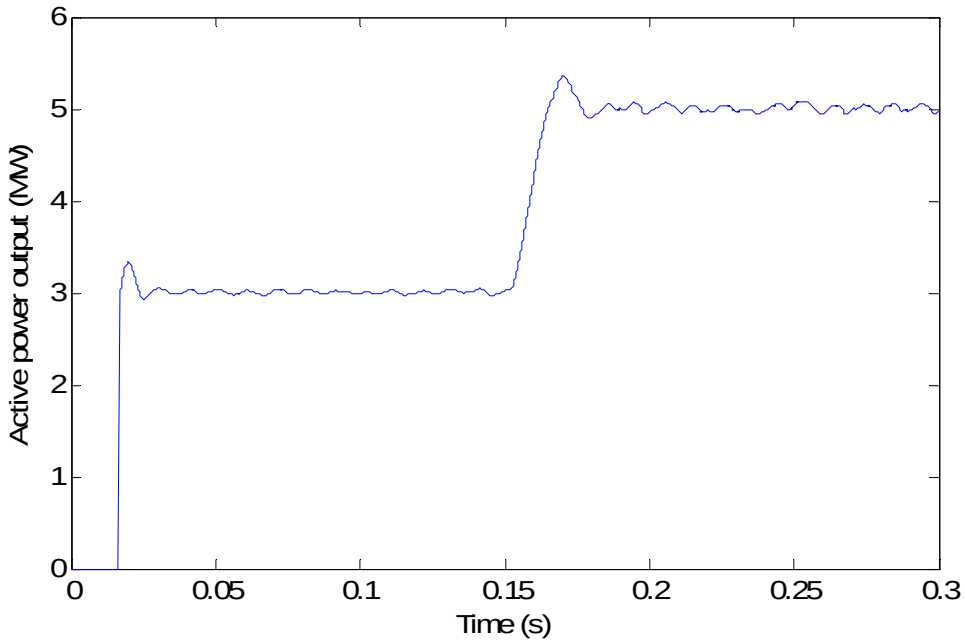

Figure 2.11 Active power output of inverter based DG with a stand alone operation, Case 2.1

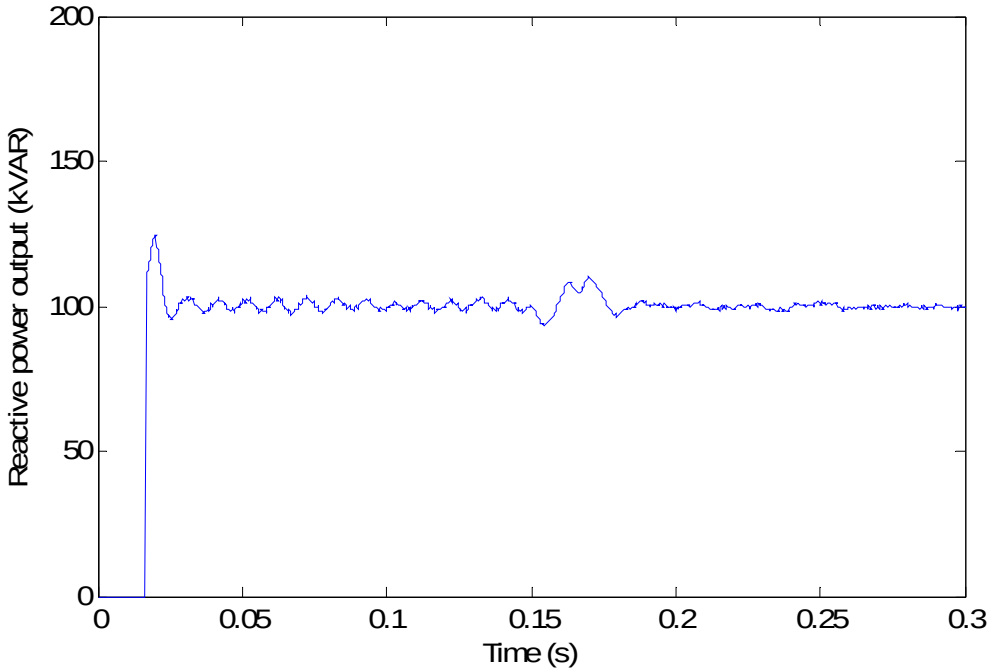

Figure 2.12 Reactive power output of inverter based DG in a stand alone operation, Case 2.1

DG connected to the grid, Case 2.2

In Case 2.2, a simple system configuration with an inverter based DG connected to the grid is given as an illustration as shown in Fig. 2.1. In this case, the amplitude controller is required to control the voltage at the reference point (1 p.u.). The angle difference controller is required to control the active power output of the inverter based DG. The simulation is built with an inverter based DG connected to the 69 kV subtransmission system through a 16 MVA, delta-wye 12.47/69 kV transformer with impedance of 0.1 p.u. The 69 kV subtransmission system is considered to be an infinite bus. The inverter based DG is applied to serve a local loads, 15 MW / 1.5 MVAR (power factor = 0.995), at 12.47 kV. Unlike Case 2.1, where the inverter based DG is programmed to control the constant output voltage at 1 p.u., the inverter based DG in Case 2.2 generates a specified active power output and also a specified output voltage. The inverter based DG parameters used in the simulation are the same as specified in Case 2.1 and shown in Table 2.1. The amplitude controller of the DG is programmed to generate the output voltage at 1.0 p.u. and the angle difference controller is programmed to provide the output at 5 MW.

According to the specific design, the output current of the inverter, based in time and frequency domains, are shown in Figs. 2.13 and 2.14. The graphs show the operation of the inverter based DG at 5 MW, 1.45 MVAR with power factor 0.96. The analysis in frequency domain is accomplished by applying the fast Fourier transform (FFT). The THD of the output current of the DG is 1.67 % for the case illustrated.

For the indicated operating condition, the voltage measured at the secondary side of the distribution transformer or PCC is 0.99 p.u. The plot of the line-neutral output

voltage is shown in Fig. 2.15. The spectrum of the output voltage is shown in Fig. 2.16 and the THD of the output voltage is 0.67%.

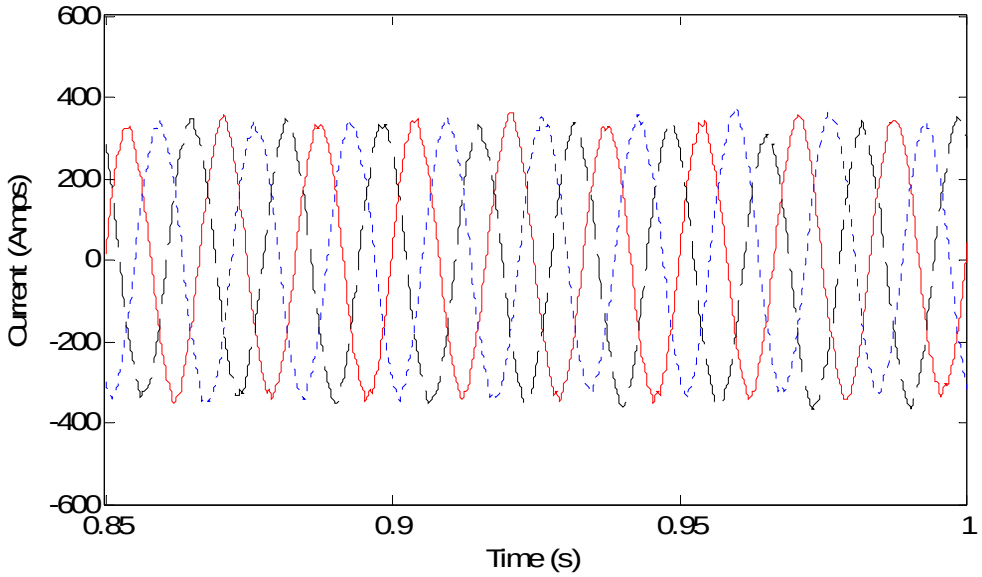

Figure 2.13 Output current of the inverter based DG – steady state operation illustrated with power output 5 MW, Case 2.2

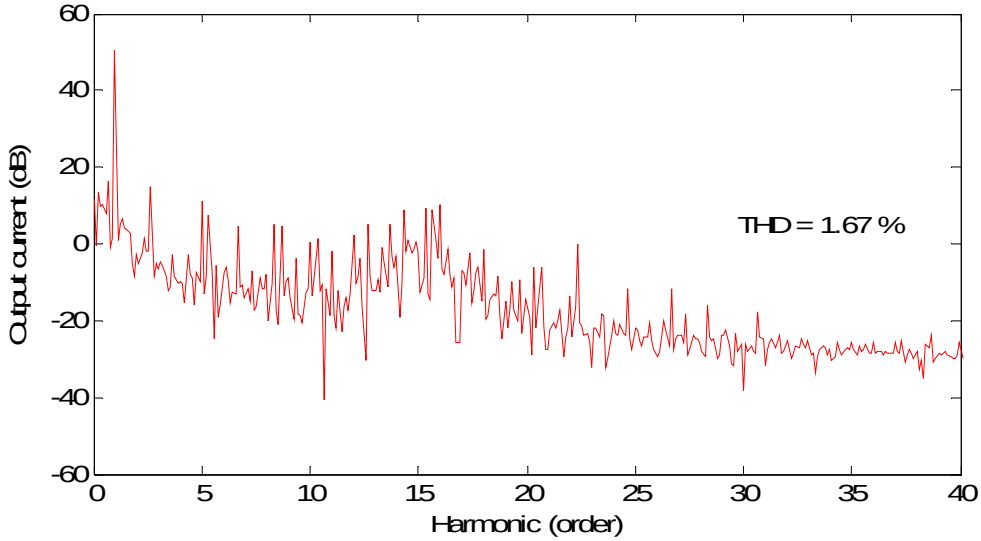

Figure 2.14 Harmonic content of the output current from inverter based DG – steady state operation illustrated with power output 5 MW, Case 2.2

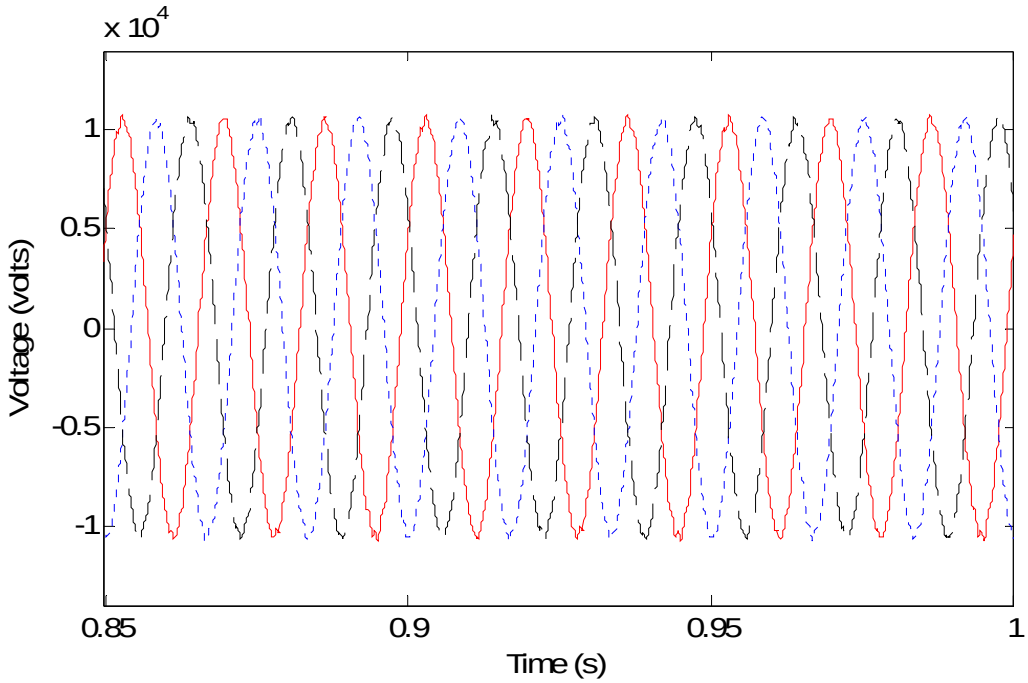

Figure 2.15 Line – neutral voltage measured at PCC – steady state operation illustrated with power output 5 MW, Case 2.2

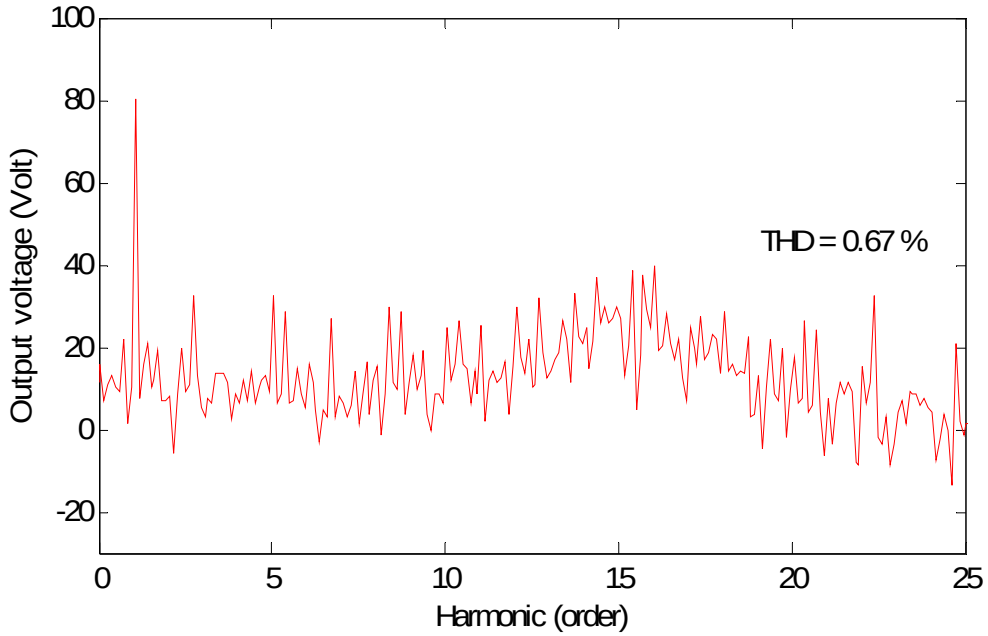

Figure 2.16 Harmonic content of the line-neutral voltage at PCC – steady state operation illustrated with power output 5 MW, Case 2.2

The plot of the active and reactive power from the DG is shown in Figs. 2.17-2.18. The plot shows power averaged over one cycle. Notice from Figs. 2.17 and 2.18 that the inverter based DG with the previously presented control strategy takes approximately 500-600 ms to reach a steady state output (from the relaxed state). Figure 2.19 shows the power factor of the inverter based DG under different reference voltages and active power outputs.

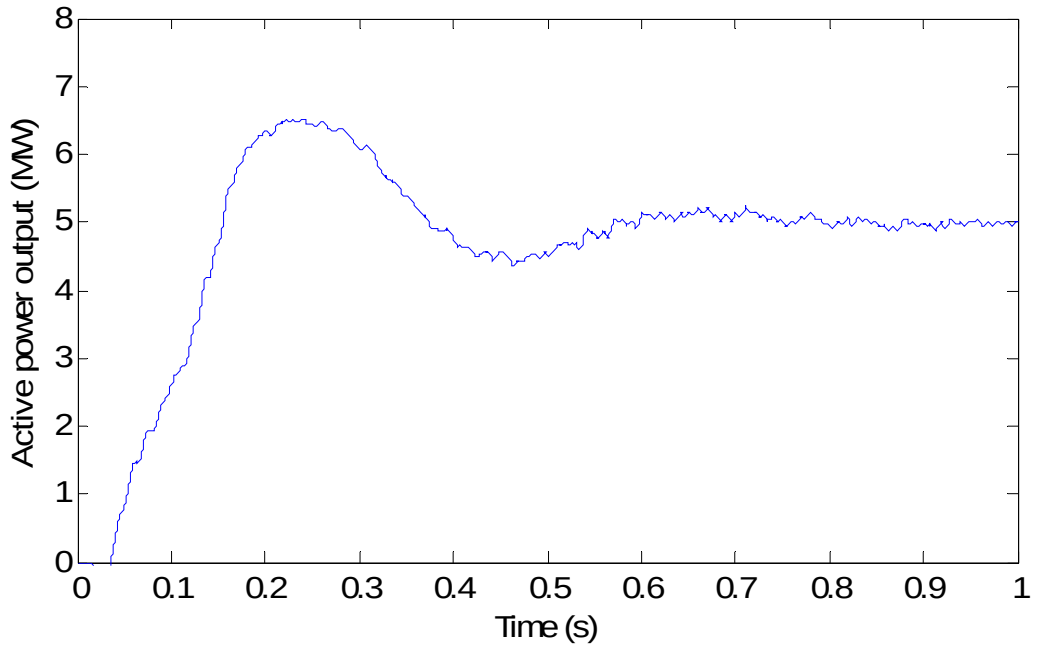

Figure 2.17 Active power output (averaged over one cycle) of inverter based DG – steady state operation illustrated with power output 5 MW, Case 2.2

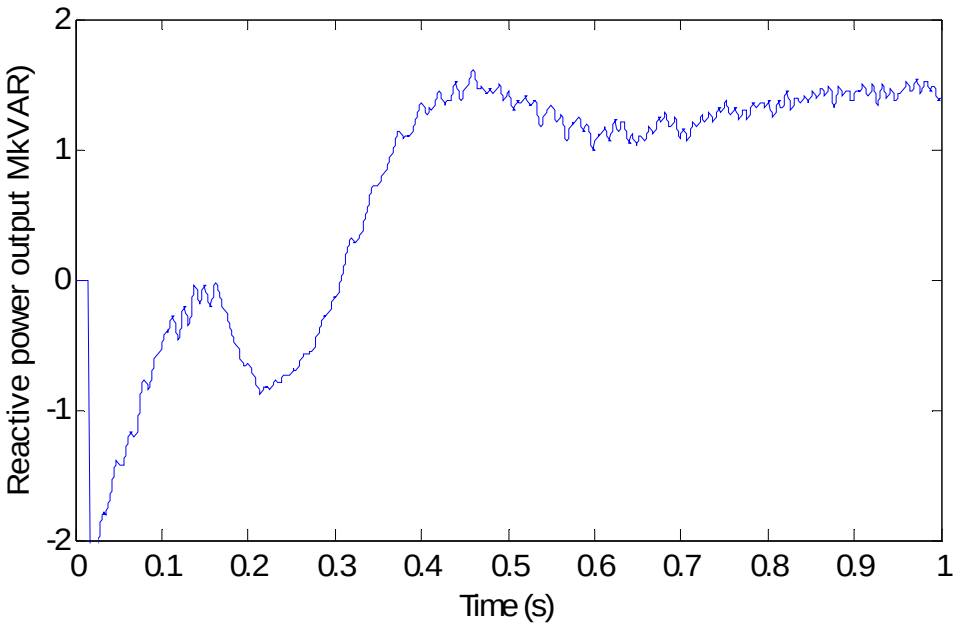

Figure 2.18 Reactive power output (averaged over one cycle) of inverter based DG – steady state operation illustrated with power output 5 MW, Case 2.2

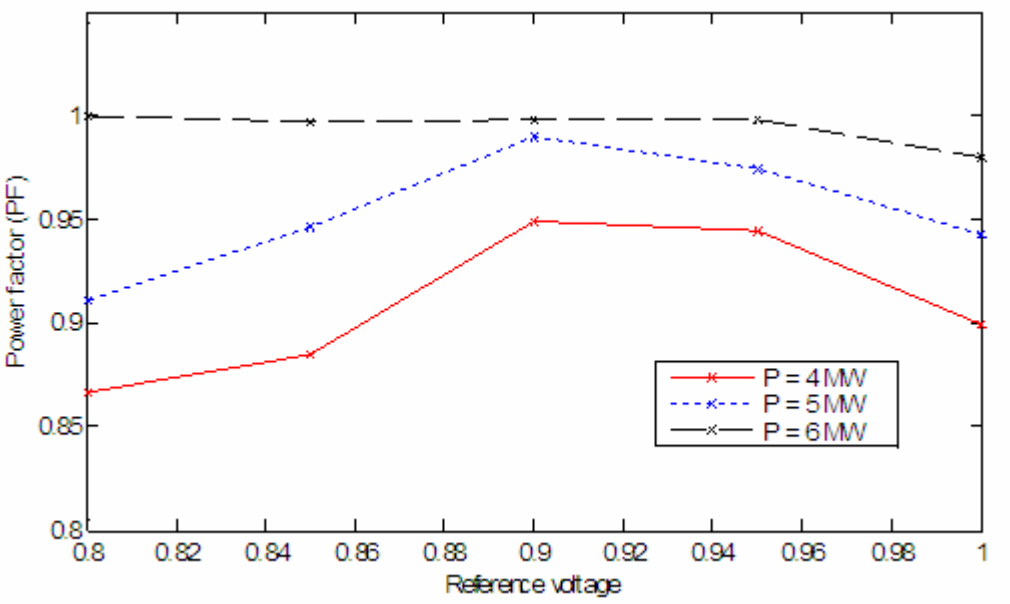

Figure 2.19 Power factor of the inverter under different reference voltages, Case 2.2

2.4 Active power output and current THD

This section discusses the variation of the total harmonic distortion of the output current under different active power outputs of the inverter based DG when the inverter is connected to the grid. The analysis is done by applying the parameters of inverter as in Table 2.1 and the test system as indicated in Case 2.2. In this analysis, the active power output of the inverter based DG is varied from 1-7 MW with the reference voltage, V_{ref}, at 1.00 p.u.

The plot of current THD versus active power output (P_{out}) of the inverter based DG with the parameters indicated in Table 2.1 is shown in Fig. 2.20. The current THD of the inverter varies depending on the active/reactive power outputs and the amplitude of the output voltage. Note that the current THD near the rated MW of the inverter (5 MW) is relatively low.

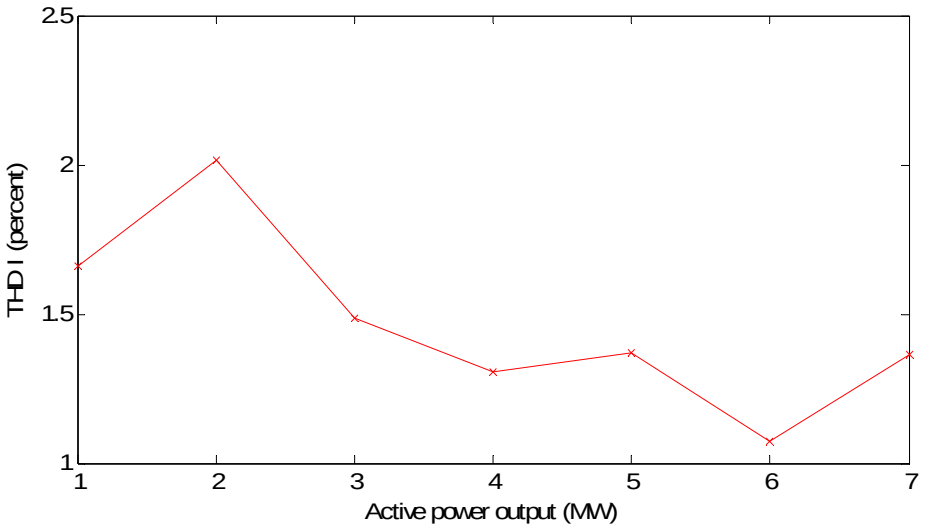

Figure 2.20 Plot of active power output vs. THD current of inverter based DGwith V_{ref} = 1.0, Case 2.2

2.5 Conclusions

This chapter describes a control strategy of an inverter based DG in a distribution system. Two distinct controllers are discussed: an amplitude controller, and an angle difference controller. The controllers are designed in an average power control configuration. In both controllers, the rotational reference frame or *abc* to *dq0* transformation is applied to calculate the phase angle of the output voltage and current. The input of the *abc* to *dq0* transformation is the power frequency of the grid system which is detected by a phase locked loop (PLL) at the PCC. The advantage of the *abc* to *dq0* transformation is the ability to obtain low frequency control signals and rapid calculations.

The illustrative cases in Section 2.3 show the operation of an inverter based DG during normal operation (steady state): stand alone operation (Case 2.1) and a DG connected to the grid system (Case 2.2). From the simulation results presented, the controls of active power and output voltage of the inverter based DG have been accomplished while maintaining acceptable power quality. Several examples are included in Cases 2.1 and 2.2 to illustrate the capabilities of the model. The proposed model is assumed to be appropriate for the analysis of a power system in the presence of inverter based DGs.

CHAPTER 3

IMPACT OF DISTRIBUTED GENERATION ON PROTECTIVE RELAYING

3.1 Introduction

Protection system planning is an indispensable part of an electric power system design. Analysis of fault level, pre-fault condition, and post-fault condition are required for the selection of interruption devices, protective relays, and their settings and coordination. Installation of DG increases the fault current throughout the system. For synchronous machine DGs, the increase of fault current due to DG installed depends on many factors, such as DG size, transient impedance, location, and pre-fault voltage of the DG. Analysis of fault current by modifying the traditional algorithm (i.e., analysis of bus impedance matrix) is discussed.

There are many technologies for distributed resources beyond the conventional synchronous machine DGs such as fuel cells, wind turbines, solar cells, and microturbines. These DGs require electronic interfaces to interconnect with the utility grid. Hence, these DGs are so called "inverter based DGs." Model of the inverter based DGs may be complicated due to complex controls. Therefore, fault analysis of the system with the inverter based DGs by the traditional algorithm may not be easy.

This chapter demonstrates a simulation technique which can be applied to access the impact of installation of DGs (i.e., synchronous machine DGs as well as inverter based DGs) in a subtransmission system. A test bed is produced for illustrative purposes and this test system is denominated as the Thunderstone system. Salt River Project

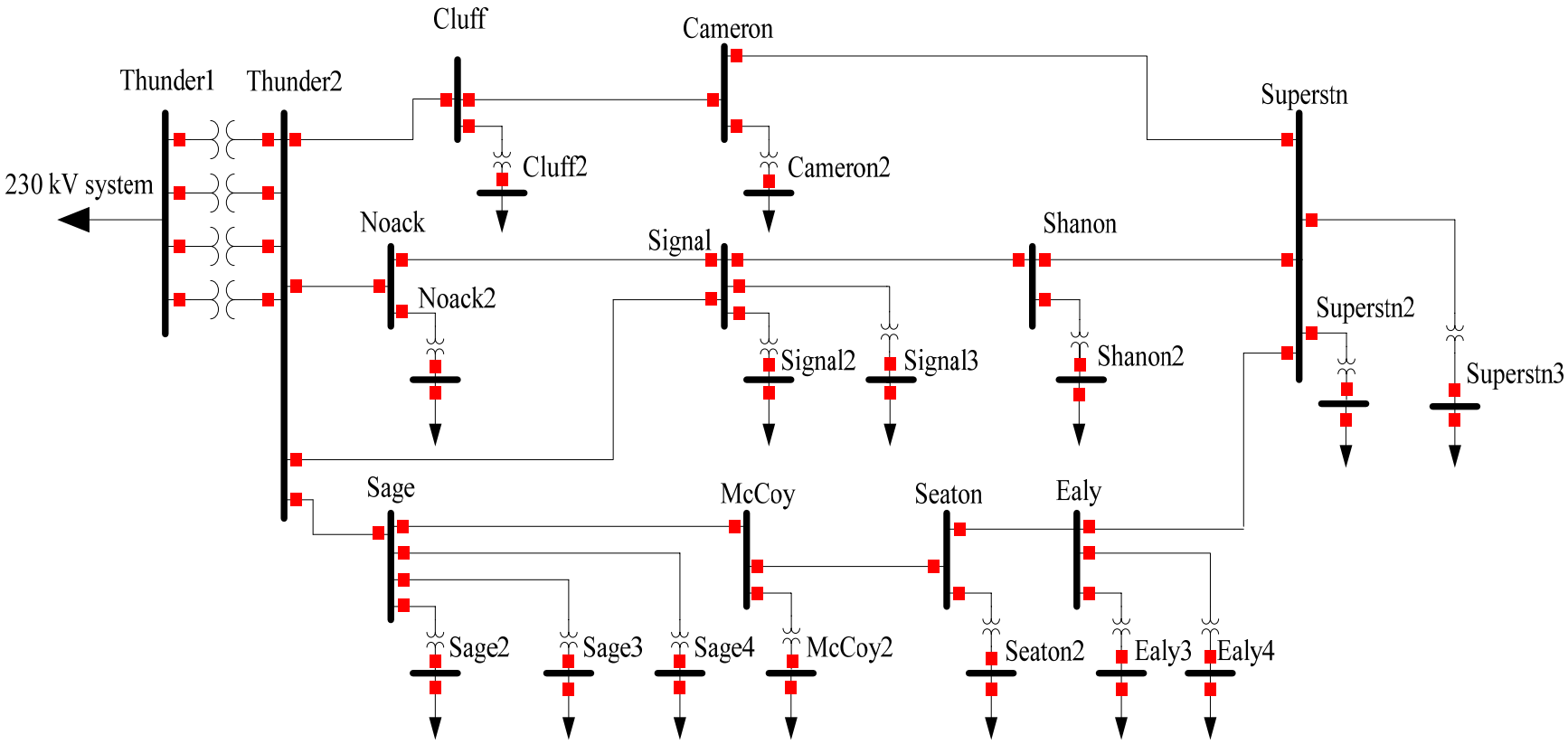

Figure 3.1 Thunderstone 69 kV transmission system

(SRP), a large electric utility company in Phoenix, AZ, supplied the Thunderstone system shown in Figure 3.1 as a test bed.

The Thunderstone system is connected to 230 kV transmission system at bus Thunder1, considered as the system slack bus. The voltage level at 230 kV from slack bus is stepped down to 69 kV at the Thunderstone substation, shown in Figure 3.1. The taps of substation transformer at 230 kV and the 12 kV distribution transformers usually operate higher than 1.0 p.u. to reduce the effect of voltage drop in the distribution level. The Thevenin equivalent impedance of 230 kV bus is $0.75728+j6.183$ ohm per phase. Note that capacitors are installed at the load sites to improved power factors. System parameters of the Thunderstone system are shown in Appendix A.

This chapter is organized as follows: Section 3.2 presents the impact on increase of fault current due to synchronous machine DGs by modifying the conventional fault current calculation. Section 3.3 discusses a simulation technique used to analyze the dynamic performance and the impact on the protection system of the system with DGs. The simulation technique can be used to analyze the system including both synchronous and inverter based DGs. Section 3.4 provides the simulation results of an illustrative case and applications to protective relaying. Finally, Section 3.5 gives conclusions.

3.2 Impact on fault current – theory

Fault analysis by means of an impedance matrix can be applied to evaluate the increase of fault current due to installation of DGs. This section discusses the fault analysis of the system with new synchronous machine DGs by modifying the algorithm of the conventional fault current calculation [73]. Positive sequence models are often adequate

for balanced short circuit studies which determine the fault response of DGs [74]. In order to calculate the fault current of the system with new synchronous machine DGs, the new impedance matrix needs to be evaluated. For inverter based systems, Z_{bus} methods are not appropriate because an inverter (plus its controls) is not a constant impedance.

Of course, for all DGs, source model parameters need to be known. The technique which is used to identity the parameters of synchronous machine DGs (i.e., transient impedance of the synchronous machines and open circuit voltage) is well studied. However, a model of inverter based DGs may be complicated due to complex controls, or may be less well understood and accepted. A simulation technique is recommended and illustrated in the following sections.

Assume that the original system can be represented by the original impedance matrix, $Z_{bus,orig}$. In this analysis, two synchronous machine DGs are installed at buses k and m. Fig. 3.2 depicts a system with two newly added DGs. The synchronous machines are simply modeled by transient impedances of $Z_{DG,k}$ and $Z_{DG,m}$ and open circuit voltages as shown in Fig. 3.2. After the addition of the synchronous machine DGs, buses p and q are added to the system.

The relationship between the bus voltages, the injected current $I_{DG,i}$, and the elements of bus impedance matrix including the new DGs can be written in matrix form as are given as,

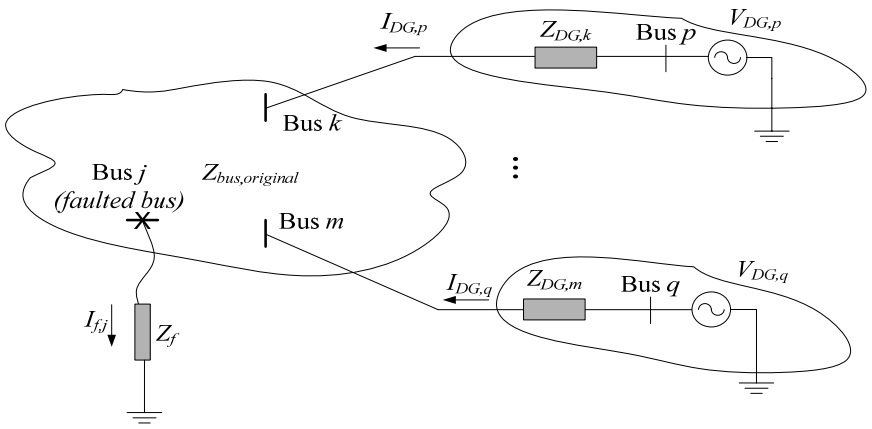

Figure 3.2 An illustrated system with new DGs added to buses *k* and *m*

$$\begin{bmatrix} V_{orig} \\ \hline V_{DG,p} \\ V_{DG,q} \end{bmatrix} = \left[\begin{array}{ccccc|cc} & & Z_{bus,orig} & & & Z_{1k} & Z_{1m} \\ & & & & & Z_{2k} & Z_{2m} \\ & & & & & \vdots & \vdots \\ & & & & & Z_{nk} & Z_{nm} \\ \hline Z_{k1} & Z_{k2} & \cdots & Z_{kn} & & Z_{kk}+Z_{DG,k} & Z_{km} \\ Z_{m1} & Z_{m2} & \cdots & Z_{mn} & & Z_{mk} & Z_{mm}+Z_{DG,m} \end{array}\right] \begin{bmatrix} I_{orig} \\ \hline I_{DG,k} \\ I_{DG,m} \end{bmatrix} \tag{3.1}$$

where *m* and *k* are buses with DGs, $Z_{bus,orig}$ is the bus impedance matrix of the system before installing DGs. Applying Kron's reduction to (3.1) [75],

$$Z_{bus,new} = Z_{bus,orig} - Z_{col,DGs}\, Z_{common}^{-1} Z_{row,DGs} \tag{3.2}$$

where

$$Z_{col,DGs} = \begin{bmatrix} Z_{1k} & \cdots & Z_{1m} \\ Z_{2k} & \cdots & Z_{2m} \\ \vdots & \vdots & \vdots \\ Z_{nk} & \cdots & Z_{nm} \end{bmatrix},$$

$$Z_{common} = \begin{bmatrix} Z_{kk}+Z_{DG,k} & & Z_{mk} \\ & \ddots & \\ Z_{km} & & Z_{mm}+Z_{DG,m} \end{bmatrix},$$

$$Z_{row,DGs} = \begin{bmatrix} Z_{k1} & Z_{k2} & \cdots & Z_{kn} \\ \vdots & \vdots & \vdots & \vdots \\ Z_{m1} & Z_{m2} & \cdots & Z_{mn} \end{bmatrix}.$$

Note that n is number of buses in the system not counting p and q where p and q are DG buses. After calculating new Z_{bus} matrix, the three phase fault current at bus j can be calculated as

$$I_j = \frac{V_j}{Z_{jj,new} + z_f} = I_{fj} \tag{3.3}$$

where $Z_{jj,new}$ is the diagonal element of bus j in the modified bus impedance, V_j is the pre-fault voltage of bus j and Z_f is the fault impedance.

The model of the added generation used above is the conventional model of a synchronous generator. Not all DGs are conventional synchronous generators. Many DGs are energy sources that produce DC which is used as the input to an inverter which ultimately interfaces with the AC system. The controls of that inverter determine how the inverter is 'seen' by the network. The full treatment of inverter based DGs may not be as easy as these remarks and procedures. DG controls are not standardized and control modeling is problematic. The following sections in this chapter propose the simulation technique to study the fault response of the system after installing inverter based DGs and/or synchronous machine DGs.

3.3 Simulation strategies

As discussed in the previous section, the analysis of fault current of the system with the presence of inverter based DGs is complicated. Hence, a simulation technique performed in Matlab Simulink is proposed. The major advantage of the simulation tech-

nique is the ability to evaluate the response of the system with complicated elements (e.g., power electronic elements). In this chapter, the strategies of the dynamic simulations of the system with synchronous machine DGs and/or inverter based DGs are discussed based on Matlab Simulink 6.0 environments.

Simulink is a software package for modeling, simulating, and analyzing dynamic systems. A graphical user interface (GUI) for building models as block diagrams is provided. The power system block sets (PSB) in Simulink are developed at TEQSIM Inc. and Hydro-Quebec. The PSB library contains Simulink blocks that represent common components and devices found in electrical power networks (e.g., transformer, transmission line, synchronous machine, and constant impedance / power load).

The simulation of synchronous machine DGs in Simulink is derived from voltage equations and flux linkage equations expressed in the rotational reference frame. Details of the synchronous machine model are discussed in [11]. The model of inverter based DGs are discussed in Chapter 2.

The simulation of the power system in Simulink is accomplished by creating the time model state space representation of the system. The simulation is performed by applying the numerical differential equations solvers (e.g., trapezoidal method, Adams method, modified Rosenbrock method and the Runge-Kutta method) [76]. The results of simulations, such as voltages and currents measured in the system, can be recorded for further analysis.

In general, the simulation time steps are 50 microseconds. This is recommended as a typical figure for a 60 Hz system. The simulation interval in the illustrative exam-

ples shown is 0 – 1 second. Longer simulation times are unlikely to be needed, but could be easily accommodated using the indicated software.

3.4 Application of the simulation technique to protective relaying: the impact of DGs on system protection

In this section, the Thunderstone system is used as a test bed to illustrate the simulation technique (data given in Appendix A). The impact of the presence of synchronous generators and inverter sources to the test bed system is investigated. The illustrative cases are separated into three parts: no DGs in the system in Case 3.1, the system with synchronous machine DGs in Case 3.2 and the system with inverter based DGs in Case 3.3. A summary of the illustrative cases are provided in Table 3.1. Appendix C lists all the cases.

In Cases 3.2 and 3.3, to study the fault response of the Thunderstone system with DGs presence, synchronous machine DGs and inverter based DGs are installed at various locations. Parameters of the synchronous machine DGs applied in the simulations (in Case 3.2) are identical and shown in Table 3.2. Same as the inverter based DGs (in Case 3.3), all machine parameters are identical and shown in Table 2.1 of Chapter 2. In all cases, a bolted fault in the Thunderstone system occurs at the midpoint of the transmission line between Superstition and Ealy (69 kV) at t = 0.4 s. Two sub-cases are considered: the fault is cleared at 500 ms or 100 ms after the fault occurs. This 100 ms fault is a commonly selected duration time for fault analysis. The impedance (Z), resistance (R) and inductance (X) measured from (i.e., "seen" from) various buses are measured near the DGs such as, Ealy2 (12.47 kV bus), Superstition (12.47 kV bus), transmission line from

Shanon to Superstition (69 kV) and transmission line from Ealy to Superstition (69 kV). Measurement points in the Thunderstone system are shown in Fig. 3.4. Note that per unit base used in all illustrative cases is 100 MVA.

For the purposes of this presentation, the notation and procedures of power system protective relaying are used with regard to *Z, R*, and *X*. These quantities are ratios of rms volts to rms amps, and the rms is carried out over one cycle (i.e., 1/60 s). The measurement at bus Ealy1 and Superstition1 is detected at the point of common coupling (PCC) or the point of DR connection at secondary side of 69/12.47 kV distribution transformer. The analysis is performed by assuming that all DGs have constant power output and loads in the system at 12.47 kV buses are considered as constant impedance loads.

In both Cases 3.2 and 3.3, DGs are installed into 12.47 kV buses at four locations: Sage4, Superstition3, Early1 and Ealy2. The generation capacity of each synchronous DG in Case 3.2 and inverter based DG in Case 3.3 are 5 MW. The penetration level in the system is approximately 7% based on the total load of Thunderstone system (300 MVA).

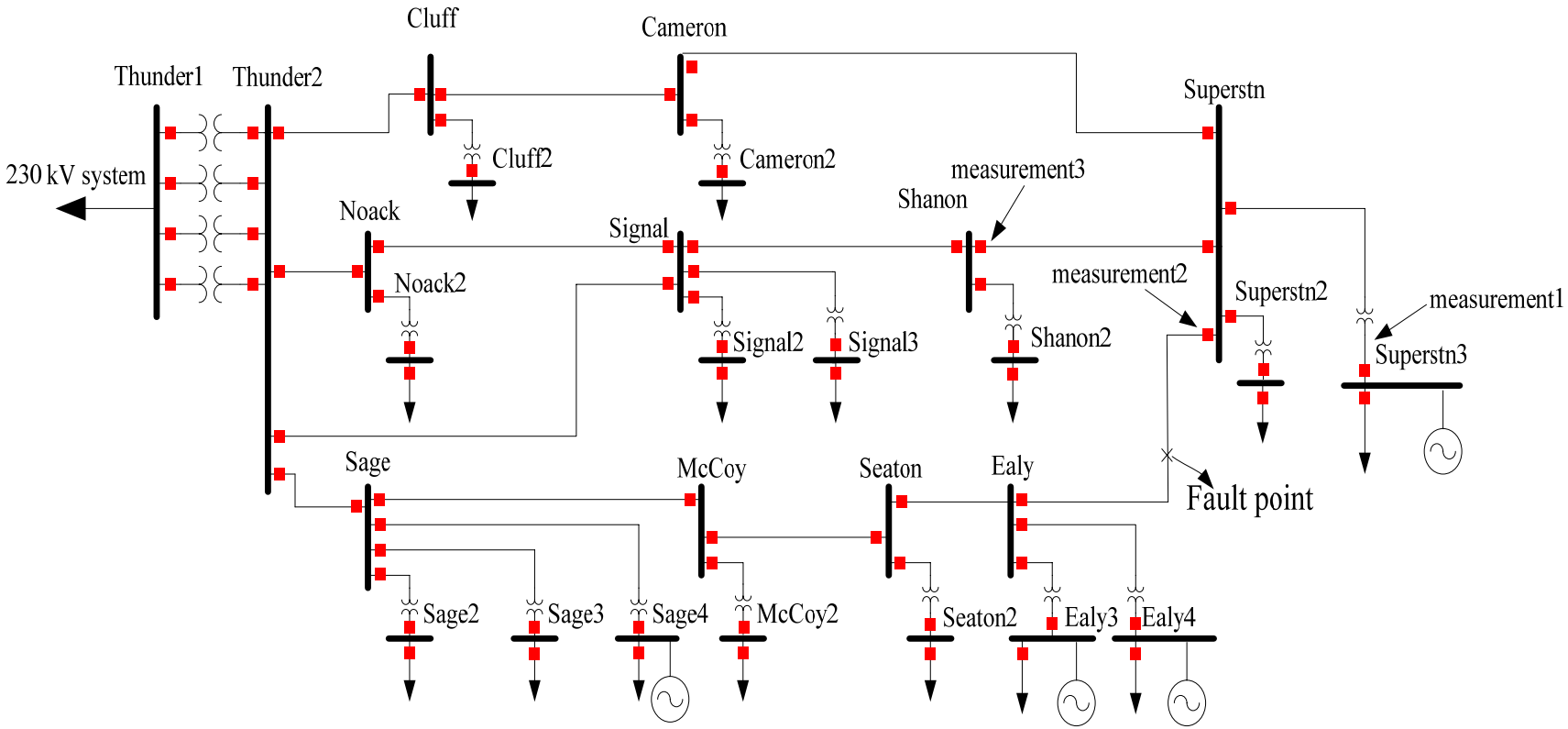

Figure 3.3 The Thunderstone system with measurement points

Table 3.1 Summary of the illustrative cases

Case	Total Output of Synchronous machine DG	Total Output of Inverter-Based DG	Source model	Type of Fault	Fault duration
3.1	None	None	Thevenin equivalent *Z*-*V* supply	3 Phase bolted fault between Superstition and Ealy (69 kV)	0.4 – 0.5 s
3.2	4 locations (4x5 MW): Sage4, Superstition3, Early1 and Ealy2	None	Park's Equations	3 Phase bolted fault between Superstition and Ealy	0.4 – 0.5 s
3.3	None	4 locations (4x5 MW): Sage4, Superstition3, Early1 and Ealy2	Constant power inverter model given in Chapter 2	3 Phase bolted fault between Superstition and Ealy (69 kV)	0.4 – 0.5 s

Table 3.2 Synchronous machine parameters

Machine parameter		Synchronous DG
Rated MVA		5 MVA
Rate output voltage		4.16 kV
Step up transformer (7 MVA)		0.074 p.u.
Synchronous reactance	X_d	1.305 p.u.
	X_q	0.474 p.u.
Transient reactance	X_d'	0.202 p.u.
	X_q'	0.243 p.u.
Subtransient reactance	X_d''	0.15 p.u.
	X_q''	0.18 p.u.

Per unit base: 5 MVA, 4.16 kV (machine); 7 MVA, 4.16 kV (transformer)

For purposes of graphic illustration, two devices are used. A three dimensional plot can be used to depict the behavior of *X, R* versus time. The three dimensional plots in Matlab is equipped with ability to zoom-in, zoom-out and rotate graphs to any orientations. This ability can not be completely demonstrated in this thesis. However, the plots of *X*, *R* versus time are shown in various angles. Although interesting in appearance, these plots may be difficult to interpret, and therefore a two dimensional plot may be used, namely |*Z*| versus time.

The cylinder in the plots of *X*-*R* vs. time represents the characteristic of the impedance relay. The impedance relay operates when the impedance measured at the bus falls within the cylinder (80% of the line impedance for protection zone 1 and 120% for

zone 2). Also note that the circle in the *X-R* plots represents the characteristic of the impedance relay. The rotating graphic capability appears to be useful to conceptualize the *R-X-t* characteristic. For example, if only the *R-X* plane is needed (i.e., the time of entry of a trajectory into a zone of protection of a relay), the plot may be rotated so that *t* is perpendicular to the page (or computer screen). If the time dial setting is needed, the plot is rotated 45° so that the entry of the trajectory into the zone of protection is visible. Other interpretations of rotated plots are also possible.

The results of calculating root-mean-square voltages and currents for relaying applications are shown in the plots of *X-R, X-R* vs. time and impedance vs. time. The plots of *X-R* and *X-R* vs. time are separated into 3 durations: before fault (T_s = 0.3–0.4 s), during fault (T_s = 0.4-0.5 s) and after the fault is cleared (T_s = 0.5-1.0 s).

Case 3.1 Simulation of three phase to ground bolted fault at Ealy (69 kV) of the Thunderstone system with no DG

In Case 3.1, no DG is installed in the Thunderstone system. A three phase bolted fault occurs at the middle of the line between Superstition and Ealy (69 kV). The purpose of the Case 3.1 is to compare the fault response of the system with other cases.

Figures 3.5 and 3.6 show the voltage and current measured at the fault location. The plots of *X-R, X-R* vs. time and the impedance vs. time measured at bus Superstition (12.47 kV) are shown in Figs. 3.7-9. The plots of impedance of the transmission line between Superstition and Ealy are shown in Figs. 3.10-11. The plots of impedance of the transmission line between Shanon and Superstition (69 kV) are shown in Figs. 3.12-14.

In Figs. 3.7-8, the plots of *X*-*R* vs. time and *X*-*R* indicate that the fault is not detected by the relay at bus Superstition in the system without DGs. In Figs. 3.10-11, the fault is detected by the distance relay when the plots fall in the cylinder at t = 0.4027 s. Since the fault occurs at 0.4 s, it takes 2.7 ms for the three phase fault to be detected by the distance relay in Case 3.1.

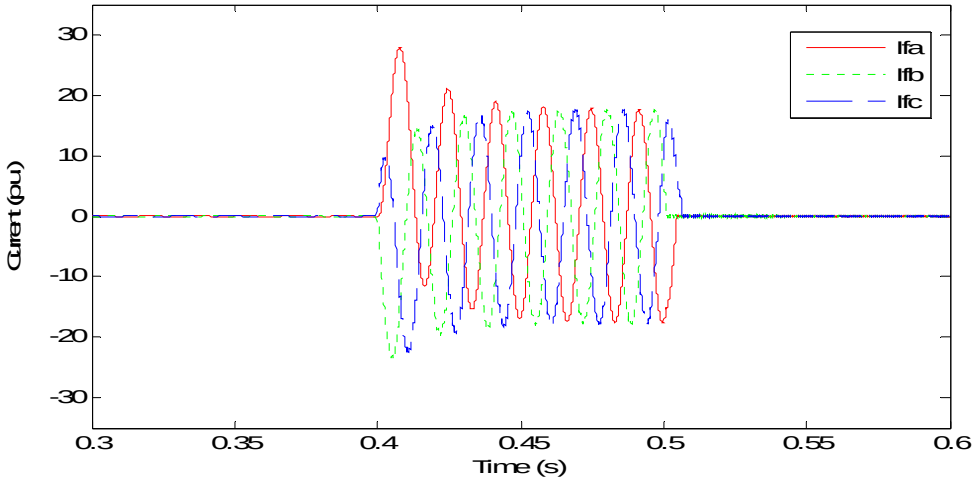

Figure 3.4 Fault current at the fault point with no DG in the system, Case 3.1 (Per unit base: 100 MVA, 69 kV)

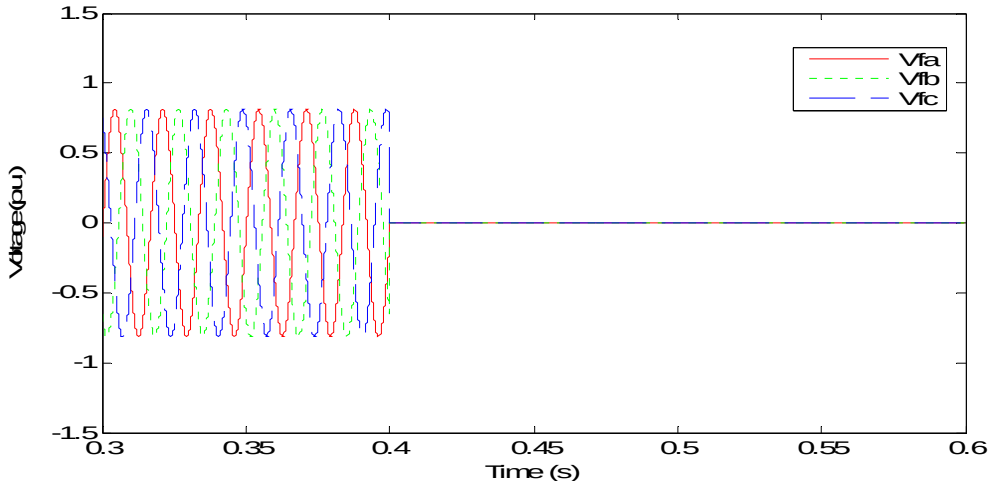

Figure 3.5 Fault voltage (line-neutral) at the fault point with no DG in the system, Case 3.1 (Per unit base: 100 MVA, 69 kV)

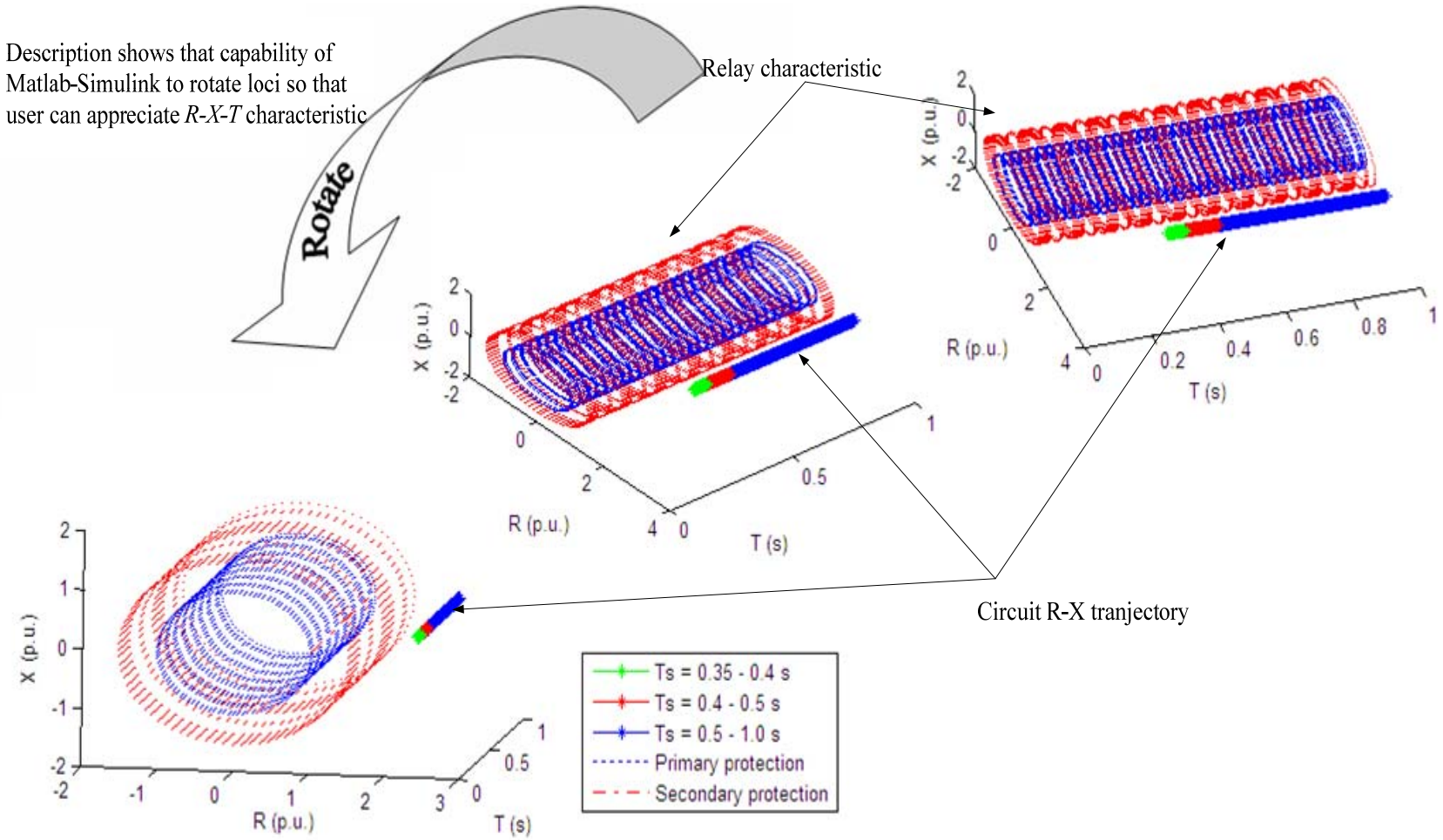

Figure 3.6 Plot of *X*-*R* vs. time at Superstition3 (12.47 kV), Case 3.1 (Per unit base: 100 MVA, 12.47 kV)

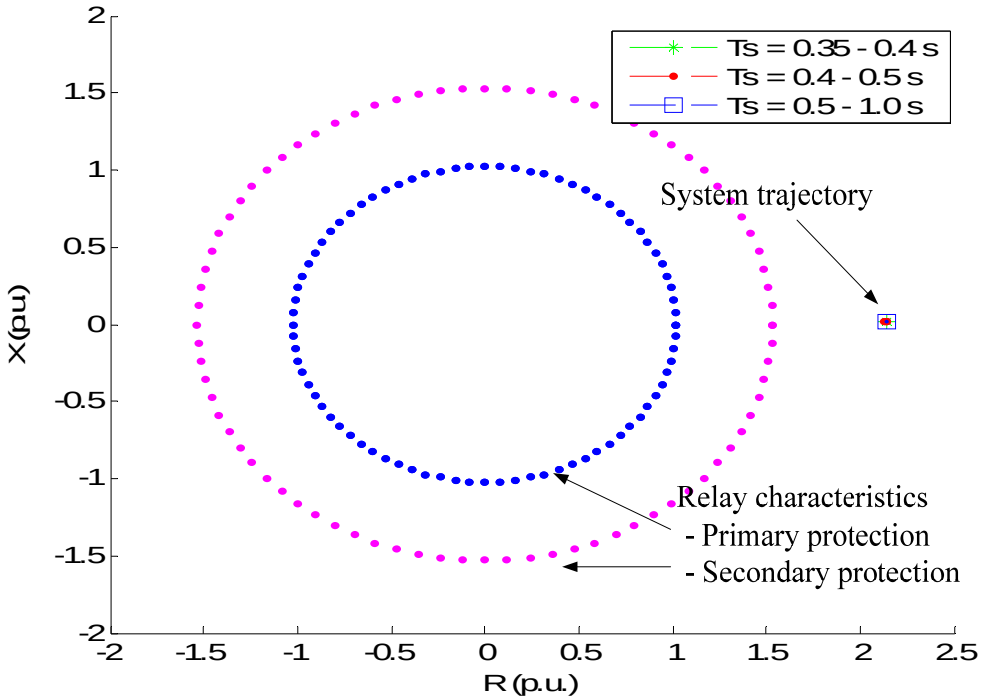

Figure 3.7 Plot of *X*- *R* at Superstition3 (12.47 kV), Case 3.1 (Per unit base: 100 MVA, 12.47 kV)

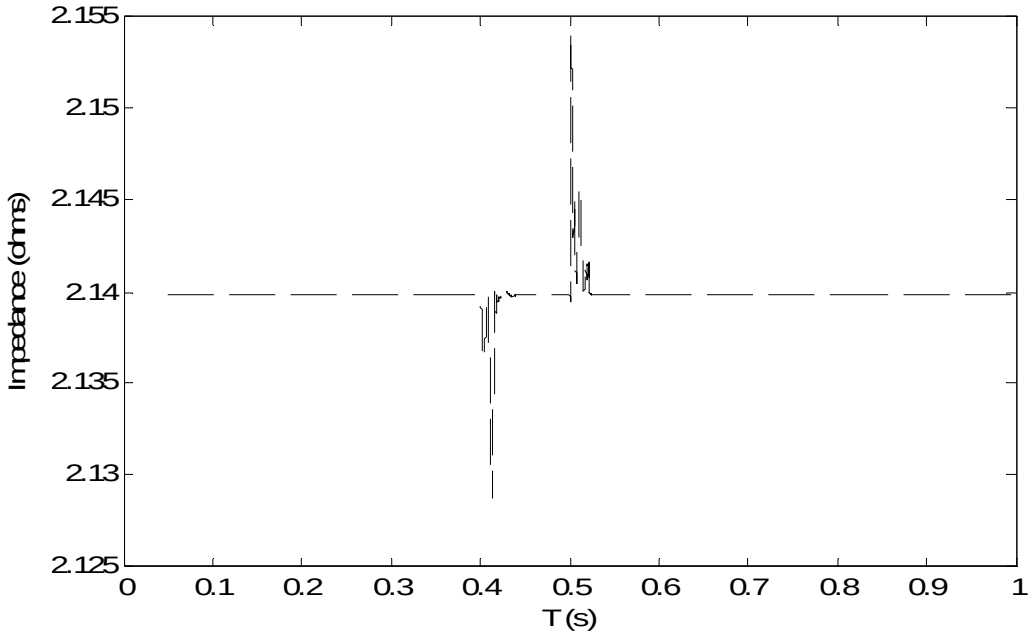

Figure 3.8 Plot of magnitude of impedance seen at Superstition3 (12.47 kV) vs. time, Case 3.1 (Per unit base: 100 MVA, 12.47 kV)

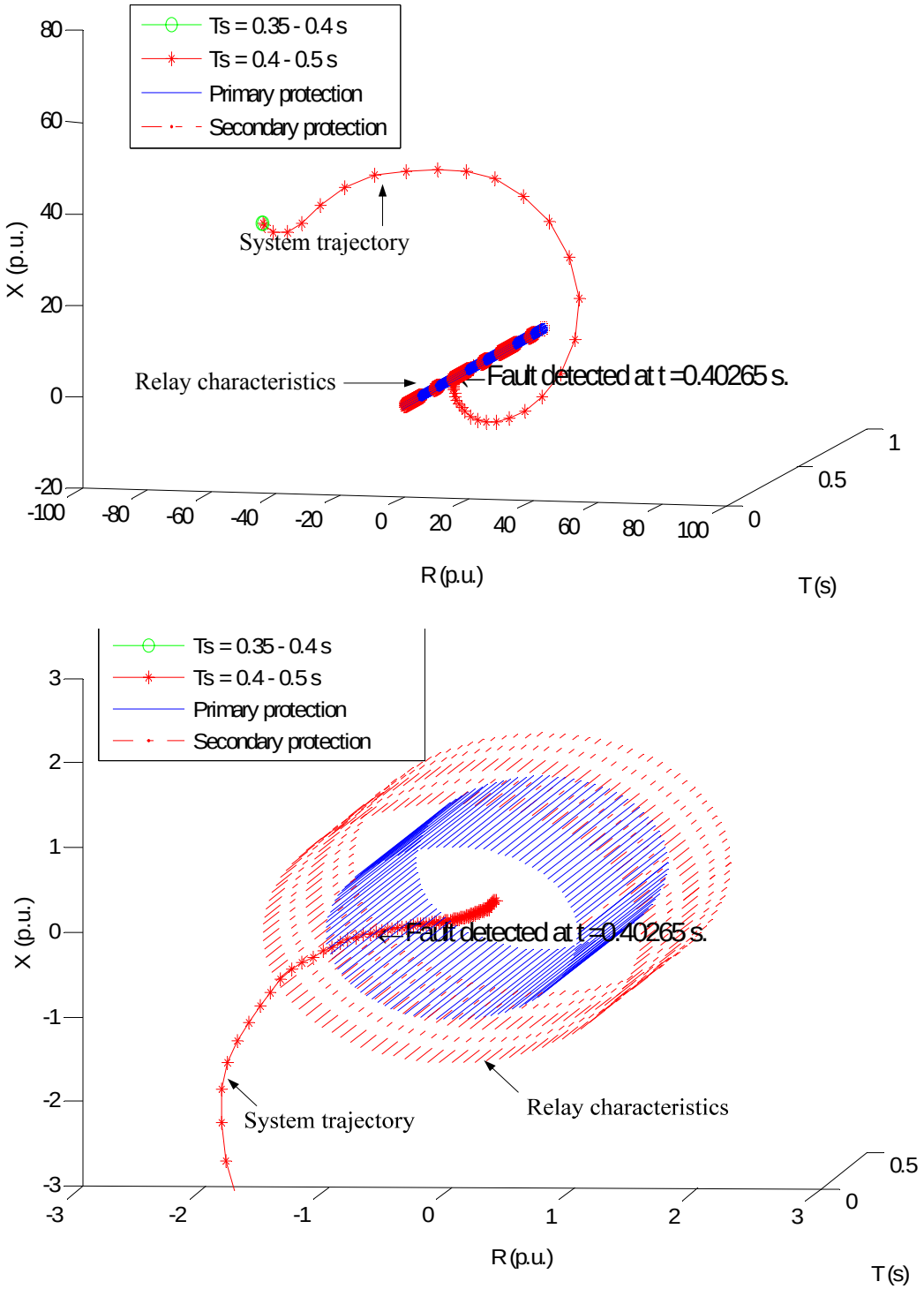

Figure 3.9 (a) Plot of *X*- *R* vs. time seen by the distance relay at transmission line from Superstition to Ealy (69 kV), Case 3.1 (b) zoom-in view (Per unit base: 100 MVA, 69 kV)

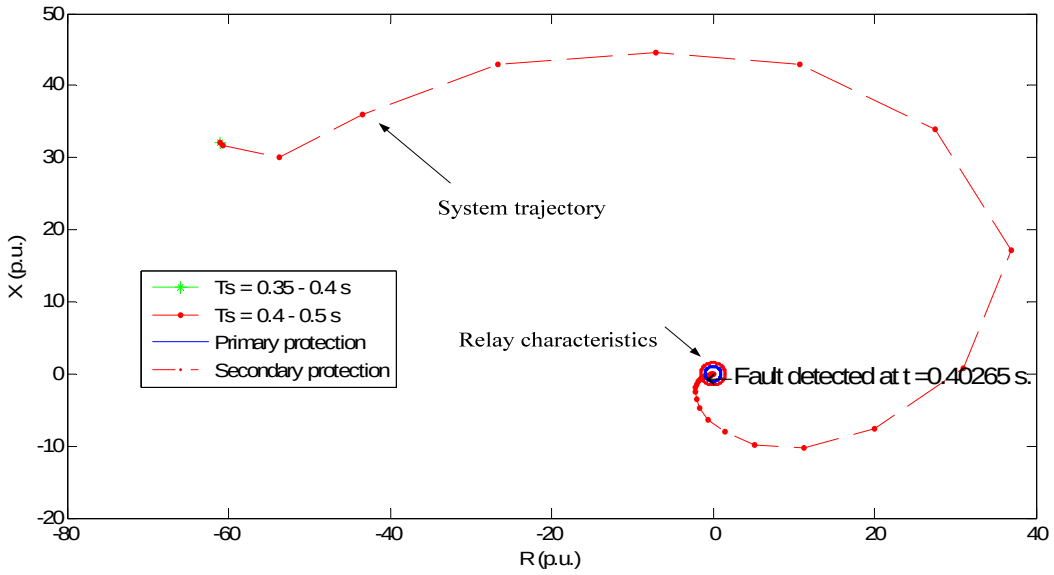

Figure 3.10 (a) Plot of *X- R* seen by the distance relay at transmission line from Superstition to Ealy (69 kV), Case 3.1 (b) zoom-in view (Per unit base: 100 MVA, 69 kV)

Case 3.2 Simulation of three phase to ground bolted fault at bus Ealy (69 kV) of the Thunderstone system with four synchronous machine DGs

In Case 3.2, four synchronous machine DGs are installed in the Thunderstone system: Sage4, Superstition3, Early1 and Ealy2. A three phase bolted fault occurs at the middle of the line between Superstition and Ealy (69 kV). The fault starts at 0.4 s and is cleared at 0.5 s.

Figures 3.15 and 3.16 show the voltage and current measured at the fault location. In Fig. 3.17-19, the plots of *X-R* and *X-R* vs. time indicate that the fault is detected by the impedance relay at bus Superstition3 (12.47 kV). Note that the *X-R* plot when the fault is detected fall into the lower half of the circle. This indicates that the fault current flows from the DG at bus Superstition3 to the fault point. The fault is detected at bus Superstition3 at $t = 0.4130$ s.

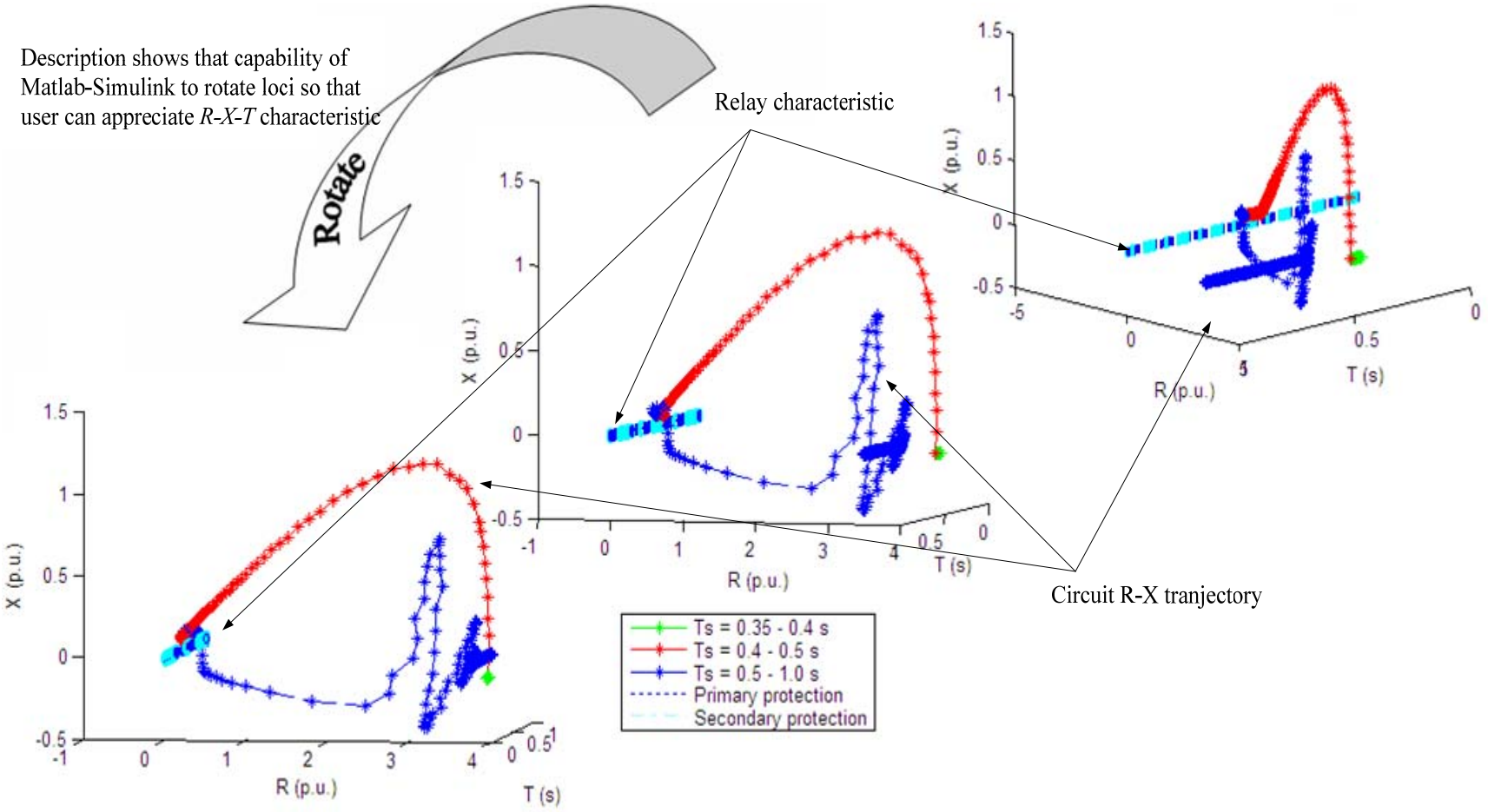

Figure 3.11 Plot of *X*- *R* vs. time seen by distance relay at transmission line between Shanon-Superstition (69 kV), Case 3.1 (Per unit base: 100 MVA, 69 kV)

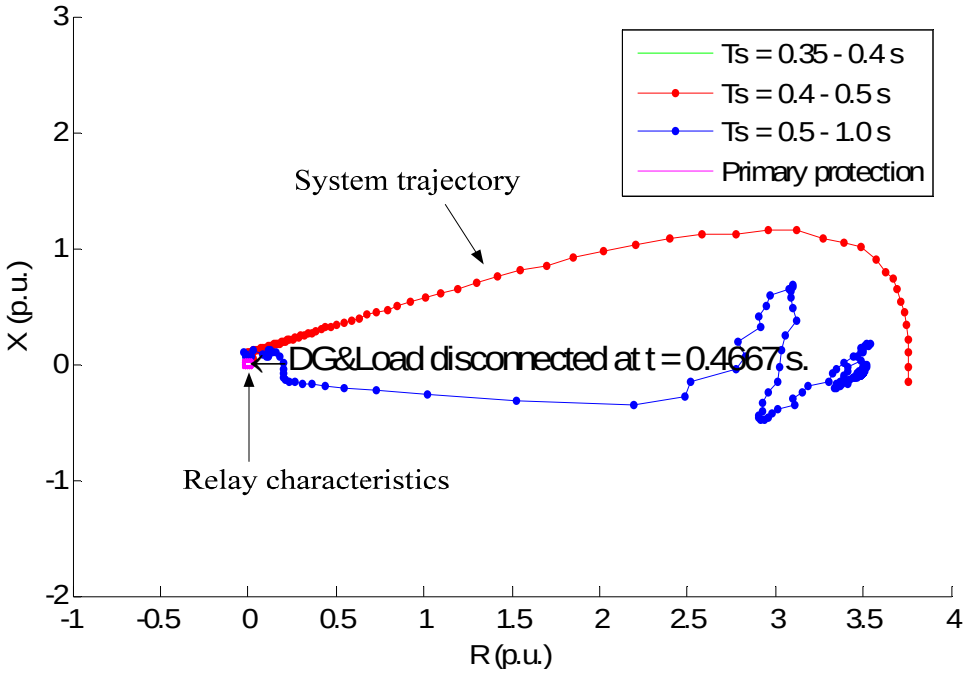

Figure 3.12 Plot of *X* and *R* seen by distance relay at transmission line between Shanon-Superstition (69 kV), Case 3.1 (Per unit base: 100 MVA, 69 kV)

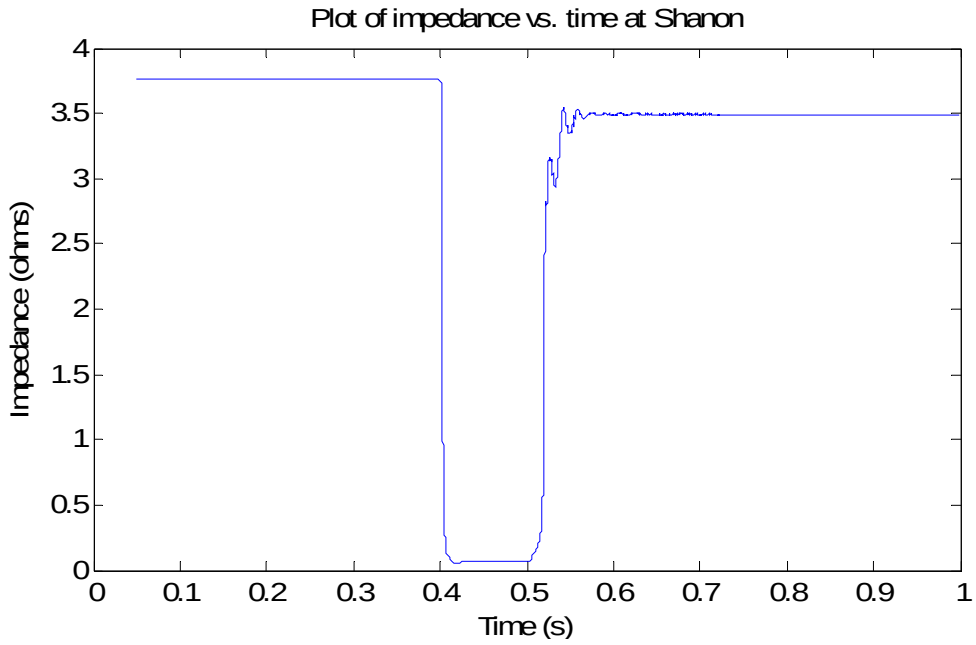

Figure 3.13 Plot of magnitude of impedance seen by distance relay at transmission line between Shanon-Superstition (69 kV), Case 3.1

The plots of impedance of the transmission line between Superstition and Ealy are shown in Figs. 3.20-21. The fault is detected at t = 0.4024 s. Due to the increase of fault current after installing the DGs the fault is detected faster than it does in Case 3.1. The plots of impedance of the transmission line between Shanon and Superstition (69 kV) are shown in Figs. 3.22-24.

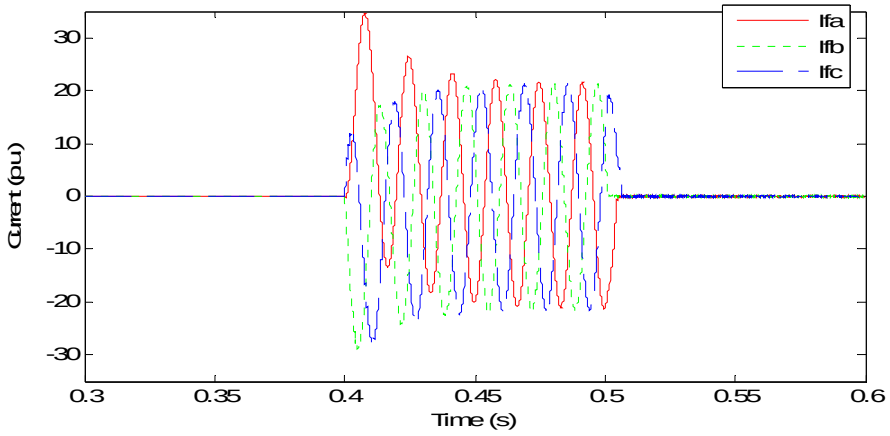

Figure 3.14 Fault current at the fault point with four synchronous machine DGs in the system, Case 3.2 (Per unit base: 100 MVA, 69 kV)

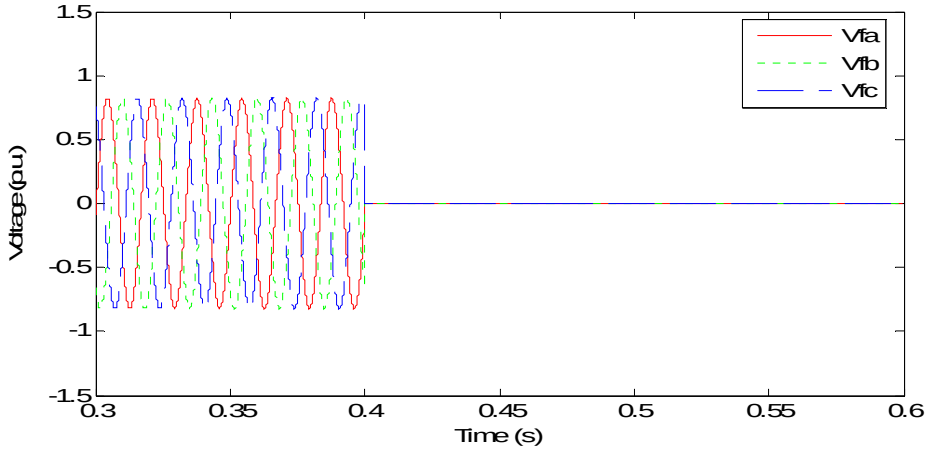

Figure 3.15 Fault voltage at the fault point with four synchronous machine DGs in the system, Case 3.2 (Per unit base: 100 MVA, 69 kV)

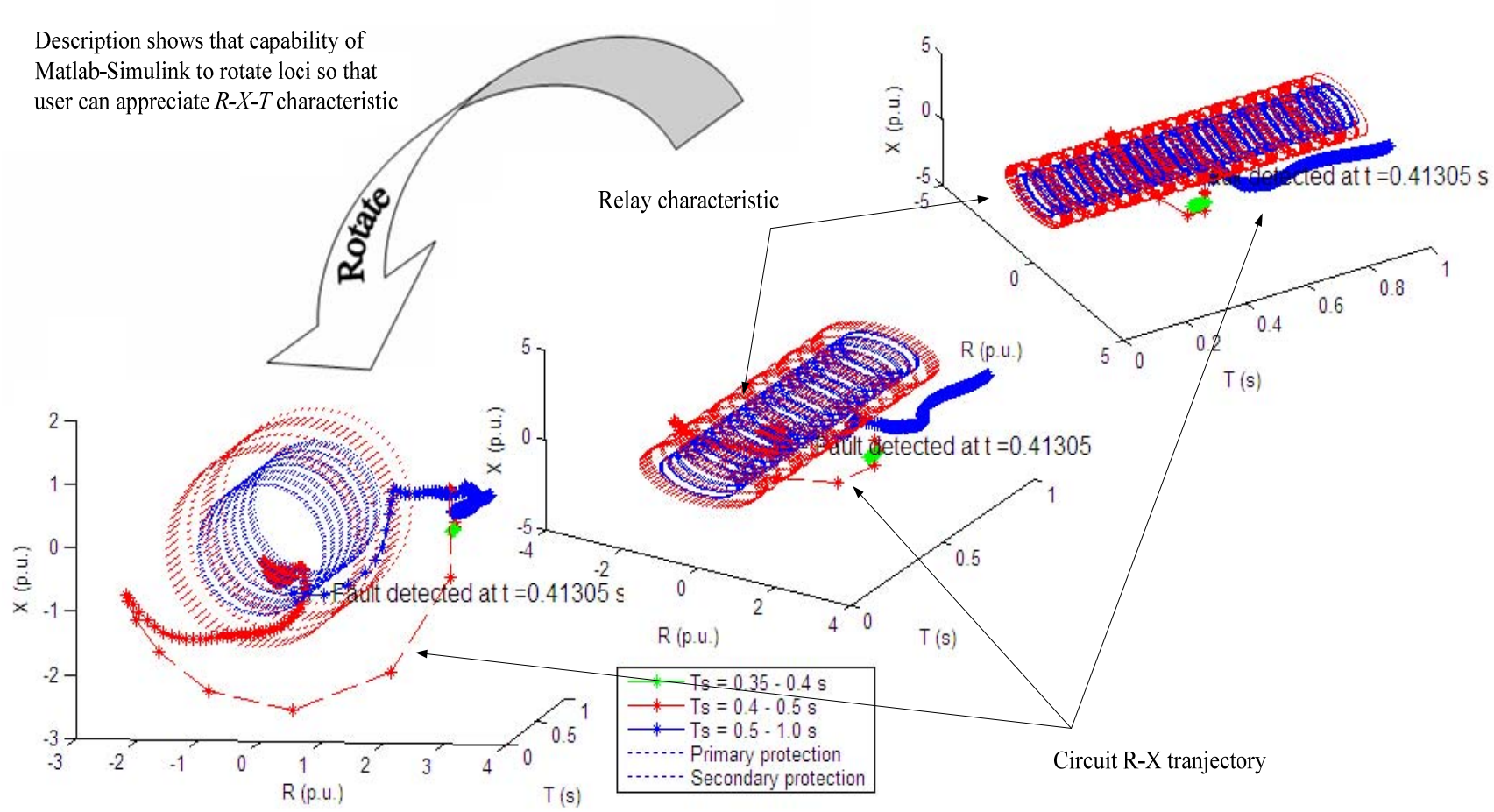

Figure 3.16 Plot of *X*-*R* vs. time at Superstition3 (12.47 kV), Case 3.2 (Per unit base: 100 MVA, 12.47 kV)

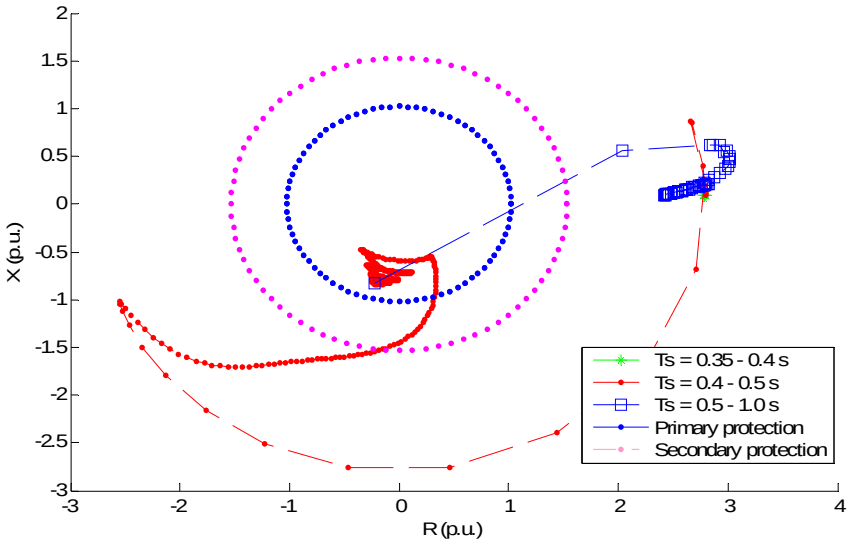

Figure 3.17 Plot of *X*, *R* at Superstition3 (12.47 kV), Case 3.2 (Per unit base: 100 MVA, 12.47 kV)

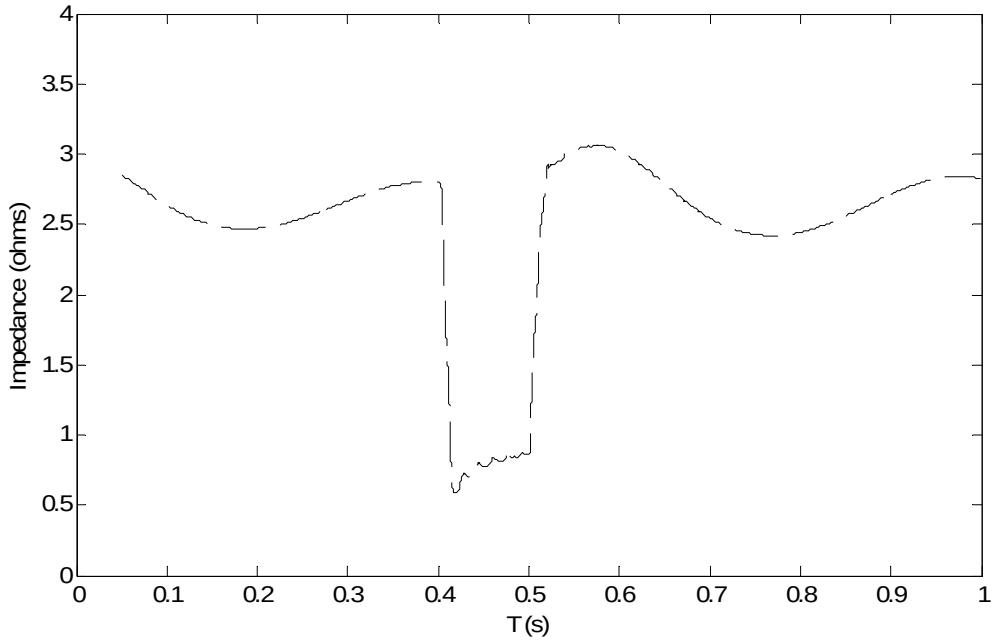

Figure 3.18 Plot of magnitude of impedance seen at Superstition3 (12.47 kV) vs. time, Case 3.2

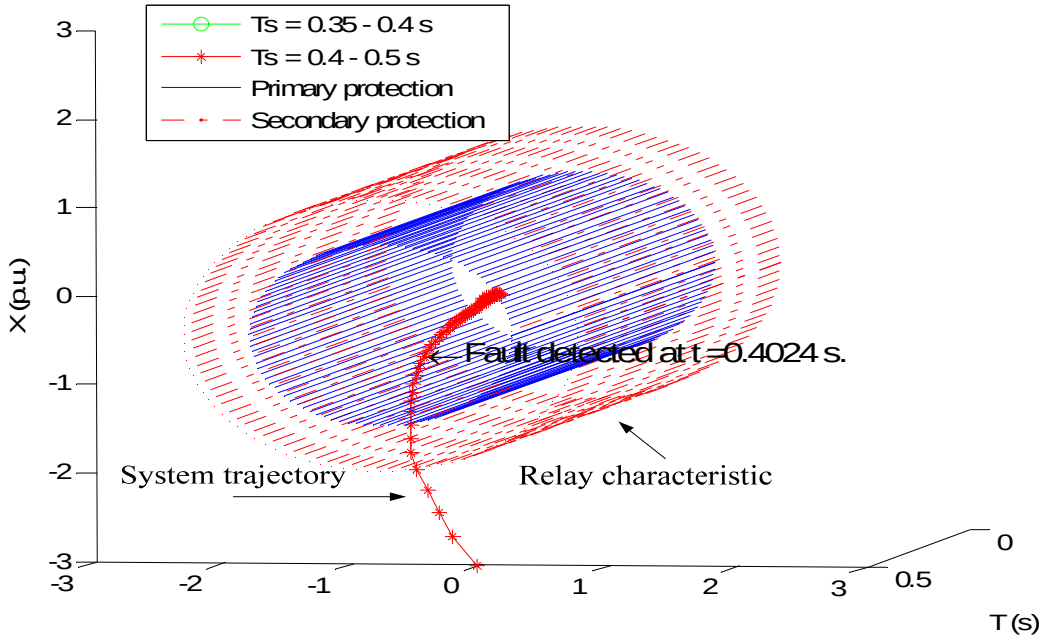

Figure 3.19 (a) Plot of *X- R* vs. time seen by the distance relay at transmission line from Superstition to Ealy (69 kV), Case 3.1 (b) zoom-in view (Per unit base: 100 MVA, 69 kV)

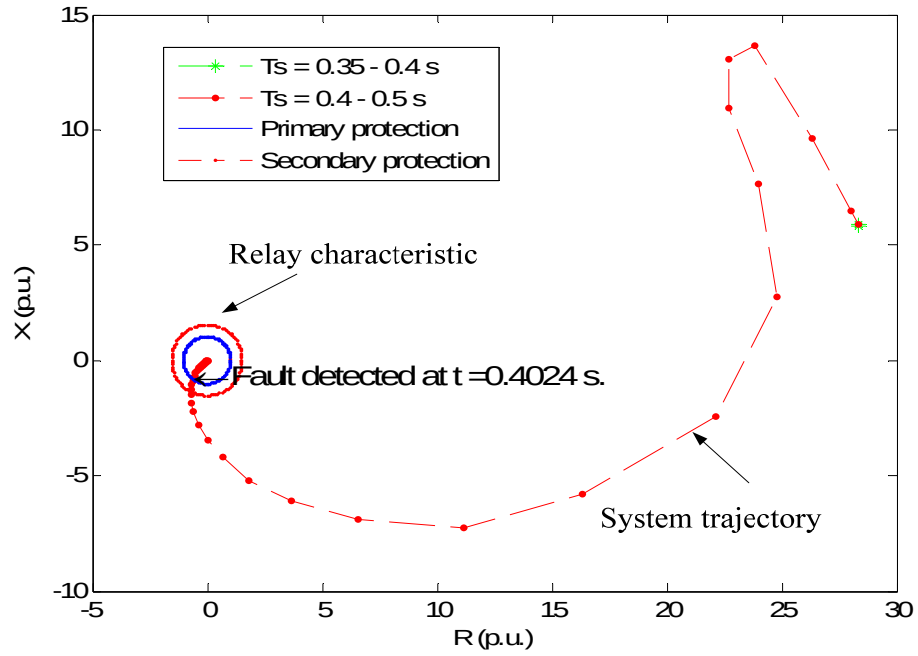

Figure 3.20 (a) Plot of *X- R* seen by the distance relay at transmission line from Superstition to Ealy (69 kV), Case 3.2 (b) zoom-in view (Per unit base: 100 MVA, 69 kV)

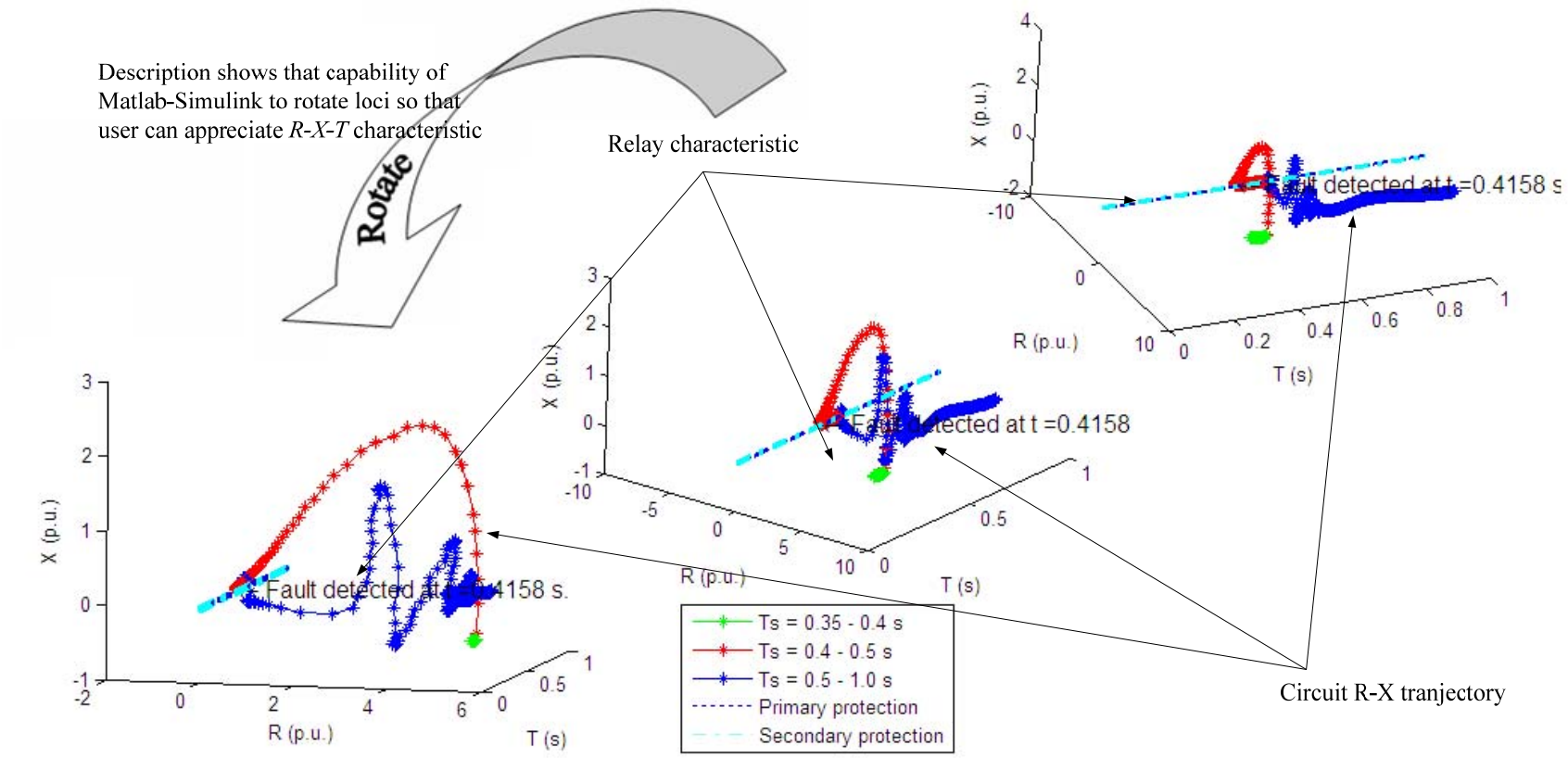

Figure 3.21 Plot of X- R vs. time seen by distance relay at transmission line between Shanon-Superstition (69 kV), Case 3.2 (Per unit base: 100 MVA, 69 kV)

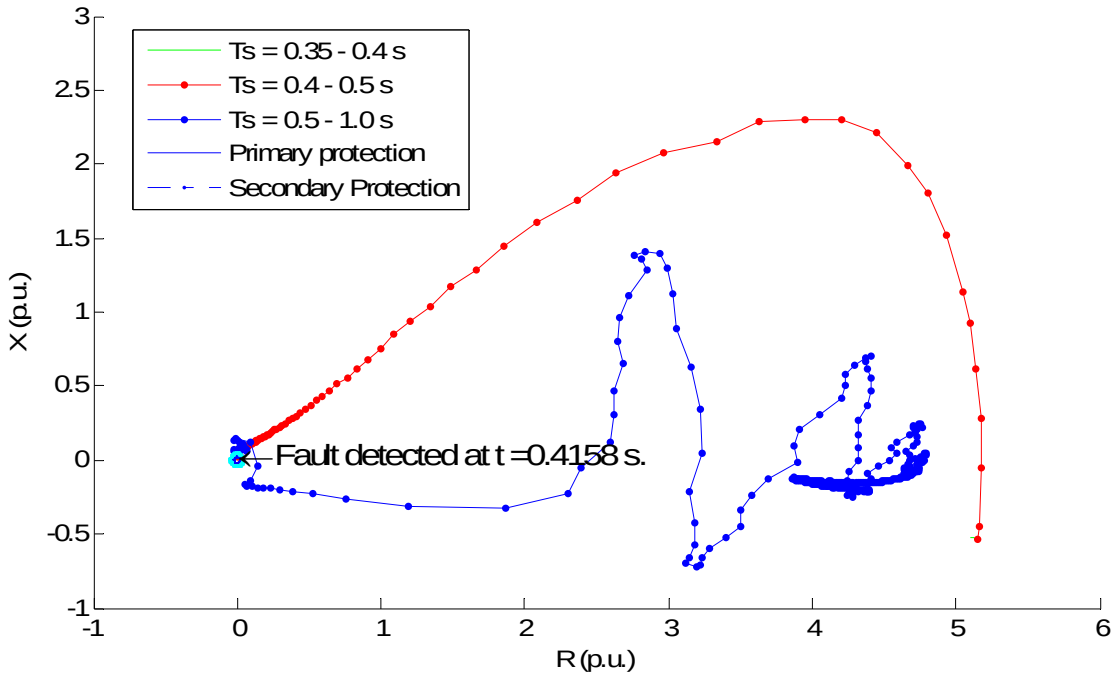

Figure 3.22 Plot of *X* and *R* seen by distance relay at transmission line between Shanon-Superstition (69 kV), Case 3.2 (Per unit base: 100 MVA, 69 kV)

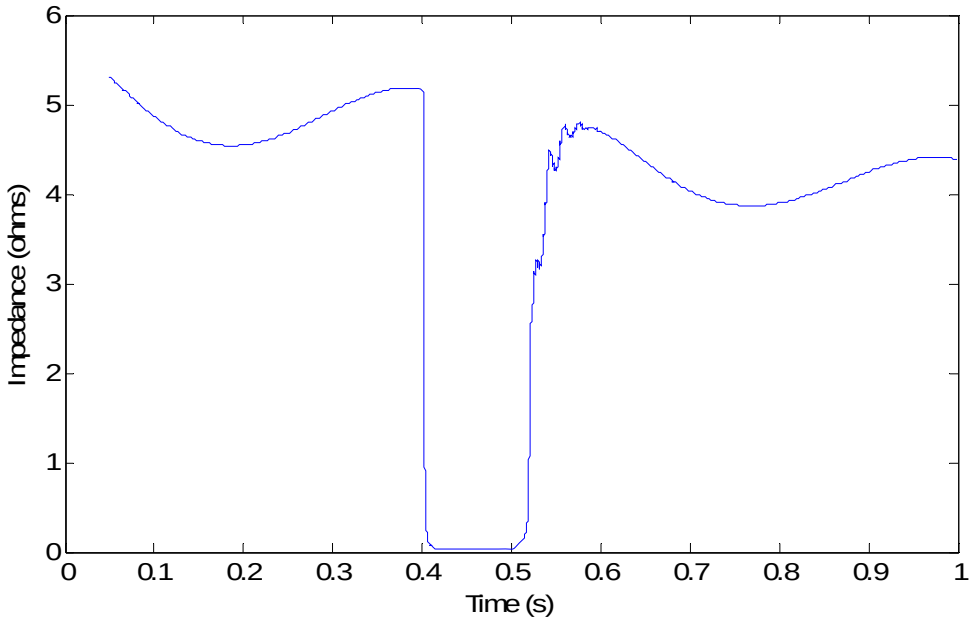

Figure 3.23 Plot of magnitude of impedance seen by distance relay at transmission line between Shanon-Superstition (69 kV), Case 3.2

Case 3.3 Simulation of three phase to ground bolted fault at bus Ealy (69 kV) with DGs of the Thunderstone system with four inverter based DGs

In Case 3.3, four inverter based DGs are installed into the Thunderstone system: Sage4, Superstition3, Early1 and Ealy2. The capacity of each DG is 5 MW which is identical to the DGs in Case 3.2. A three phase bolted fault occurs at the middle of the line between Superstition and Ealy (69 kV). The fault starts at 0.4 s and is cleared at 0.5 s.

Figures 3.25 and 3.26 show the voltage and current measured at the fault location. In Fig. 3.27-29, the plots of *X*-*R* and *X*-*R* vs. time indicate that the fault is not detected by the impedance relay at bus Superstition3 (12.47 kV). The fault current that flows from the inverter based DG at bus Superstition3 to the fault point is not high enough to be detected by the primary protection system.

The plots of impedance of the transmission line between Superstition and Ealy are shown in Figs. 3.30-3.32. The fault is detected at t = 0.4024 s. Due to the increase of fault current after installing the DGs the fault is detected faster than it does in Case 3.1. The plots of impedance of the transmission line between Shanon and Superstition (69 kV) are shown in Figs. 3.33-35.

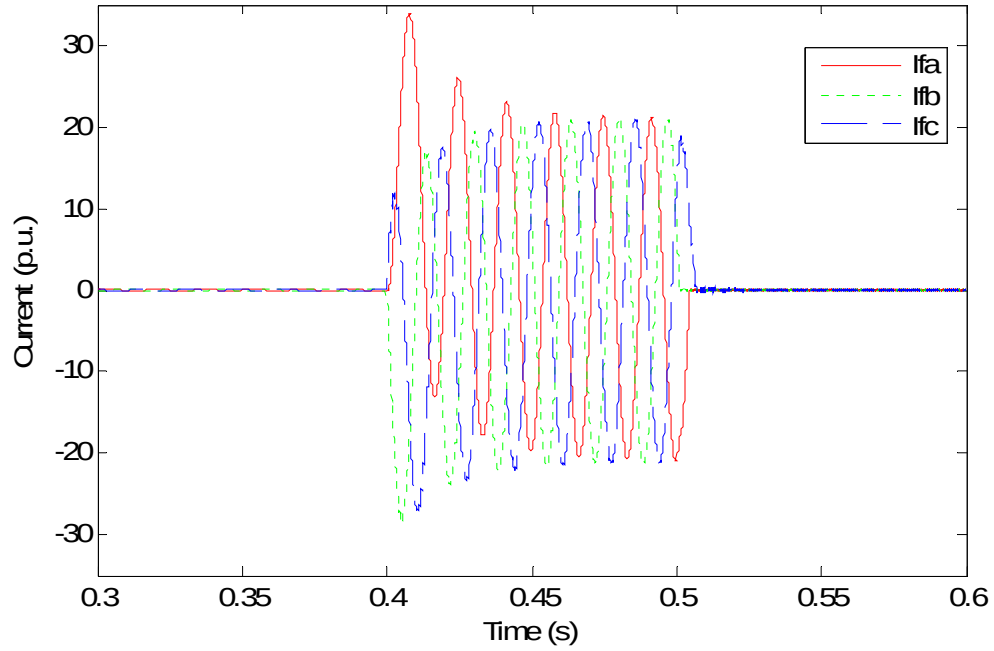

Figure 3.24 Fault current at the fault point with four synchronous machine DGs in the system, Case 3.3 (Per unit base: 100 MVA, 69 kV)

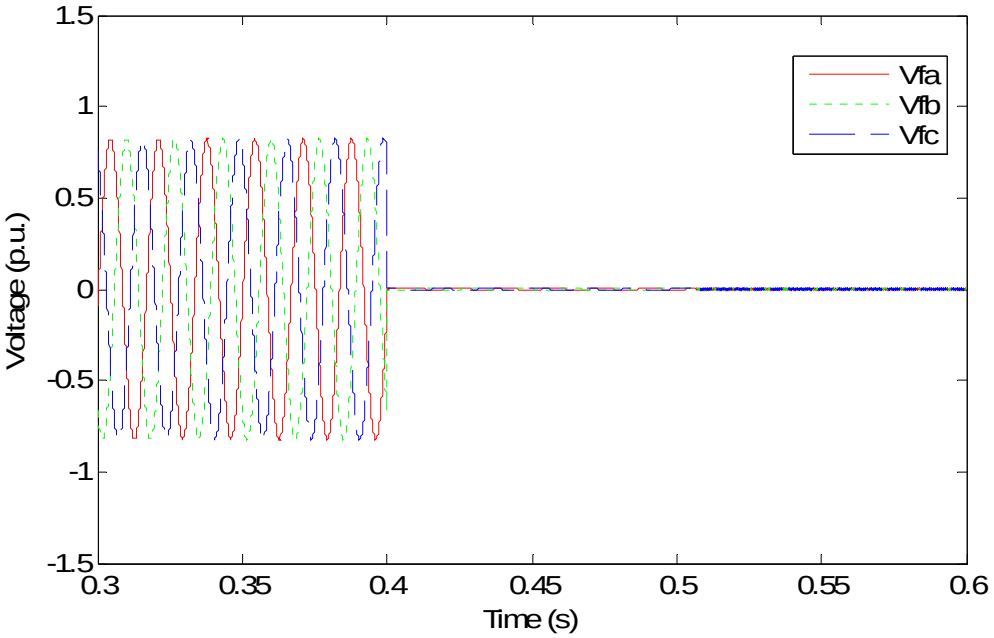

Figure 3.25 Fault voltage at the fault point with four synchronous machine DGs in the system, Case 3.3 (Per unit base: 100 MVA, 69 kV)

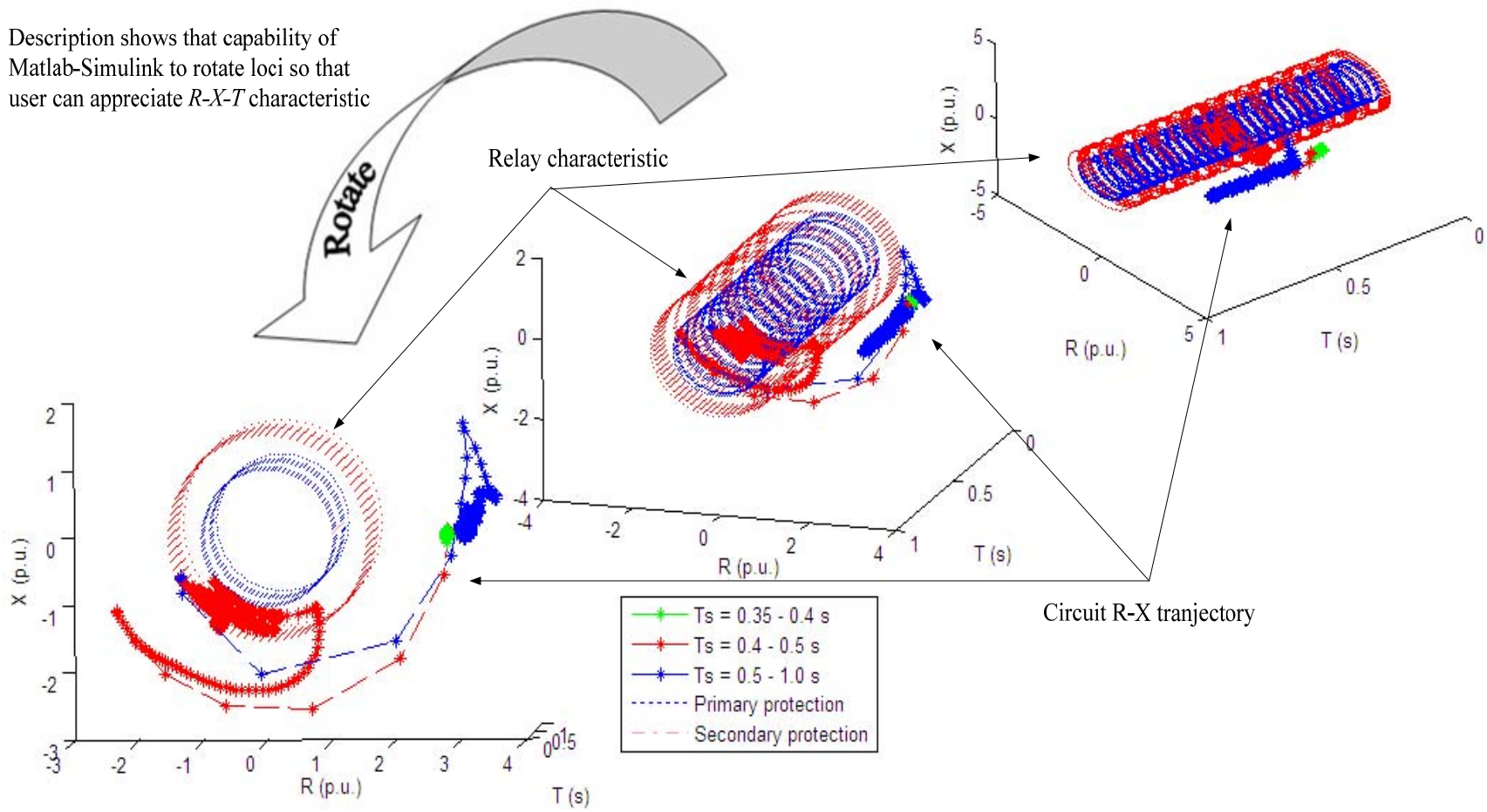

Figure 3.26 Plot of *X*-*R* vs. time at Superstition3 (12.47 kV) with various angles, Case 3.3 (Per unit base: 100 MVA, 12.47 kV)

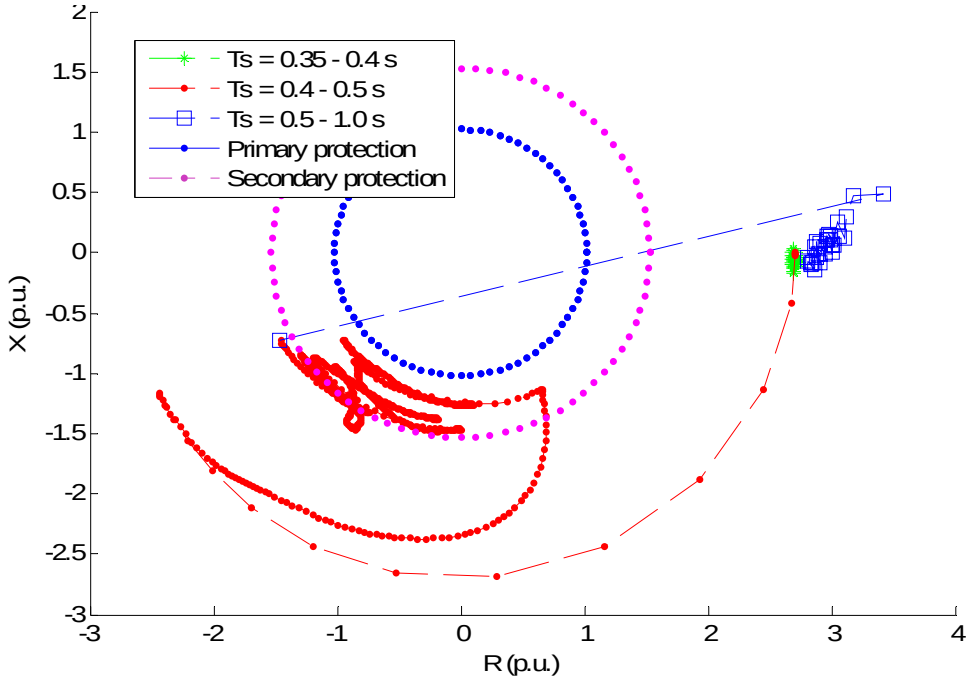

Figure 3.27 Plot of *X*, *R* at Superstition3 (12.47 kV), Case 3.3 (Per unit base: 100 MVA, 12.47 kV)

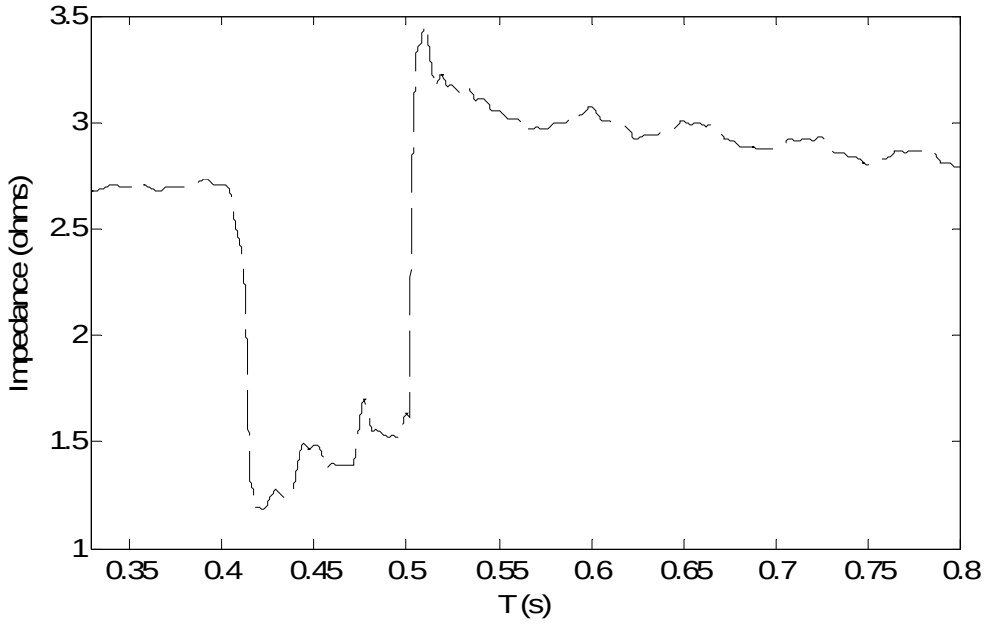

Figure 3.28 Plot of magnitude of impedance seen at Superstition3 (12.47 kV) vs. time, Case 3.3

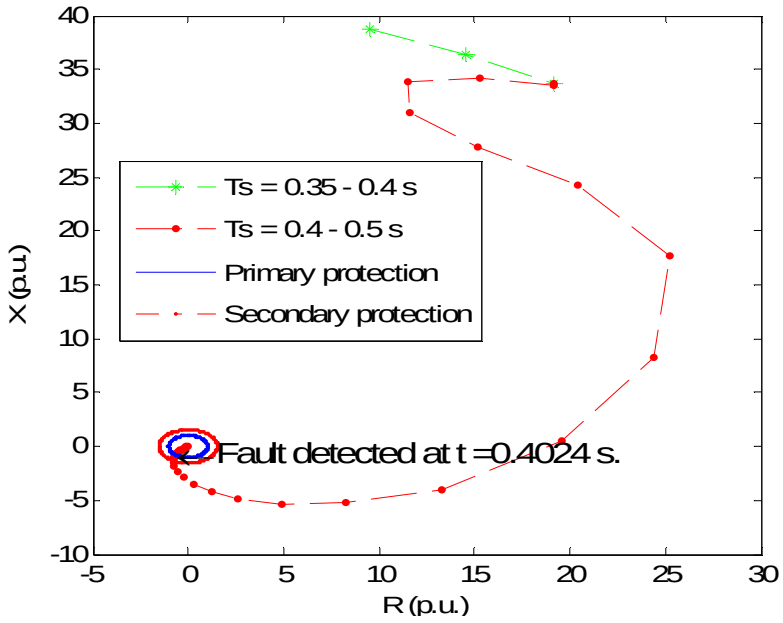

(a)

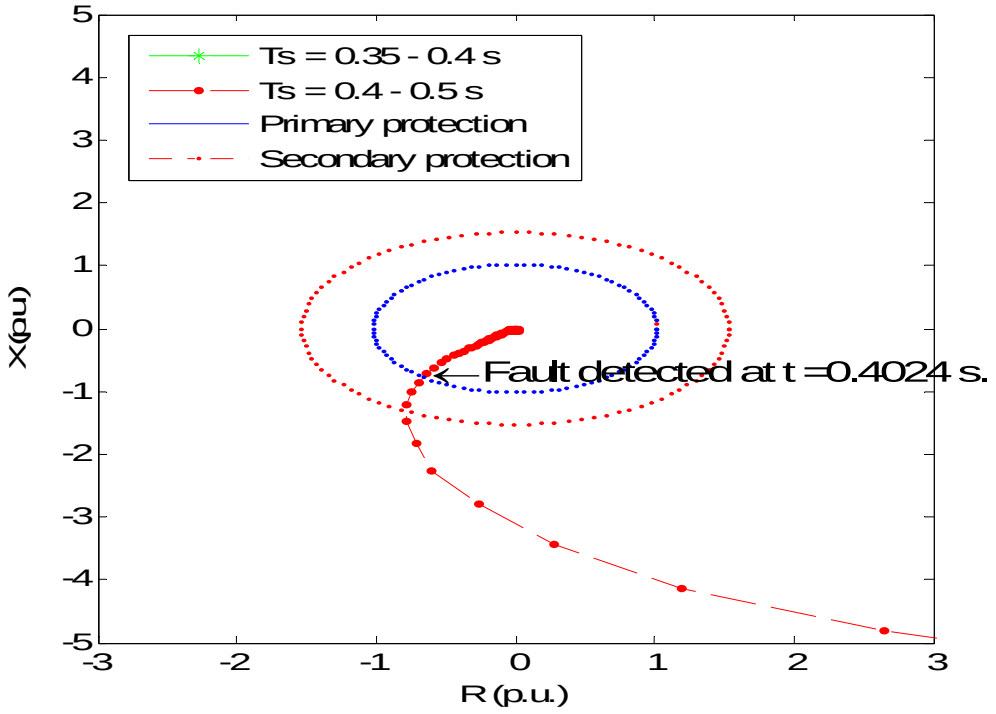

(b)

Figure 3.29 (a) Plot of X- R seen by the distance relay at transmission line from Superstition to Ealy (69 kV), Case 3.3 (b) zoom-in view (Per unit base: 100 MVA, 69 kV)

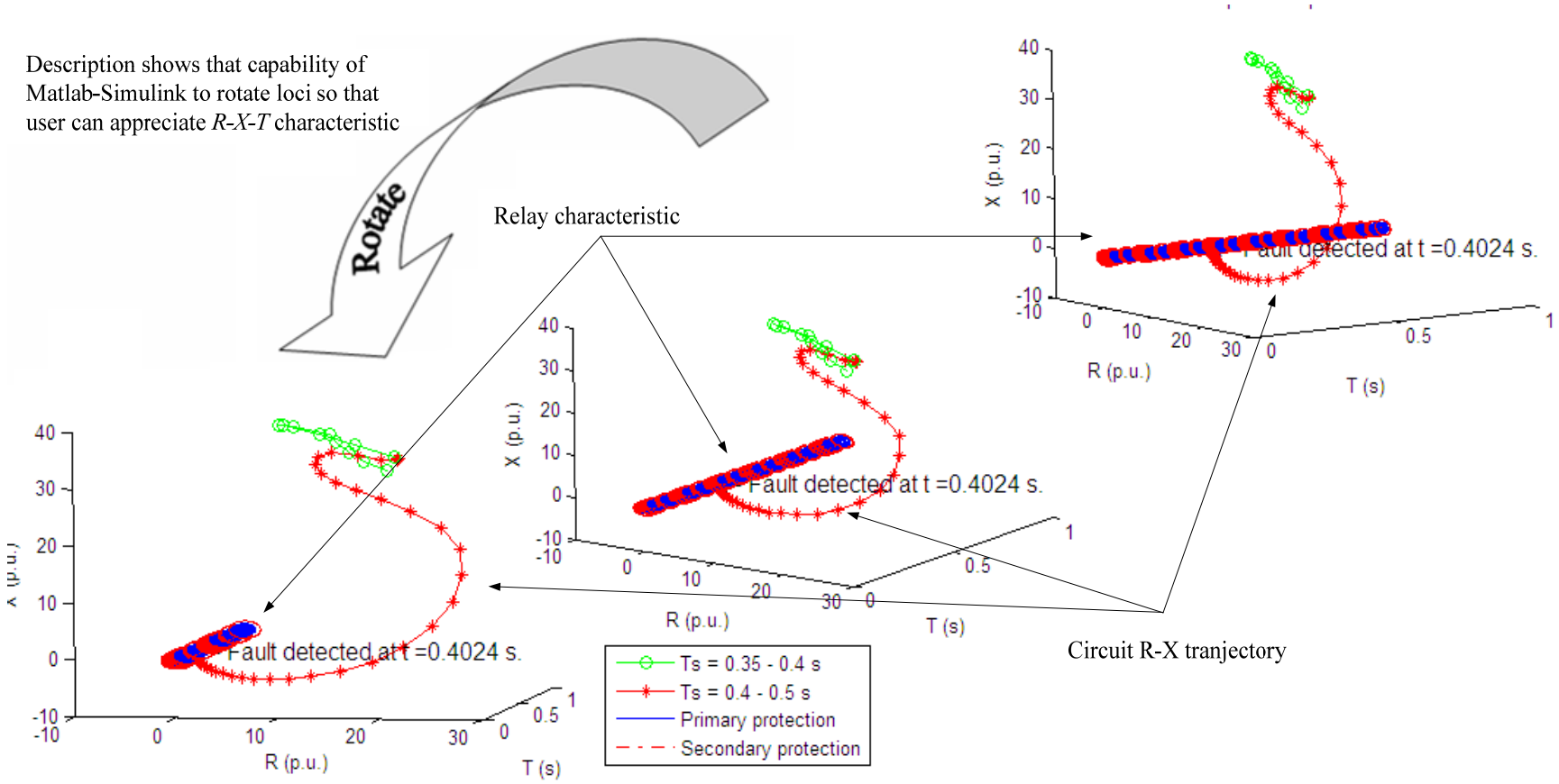

Figure 3.30 Plot of *X*- *R* vs. time seen by the distance relay at transmission line from Superstition to Ealy (69 kV), Case 3.3 (Per unit base: 100 MVA, 69 kV)

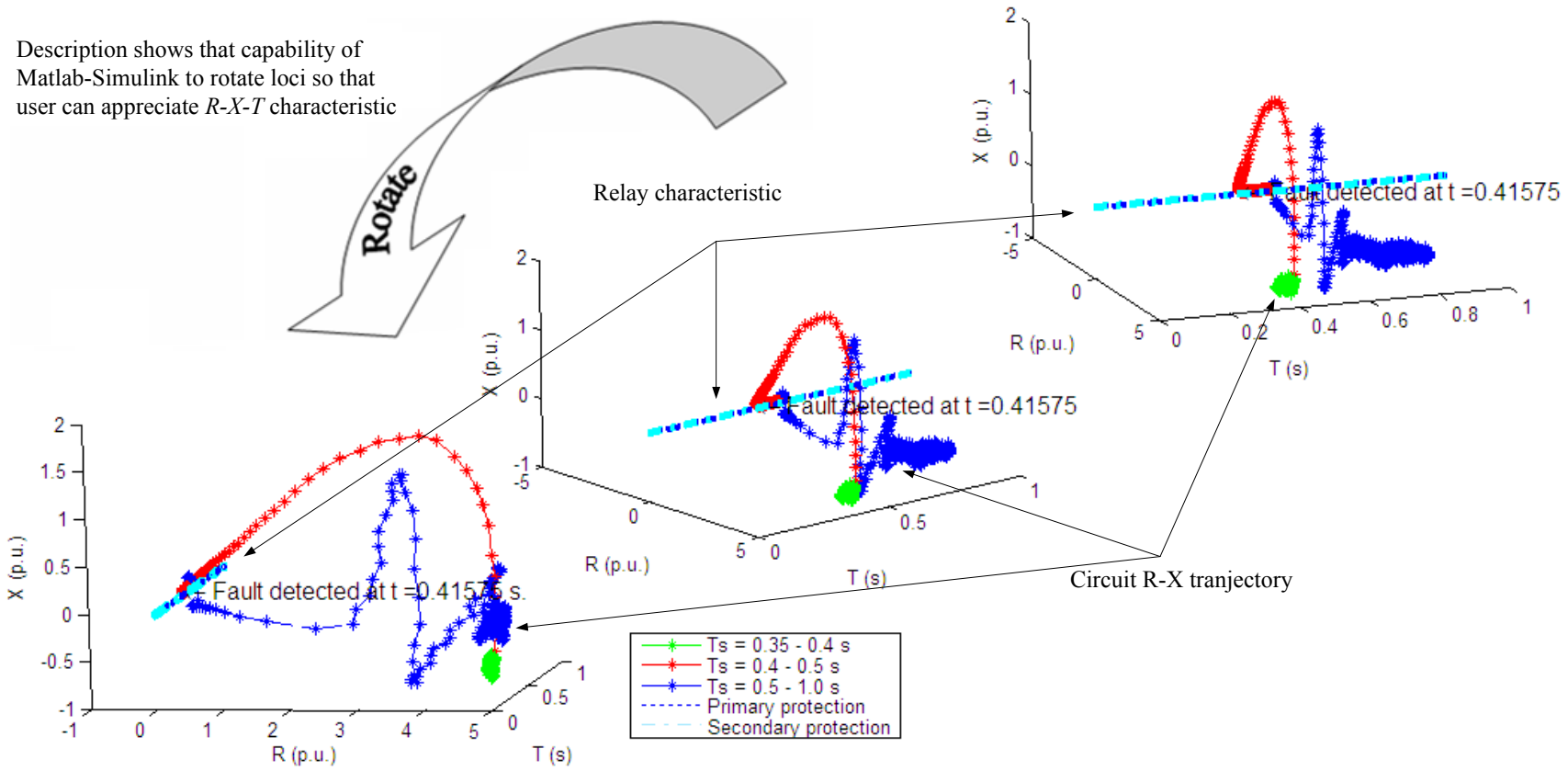

Figure 3.31 Plot of *X* and *R* seen by distance relay seen from bus Superstition at transmission line between Shanon-Superstition (69 kV), Case 3.3 (Per unit base: 100 MVA, 69 kV)

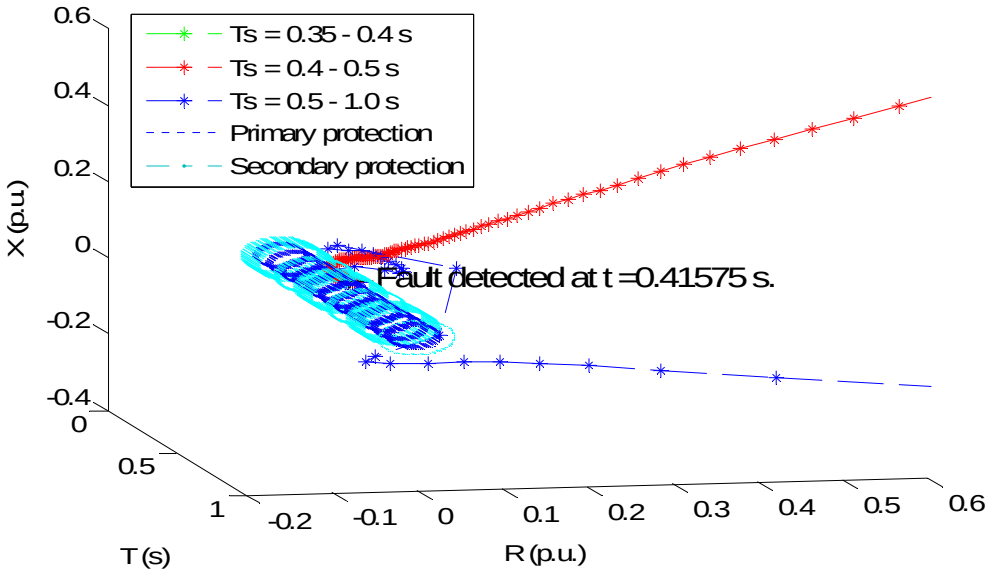

Figure 3.32 Zoom-in view of *X* and *R* seen by distance relay from bus Superstition at transmission line between Shanon-Superstition (69 kV), Case 3.3 (Per unit base: 100 MVA, 69 kV)

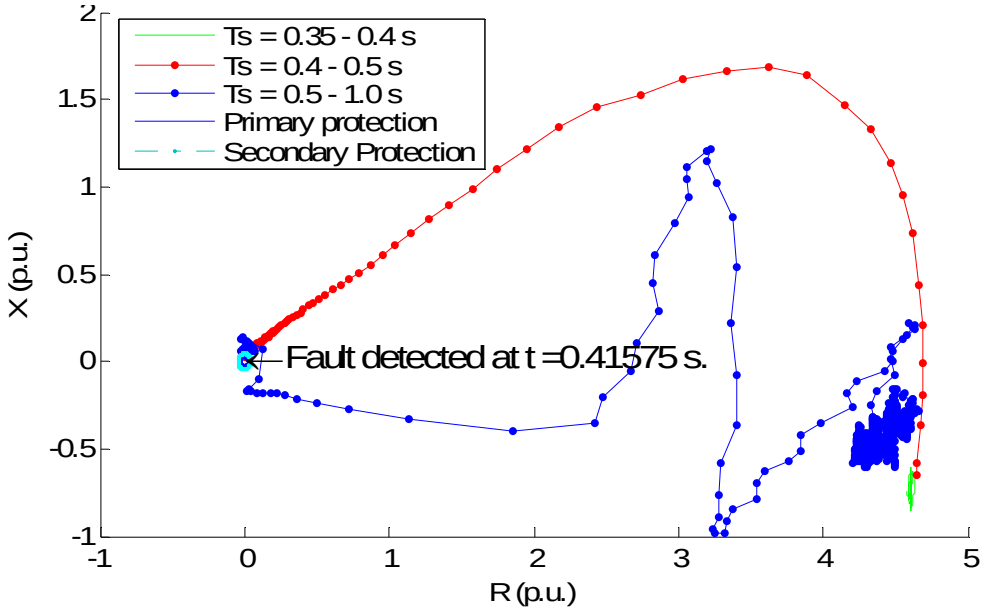

Figure 3.33 Plot of *X* and *R* seen by distance relay from bus Superstition at transmission line between Shanon-Superstition (69 kV), Case 3.3 (Per unit base: 100 MVA, 69 kV)

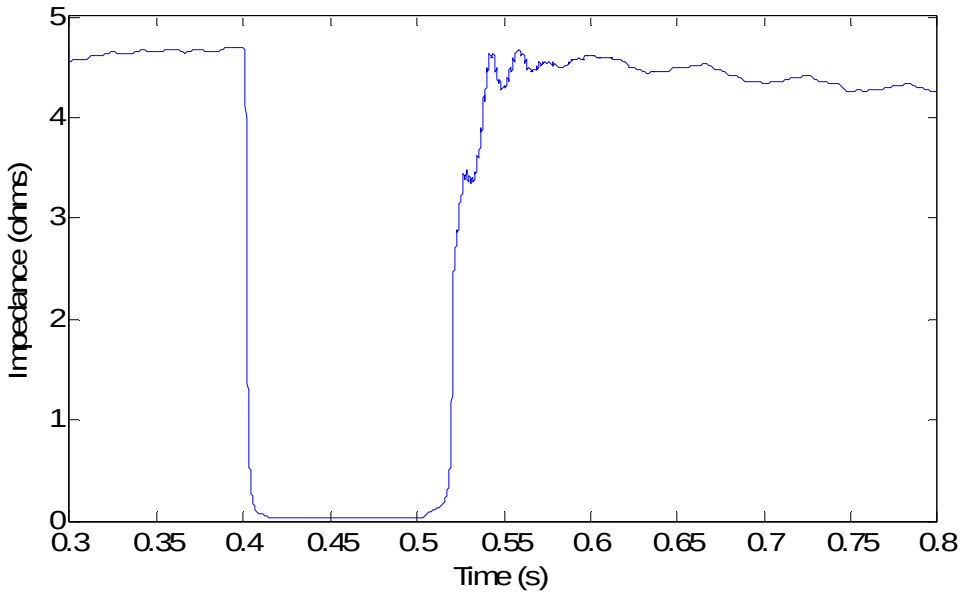

Figure 3.34 Plot of magnitude of impedance seen by distance relay at transmission line between Shanon-Superstition (69 kV), Case 3.3

3.5 Conclusion

This chapter discusses the fault analysis of the subtransmission system with the presence of DGs. The modified bus impedance matrix is applied in the illustrative example (Section 3.2) to calculate the fault current of the Thunderstone system with synchronous machine DGs. This can be used to design the size of protection system such as circuit breaker (CB), fuse and relays. However, it is inconvenient to applied this method to analyze the system with inverter based DGs because of inverters are nonlinear. A simulation technique is proposed to analyze the system dynamic and change of the fault response of the system with inverter based DGs. Simulations of the synchronous and inverter based DGs in subtransmission system are presented in this chapter. The Thunderstone system is applied as the test bed. The model of inverter based DGs in the illustra-

tive example (Case 3.3) is discussed in Chapter 2. Simulation results are summarized in Table 3.3.

Table 3.3 Summary of the simulations, Cases 3.1 – 3.3

Location of measurements	Case 3.1 Figures	Case 3.2 Figures	Case 3.3 Figures
Voltage and Current at the fault point	3.5, 3.6	3.15, 3.16	3.25, 3.26
X-*R* and *X*-*R*-time seen by distance relay at Superstition3 (12.47 kV)	3.7, 3.8	3.17, 3.18	3.27, 3.28
Impedance vs. time seen by distance relay at Superstition3 (12.47 kV)	3.9	3.19	3.29
X-*R* and *X*-*R*-time seen by distance relay at transmission line between Superstition – Ealy (69 kV)	3.10, 3.11	3.20, 3.21	3.30, 3.31
X-*R* and *X*-*R*-time seen by distance relay at transmission line between Superstition – Ealy (69 kV)	3.12, 3.13	3.22, 3.23	3.32, 3.33
Impedance vs. time seen by distance relay at Shanon-Superstition	3.14	3.24	3.34

Conclusions can be drawn from the simulations in this chapter as:

- Installation of DGs in the distribution system increases the fault current throughout the system. This situation may change the way protective relays react to the faults. Circuit breakers, fuses and setting of relays may need to be adjusted to the new appropriate range.

- The simulation results show that severity of increase of fault current from synchronous machine DGs is higher than that from inverter based DGs. Fault currents from the three-phase to ground bolted fault in Cases 3.1-3 are shown in Fig. 3.36.
- The protection system may lose coordination upon installation of DGs. This point is illustrated as follows: before installing distributed generation (Case 3.1), distance relay at Superstition3 (12.47 kV) should not operate to clear the fault. This is due to the upstream fault on the subtransmission system. The fault should be cleared by the distance relays of the line between Superstition and Ealy (69 kV). When synchronous machine DGs are installed (Case 3.2), the fault current flows from DG at Supertition3 to the fault point and the relay at Superstition3 (12.47 kV) might operate (see Fig. 3.7). This situation depends on the coordination of protections system before installing DGs. Thus, the protection system might lose coordination for the case of installed synchronous machine DGs. However, in Case 3.3, when a three-phase fault occurs at the middle of the line between Superstition and Ealy, the fault current from inverter based DGs are less severe than in Case 3.2. Simulation results show that distance relay at Superstition3 does not detect the fault. The protection system operates the same as in Case 3.1 to clear the fault.
- The results of simulation can be used to analyze the setting of relays in the system in the presence of DGs. For example, Fig. 3.37 shows the operation time of the distance relay at Superstition3 (12.47 kV). This plot provides important information to analyze the coordination of the protection system.

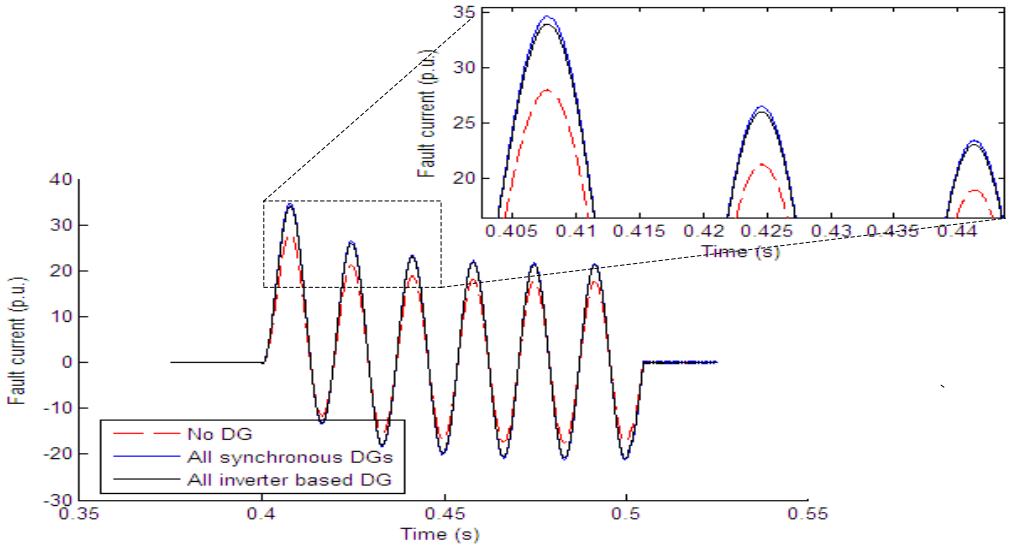

Figure 3.35 Comparison of the fault currents (p.u.) from three phase to ground bolted fault at the middle of the line between Superstition – Ealy (69 kV), Cases 3.1-3.3 (Per unit base: 100 MVA, 69 kV) , taken from [72]

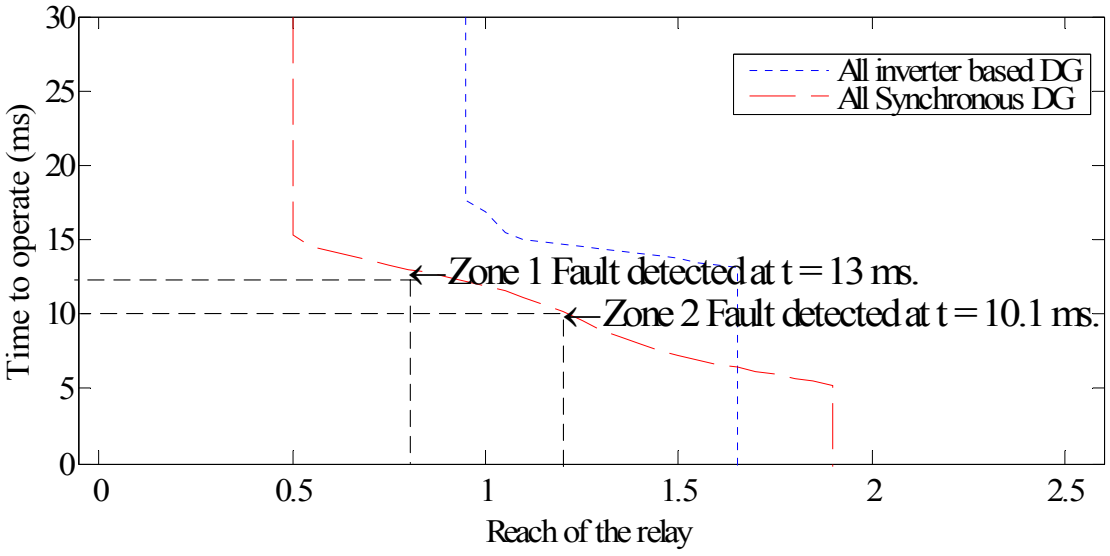

Figure 3.36 Plot of time to operation of the distance relay at bus Superstition3 (12.47 kV) vs. reach of the relay, Case 3.2 and 3.3 (Per unit base: 100 MVA, 12.47 kV) , taken from [72]

CHAPTER 4

ONLINE CALCULATION OF FAULT CURRENT IN THE PRESENCE OF DG

4.1 Introduction

Analysis of fault current by applying the conventional technique is well studied in many references such as [36, 56, 57]. This procedure is standardized and considered critical. Calculation of fault current in the conventional technique is based on the system parameters and system configuration. That is, all parameters of the system, such as line parameters, transformers and loads, are required in the conventional technique.

K. Sriniwasan, C. Lafond and R. Jutras propose a fault current estimation technique in [55]. The proposed technique applies a statistical knowledge to evaluate three phase bolted fault current of a load bus in a distribution system. The calculation is accomplished by using the variations of voltage and current measured at the load. The voltage and current variations are created from changes of the load. Figure 4.1 conceptualizes the ideal of online fault current estimation.

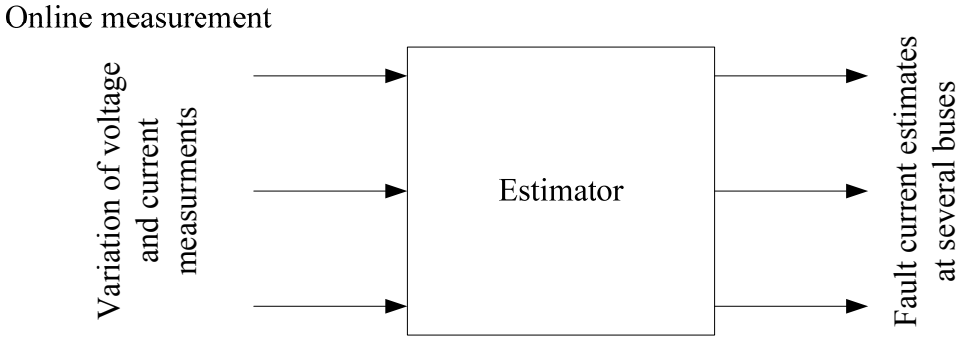

Figure 4.1 On-line fault current estimation

These variations may be used to estimate the fault current at the measured location. Parameters and configuration of the system is not required in this estimation technique. Based on the fault current estimation technique, the fault current at the measurement locations can be estimated by using only the filed measurement data. The method in [55] is essentially based on a statistical analysis and this concept is adapted here for the case of DG penetration.

In practical operation, the increase of fault current in a system may also occur due to the installation of new DGs, change of system configuration, or change of breaker topology. This estimation technique can be used to secure the system from the increase of fault current. The online assessment of fault current is necessary to inform the operator to avoid these unsafe operation conditions. Such advice may be in the form of an alarm.

This chapter demonstrates an online fault current estimation technique. A test bed, denominated as the Thunderstone system, is produced for illustrative purposes. The Thunderstone system is described in Section 3.1.

This chapter is organized as: Section 4.2 discusses the theory of online fault current estimation; Section 4.3 contains an illustrative example on the test bed system; Section 4.4 discusses the interpretation of the results from online estimation technique.

4.2 Summary of existing work – fault current estimation

This section discusses the theory and equations used for fault current estimation. By applying an estimation technique, the fault current at major load points can be estimated based on voltage and current measurements at each load point. Voltage and current variations, due to the change of loads, at the estimated point are used in this calcula-

tion. The voltage and current are recorded in rms values. The voltage and current variation might occur from the load side or the source side or happen simultaneously. The recorded signals, normally a few hundred snapshots, are used as the input of this calculation.

Equations used in this estimation technique are derived from system voltage equations at a PCC. The Thevenin equivalent circuit of a power system at a PCC can is depicted in Fig. 4.2. The load in Fig. 4.2 is represented by a constant impedance. The voltage equations of the Thevenin equivalent circuit can be written as,

$$V = E - IZ_s \tag{4.1}$$

$$V = IZ_L \tag{4.2}$$

where V is the voltage a PCC, I is the current to the load, Z_s is the equivalent impedance of the source side, E is the equivalent voltage at the source side, Z_L is the load impedance.

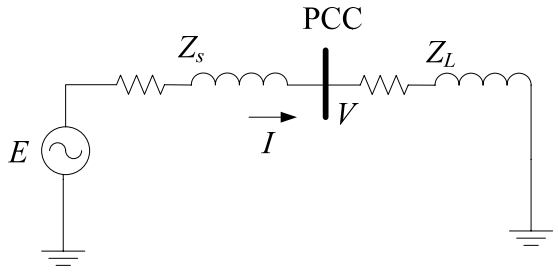

Figure 4.2 The Thevenin equivalent circuit at a PCC

As mentioned in the previous section, the fault current estimation is based on the analysis of voltage and current variations. The fault current estimation is derived by applying the analysis of small signal variations. The derivation is done under the assumption that the second order terms are negligible. From (4.1-4.2), voltage equations with small signal variations can be written as follows [55],

$$V + \delta V = (E + \delta E) - (I + \delta I)(Z_s + \delta Z_s)$$

$$V + \delta V = (I + \delta I)(Z_L + \delta Z_L)$$

or

$$\delta Z_L = \frac{\delta V}{I} - \frac{V}{I^2}\delta I \tag{4.3}$$

$$\frac{\delta E}{I} - \delta Z_s + \frac{(E - V)}{I^2}\delta I = \frac{\delta V}{I}. \tag{4.4}$$

Multiply (4.4) by (4.3) and take the average over a large number of measured voltages and currents, Equation (4.4) can be expressed as [55],

$$E - V = \frac{I^* R_{VV} - V^* R_{VI}}{V^* \dfrac{R_{II}}{I} - I^* \dfrac{R_{VI}^*}{I}} \tag{4.5}$$

where R_{xy} denotes the covariance of variables x and y.

Note that, from (4.5), the fault current estimation is partially related to the covariance of the voltage and current at the estimated bus. The covariance of two variables, x and y, provides a statistical measure of how strongly correlated these variables are. The definition of the covariance of complex variables x and y, R_{xy}, is given by [77],

$$R_{xy} = \left\langle (x - \mu_x)(y - \mu_y) \right\rangle$$

$$= \left\langle x_i y_i \right\rangle - \mu_x \mu_y ,$$

where $\mu_x = \left\langle x_i \right\rangle$ and $\mu_y = \left\langle y_i \right\rangle$ is the mean value of x_i and y_i. Note that the impedance of the load side, Z_L, has no statistical correlation with the impedance of source side, Z_s. In other words, the impedance of the load size is statistically independent from the impedance of source side (see Fig. 4.2). Hence, the covariance of variable Z_L and Z_s is zero

($R_{Z_L Z_S} = 0$). The same reason can be applied to source voltage, E, and load impedance, Z_L. The covariance of variable E and Z_s is zero ($R_{EZ_S} = 0$).

From (4.1) and (4.5), the equivalent impedance of the system, Z_s, at the PCC is

$$Z_s = \frac{I^* R_{VV} - V^* R_{VI}}{V^* R_{II} - I^* R_{VI}^*}. \tag{4.6}$$

where I^* represents the complex conjugate of I.

The fault current, I_f, at buses with measurement can be expressed, from (4.1) and (4.6), as

$$I_f = \frac{V + IZ_s}{Z_s} = I + \frac{V}{Z_s} = I + V \frac{\left(V^* R_{II} - I^* R_{VI}^*\right)}{\left(I^* R_{VV} - V^* R_{VI}\right)}. \tag{4.7}$$

4.3 Illustrative example – application to the subtransmission system with DGs

In this section, the Thunderstone system as shown in Fig. 3.1 is used as the test bed system to demonstrate the fault current estimation technique. To evaluate the accuracy of the estimation technique, fault current at some load buses calculated by using the conventional algorithm are compared to the calculation by the estimation technique. As also mention in Chapter 3, installation of DGs increases faults current throughout the system. The demonstration in this section shows the ability to detect the increased of fault current due to these DGs. The demonstrations in this chapter are separated to 2 cases:

- Thunderstone system without DG denominated as “Case 4.1”.
- The Thunderstone system with DGs denominated as “Case 4.2”. In this case, DGs are installed at 5 locations. Parameters of DGs and locations are shown in Table 4.1

Note that all examples are listed in Appendix C.

In both cases, assume that voltage and current are recorded at 12 kV load buses at 7 locations: Cameron, Cluff2, Signal3, Shanon2, Sage2, Ealy3, Ealy4 and Seaton. Figure 4.3 redraws the Thunderstone system with the measurement points and location of DGs.

The conventional fault current calculation is discussed in Section 3.2 and [73]. Three phase fault current at each bus, in Cases 4.1 and 4.2, can be calculated by (3.3). The prefault voltage in (3.3) is given by the load flow solution of the system. The diagonal element of the bus impedance matrix of bus j, Z_{jj}, can be calculated by (3.2).

In the fault current estimation technique, the calculation is done based on variations of voltage and current rms measurements due to the change of loads. Instead of actual measurements over a period of time, voltage and current measurements from one hundred events used in this demonstration are created from the results of load flow calculations. Changes of active and reactive power of loads in each event are generated psedorandomly by following the Gaussian distribution. The intent is not to claim that operating points and DG levels are random variables but only to illustrate the variation of fault response with load and operating point. The variations of active and reactive power of loads in the system are quantified by mean values and standard deviations of the loads. In the illustrative examples, mean values of active and reactive power are given in Table A.2 (Appendix A). In each event, the standard deviations of active and reactive power of each load are fixed at 5 and 0.4, respectively.

Table 4.1 Locations and parameters of DGs in Case 4.2

Locations	Size (MVA)	Transient impedance (p.u.)*
Superstition3	10.0	0.0005+*j0.*125
Seaton2	20.0	0.001+*j*0.224
Ealy3	30.0	0.0015+*j*0.339
Ealy4	45.0	0.0001+*j*0.4
Sage3	40.0	0.002+*j*0.38

* Per unit based on machine rating MVA, 12.47 kV

The three phase bolted fault current at each bus is calculated by applying (4.7). Results of calculation from the conventional technique and the estimation technique are shown Tables 4.2 and 4.3. Plots of the fault current calculation by the estimation technique are shown in Figs. 4.4-4.10. For example, the histogram in Fig. 4.4 shows the amplitude of the fault current at bus Cameron versus the number of occurrences in Cases 4.1 and 4.2. The dotted line in the plots represents the average value of the estimated fault currents. Note that the error of the fault current estimation form the conventional technique is in the range of 5 percent. The cited tables and figures are for given selection of statistics of operating point in this example. It is expected that similar results would be obtained for other probability distributions.

Table 4.2 Three phase fault current of the Thunderstone system "without DG", Case 4.1

Bus	Three phase fault current (p.u.)		Error (Percent)
	Conventional Calculation, $\lvert I_f \rvert$	Estimation Technique, $\lvert \bar{I}_f \rvert$	
Cameron (5)*	18.84	19.05	1.11
Signal3 (11)**	12.37	12.90	4.31
Shanon2 (13)**	14.37	14.77	0.85
Superstition2 (15)**	10.83	11.07	2.23
Sage2 (18)**	11.43	11.74	2.70
McCoy2 (20)**	14.66	14.53	0.85
Seaton (21)**	17.68	17.38	1.69

* Per unit based on 12 MVA, 12.47 kV ** Per unit based on 100 MVA, 69 kV

Table 4.3 Three phase fault current of the Thunderstone system "with DGs", Case 4.2

Bus	Three phase fault current (p.u.)*		Error (Percent)
	Conventional Calculation, $\lvert I_f \rvert$	Estimation Technique, $\lvert \bar{I}_f \rvert$	
Cameron (5)*	19.89	19.98	0.45
Signal3 (11)**	12.50	12.96	3.67
Shanon2 (13)**	14.58	14.89	2.17
Superstition2 (15)**	10.94	11.16	1.90
Sage2 (18)**	11.57	11.75	1.59
McCoy2 (20)	14.83	14.79	0.28
Seaton (21)**	19.67	19.82	0.76

* Per unit based on 100 MVA, 12.47 kV ** Per unit based on 100 MVA, 69 kV

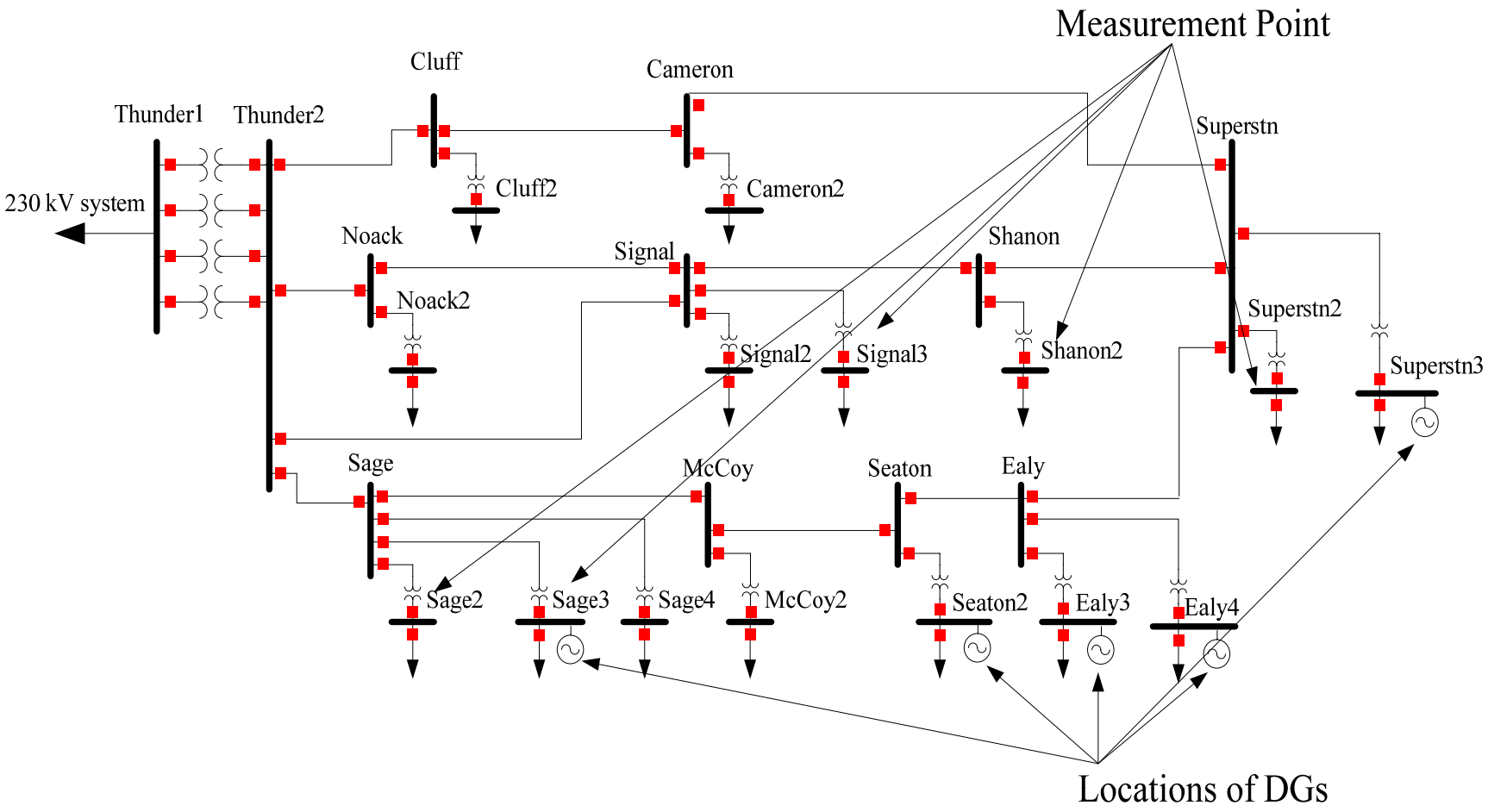

Figure 4.3 The Thunderstone system with 5 DGs and measurement points

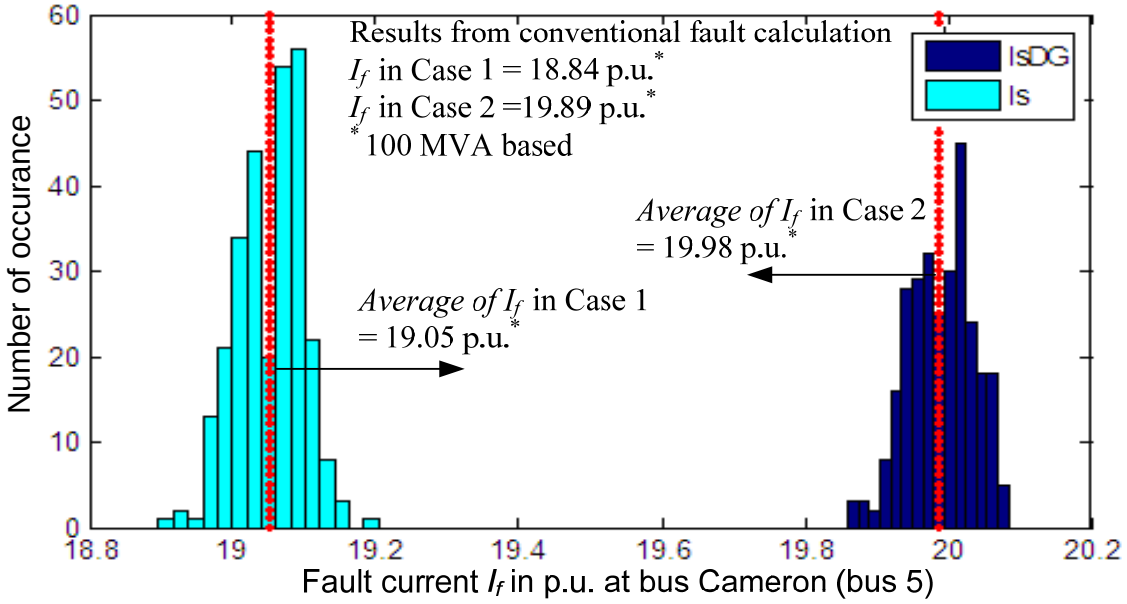

Figure 4.4 Three phase bolted fault current at bus Cameron from the estimation technique (Per unit based on 100 MVA, 69 kV), Cases 1 and 2

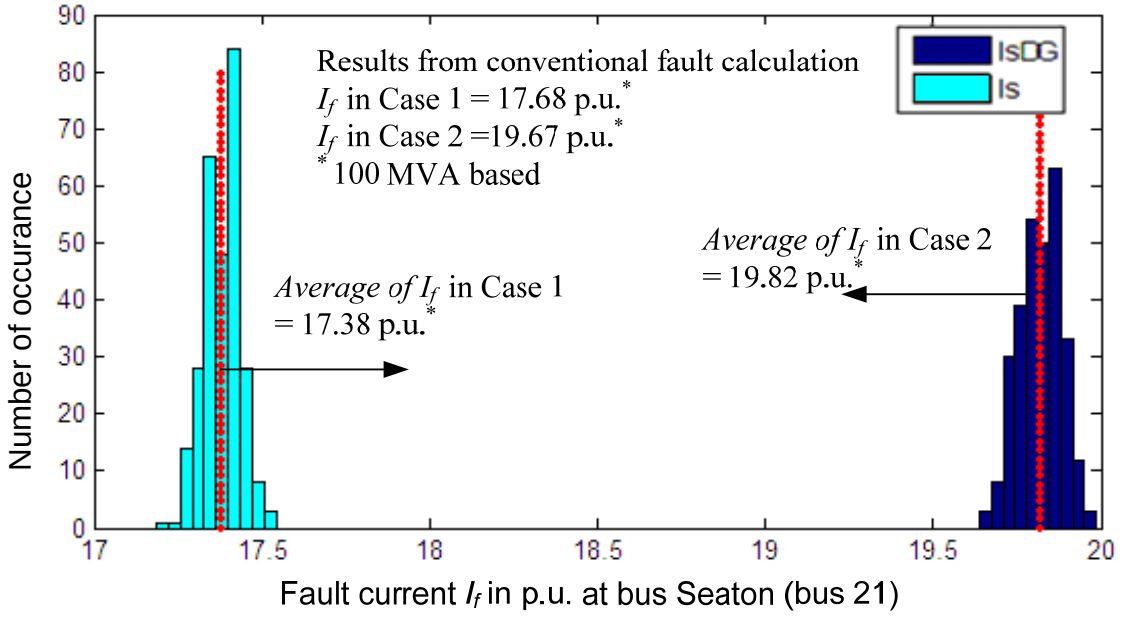

Figure 4.5 Three phase bolted fault current at bus Seaton from the estimation technique (Per unit based on 100 MVA, 69 kV), Cases 1 and 2

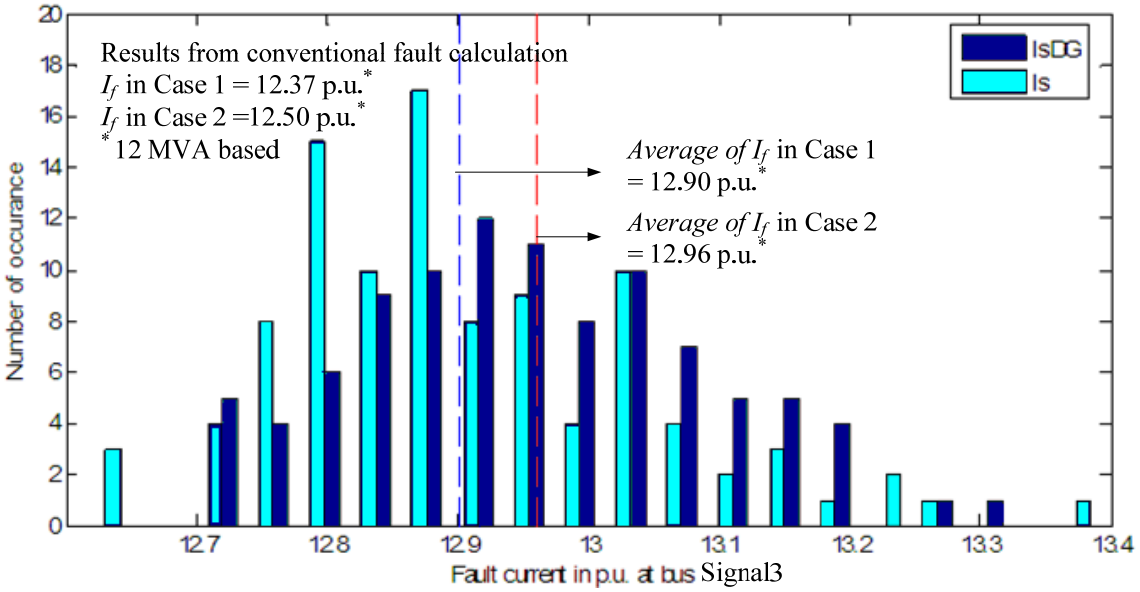

Figure 4.6 Three phase bolted fault current at bus Signal3 from the estimation technique

(Per unit based on 12 MVA, 12.47 kV), Cases 1 and 2

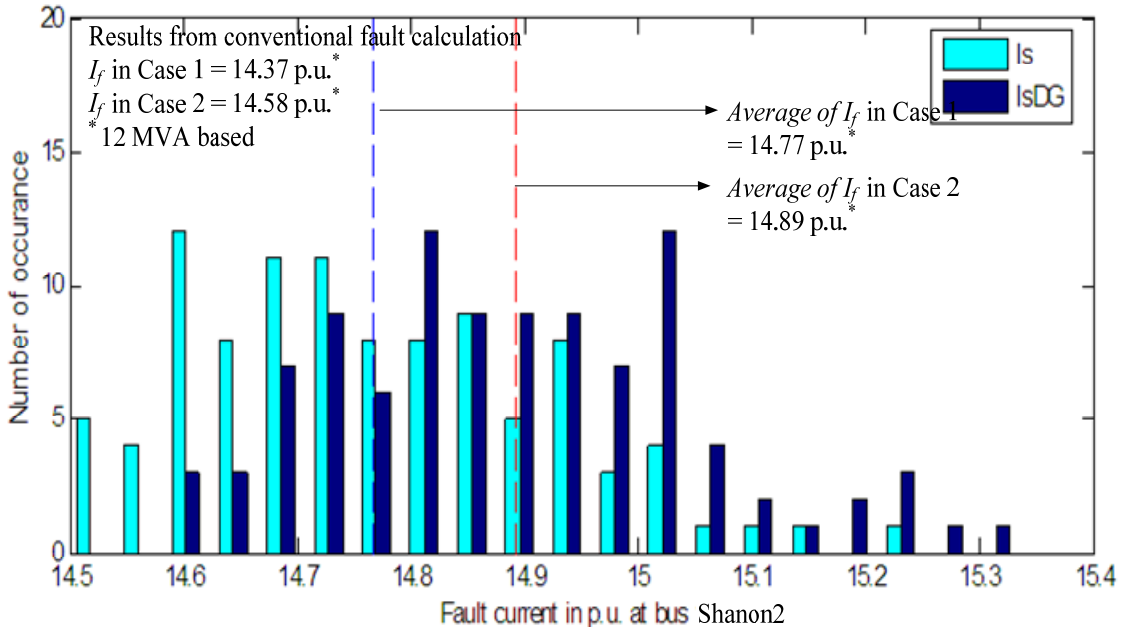

Figure 4.7 Three phase bolted fault current at bus Shanon2 from the estimation technique

(Per unit based on 12 MVA, 12.47kV), Cases 1 and 2

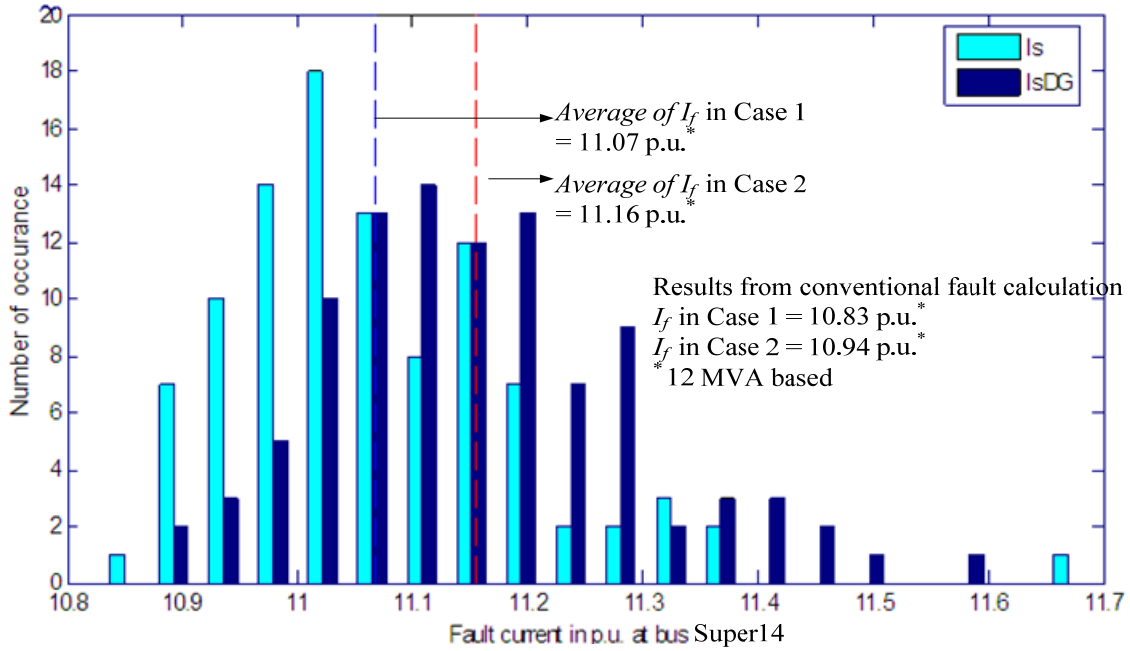

Figure 4.8 Three phase bolted fault current at bus Superstiton4 from the estimation technique (Per unit based on 12 MVA, 12.47kV), Cases 1 and 2

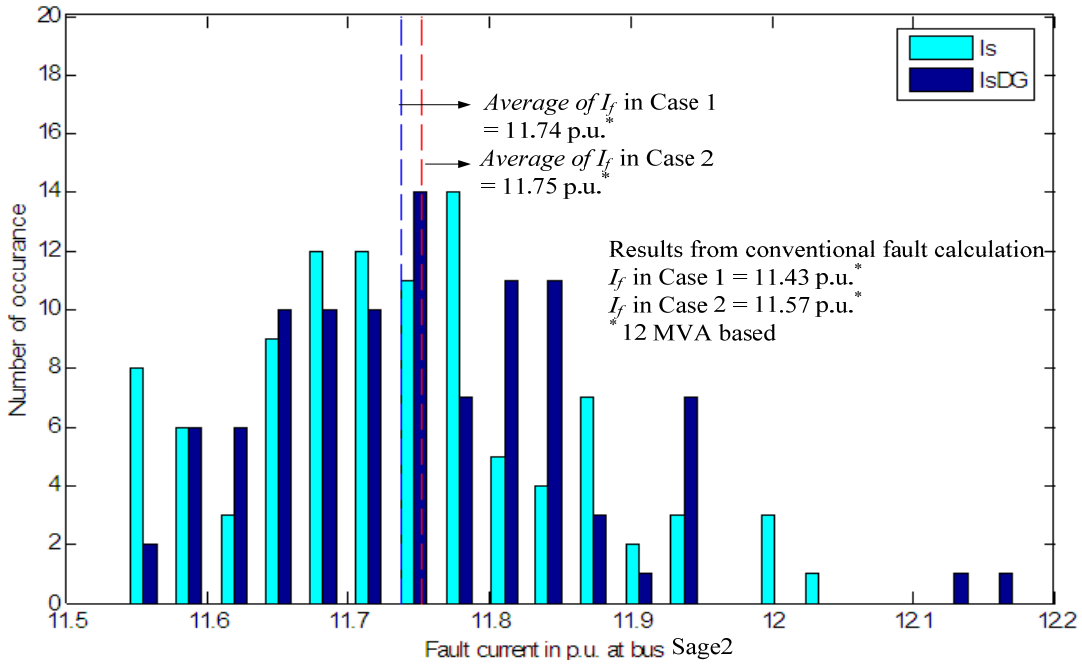

Figure 4.9 Three phase bolted fault current at bus Sage2 from the estimation technique (Per unit based on 12 MVA, 12.47 kV), Cases 1 and 2

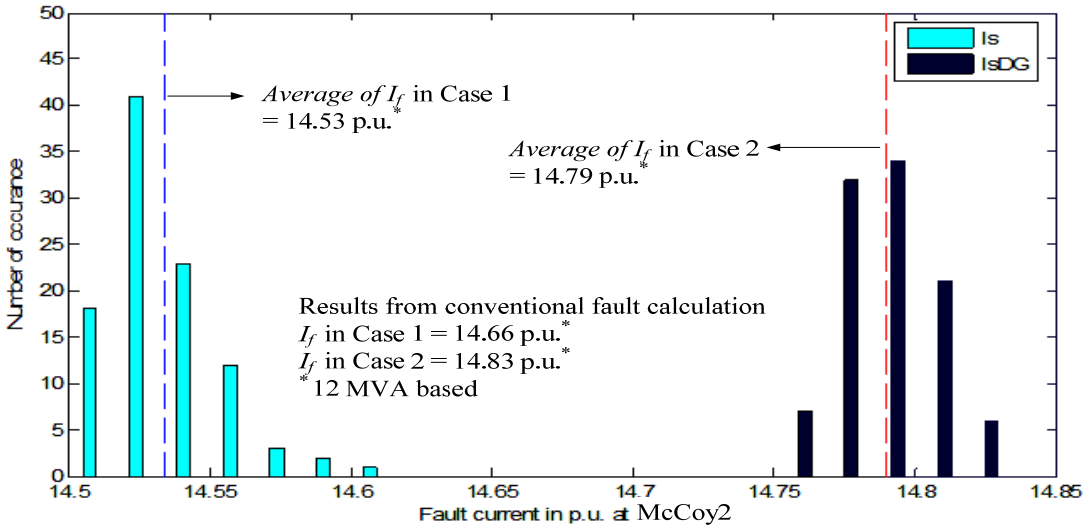

Figure 4.10 Three phase bolted fault current at bus McCoy2 from the estimation technique (Per unit based on 12 MVA, 12.47kV) , Cases 1 and 2

4.4 Online assessment of fault current

The fault current estimation discussed in the previous sections provides a technique to calculate the fault from the voltage and current measurements. In practice, these voltage and current variations can be taken from the supervisory control and data acquisition system (SCADA). By applying the technique shown here, the increase of fault current attributed to DGs or change of system topology can be observed without knowing the change of a specific system parameters. The results of fault current estimation should be compared to the interrupting capability of circuit breaker in each location. This estimation technique can be utilized as an online assessment of the fault current which is necessary to help the operator to avoid unsafe operating conditions. That is, if high fault current is estimated and the fault current exceeds circuit breaker ratings, the several DGs may be removed from service before interrupting the fault current.

CHAPTER 5

AVERAGE CHANGE OF FAULT CURRENT

5.1 Introduction

Power system planning is one of the indispensable parts of electric power system design. Analysis of fault level, pre-fault condition, and post-fault condition are required for the selection of interruption devices, protective relays, and their coordination. Systems must be able to withstand a certain limit of fault current which also affects reliability indices.

The appearance of co-generation, distributed generation, and unconventional generation collectively known as distributed resources (DRs) may result in the change of the fault response. Circuit breaker capability and configuration of protective relays that were previously designed for the system without DRs may not safely accommodate faults. In order to assess the severity (i.e., amplitude) of the increase in fault current in the system due to installing DRs, fault current analysis has to be done, and this procedure is standardized and considered critical.

This chapter is organized as follows: in Section 5.2, a new index called "*ACF*" is proposed as a new system-wide measure of the change in fault current in the system. In Section 5.3, an estimation technique is proposed to calculate the ACF value of a system. The application of the proposed estimation technique is illustrated in Section 5.4. Sections 5.5 and 5.6 discuss the confidence interval of the least squares estimator coefficients and the mean response of the ACF, respectively.

5.2 Average change of fault current (ACF)

At this point, a new index is suggested for the purpose of quantifying the increase of fault current system-wide. The severity of increase of fault currents in the

system can be indicated by applying a new index, the average change of fault current (*ACF*) [78],

$$ACF = \frac{\sum_{n=1}^{nbus} \left| \frac{I_{f,n} - I_{fDG,n}}{I_{f,n}} \right| \times 100}{(number\ of\ 69\ kV bus - 1)} \tag{5.1}$$

where $I_{f,n}$ is the fault current at bus n before installing a new DR, $I_{fDR,n}$ is the fault current at bus n after installing new DRs, and *nbus* is the total number of buses in the system. The 'minus 1' in the denominator of (5.1) allows for no change in fault current at the system slack bus. The term "Average Change of Fault current" is proposed as suitable to quantify the change of fault currents at system buses due to the addition. And these changes are averaged over all system buses. Note that

$$\left| \frac{I_{f,n} - I_{fDG,n}}{I_{f,n}} \right| \times 100$$

is the percent change of amplitude of the fault currents at the 69 kV buses. To conceptualize the ACF, refer to Fig. 5.1.

The foregoing concept is that an index be utilized to determine the percentage of upgrade costs that should be equitably attributed to owners of new DRs. If a single DR is added, there is no issue on the attribution of cost. However, if several DRs are installed – more or less at the same time – it may not be clear as to who should pay for upgrade costs. The envisioned concept is that costs associated with the purchase and installation of circuit protection hardware, including circuit breakers, shall be evaluated at the time that the added DRs are commissioned. Only synchronous generator DRs are addressed in this chapter – although inverter based DRs are predominant at the lower power levels. The issues of inverter based DRs deserve special attention.

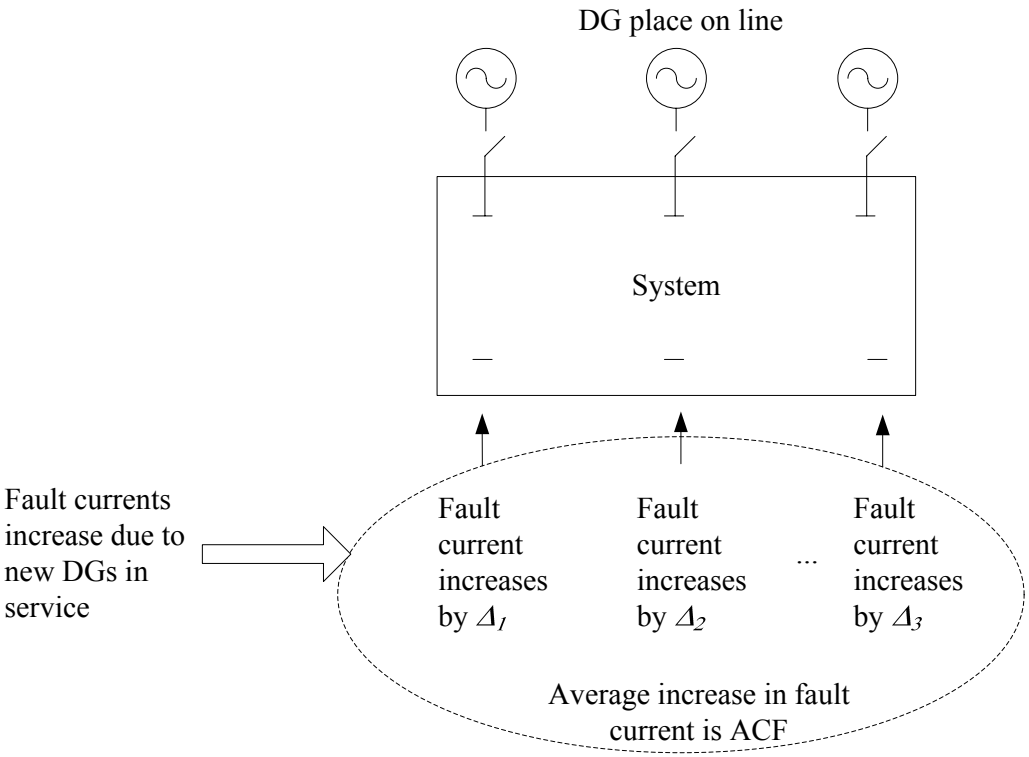

Figure 5.1 Concept of "ACF"

One of the applications of ACF is to indicate the severity of the increase of fault currents in the system due to the installation of each DG or merchant plant. The least squares method for calculating the ACF is discussed in the following sections.

5.3 Least squares estimate of ACF

The ACF index, however, is not simply calculated because several complex subprocedures must be done. One way to reduce complexity is to create an estimator of the ACF for a given system on the basis of several previously analyzed cases. Figure 5.2 shows the approach. Details of the least squares estimate of ACF are discussed as follows.

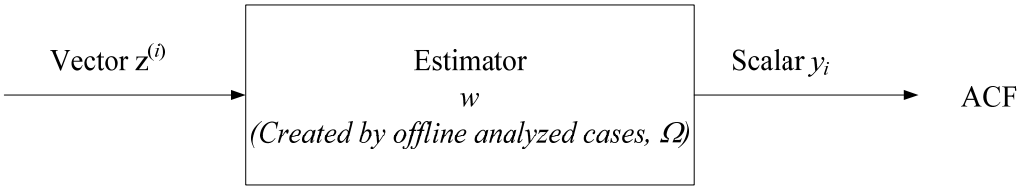

Figure 5.2 System diagram of a least square estimator

In Fig. 5.2, offline, previously calculated cases are denoted as the set Ω. In each of the cases in Ω, a datum vector $z^{(i)}$ is used. The superscript (i) refers to the sample number. When the vectors $z^{(i)}$ are arranged column by column in a matrix, for all cases in Ω, the matrix Z results. Similarly, the ACF resulting from the use of vector $z^{(i)}$ is denoted as the scalar value y_i. When all the case results in Ω are arranged in a matrix, the vector y results. The question of how y_i is related to $z^{(i)}$ (for case i in Ω) is now considered. Let several functions of $z^{(i)}$ appear in a linear combination to generate y_i

$$y_i = \text{Linear combination } \{f_1(\mathbf{z^{(i)}}), f_2(\mathbf{z^{(i)}}), \ldots\}. \tag{5.2}$$

The f_k functions may be linear or nonlinear. But (5.2) is a linear combination of the $f_k(Z^{(i)})$ scalar functions.

At this point, relate the linear combination concept above to the calculation of ACF. Note that the ACF in case i (in Ω) depends on the impedance of newly added DGs at m different locations. That is, m DGs are added, and the ACF is calculated. Then [78],

$$y_i = ACF_i = \sum_{j=1}^{k}\sum_{\ell=1}^{m} w_{j,\ell} f_j\left(z_{DG,\ell}^{(i)}\right). \tag{5.3}$$

In (5.3), $w_{j,\ell}$ denotes the linear combination coefficients mentioned in (5.2). The intent is that the y_i be a formula for ACF in case i, and the formula should have constant

coefficients (i.e., the $w_{j,\ell}$ coefficients are not a function of *i*). Also note in (5.3) that *k* is the number of functions used in the linear combination shown in (5.2). For example, if $k = 2$, y_i is a linear combination of $f_1(z_{DG,\ell})$ and $f_2(z_{DG,\ell})$ for all newly added DGs.

Consider of cases in the sample ensemble Ω. That is, in (5.3), $i = 1, 2, \ldots, q$. From the vector *y* as a *q*–vector of calculated ACF values in each of the *q* cases in Ω. Then, the method of minimum least squares is to minimize the scalar residual *r*,

$$r^2 = \left(y_i - \sum_{j=1}^{k} \sum_{\ell=1}^{m} w_{j,\ell} f_j(z_{DG,\ell}^{(i)}) \right)^2 . \tag{5.4}$$

Note that when $r = 0$, all ACF values in Ω calculated by (5.3) agree with the correct (full calculations) values y_i. The $w_{j,\ell}$ coefficients may be arranged in a vector as follows

$$w = \begin{bmatrix} w_{1,1} & w_{1,2} & w_{1,3} & \cdots & w_{1,m} & w_{2,1} & w_{2,2} & \cdots & w_{2,m} & w_{3,1} & \cdots & w_{k,m} \end{bmatrix}' .$$

Thus, Equation (5.3) can be written as

$$ACF = y = F w \tag{5.5}$$

and the least squares estimate of the vector of linear combination coefficients, $\hat{w}$, is

$$\hat{w} = F^{+} y \tag{5.6}$$

where F^{+} denotes the pseudoinverse. For this case, F^{+} is $(F'F)^{-1}F'$ [37, 79], and *F* is a *q* by *mk* matrix,

$$F = \begin{array}{c} \longleftarrow mk \longrightarrow \\ \\ q \\ \\ \end{array} \begin{bmatrix} f_1(z_{DG,1}^{(1)}) & f_1(z_{DG,2}^{(1)}) & \cdots & f_1(z_{DG,m}^{(1)}) & f_2(z_{DG,1}^{(1)}) & \cdots & f_k(z_{DG,m}^{(1)}) \\ f_1(z_{DG,1}^{(2)}) & & & \cdots & & & f_k(z_{DG,m}^{(2)}) \\ \vdots & & & \ddots & & & \vdots \\ f_1(z_{DG,1}^{(q)}) & & & \cdots & & & f_k(z_{DG,m}^{(q)}) \end{bmatrix} \tag{5.7}$$

where $z_{DG,a}^{(b)}$ refers to the impedance of a newly added DG at bus *a* for case *b* in $\{\Omega\}$. References [77, 79] document the unbiased least squares approach indicated by (5.6). To review, Equation (5.6) is

$$\hat{w} = \text{Estimate of } w$$

$$= F^{+} y \ .$$

where $\hat{w}$ is a *mk* vector, *y* is *q* vector and F^{+} is *q* by *mk* matrix. To assist the reader in following the mathematics, Table 5.1 is offered.

In the foregoing, the general case of *k* terms is used to estimate ACF for each newly added DG bus. The selection of *k* and the functional forms of the $f_j, j = 1,\ldots, k$ terms in (5.3) need to be made.

In this application, the least squares estimator is applied to calculate the ACF of the system corresponding to the impedance of DGs as shown in Fig. 5.2. The unknown system can be modeled as the following functions that are linear in the *w* terms [78],

First order ($k = 1$): $$ACF_i = y_i = \sum_{\ell=1}^{m} w_{1,\ell} \cdot \left| z_{DG,\ell}^{(i)} \right| \qquad (5.8a)$$

Second order ($k = 2$): $$ACF_i = y_i = \sum_{\ell=1}^{m} w_{1,\ell} \cdot \left| z_{DG,\ell}^{(i)} \right| + \sum_{\ell=1}^{m} w_{2,\ell} \cdot \left| z_{DG,\ell}^{(i)} \right|^2 \qquad (5.8b)$$

Third order ($k = 3$):

$$ACF_i = y_i = \sum_{\ell=1}^{m} w_{1,\ell} \cdot \left| z_{DG,\ell}^{(i)} \right| + \sum_{\ell=1}^{m} w_{2,\ell} \cdot \left| z_{DG,\ell}^{(i)} \right|^2 + \sum_{\ell=1}^{m} w_{3,\ell} \cdot \left| z_{DG,\ell}^{(i)} \right|^3 \qquad (5.8c)$$

Reciprocal of $\left| Z_{DG,\ell} \right|$ ($k = 1$): $$ACF_i = y_i = \sum_{\ell=1}^{m} w_{1,\ell} \cdot \left| z_{DG,\ell}^{(i)} \right|^{-1} \qquad (5.8d)$$

Reciprocal of $\left| Z_{DG,\ell} \right|$ squares ($k = 2$) :

$$ACF_i = y_i = \sum_{\ell=1}^{m} w_{1,\ell} \cdot \left| z_{DG,\ell}^{(i)} \right|^{-1} + \sum_{\ell=1}^{m} w_{2,\ell} \cdot \left| z_{DG,\ell}^{(i)} \right|^{-2} \qquad (5.8e)$$

Table 5.1 Dimensions of several quantities used in the least squares estimation of ACF

Quantity		Rows	Columns
r	Residual of the least squares estimation	1	1
y	Vector of output data from linear combination	mk	1
y_i	Value of ACF	1	1
$f_1, f_2, \ldots$	Functions used to approximate ACF	1	1
$z^{(i)}$	Vector of input data for estimate, case (i)	m	1
Z	Matrix of input data for estimate, all case	q	m
$w_{j\ell}$	Element of vector w, linear combination coefficient	1	1
w	Linear combination coefficient	mk	1
F	Relationship matrix	q	mk
F^+	Pseudoinverse of relationship matrix	q	mk
$\hat{w}$	Estimate of linear combination coefficient	mk	1
m	Number of bus with possibly DG added	1	1
k	Order of the ACF model	1	1
q	Number of case in Ω	1	1

Reciprocal of $\left|Z_{DG,\ell}\right|$ cubes ($k = 3$) :

$$ACF_i = y_i = \sum_{\ell=1}^{m} w_{1,\ell} \cdot \left|z_{DG,\ell}^{(i)}\right|^{-1} + \sum_{\ell=1}^{m} w_{2,\ell} \cdot \left|z_{DG,\ell}^{(i)}\right|^{-2} + \sum_{\ell=1}^{m} w_{3,\ell} \cdot \left|z_{DG,\ell}^{(i)}\right|^{-3} \tag{5.8f}$$

where $z_{DG,\ell}^{(i)}$ is the impedance of the added DGs in case i and $w_{1,\ell}$, $w_{2,\ell}$ and $w_{3,\ell}$ is the coefficient of the first, the second and the third order, respectively.

Calculation of the linear coefficient vector, $w_{j,\ell}$, used in (5.6) is comparable to the parameter estimation techniques [37, 79]. Equation (5.5) from the least squares method can be written in the state estimation sense as,

$$Hx = z \ ,$$

where x or the coefficients of linear function is equivalent to the coefficient vector, w, the incident matrix H is equivalent to the relationship matrix F shown in (5.7) and z or the vector of measured values is equivalent to the vector of the ACF.

5.4 Application of the least squares method to the Thunderstone system, Case 5.1

To illustrate the application of the proposed index, a sample system is used to demonstrate the potential economic impact due to the high levels of DG and merchant plant penetration. The Thunderstone system as shown in Fig. 3.4 is used as the test bed system to demonstrate the calculation of the coefficient matrix, W_{mk}, and an application of the ACF index. Details of the Thunderstone system are discussed in Chapter 3. All system parameters are shown in Appendix A. By applying the reciprocal of $|Z_{DR}|$ cubes model,

$$ACF_i = y_i = \sum_{\ell=1}^{m} w_{1,\ell} \cdot \left| z_{DG,\ell}^{(i)} \right|^{-1} + \sum_{\ell=1}^{m} w_{2,\ell} \cdot \left| z_{DG,\ell}^{(i)} \right|^{-2} + \sum_{\ell=1}^{m} w_{3,\ell} \cdot \left| z_{DG,\ell}^{(i)} \right|^{-3} \tag{5.9}$$

In this calculation, the least squares estimator model is created from 500 cases each with a different Z_{DR}. The impedances of DRs installed at 12 kV buses are pseudorandom, uniformly distributed. The transient impedances of each DR are in the range 0.005+j0.83 to 0.005+j0.92 per unit. From (5.9), the ACF model can be written as

$$ACF = \sum_{j=1}^{k} \sum_{i=1}^{m} w_{j,i} f_j\left(Z_{DR,i}\right) = FW$$

where f_j is a function applied in the power series (i.e., $\left|Z_{DR}\right|^{-k}$) and F is the matrix of $f_j(Z_{DR,i})$ terms. The coefficient vector, W, calculated using the least squares method is $W = \left(F'F\right)^{-1} F'\left(ACF\right)$. This is comparable to the parameter estimation technique in [37].

Assume that the DGs are installed at 6 locations: Cameron2, Signal3, Seaton2, Ealy3, Ealy4 and Sage3. The transient impedances of each DG are shown in Table 5.2.

Table 5.2 List of the buses with new DG in Case 5.1

Bus name	Transient impedance of the DG (p.u.)*
Cameron2 (6)	$0.005 + j0.81$
Signal3 (11)	$0.005 + j0.90$
Seaton2 (22)	$0.005 + j0.83$
Ealy3 (24)	$0.005 + j0.85$
Ealy4 (25)	$0.005 + j0.92$
Sage3 (26)	$0.005 + j0.84$

* Per unit based on 100 MVA, 12 kV

The coefficient vector of the model is calculated by applying (5.6). Note that the coefficient vector, *w*, can be separated into *k* groups depending on the order of each model. For example, in the reciprocal of $z_{DG,\ell}$ cubes ($k = 3$), the first order coefficient of the coefficient vector, $w_{1,\ell}$, is *m* by one sub-vector. For this reason, the coefficient vector, *w*, is *mk* by one vector. The coefficient vector, *w*, of the Thunderstone system is,

$$w = \begin{bmatrix} w_{1,\ell} & w_{2,\ell} & w_{3,\ell} \end{bmatrix}^T,$$

Where

$$w_{1,\ell} = \begin{bmatrix} 2.2048 \\ 2.5609 \\ 1.7878 \\ 2.3637 \\ 2.3148 \\ 2.7164 \\ 2.4916 \\ 2.3671 \\ 2.3834 \\ 2.6878 \\ 2.8195 \\ 2.8508 \\ 2.3576 \\ 2.2561 \end{bmatrix}, \quad w_{2,\ell} = \begin{bmatrix} -1.1148 \\ -1.2409 \\ -0.8427 \\ -1.1276 \\ -1.1037 \\ -1.1208 \\ -1.1090 \\ -1.1408 \\ -1.2601 \\ -1.2799 \\ -1.1144 \\ -1.4519 \\ -1.2003 \\ -1.1449 \end{bmatrix} \text{ and } \quad w_{3,\ell} = \begin{bmatrix} 0.2317 \\ 0.2641 \\ 0.1711 \\ 0.2298 \\ 0.2259 \\ 0.2100 \\ 0.2113 \\ 0.2252 \\ 0.2692 \\ 0.2643 \\ 0.2006 \\ 0.2991 \\ 0.2523 \\ 0.2447 \end{bmatrix}.$$

The impedance of the added DGs in this case is

$$|z_{DG}| = \begin{bmatrix} 0 & 0.81 & 0 & 0 & 0.90 & 0 & 0 & 0 & 0 & 0.83 & 0.85 & 0.92 & 0.84 & 0 \end{bmatrix}.$$

The ACF of the system from (5.8) is

$$ACF = y = \begin{bmatrix} 0.0000 \\ 1.2345 \\ 0.0000 \\ 0.0000 \\ 1.2500 \\ 0.0000 \\ 0.0000 \\ 0.0000 \\ 0.0000 \\ 1.2048 \\ 1.1765 \\ 1.0869 \\ 1.1905 \\ 0.0000 \end{bmatrix}^t \hat{w}_{1,\ell} + \begin{bmatrix} 0.0000 \\ 1.5241 \\ 0.0000 \\ 0.0000 \\ 1.5624 \\ 0.0000 \\ 0.0000 \\ 0.0000 \\ 0.0000 \\ 1.4515 \\ 1.3840 \\ 1.1814 \\ 1.4172 \\ 0.0000 \end{bmatrix}^t \hat{w}_{2,\ell} + \begin{bmatrix} 0.0000 \\ 1.8816 \\ 0.0000 \\ 0.0000 \\ 1.9530 \\ 0.0000 \\ 0.0000 \\ 0.0000 \\ 0.0000 \\ 1.7488 \\ 1.6282 \\ 1.2842 \\ 1.6871 \\ 0.0000 \end{bmatrix}^t \hat{w}_{3,\ell} \tag{5.10}$$

$$= 10.63\ \%.$$

Note that the ACF from the conventional fault calculation is 10.87 %. The error from the least squares estimator compared to the conventional fault calculation is 2.25 %.

The accuracy of the least squares model can be measured by the norm of the scalar residual r_i,

$$\frac{\|r\|}{\|F\hat{w}\|} = \frac{\|y - F\hat{w}\|}{\|F\hat{w}\|} \text{ p.u. },$$

where y is the vector ACF from the conventional fault calculation (full calculation).

In this calculation, the least squares estimator is created from 500 cases. The impedances of DGs installed at 12 kV buses are generated randomly under the same base MVA. Among the model in (5.8), the reciprocal of $Z_{DG,\ell}$ cubes shown in (5.8f) has the highest accuracy. The norm of the scalar residual of each model is shown in Table 5.3. The histogram of the residual from the least squares model is shown in Fig. 5.3.

Table 5.3 Norm of residual of Case 5.1

Model	Equation	Norm of residual*
First order	(5.8a)	0.135
Second order	(5.8b)	0.0432
Third order	(5.8c)	0.0127
Reciprocal of $\left\|z_{DG,\ell}\right\|$	(5.8d)	0.046
Reciprocal of $\left\|z_{DG,\ell}\right\|^2$	(5.8e)	0.00655
Reciprocal of $\left\|z_{DG,\ell}\right\|^3$	(5.8f)	0.00119

* expressed as a fraction, e.g., 0.135 = 13.4%

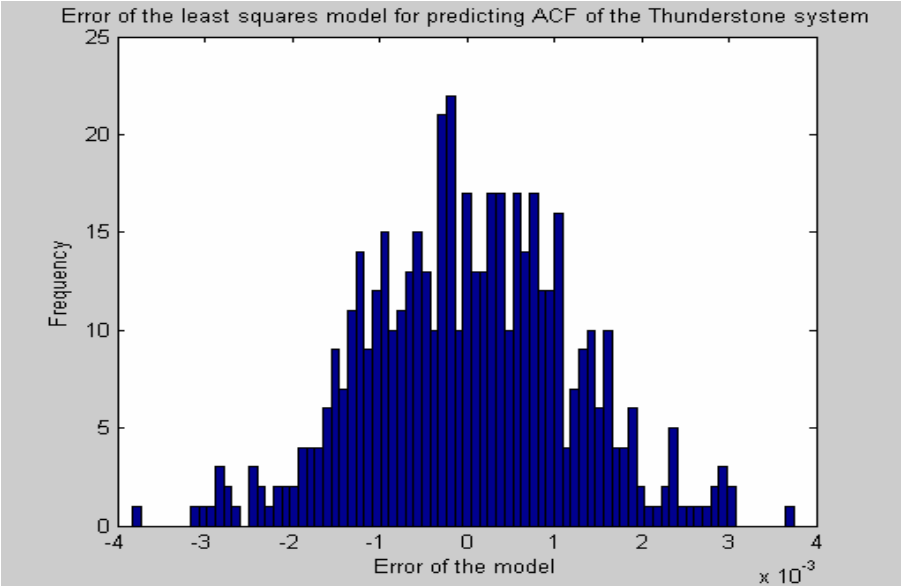

Figure 5.3 Residual of the least squares estimator, Case 5.1 (residual expressed as a fraction as in Table 5.3)

Note that (5.10) can be independently written as 14 components according to fourteen 12 kV buses. Each component $ACF_{(bus)}$, called "bus ACF", relates to the contribution of the DG to the total ACF. The plot of bus ACF and the total ACF is shown in Fig. 5.4. For instance, the contribution of the DG at bus 6 (Cameron2), 11 (Signal3), 22 (Seaton2), 24 (Ealy3), 25 (Ealy4) and 26 (Sage3) to ACF are

$$ACF_{(6)} = 2.5609 \cdot \frac{1}{|z_{DG,6}|} - 1.2409 \cdot \frac{1}{|z_{DG,6}|^2} + 0.2641 \cdot \frac{1}{|z_{DG,6}|^3}, \quad (5.11a)$$

$$ACF_{(11)} = 2.3148 \cdot \frac{1}{|z_{DG,11}|} - 1.1037 \cdot \frac{1}{|z_{DG,11}|^2} + 0.2259 \cdot \frac{1}{|z_{DG,11}|^3}, \quad (5.11b)$$

$$ACF_{(22)} = 2.6878 \cdot \frac{1}{|z_{DG,22}|} - 1.2799 \cdot \frac{1}{|z_{DG,22}|^2} + 0.2643 \cdot \frac{1}{|z_{DG,22}|^3}, \quad (5.11c)$$

$$ACF_{(24)} = 2.8195 \cdot \frac{1}{|z_{DG,24}|} - 1.1144 \cdot \frac{1}{|z_{DG,24}|^2} + 0.2006 \cdot \frac{1}{|z_{DG,24}|^3}, \quad (5.11d)$$

$$ACF_{(25)} = 2.8508 \cdot \frac{1}{\left|z_{DG,25}\right|} - 1.4519 \cdot \frac{1}{\left|z_{DG,25}\right|^2} + 0.2991 \cdot \frac{1}{\left|z_{DG,25}\right|^3}, \quad (5.11e)$$

$$ACF_{(26)} = 2.3576 \cdot \frac{1}{\left|z_{DG,26}\right|} - 1.2003 \cdot \frac{1}{\left|z_{DG,26}\right|^2} + 0.2523 \cdot \frac{1}{\left|z_{DG,26}\right|^3}. \quad (5.11f)$$

Figure 5.4 shows the comparison of the least squares estimator model and the conventional fault calculation. The accuracy of the least squares estimator when the DG transient impedance lies between *j*0.5 to *j*1.5 p.u., which is the usual range, is tolerable. Reasons for the error are:

- the historical data used to create the model range from *j*0.5 to *j*1.5 p.u.
- the pre-fault voltage is not included into the model. However, while calculating the historical data, the pre-fault voltages after installing DGs are updated and applied to the fault current calculation. For this reason, results of the pre-fault voltages after installing DGs are also included into the calculation of the ACF.

5.5 Confidence interval of the least squares estimator coefficient

Assuming that the residuals of the least squares estimator are normally and independently distributed with mean zero and variance, σ_r^2. The linear coefficient vector, $\hat{w}$, is normally distributed with the mean vector *w* and the covariance matrix $\sigma_r^2 (F'F)^{-1}$. For the same reason, the marginal distribution of any least squares estimator, $\hat{w}_{j,\ell}$, is normal with mean $w_{j,\ell}$ and variance $\sigma_r^2 C_{jj}$, where C_{jj} is the *j*th diagonal element of the $(F'F)^{-1}$ matrix.

Therefore, the 100(1-α) percent confidence interval for the least squares estimator coefficient $w_{j,\ell}$ is [77]

$$\hat{w}_{j,\ell} - t_{\alpha/2,n-p}\sqrt{\hat{\sigma}_r^{\,2} C_{ii}} \le w_{j,\ell} \le \hat{w}_{j,\ell} + t_{\alpha/2,n-p}\sqrt{\hat{\sigma}_r^{\,2} C_{ii}}\,, \qquad (5.12)$$

where $t_{\alpha/2,n-p}$ is the value from *t*-distribution, *n* is the number of all historical data, *p* is number of coefficient of the least squares estimator and $\hat{\sigma}_r^{\,2}$ is the estimation of variance of residual. The estimation of variance of residual, $\hat{\sigma}_r^{\,2}$ is,

$$\hat{\sigma}_r^{\,2} = \frac{SS_{\mathrm{Res}}}{n-p} = \frac{y'y - \hat{w}'F'y}{n-p},$$

where SS_{Res} is the residual sum of squares [77].

Applying (5.12), the 95 percent confidence intervals on the coefficient of the ACF model for the Thunderstone system, Case 5.1, are shown in Table 5.4

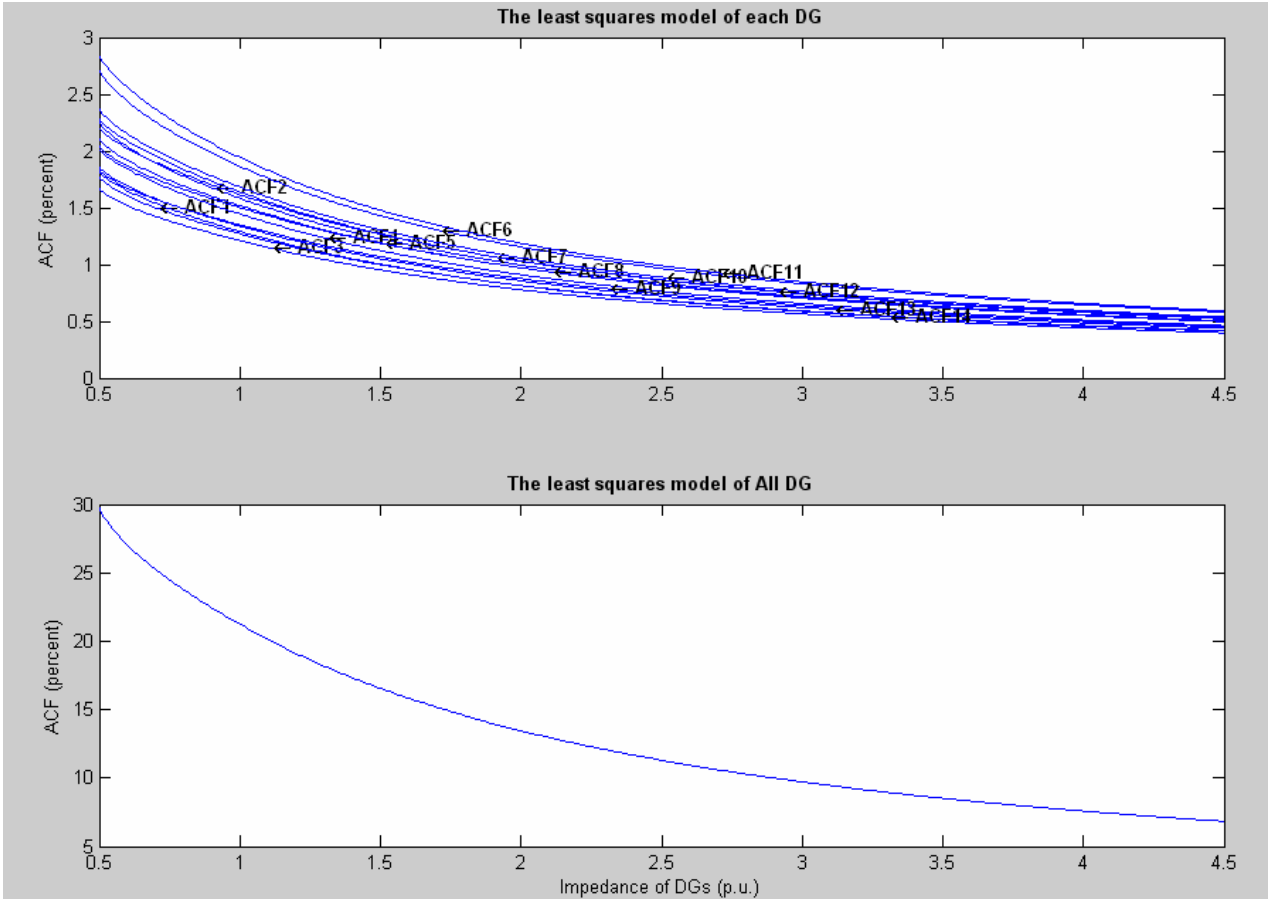

Figure 5.4 Plot of the bus ACF and the total ACF, Case 5.1

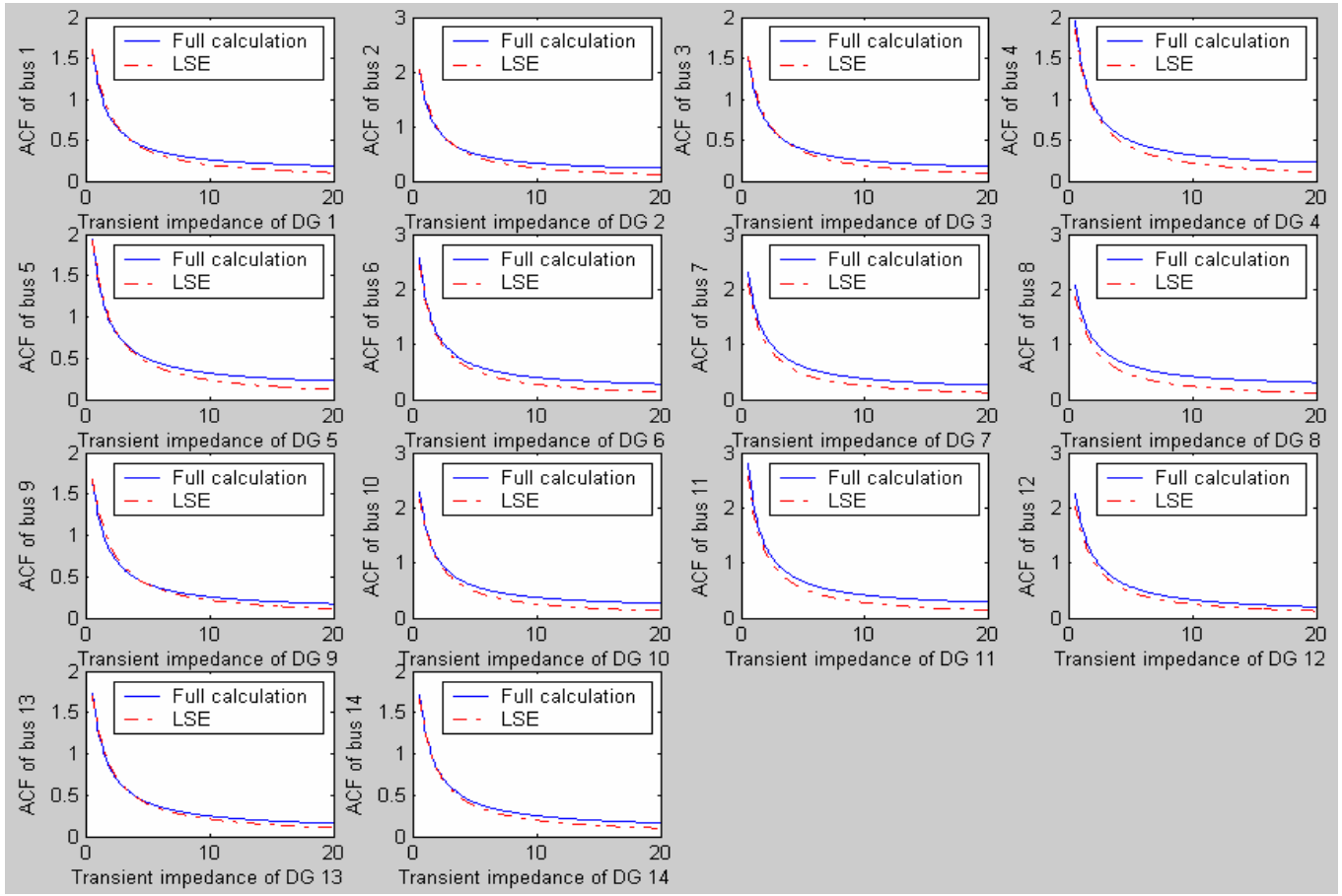

Figure 5.5 Comparison between the full fault calculation and the least squares estimator model, Case 5.1

5.6 Confidence interval estimation of the mean response of ACF

Define a particular situation when the input of the ACF model is

$$f_0 = [f_1(z_{DG,1}^{(0)}) \quad \cdots \quad f_1(z_{DG,m}^{(0)}) \quad f_2(z_{DG,1}^{(0)}) \quad \cdots \quad f_2(z_{DG,m}^{(0)}) \quad f_3(z_{DG,1}^{(0)}) \quad \cdots \quad f_3(z_{DG,m}^{(0)})].$$

For example, if considering the reciprocal of $\left|z_{DG,\ell}\right|^3$ as the ACF model, the input matrix of the ACF model is,

$$f_0 = [\left|z_{DG,1}\right|^{-1} \quad \cdots \quad \left|z_{DG,m}\right|^{-1} \quad \left|z_{DG,1}\right|^{-2} \quad \cdots \quad \left|z_{DG,m}\right|^{-2} \quad \left|z_{DG,1}\right|^{-3} \quad \cdots \quad \left|z_{DG,m}\right|^{-3}].$$

The ACF value can be estimated as $\hat{ACF}$ at a particular point by applying (5.8f),

$$\hat{ACF} = \hat{y} = \sum_{\ell=1}^{m} \hat{w}_{1,\ell} \cdot \left|z_{DG,\ell}\right|^{-1} + \sum_{\ell=1}^{m} \hat{w}_{2,\ell} \cdot \left|z_{DG,\ell}\right|^{-2} + \sum_{\ell=1}^{m} w_{3,\ell} \cdot \left|z_{DG,\ell}\right|^{-3}.$$

The variance of the $\hat{ACF}$ is

$$Var(\hat{ACF}) = \sigma^2 f_0'(F'F)^{-1} f_0.$$

Therefore, the 100(1-α) percent confidence interval on the mean response of the ACF model with f_0 as the input is [64],

$$\hat{ACF}_0 - t_{\alpha/2,n-p}\sqrt{\hat{\sigma}_r^{\,2} f_0'(F'F)^{-1} f_0} \le E(ACF|f_0) \le \hat{ACF}_0 + t_{\alpha/2,n-p}\sqrt{\hat{\sigma}_r^{\,2} f_0'(F'F)^{-1} f_0}\,. \tag{5.13}$$

For instance, the 95 percent confidence interval of the ACF of the Thunderstone system with new DGs shown in Table 5.2 for Case 5.1 is,

$$10.63 - t_{0.025,467}\sqrt{\hat{\sigma}_r^{\,2} f_0'(F'F)^{-1} f_0} \le E(ACF|f_0) \le 10.63 + t_{0.025,467}\sqrt{\hat{\sigma}_r^{\,2} f_0'(F'F)^{-1} f_0}\,,$$

or

$$10.53 \le E(ACF|f_0) \le 10.819\ \%\,.$$

Table 5.4 Confidence interval of the Coefficient of the ACF model, Case 5.1

Model coefficient, $w_{j,\ell}$	Ninety five percent Confidence interval	95% confidence interval / Coefficient $w_{j,\ell}$
2.2048	± 0.2650	0.1202
2.5609	± 0.2433	0.0950
1.7878	± 0.2457	0.1374
2.3637	± 0.2564	0.1085
2.3148	± 0.2470	0.1067
2.7164	± 0.2310	0.0850
2.4916	± 0.2503	0.1005
2.3671	± 0.2548	0.1076
2.3834	± 0.2554	0.1072
2.6878	± 0.2830	0.1053
2.8195	± 0.2372	0.0841
2.8508	± 0.2695	0.0945
2.3576	± 0.2477	0.1051
2.2561	± 0.2572	0.1140
-1.1148	± 0.2195	0.1969
-1.2409	± 0.2001	0.1613
-0.8427	± 0.2009	0.2384
-1.1276	± 0.2126	0.1885
-1.1037	± 0.2021	0.1831
-1.1208	± 0.1879	0.1676
-1.1090	± 0.2057	0.1855
-1.1408	± 0.2113	0.1852
-1.2601	± 0.2104	0.1670
-1.2799	± 0.2342	0.1830
-1.1144	± 0.1945	0.1745
-1.4519	± 0.2254	0.1552
-1.2003	± 0.2052	0.1710
-1.1449	± 0.2126	0.1857
0.2317	± 0.0579	0.2499
0.2641	± 0.0523	0.1980
0.1711	± 0.0521	0.3045
0.2298	± 0.0559	0.2433
0.2259	± 0.0526	0.2328
0.2100	± 0.0485	0.2310
0.2113	± 0.0537	0.2541
0.2252	± 0.0556	0.2469
0.2692	± 0.0552	0.2051
0.2643	± 0.0617	0.2334
0.2006	± 0.0505	0.2517
0.2991	± 0.0601	0.2009
0.2523	± 0.0541	0.2144
0.2447	± 0.0559	0.2284

There is ninety five percent probability that the true ACF of Case 5.1 stays in the indicated interval. Table 5.5 shows the confidence interval of the mean response of the ACF model with various percent confidence, α.

Table 5.5 Percent confidence and their confidence intervals for the mean response of the ACF of the Thunderstone system, Case 5.1

Percent confidence	Confidence interval, $E(ACF\|f_0)$
98	10.63 ± 0.21 %
95	10.63 ± 0.18 %
90	10.63 ± 0.15 %
80	10.63 ± 0.12 %

5.7 Allocation of the responsibility for the system upgrades to the owner of DGs

This section proposes a technique to allocate the responsibility of each DG owner due to the system upgrades by applying the ACF index. Theoretically, the owner of DGs should share the cost for the system upgrades, depending on the severity of the change of fault created by their own DGs. According to the illustrated system, six DGs are installed at the subtransmission or primary distribution bus. From conventional fault current calculations, as the consequence of installing these DGs, the CBs at 2 locations need to be upgraded. The contributions of the DG at each bus are calculated as in (5.11).

The owners of DG should pay for the cost of upgrading the protection system,

such as IC of CBs and fuses, proportional to the ACF_i. For this reason, the cost for each owner of DG is distributed according to the following allocation,

Price to the owner of DG at bus *i*

$$= \frac{\text{Total cost for upgrades system}}{\sum_{i}^{N} ACF_i} \cdot ACF_i , \tag{5.14}$$

where *N* is the number of the bus with DG.

Assuming that the cost of upgrading the CB at each of two locations is 50,000 dollars, that is, the total upgrade cost is 100,000 dollars. Then, the costs of upgrading the system for each owner of a DG are shown in Table 5.6.

Table 5.6 Cost for upgrades the system due to installing new DGs

Bus name	Cost of upgrading the system, dollars
Cameron2 (6)	16,639.98
Signal3 (11)	15,161.50
Seaton2 (22)	17,355.68
Ealy3 (24)	19785.29
Ealy4 (25)	16,639.98
Sage3 (26)	14,417.55

In (5.14), it is assumed that the entire CB upgrade costs should be assigned to the DG owners. If some fraction *F* of the total cost is to be paid by the utility company, then 1-*F* is paid by the DG owner,

Price to the owner of DG at bus *i*

$$= (1 - F) \cdot \frac{\text{Total cost for upgrades system}}{\sum_{i}^{N} ACF_i} \cdot ACF_i .$$

5.8 Conclusion

This chapter proposes the average change of fault current or ACF index which can be used to quantify the change of fault current in a system upon the commission of DG. The least squares technique is applied to estimate the ACF. The illustrative example in this chapter focuses on the application of the ACF index to quantify the contribution of fault current from the installation of DGs. The error of the least squares method to estimate ACF as compared to the full calculation is in the range of 5 percent.

The cost of system upgrades due to the installation of DGs can be allocated by using the method in Section 5.7. The cost of upgrades the system for each owner of DG mainly depends on the transient impedance of the DGs and the configuration of the system.

CHAPTER 6

IMPLICATION OF FAULT CURRENT ON UNIT COMMITMENT

6.1 Introduction

This chapter introduces a study on the implications of operating economics imposed by increased fault current due to the addition of DGs and/or merchant plans to a power system. In some cases, especially when the system has high penetration level, the fault current after connecting these generation sources may be higher than the interrupting capability of some circuit breakers (CBs) in the system. This means that the CBs may fail to interrupt fault current and may create a safety hazard.

Increased system fault currents resulting from DG installation and the effects of increased fault currents on operating economics is discussed in this chapter. A technique used to evaluate the unit commitment (UC) with fault level constraint after installing DGs is analyzed, and an example is given.

Unit commitment is the problem of determining the optimal schedule of committing (i.e., making available for dispatch) generation subject to operating constraints. The operating constraints include minimum start up / shut down times and the generator maximum and minimum limits. The general objective of the UC problem is to minimize the system total operating cost while satisfying all of the constraints so that a given security level can be met. Fault level constraints (FLCs) are considered as one of the constraints in the UC problem.

6.2 UC problem formation

The UC problem is to find the schedule up / down (i.e., commit / decommit) for available units and their generation levels at each period of time in the time horizon. This is done in order to minimize the total operating cost (OC) while satisfying various constraints.

Objective function

The UC problem can be formulated as,

$$OC = \min \sum_{t}^{T} \sum_{I=1}^{L} [\mathrm{P}_{\mathrm{cost}}(\mathrm{t}, \mathrm{I}) + \mathrm{S}_{\mathrm{cost}}(\mathrm{t}\text{-}1, \mathrm{J} : \mathrm{t}, \mathrm{I})]$$

where

- Production cost can be modeled as a quadratic function,

$$P_{cost}(t, I) = \sum_{i}^{I} \left(a_i + b_i P_{it} + c_i P_{it}^{\,2} \right).$$

- Transition cost, S_{cost} is the total start up / shut down cost of each unit of the time *t*. The start up cost depends on the number of hours it has been off-line (hot start/cold start).

Constraints

The constraints for the problem are,

- Power flow equation of the power network
- The inequality constraint on reactive power generation at each *PV* bus. The reactive power output must stay in the specific range,

$$Q_i^{\min} < Q_i < Q_i^{\max}.$$

- The inequality constraint on voltage magnitude $|V|$ of each PQ bus

$$V_i^{\min} < V_i < V_i^{\max}.$$

- Unit generation limits: generation of unit *i* at time *t* is limited by minimum and maximum physical and operational limits,

$$G_{it}^{\min} < G_{it} < G_{it}^{\max}.$$

- Spinning reserve constraint: the spinning reserve is the total amount of power generation available from all units minus the present load and losses. The reserve is a specified amount or percent of the forecasted peak demand of each period.

$$\sum_{i=1}^{N} P_{\max,i} \cdot U_{it} \geq Load_t + R_t.$$

In this illustration, the spinning reserved is fixed at 10 percent of the forecasted peak demand

- Fault current level constraints: three phase fault currents $\left|I_{fi}\right|$ can be calculated by applying (3.2) and (3.3), where

$$|I_{fi}| < IC_i.$$

- Unit minimum up and down time constraints. Once the unit is running or decommited, there is a minimum time before changing its status.

$$Ton_i \geq Tup_i$$

and

$$Toff_i \geq TDown_i.$$

Short term commitment schedules

Unit commitment is frequently done on a weekly or monthly basis with a time resolution of about one hour. For small generating units such as DGs, a smaller time resolution might be used, and a much shorter time horizon may be employed. In the subsequent section, some experimental results are shown utilizing a time resolution of one hour and a time horizon for the study of one day. The examples are intended as illustrations but the time resolution and horizon may not be illustrative of all DG applications.

6.3 Illustrative examples

To illustrate the results from a dynamic programming / unit commitment study (DPUC), a 24 hour schedule of the test bed system (see Fig. 3.1) is used to demonstrate the potential economic impact due to the high levels of DG and merchant plant penetration. The Thunderstone system is used as the test bed system. Details of the Thunderstone system are discussed in Section 3.1. All parameters are shown in Appendix A.

In this demonstration, eight DGs are installed at the 12 kV buses of the sample system. The CBs at the bus with DGs is assumed to be upgraded by the owners. It is assumed that the power delivered from the grid is limited at 200 MVA. Tables 6.1-6.3 show the data of several DGs and merchant plants. Note that the per unit reactances are given on the DG unit base.

The results of the DPUC study are shown in the Tables 6.5-6.6. In Table 6.5, the following factors are modeled:

- Minimum start up and shut down times

- Operating cost using a quadratic cost function
- Start up and shut down costs
- Spinning reserve requirements
- Distinction between hot start and cold start in start up costs.

With reference to the Tables 6.5 and 6.6, in Table 6.5, a '0' denotes a decommitted unit, and '1' denotes a committed unit. The system demand is listed in Table 6.5 as 'load'. Losses are not modeled for this study. Note that 'spinning reserve' requirements are 10% of the forecast demand. Table 6.4 lists the location of DG used in this study.

Table 6.1 Generating unit characteristics

Unit#	Min (MW)	Max (MW)	Hot start Cost ($)	Cold start Cost ($)	Cold start Time (h)	Shut Down Cost ($)
Grid	-	200	-	-	-	-
1	3	11	150	500	3	150
2	3	10	120	450	3	130
3	1	8	130	400	3	110
4	3	15	170	620	2	150
5	1	7	35	130	2	90
6	3	12	250	500	4	160
7	1	6	30	100	5	20
8	5	13	45	150	3	125

Table 6.2 Unit fuel costs

Unit#	Initial conditions Hours off line (-) Hours on line (+)	Cost coefficients*		
		a_i	b_i	c_i
Grid	-	450	4.500	0.03653
1	2	580	9.910	0.00690
2	1	600	10.100	0.00630
3	3	720	12.500	0.01850
4	-1	481	9.210	0.00487
5	-1	580	11.300	0.00900
6	-1	550	9.810	0.00620
7	2	610	11.500	0.00800
8	3	575	9.950	0.00650

*The units of the a_i are dollars, the b_i are in \$/MWh, and the c_i are in \$/(MW)^{2}h

Table 6.3 Unit transient impedances X'_d

New DG at bus	DGs impedance (per unit)*	Machine rating (MVA)
6	$0.005 + j0.40$	11.0
11	$0.005 + j0.30$	10.1
15	$0.005 + j0.37$	8.3
16	$0.005 + j0.25$	15.0
22	$0.005 + j0.59$	7.1
24	$0.005 + j0.33$	12.2
25	$0.005 + j0.65$	6
26	$0.005 + j0.35$	13.0

* per unit based on the machine rating and 12.47 kV

Table 6.4 Location and type of DG used in sample study

DG number	DG location (bus number)
1	Cameron2
2	Signal13
3	Super14
4	Super15
5	Seaton2
6	Early3
7	Early4
8	Sage3

When fault current limitations are added to the DPUC, the unit commitment will change. This occurs because in the progress of the dynamic programming algorithm, each state is checked versus fault current maxima. That is, for every state in the dynamic programming chart, the fault currents at all system busses are calculated. If a fault current exceeds the IC_i (which come from the design of the fault current interruption equipment), the DPUC state is considered to be a 'forbidden state'. The results of the modified DPUC are shown in Table 6.6.

Table 6.5 Unit scheduling: without fault current limitation

Period	Status									Max Gen	Load	Cost	Total
	Grid	1	2	3	4	5	6	7	8	(MW)	(MW)	($)	Cost ($)
1	1	0	0	0	0	0	0	0	0	200.0	155.1	2561.7	2561.7
2	1	0	0	0	1	0	0	0	0	215.0	195.0	3683.8	6245.5
3	1	0	0	0	1	0	0	0	0	215.0	195.3	3069.1	9314.7
4	1	0	0	0	1	0	1	0	0	227.0	196.0	4542.7	13357.3
5	1	0	0	0	1	0	1	0	0	227.0	197.0	4559.6	16916.9
6	1	0	0	0	1	0	1	0	1	240.0	210.0	5265.0	21331.9
7	1	0	0	0	1	0	1	0	1	240.0	212.0	5299.0	25631.0
8	1	1	0	0	1	0	1	0	1	251.0	226.0	6040.4	31171.3
9	1	1	0	0	1	0	1	0	1	251.0	227.2	5061.2	36232.5
10	1	1	0	0	1	1	1	0	1	258.0	230.5	6656.9	42019.5
11	1	1	0	0	1	1	1	0	1	258.0	231.5	6674.1	47693.5
12	1	1	0	0	1	1	1	0	1	258.0	230.2	6651.8	53345.3
13	1	0	0	0	1	0	1	0	0	227.0	162.2	4015.0	56725.3
14	1	0	1	0	1	0	1	0	0	237.0	215.1	4850.7	61576.0
15	1	1	0	0	1	0	1	0	1	251.0	220.3	5943.0	66844.0
16	1	1	0	0	1	0	1	0	1	251.0	226.5	5049.0	71893.1
17	1	1	0	0	1	0	1	0	1	251.0	225.2	6026.6	76919.6
18	1	1	0	0	1	0	1	0	1	251.0	228.1	5076.8	81996.5
19	1	1	0	0	1	0	1	1	1	257.0	230.1	6687.0	87783.5
20	1	0	0	0	1	0	1	0	1	240.0	215.5	5359.2	92312.6
21	1	0	0	0	1	0	1	0	1	240.0	214.1	5335.0	96647.7
22	1	0	0	0	1	0	1	0	1	240.0	212.1	5300.7	100948.4
23	1	0	0	0	0	0	0	0	0	200.0	175.4	2798.2	103746.5
24	1	0	0	0	0	0	0	0	0	200.0	160.5	2113.3	105859.8

As shown in the Tables 6.5 and 6.6, the total cost of operations for unit scheduling with and without the fault level constraints are 105,859.8 and 110627.6 $/day, respectively. Note that the unit scheduling of the systems are changed when the total MW capacity of each period is higher than 240 MW while in this example is period 6. In this period, the unit schedule when the FCL constraint is ignored are {1,0,0,0,1,0,1,0,1}. This unit combination violates the FCL constraint while {1,0,0,0,1,0,1,1,0} comply with the constraint but it is more expensive. Figure 6.1 shows the forecasted demand and total MW capacity in each period. The increase of fault current creates some forbidden states in DPUC which might be the cheapest path. For this reason, when including the FCL constraint, the smaller units with higher transient impedance and higher fuel cost are interconnected to serve the demand.

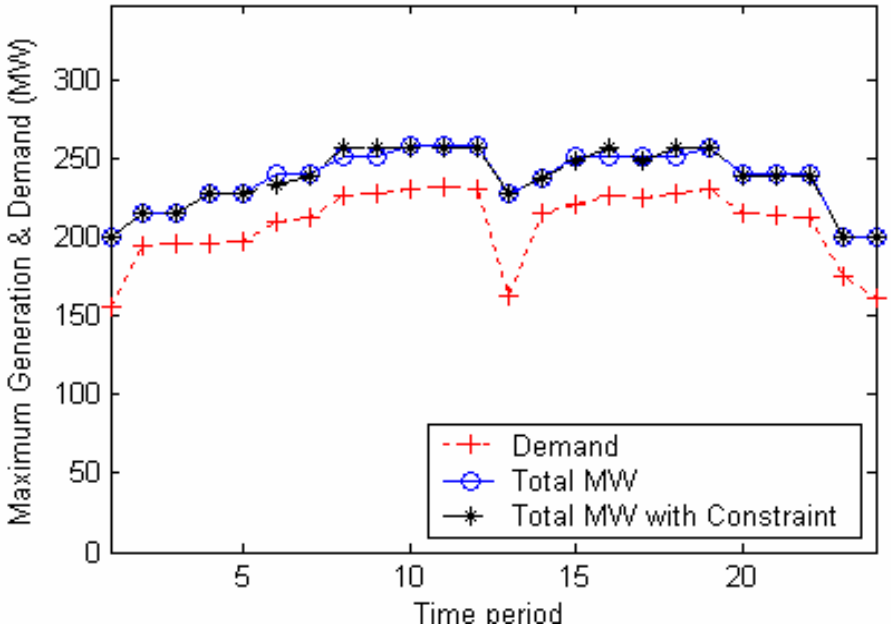

Figure 6.1 Total MW capacity committed and demand in each period

For the examples shown, a one hour time resolution is used, and the study is carried over a time horizon of 24 hours. Other (perhaps shorter, e.g., 30 minute) time resolutions might be used, and other time horizons (perhaps shorter, e.g., 6 hours) might be used depending on the specifics of the DG types, available load forecast, and start up / shut down cost characteristics.

6.4 Conclusions

There are advantages that arise from installing DGs in power systems, such as improving reliability, potentially improving power quality, and potentially enhancing the environment. However, a well planned system is also required to avoid problems from system generation capacity additions. The UC problem with fault level constraint is discussed in this chapter. The modification of system impedance matrix is utilized to evaluate increased fault currents.

Application of dynamic programming for solving the unit commitment problem with fault current level constraint is demonstrated. The case study shows that the generation of the merchant plants under the fault current level constraint may result in higher cost of operation than the operation without this constraint. For the example studied, about 5% increase in operating cost occurs when fault current limitations are included in the UC.

CHAPTER 7

COORDINATION OF PROTECTIVE RELAYS BY ARTIFICIAL ANT COLONY OPTIMIZATION

7.1 Artificial ant colony optimization

Artificial ant colony optimization (ACO) is a novel optimization algorithm which can be applied to solve discontinuous or nonlinear constrained optimization problems. The ACO is inspired by the behavior of real ant colonies. The ACO algorithm is introduced by Dorigo and Maniezzo in [65] to solve the symmetric/asymmetric traveling salesman problem (TSP).

The core of the ACO technique is to apply a parallel search by a set of agents, called *ants*. The agents or ants search for a good solution. At the same time, real ants coordinate their activities by applying indirect communication via the use of chemicals produced by the ants. These chemicals are called *pheromones*. In fact, many ant species are completely blind; ants communicate among the individuals by applying pheromone. By sensing the pheromone trails, ants can follow a path to food discovered by other ants. For the case of real ants, the shorter path for moving from the nest to food locations requires less time. For this reason, the amount of pheromone laid on the short path is higher than the longer path. Thus, the probability that ants will choose the shorter path is higher. This is equivalent to a better objective function in generic optimization problems. The shortest path from the nest to the food location is analogous to the best solution in an optimization problem. Figure 7.1 illustrates this point. The pheromone deposition and

foraging behavior of ants have been investigated by several researchers. Deneubourg, Gross, Franks, Detrain and Chretien in [80] propose a simple stochastic model that describes the dynamic model of an ant colony.

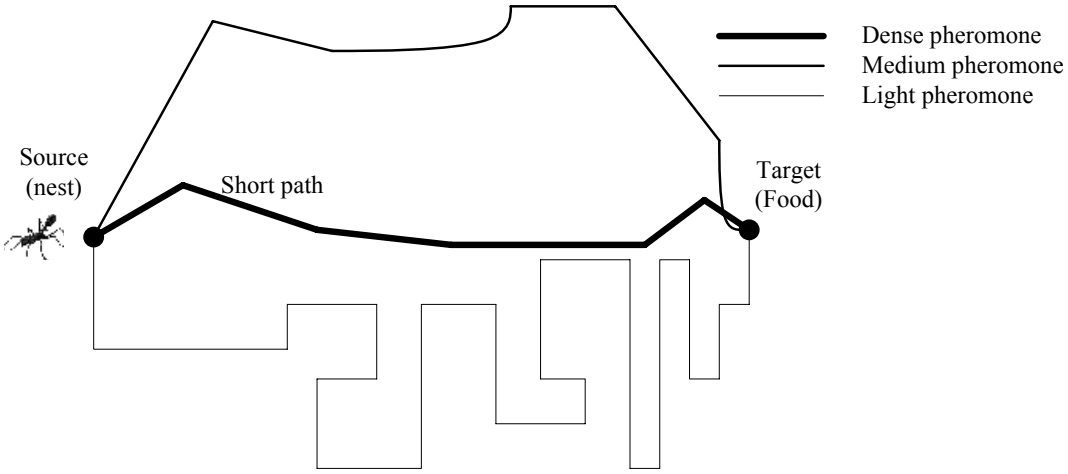

Figure 7.1 Illustration of search path in the ant colony algorithm

In this chapter, the ACO algorithm is applied to search for optimal settings of power system protective relays. The coordination of protective relays in power systems can be stated as a constrained discrete optimization problem. The objective of this optimization is to minimize the sum of the operation times of overcurrent relays and distance relays in power systems. The constraints in this optimization problem are the coordination interval (CI), limits of settings of relays, relay operating characteristics and bounds on operation times. References [62, 63] state the optimal coordination of the inverse time directional overcurrent relays (ITDOC) and solve the problem by a applying linear programming technique. Reference [64] states the optimal coordination of the mixed scheme protection between ITDOC relays and distance relays using a genetic algorithm.

Reference [65] relates to ACO applications in engineering, in general, and [67-69, 81] relate to power engineering in particular.

7.2 Formulation of the protective relaying coordination problem as an ACO problem

Typical protection systems consist of overcurrent relays and distance relays. In traditional methods, the setting and coordination of relays are done on each type individually [64].

In network systems with multiple sources, coordination of ITDOC relays becomes very complicated or impossible in some cases [74]. To solve this problem, a relay operating on the basis of voltage to current ratio or distance relay is recommended. The distance relay provides higher sensitivity to faults than using only overcurrent relay. During a three phase fault, the apparent impedance seen by distance relay decreases. ITDOC relays are applied in this design to demonstrate the application of ACO for coordinating the protective relays.

The protection system should be designed such that the primary protection sends the trip signal to the corresponding circuit breakers as fast as possible. In case the primary protection fails to operate, the back up protection should operate within a coordination interval (e.g., 0.2 to 0.3 s for distribution system [82]). The optimization technique discussed in this chapter is applied to setting the relays such that the coordination interval of relays is satisfied. Note that, in the distribution network, setting of relays must be done by taking into consideration of the effect on all protection system. The objective function of this optimization problem can be formulated as [64],

Minimize:

$$\text{Objective} = A * \sum_{k} \sum_{i} R_{ik} + B * \sum_{k} \sum_{j} CI_{jk} + C * \sum_{k} CV_{k}^{D} \tag{7.1}$$

Subject to:

$$R_{min} \leq R_{ik} \leq R_{max}$$

$$CI_{jk} \geq CI$$

where R_{ik} is the operation time of the primary protection relay i for fault k, CI_{jk} is the difference of operating time (coordination interval) between the primary protection and the backup relays j for fault k, CV_k is the number of constraint violations for fault k (e.g., the difference between the operating time of primary protection and back up protection is higher than coordination interval, CI). In (7.1), A, B, and C are the coefficients which indicate the contribution of each term in the objective function. The constant A indicates the contribution of the operation time of primary protection. The constant B indicates the contribution of the coordination time and the constants C and D indicates the contribution of the number of constraint violations.

The physical meaning of the objective function is that when this function is low, the system is well coordinated. When the objective function is high, the system is not well coordinated. Typical values of an acceptable objective function depend on the A, B and C parameters. For the test bed shown in this chapter, and for typical values of A, B and C parameters, the optimal objective function is about 80.

Fig. 7.2 shows a simple case of coordinating protective relays in a radial system. Assuming that all relays applied in this system are ITDOC relays. From Fig. 7.2, in case the fault occurs at *F1*, the relay *R1* and *R2* should operate to clear the fault. The relay *Rb*

is the backup for relay *R1*. Note from Fig. 7.2 that the difference between the operation time of *R1* and *Rb* must be adjusted such that $t(Rb) - t(R1)$ is higher than *CI*. A typical value of *CI* is 0.3 s for distribution systems.

Operation time of relays

The proper representation of the characteristic of relays is very important for coordinating the protection system. Operating time of relays can be calculated depending on the operational mechanism of each relay unit (i.e., definite time delay overcurrent relay , ITDOC relay and distance relay).

The operation time of ITDOC and distance relay depend on the delay time setting, t_{delay}. For the ITDOC, the operation time can be calculated as [61],

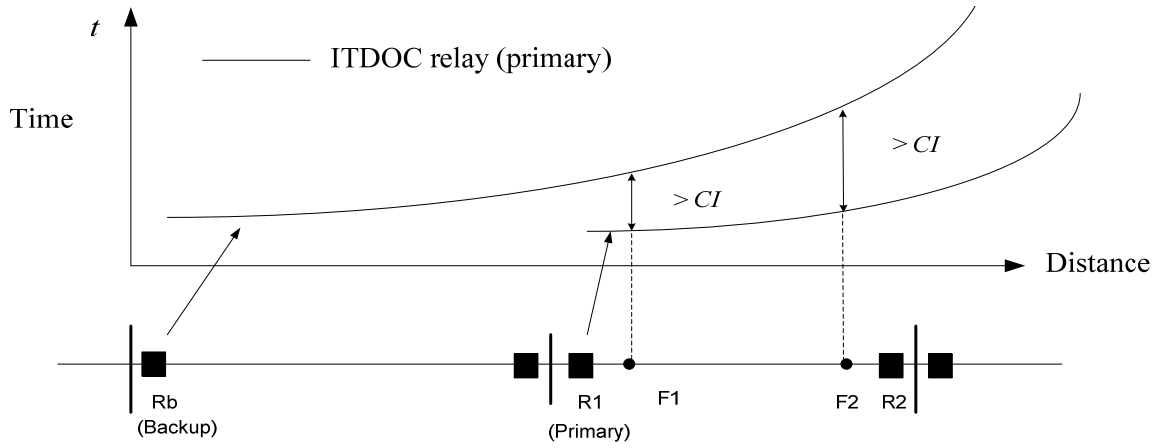

Figure 7.2 Coordination of ITDOCs

$$t(I) = TD\left(\frac{A}{M^{p}-1} + B\right) \tag{7.2}$$

where *M* is the multiple of the pickup current, *TD* is the time dial setting, *A*, *B* and exponent *p* imitate the curve shape of the trip characteristic.

Two main series of ITDOC relays are used in North America: model A (CO induction relay) and model B (IAC induction relay). The constants A, B and p for moderately, very, extremely inverse characteristics of each series are provided in Table 7.1 – 7.2. Table 7.1 shows the data for model A, type CO induction relay. Table 7.2 shows the data for model B, type IAC induction relay. This data are taken from the IEEE standard inverse-time characteristic equations for over current relays in [61].

Table 7.1 Model A - CO induction relay

(from [61])

Constant	Moderately inverse	Very inverse	Extremely inverse
A	0.047	18.92	28.08
B	0.183	0.492	0.130
p	0.02	2.00	2.00

Table 7.2 Model B - IAC induction relay

(from [61])

Constant	Moderately inverse	Very inverse	Extremely inverse
A	0.056	20.29	20.33
B	0.045	0.489	0.081
p	0.02	2.00	2.00

Fig. 7.3 shows the comparison of the time-current characteristic of an ITDOC for extremely inverse induction in both models A and B.

7.3 Basis of the ACO for coordinating relays

The ant colony algorithm mimics several behaviors of real ants. The processes in the ACO are: tour construction, pheromone trail update, local search, fitness evaluation and statistical update. This section is dedicated to explain the application of the ACO to coordinate ITDOC relays. The overview of the ACO for coordinating relays is shown in Fig. 7.4.

Details of each process shown in Fig. 7.4 are discussed in the following sections. The coordination problem is comparable to the multidimensional traveling salesman problem. That is, the setting of relays is analogous to the location of a city in the TSP problem. For example, for a ITDOC, the setting of each relay consists of the time dial setting (TD), current transformer (CT) ratio, type of relay (moderately, very ,and extremely inverse) and tap setting. Thus, this coordination problem is analogous to a four-dimensional TSP problem (see Fig. 7.5).

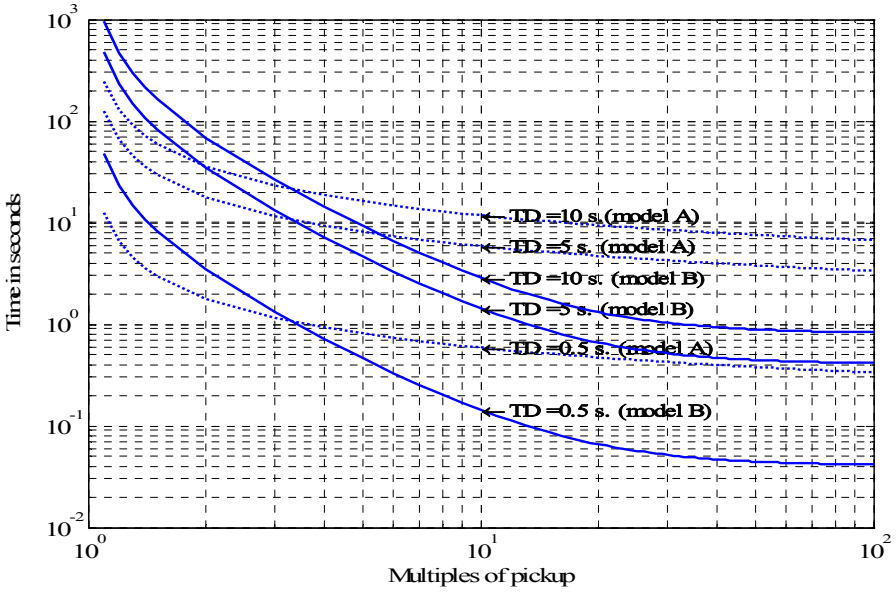

Figure 7.3 Plot of time-current characteristic of ITDOC for model A and B (extremely inverse).

Figure 7.5 shows an example of a search path for the ants in this optimal coordination problem. Note that each dot represents the setting of an ITDOC relay {CT, Type, Tap, TD}. The standard values for each setting are [61],

CT ratio = 20:1, 40:1, 60:1, 80:1, 100:1, 120:1,160:1,180:1,200:1 and 240:1

Type of relay = moderately inverse (type = 1), very inverse (type = 2) and extremely inverse (type = 3)

Tap setting = 1.0, 1.2, 1.5, 2.0, 2.5, 3.0, 3.5, 4.0, 5.0, 6.0, 7.0, 8.0, 10.0 and 12.0

Time dial setting = 1/2, 1, 2, 3, 4, 5, 6, 7, 8, 9, 10 and 11

For example, when considering the setting of relay 1, the setting {200, 2, 2.5, 5} means that the agents (i.e., ants) choose the optimal setting of relay 1 as follows: CT ratio is 200:1, type of relay is very inverse time characteristic, tap setting is 2.5, and time dial setting is 5.

Tour construction

Initially, ants (i.e., the agents) choose the sequence of relay units to be adjusted randomly. Since the setting of each relay has effects on coordination of all protection systems, the optimal solution may not come from setting relays sequentially (i.e., relay settings calculated one at a time in sequence assuming that previously calculated setting are correct).

The search for the optimal solution to a problem using ACO entails searching a given multidimensional space. The trajectory of the sequential search is termed a *tour* in keeping with the analog to ant behavior. The illustration of tour construction is shown in Fig. 7.5. Let the ant k be located at the setting of relay i $\{CT_i, Type_i, Tap_i, TD_i\}$ repre-

sented by the asterisk. Ant k moves to the setting of relay i+1 $\{CT_{i+1}, Type_{i+1}, Tap_{i+1}, TD_{i+1}\}$ by following the *pseudorandom proportional* rule [66]:

$$\text{Setting of relay } i+1 = \begin{cases} \arg\max_{\ell \in N_i^k} \left\{ \tau_{i\ell} [\eta_{i\ell}]^{\beta} \right\}, & \text{if } q \le q_0 \\ J, & \text{otherwise} \end{cases} \tag{7.3}$$

where q is a random variable which has uniform distribution in [0, 1], q_0 is a parameter which determines the selection technique ($0 < q_0 < 1$), β is a parameter which determines the impact of objective function value in tour construction, J is a random setting selected by using the roulette wheel technique or so called random proportional rule (details are discussed in the next section), ℓ is a relay setting which is a subset of the feasible neighborhood of relay i for ant k or so called N_i^k. The variable $\tau_{i\ell}$ is the amount of pheromone laid on the path from setting i to ℓ and $\eta_{i\ell}$ is the inverse of the objective function when changing the setting of relay i+1 to ℓ (see Fig. 7.6).

The application of the ACO algorithm to a given problem entails skill in the selection of search parameters. For example, typical values for q_0 and β for this power system protection optimization problem are 0.8 and 2.2, respectively. Equation (7.3) can be separated into two parts: $q \le q_0$ and $q > q_0$. When the random variable q is lower than q_0, the ants make the best possible move by choosing the minimum objective function. This is accomplished incorporating the maximum amount of pheromone laid on the path. In this case, the ant is exploiting the learned knowledge left on the path.

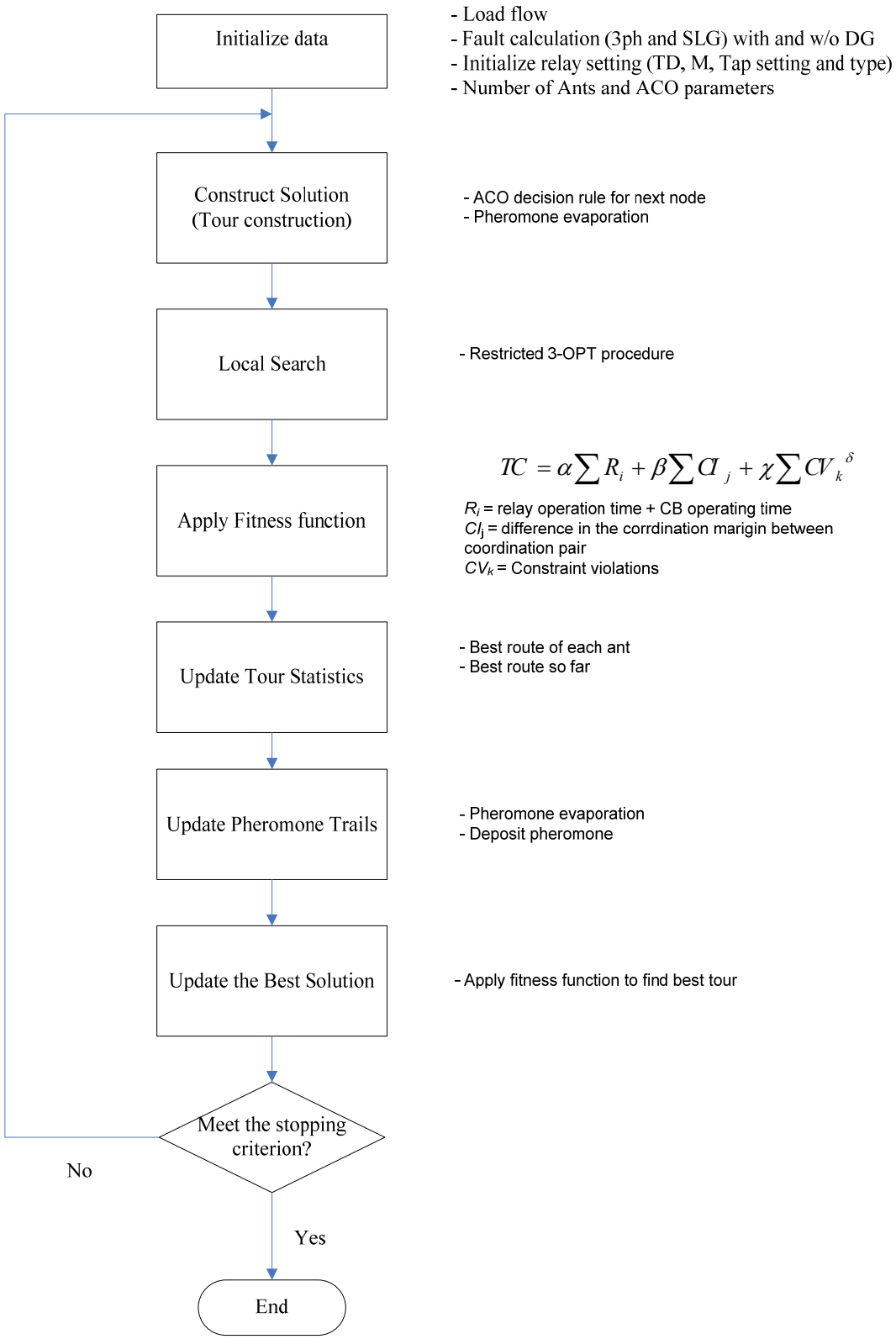

Figure 7.4 ACO application for coordinating protective relays

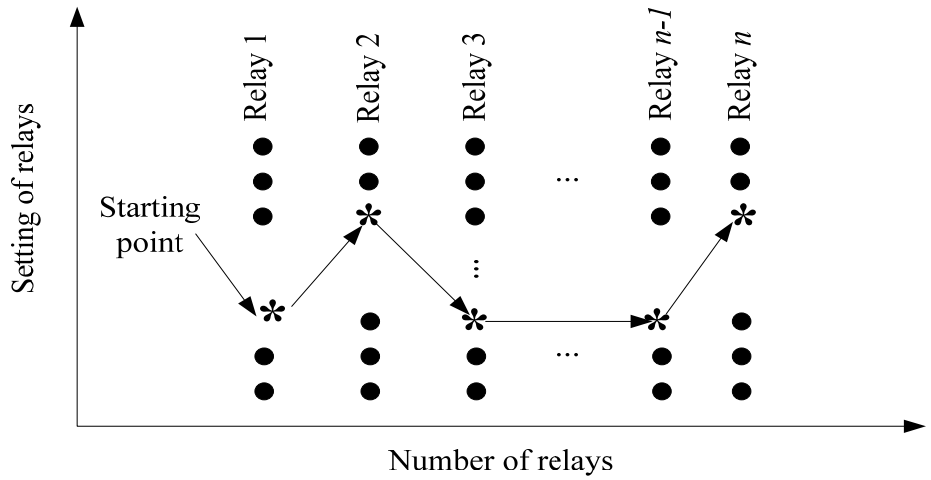

Note : each dot represents the possible setting of each relay {CT_i, $Type_i$, Tap_i, TD_i}
asterisk represents the selected choice of ants

Figure 7.5 Search path of ACO algorithm

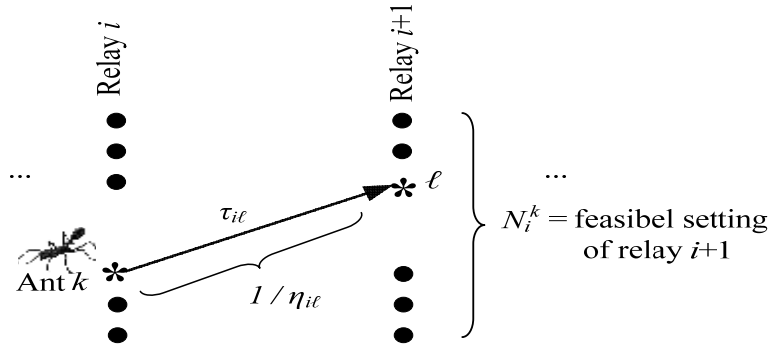

Note : each dot represents the possible setting of each relay {CT_i, $Type_i$, Tap_i, TD_i}
asterisk represents the selected choice of ants

Figure 7.6 Artificial ant colony algorithm

When the random variable q is higher than q_0, the ants choose the setting of relay i+1 by using the random proportional rule. That is, the probability in which ant k, located at relay i, chooses to go to setting ℓ of relay i+1 is

$$p_{i\ell}^{k} = \frac{[\tau_{i\ell}]^{\alpha}[\eta_{i\ell}]^{\beta}}{\sum_{\ell \in N_i^k}[\tau_{i\ell}]^{\alpha}[\eta_{i\ell}]^{\beta}}, \tag{7.4}$$

where $\eta_{i\ell}$ is the inverse of the objective function value when the ant located at relay i and this ant chooses the setting of relay i+1 to be ℓ. The constants α and β are the parameters which determine the impact of pheromone and the objective function value. After all of the probabilities from the setting of relay i to the feasible neighbors (N_i^k) are calculated using equation (7.4), the setting of relay i+1 can be chosen using the concept of the roulette wheel described below.

The roulette wheel technique can be imagined as spinning a roulette wheel with different sizes of each slot (see Fig. 7.7). The width of each slot is proportional to the probability $p_{i\ell}^{k}$. Thus, the setting of the relay with higher amount of pheromone and lower objective value dominates all the others. Roulette wheel selection can be implemented as follows:

1. sum the probability of all the feasible neighbor ($p_{i\ell}^{k}$) called *TF*
2. generate a random number *n*, between 0 and *TF* (i.e., the total feasible state).
3. setting of relay i+1 is the setting corresponding to the cumulative probability greater than or equal to *n.*

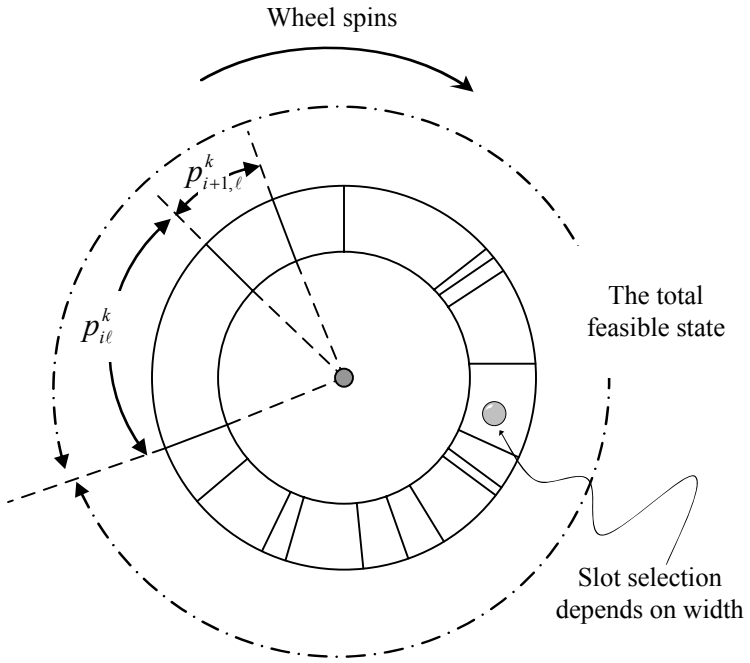

Figure 7.7 Roulette wheel with variable slot width

Local search

The literature [65, 66, 83] suggests that combining the ACO algorithm with local search improves the quality of final problem solutions. The local search procedure can be explained as follows. Once ants have completed their solution construction, the best solution from ants might be improved by applying heuristic information. In the application of relay coordination, the local search procedure can be illustrated by pseudocode in Fig. 7.8. Note that the application of a local search helps the ACO algorithm to find the local optimum while the artificial ants provide good starting solutions. After the local search procedure, the pheromone on each trail is updated by this local optimum solution. Comparison of the ACO algorithms with and without the local search procedure for ge-

neric problems can be found in [66]. The Matlab code for the local search procedure can be found in Appendix D.

Procedure LocalSearch
for relay = 1 : length(RelayData)
if CIout(relay) > 0.3 % if it's longer than 0.3
while CIout(relay) < 0.3 and Objective function is improved
- decrease the tap setting or/and time dial setting of the corresponding relays (adjacent bus)
- Calculate new objective function.

end
elseif CIout(relay) < 0.3 % if it's longer than 0.3
while CIout(relay) > 0.3 and Objective function is improved
- Increase the tap setting or/and time dial setting of the corresponding relays (adjacent bus)
- Calculate new objective function.

end
end
end

Figure 7.8 Pseudocode of the local search procedure for application of ACO in coordinating relays

Fitness evaluation and statistical update

The fitness evaluation can be done by applying the objective function in (7.1). This equation assesses quantitatively the operation time of primary and back up protection for all busbar faults. The results from (7.1) are analogous to the distance between cities in TSP problem. All of the relay settings chosen by artificial ants are evaluated. The best solution over the process is used in the pheromone update procedure.

Pheromone trail update

Only the ant which chooses the setting with the best objective value (i.e., the best solution up to this iteration) is allowed to add the pheromone after each iteration. The updated pheromone can be calculated as

$$\tau_{i\ell} \leftarrow (1-\rho)\tau_{i\ell} + \rho\Delta\tau_{i\ell}^{bs}$$

where $\Delta\tau_{i\ell}^{bs}$ is $1/C_{bs}$, C_{bs} is the best objective function value and ρ is the discount factor of the deposited pheromone. This procedure updates the pheromone trail by applying the weighted average between the amounts of old pheromone, $(1-\rho)\tau_{i\ell}$, and the pheromone deposited $\rho\Delta\tau_{i\ell}^{bs}$. A typical range of values for ρ *is* 0.6 – 0.8.

Pheromone trail evaporation

The objective of pheromone evaporation is to avoid quick convergence of all ants to a local optimum point. The evaporation procedure decreases the amount of pheromone in all trails with a constant (1-ρ),

$$\tau_{ij} \leftarrow (1-\rho)\tau_{ij}.$$

The pheromone evaporation is more important to the complex optimization problem compared to the simple problem. This process is done to all paths after updating the pheromone trail.

7.4 Consideration of distance relays

A fair number of network systems have ITDOC relays that operate together with distance relays as the second zone of protection. The distance relay operates when the

impedance seen at the location of relay is lower than the reach of zone 2 (see Fig. 7.9). Once the operating condition is met, the distance relay operates with pre-specified time delay, t_{zone2}. This section discusses a technique to set the reach and operating time (t_{zone2}) of the back up system (secondary zone).

After applying the ACO algorithm to coordinate the ITDOC relays, the operating time of distance relays can be decided by applying two constraints [63]:

$$t_{zone2,Rb} - t_{R1}(F1) \geq CI' \tag{7.5}$$

$$t_{Rb}(F2) - t_{zone2,R1} \geq CI' \tag{7.6}$$

where t_{zone2} is the operating time of back up protection, $t_{R1}(F1)$ is the operating time of relay *R1* when a fault occurs at *F1* (see Fig. 7.9), CI' is the coordination interval of the ITDOC and distance relay. In this illustration, the fault locations F1 and F2 are located at 20% and 80% of the line length.

The constraint in (7.5) states that the operating time of secondary protection *Rb* must be slower than the operating time of the primary protection (ITDOC) at *R1* at least by *CI'*. Note that the coordination time in this case (*CI'*) is not necessarily equal to the *CI* in the coordination between ITDOCs in Section 7.2 (Fig. 7.2). This constraint considers the coordination time, *CI'*, of the back up protection located at *Rb* when primary protection at *R1* fails to operate.

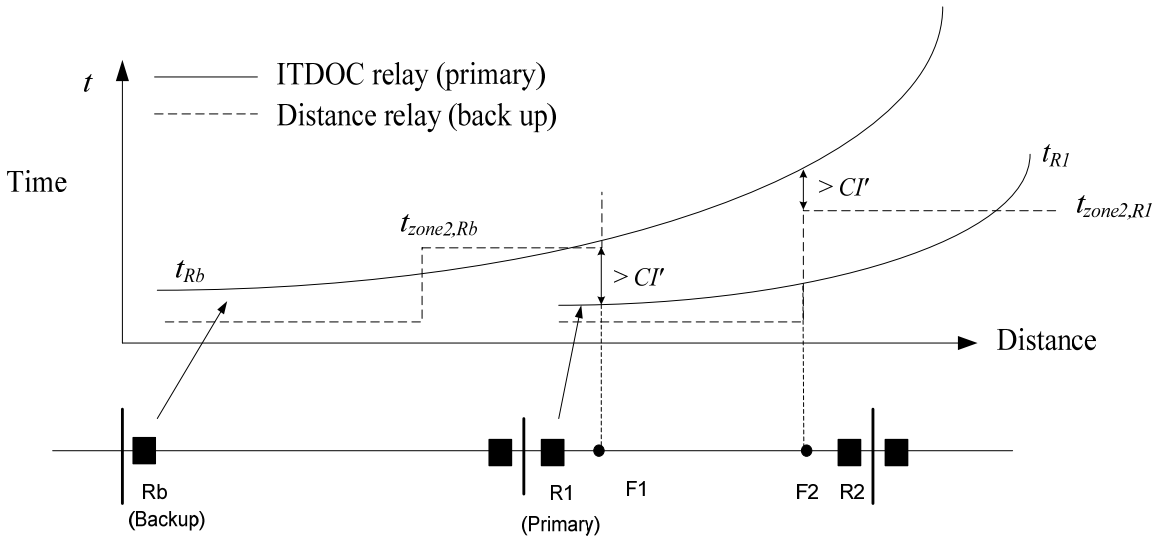

Figure 7.9 Coordination between ITDOCs and distance relay

Similarly, the second constraint in (7.6) states that the operating time of the primary protection (ITDOC) at *Rb* when a fault occurs at *F2* must be slower than the operating time of the distance relay at *R1* by at least *CI'*. This constraint considers the coordination time, *CI'*, of the distance relay located at *R1*. These two constraints must be applied to set up the operating time of all distance relays in the distribution system.

The reach of the distance relay should be adjusted to protect the line impedance plus 20% [84] of the next shortest line impedance. That is, assuming that line impedance $k < \ell$ (see Fig. 7.10), the reach of the distance relay at R_b is $m + 0.2*k$.

7.5 Illustration of the ACO algorithm for relay coordination

To illustrate the application of ACO optimization technique, a distribution network is used as a test bed system (see Fig. 7.11). Let this test bed system called Case 7.1. The ACO technique is applied to set the overcurrent relays. The test bed system is a six bus system with eight distribution lines and sixteen ITDOC relays. Characteristics of the

test bed system are shown in Table 7.3. The per unit bases of this study are 25 MVA and 12 kV.

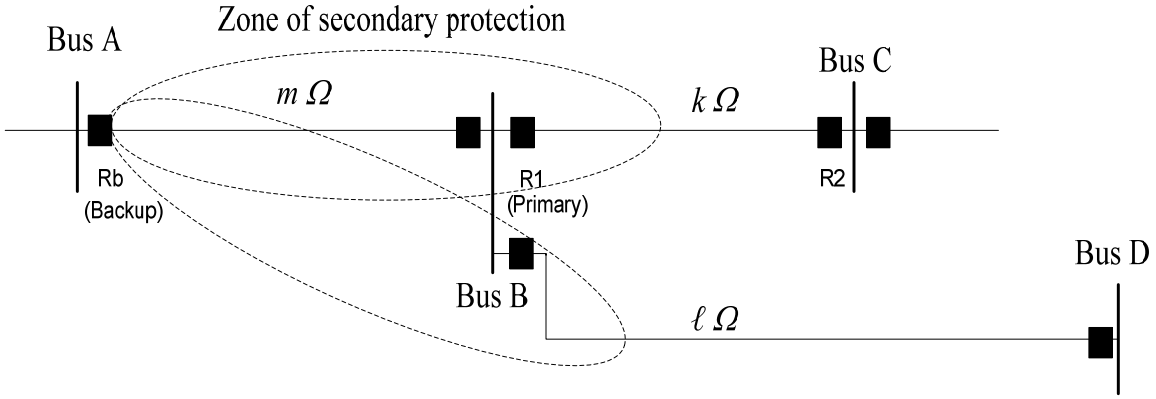

Figure 7.10 Protective zone of a distance relay

In this demonstration, a single line to ground (SLG) fault is considered in the setting of relays. The standard values for the setting of ITDOC relays are [61]:

CT ratio = 20:1, 40:1, 60:1, 80:1, 100:1, 120:1,160:1,180:1,200:1 and 240:1

Type of relay = moderately inverse (type = 1), very inverse (type = 2) and extremely inverse (type = 3)

Tap setting = 1.0, 1.2, 1.5, 2.0, 2.5, 3.0, 3.5, 4.0, 5.0, 6.0, 7.0, 8.0, 10.0 and 12.0

Time dial setting = 1/2, 1, 2, 3, 4, 5, 6, 7, 8, 9, 10 and 11.

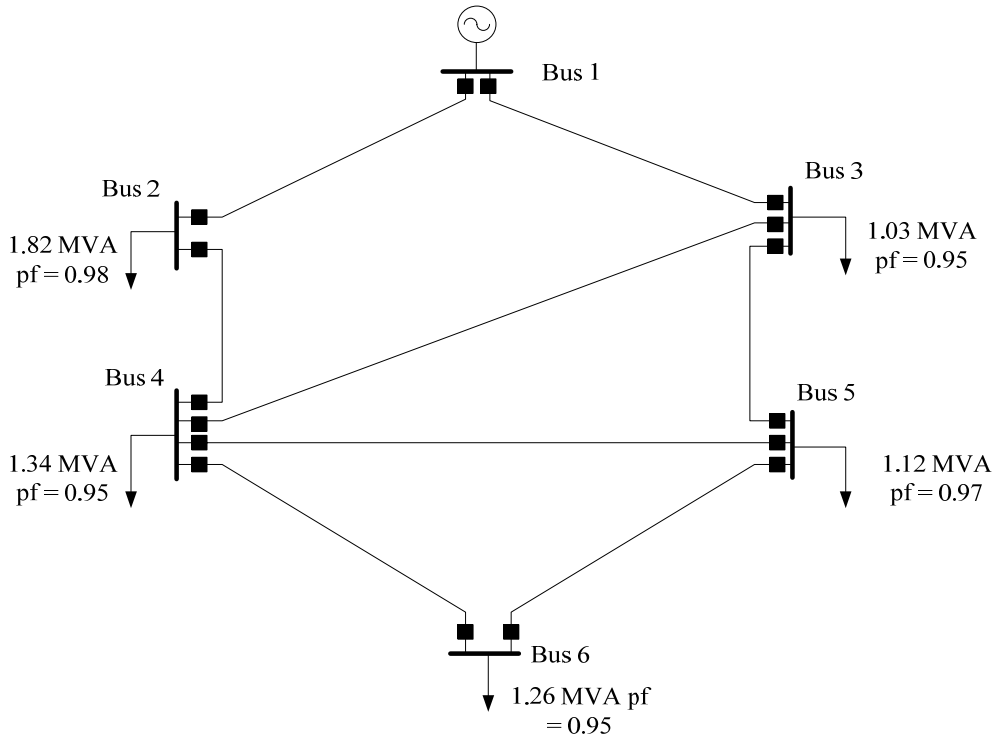

Figure 7.11 A test bed system, Case 7.1

Table 7.3 Characteristics of the distribution system in Case 7.1

From bus	To bus	*R* (pu.*)	*X* (pu.*)	*R0* (pu.*)	*X0* (pu.*)
1	2	0.0323	0.0761	0.0244	0.07135
1	3	0.03525	0.0830	0.0267	0.0778
2	4	0.0206	0.0484	0.0156	0.0454
3	4	0.0646	0.1522	0.0489	0.1427
3	5	0.0441	0.1038	0.0333	0.0973
4	5	0.0558	0.1314	0.0422	0.1232
4	6	0.0162	0.0380	0.0122	0.0357
5	6	0.0411	0.0968	0.0311	0.0908

* base 25 MVA and 12 kV

Table 7.4 Parameters of the ACO algorithm for Cases 7.1 and 7.2

Parameter	Value
Number of artificial ants	25
Number of travel round	10
Contribution of the operation time of primary protection, A^*	1.0
Contribution of the coordination time, B^*	0.8
Contribution of the number of constraint violation, C^*	1.0
Contribution of the number of constraint violation, D^*	2.0
Impact of pheromone in tour construction, α	2.0
Impact of objective value in tour construction, β	2.2
Pheromone constant, ρ	0.2

* see objective value in (7.1)

The ACO algorithm is applied to coordinate the relays for the test bed system in Fig. 7.11. This test bed is a 12 kV network primary distribution system. Although networked distribution system are not common, they do exist in urban settings, and in this case of systems intended for distributed generation, networking may be advantage. Although this test bed utilizes a distribution engineering environment, the same concepts would apply to networked subtransmission systems. The darkened boxes in Fig. 7.11 denote circuit breakers and ITDOC relays. This test bed is used with ITDOC relays and distance relays in Case 1; the same test bed is used in the presence of DG in Case 2.

In Fig. 7.12, results of relay coordination by ACO algorithm are separated into three parts. The first part shows the parameters used in the ACO algorithm. The second

part of the results shows the results of the coordination by using only ITDOC relays (without consideration of distance relays). Results from the second part of Fig. 7.12 can be interpreted as follows. In Fig. 7.11, let the relay located at bus *a* which protects the line between bus *a* and *b* be called Rab (e.g., the relay R12 is the relay between line 12 located at bus 1). When a SLG fault occurs at the line between bus 2 and 4 (close to bus 2), the primary protection (R24) operates at 0.499 s. In case that the relay R24 fails to operate, the backup protection (i.e., R35 and R65) will operates within 0.300 s.

The third part of the results in Fig. 7.12 shows the best set of relay settings from the ACO technique. The settings of CT ratio, tap and time dial (TD) are shown in columns 4, 6 and 7 respectively. Reach of the distance relay (zone 2), *Z2* and operating time (Timer) are shown in columns 7 and 8. The operating time of distance relays can be decided by constraints in (7.5) and (7.6). The target of coordination interval (CI') in this case is 0.25 s. For example, from the relay data in Fig. 7.12, the settings of ITDOC relay R54 are: CT ratio = 20:1 or 100:5, tap setting = 5 and time dial setting = 1. The settings of distance relay R54 are: reach = 0.229 Ω and timer = 0.772 s. Note that the objective function in this design is 28.1.

7.6 Coordination of protective relays in the presence of DG

The appearance of DGs in distribution systems might increase fault currents. The previously designed system without DGs may not safely manage faults. This section shows the change of relay coordination with the presence of DGs. The test bed system shown in Fig. 7.11 is used to illustrate this fact. The test bed used is the same as that in Case 7.1 except that the single DG is located at bus 6 and is rated 5 MW. This size DG is

intended to be representative of a unit that is likely to be installed at a distribution substation. In this case, the 1.26 MVA load at the same substation is substantially less than the DG output – and it is clear that the DG is intended for system support rather than only local load support. The application illustrated here implies that DG is sited at a substation – a widely suggested concept which has not been widely implemented. The technique shown in this analysis is not dependent, however, on whether bus 6 is a substation or not.

Assuming that after setting the relays as discussed in Section 7.5, a five megawatt DG is installed at bus 6. This scenario is denominated as Case 7.2. The test bed system with DG is shown in Fig. 7.13. Installing the DG at bus 6 results in increase of fault currents. The coordination of the ITDOC relays by applying the previous designed (without DG) is shown in Fig. 7.14. Note that the objective function in Case 2 increases from 28.1 to 80.9. Applying the ACO technique to redesign the coordination of relays one finds that the CI between ITDOC relays after applying the ACO for Case 2 is as shown in Fig. 7.15

```
Coordination of inverse time overcurrent relay by ACO
-----------------------------------
ACO Characteristics:
-----------------------------------
Number of Ants: 25
Number of Round: 10
alpha: 2
beta: 2.2
rho: 0.2
q0: 0.8
-----------------------------------
-------------------------------------
-----   Time to operate (s)  ---------
   Relay      Primary        CI
-------------------------------------
   1 - 2       0.516          -
   2 - 1       0.503        0.178
   1 - 3       0.522          -
   3 - 1       0.500        0.390
   2 - 4       0.544        0.312
   4 - 2       0.516        0.475
   3 - 4       0.523        0.323
   4 - 3       0.503        0.349
   3 - 5       0.539        0.352
   5 - 3       0.502        0.337
   4 - 5       0.510        0.480
   5 - 4       0.499        0.300
   4 - 6       0.558        0.433
   6 - 4       0.500        0.332
   5 - 6       0.520        0.319
   6 - 5       0.511        0.163
-------------------------------------
```

Parameters of ACO algorithm

Coordination interval (CI) between ITDOC relays

```
-------------------------------------RelayData-------------------------------------
    (1)       (2)       (3)       (4)       (5)       (6)       (7)       (8)       (9)
 LineFrom    LineTo    Line#      CT       Type      Tap     TimeDial     Z2      Timer
 ---------------------------------------------------------------------------------------
     1         2         1        60         2       3.5         6     0.161     0.769
     2         1         1        20         2        10       0.5     0.198     0.783
     1         3         2        20         2        10         8     0.231     0.776
     3         1         2        40         2         1        11     0.201     0.775
     2         4         3       180         2         1         3      0.11     0.781
     4         2         3        60         2         1        11     0.152     0.745
     3         4         4       180         2         1         2     0.258     0.772
     4         3         4        20         2         4         3     0.307     0.754
     3         5         5       180         2         1         3     0.253     0.758
     5         3         5        60         2         1         4     0.238      0.75
     4         5         6        20         2         5         3     0.292     0.755
     5         4         6        20         2         5         1     0.229     0.772
     4         6         7        20         2         5        11     0.159     0.754
     6         4         7        60         2         1         3     0.107     0.753
     5         6         8        20         2         5         4     0.179     0.746
     6         5         8        20         2         8         1     0.251     0.747
 ---------------------------------------------------------------------------------------
Best Objective function = 28.0988
```

Note: TPri = operating time of ITDOC relay when fault occurs close to the location of relay, CT = current transformer ration, Tap = tap setting of ITDOC relays, TD = time dial setting of ITDOC relays, Z2 = reach of distance relays, Timer = time setting of distance relays.

Figure 7.12 Results of relay coordination by ACO algorithm, Case 7.1

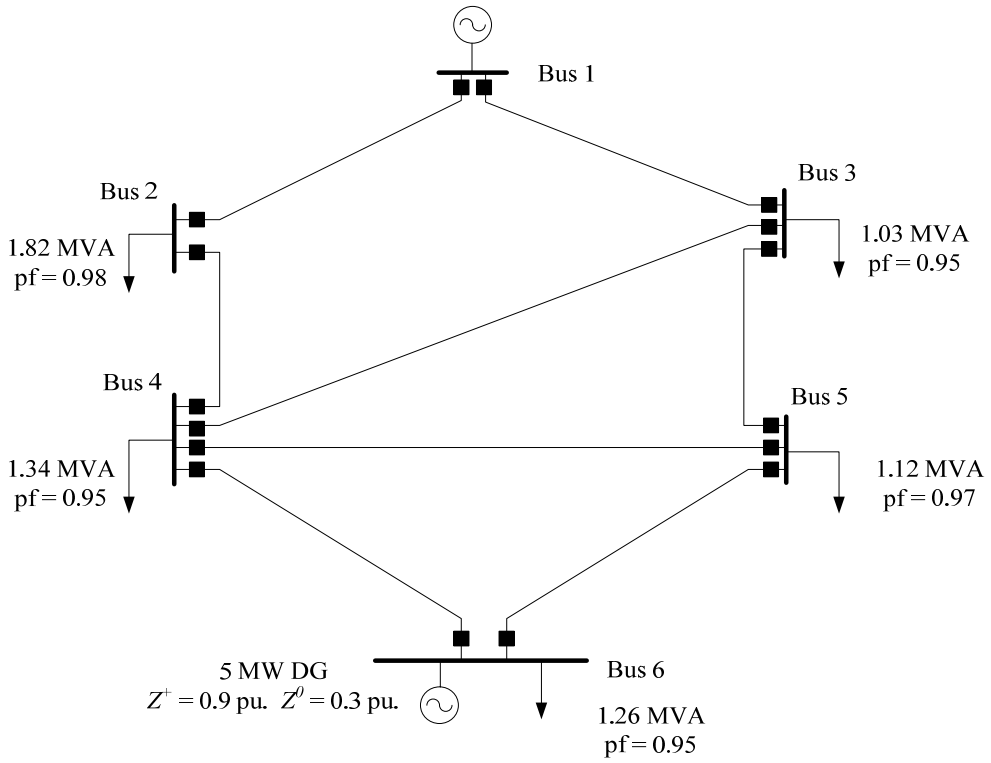

Figure 7.13 Test bed system, Case 7.2

```
Coordination of inverse time overcurrent relay by ACO

--------------------------------------
-----   Time to operate (s)  ---------
   Relay      Primary        CI
--------------------------------------
   1 - 2       0.514          -
   2 - 1       0.501         0.130
   1 - 3       0.519          -
   3 - 1       0.499         0.261
   2 - 4       0.538         0.307
   4 - 2       0.511         0.459
   3 - 4       0.519         0.307
   4 - 3       0.501         0.326
   3 - 5       0.532         0.294
   5 - 3       0.500         0.271
   4 - 5       0.506         0.463
   5 - 4       0.498         0.278
   4 - 6       0.545         0.425
   6 - 4       0.498         0.324
   5 - 6       0.515         0.261
   6 - 5       0.506         0.162
--------------------------------------
Best Objective function = 80.923
```

Figure 7.14 Coordination of the ITDOC relays in the test bed system with the presence of DG at bus 6 by using the setting in previous designed

```
Coordination of inverse time overcurrent relay by ACO

-----------------------------------
ACO Characteristics:
-----------------------------------
Number of Ants: 25
Number of Round: 10
alpha: 2
beta: 2.2
rho: 0.2
q0: 0.8
-----------------------------------
```

Parameters of ACO algorithm

```
--------------------------------------
-----   Time to operate (s)  ---------
   Relay      Primary        CI
--------------------------------------
   1 - 2       0.515          -
   2 - 1       0.540         0.070
   1 - 3       0.518          -
   3 - 1       0.622         0.332
   2 - 4       0.535         0.336
   4 - 2       0.509         0.376
   3 - 4       0.509         0.357
   4 - 3       0.509         0.375
   3 - 5       0.541         0.413
   5 - 3       0.508         0.314
   4 - 5       0.509         0.317
   5 - 4       0.499         0.359
   4 - 6       0.539         0.346
   6 - 4       0.511         0.311
   5 - 6       0.512         0.346
   6 - 5       0.517         0.152
--------------------------------------
```

Coordination interval (CI) between ITDOC relays

```
 ------------------------------------RelayData-----------------------------------------
    (1)       (2)       (3)       (4)        (5)       (6)       (7)        (8)       (9)
 LineFrom    LineTo    Line#      CT        Type       Tap     TimeDial     Z2      Timer
-------------------------------------------------------------------------------------------
     1         2         1       240         2         1         5      0.161     0.769
     2         1         1        20         2         5        11      0.198     0.783
     1         3         2        20         2        10         8      0.231     0.787
     3         1         2       240         2         1         6      0.201     0.778
     2         4         3       180         2         1         3       0.11     0.781
     4         2         3        60         2         1        11      0.152     0.756
     3         4         4        60         2       3.5         1      0.258     0.772
     4         3         4        20         2        10         1      0.307     0.786
     3         5         5       180         2         1         4      0.253     0.758
     5         3         5        80         2         1         5      0.238     0.786
     4         5         6        20         2         5         4      0.292     0.755
     5         4         6       120         2         1         1      0.229     0.772
     4         6         7        20         2         5        11      0.159     0.765
     6         4         7        60         2         1        11      0.107     0.753
     5         6         8        20         2         5         4      0.179     0.755
     6         5         8        20         2         8         2      0.251     0.752
 -------------------------------------------------------------------------------------------
Best Objective function = 37.321
```

Note: TPri = operating time of ITDOC relay when fault occurs close to the location of relay, CT = current transformer ration, Tap = tap setting of ITDOC relays, TD = time dial setting of ITDOC relays, Z2 = reach of distance relays, Timer = time setting of distance relays.

Figure 7.15 Results of relay coordination by ACO algorithm for the system with the presence of the DG at bus 6, Case 7.2

7.7 Conclusion

This chapter proposes an application of the ACO algorithm to set the coordination of protective relays. The ACO algorithm is a discrete optimization technique which mimics the nature of real ants. The ACO algorithm performs well in an off-line, discrete, constrained optimization. The relay coordination problem is analogous to the multidimensional TSP problem. The objective of the coordination optimization problem is to minimize the total operation time of the relays in the system. The total operating time is proportional to the time to operate considering a SLG fault at every bus plus the operating time of backup protection.

Section 7.2 explains the setting of ITDOC relays in distribution systems. Modeling of the relays in this calculation is accomplished by following the IEEE standard inverse-time characteristic equations for overcurrent relays [61].

Section 7.3 considers the mixed scheme protection between distance relays and ITDOC relays. The distance relays operate as the backup protection. In the mixed scheme protection, the coordination of relays in the distribution system must be computed by taking into consideration both types of relays. Separate relay computation leads to loss of selectivity and security of the protection system. That is, the protection system should not operate falsely, must remove the least amount of equipment, and must result in minimum damages.

Section 7.4 discusses the consequence of installing DG in the distribution system. The increase in fault currents resulting from installing DG might result in the need of redesign of the protection system.

In fact, this coordination problem can be solved by applying various types of optimization such as linear programming [85] and a genetic algorithm [64]. However, the main disadvantage of the linear programming methodology is the large dimensionality of the problem. The problem is more complicated when two or more relays with different operating principles are required to coordinate in the protection system.

Both the formulation of protection coordination and typical results are shown using ACO technique. Two cases are used to exemplify typical designs. Case 7.1 relates to the design of a protection system without DG present, and Case 7.2 to a system with DG. The results of these cases indicate that systems with DG result in a larger objective function which means that the system with DG is not as well coordinated. The ACO solution, however, is applicable in both cases.

CHAPTER 8

CONCLUSIONS AND RECOMMENDATAIONS

8.1 Conclusions

According to the demands of clean energy, consumer perceptions, high reliability and power quality for sensitive loads, the demand for distributed resources is gradually rising. Moreover, the distributed resources may decrease or defer the investment of the system upgrades (i.e., transmission line capacity, transformer) due to the increasing of the energy demand. Distributed resources, such as fuel cells, microturbines, solar cells and wind turbines, are mostly based on electronic inverters. These inverters interface with the AC network result in changing of the fault response throughout the system. In order to analyze the effects from the increase of fault current due to the installation of inverter based DGs, model of these DGs are need to be studied. The model of inverter based DGs proposed in Chapter 2 are accomplished by applying the *abc* to *dq0* transformation. The control strategy can be separated into two parts: voltage controller and angle difference controller. Simulation results of the stand alone operation and the grid connection of the inverter based DG are analyzed in both time and frequency domains. The main drawn is that the *dq0* transformation, originally designed for rotating machinery, is suitable for controller design for inverter based DG. The voltage and phase controllers, based on the *dq0* transformation have been illustrated for inverter based DG transient operation.

Fault calculations in power systems are used to determine the interrupting capability of circuit breakers. The calculation of fault current at the system buses is done conventionally by applying the system Z_{bus} matrix. The effects of merchant plants, such as independent power producers (IPP), are not taken into consideration in the classical fault current calculation. New developments in dereguration have brought new generation sources to the system. The appearance of DGs is a cause of increasing fault currents that has not previously been envisioned. A modification of the conventional fault current calculation is discussed in Section 3.2 to accommodate fault calculation in the case of addition of DGs. The main conclusion is that the modification of the Z_{bus} method for fault current calculation is suitable to individual or widespread synchronous machine DG implementation.

Especially in the presence of inverter based DG, the calculation of fault current by applying the Z_{bus} matrix may not be convenient due to the complexity in estimating the transient impedance of the inverter based DGs. Chapter 3 discusses a simulation strategy which can be applied to calculate the fault current and also the coordination of protection systems. A model of the inverter based DG described in Chapter 2 is used in illustrative examples in the case with the presence of inverter based DGs. Two dimensional plots of R vs. X and three dimensional plots of t, R and X seen by protective relay are used as a graphic tool to visualize the system trajectory. General conclusions drawn from the results of simulations in Chapter 3 are:

- Installation of DGs in the distribution system increases the fault current throughout the system.

- The equivalent impedance seen by the system in case of synchronous machine DGs is higher than that of the inverter based DGs. Hence, inverter based generation sources appear to be 'softer' in the sense that their fault currents are not as severe as in the case of synchronous machine sources.
- Depending on the penetration level, locations, type of DGs, the protection system may lose coordination upon installation of DGs.
- The results of simulations provide important information to analyze the coordination of the protection system.

Chapter 4 describes the fault current estimation technique. The fault current estimation is done based on the statistical analysis of voltage and current variations. The estimation technique is applied to the test bed system at some locations. This estimation technique can be utilized as an *online assessment* of the fault current which is necessary to help the operator to avoid unsafe operating conditions.

Chapter 5 introduces an index called the average change of fault current or "ACF" which can be used to quantify the increase of fault current system-wide. Also, a method to approximate the ACF of a system is proposed. A model for calculating ACF has been shown. The least squares method is applied to estimate the coefficients of the ACF model. One of the applications of the ACF is to assign the cost of protective upgrades due to the commissioning of the several DRs. The general conclusion on the basis of testing is that the ACF is accurate in the 10% range. Note that, it is suggested to use the ACF as a system-wide measure, but it is not proposed to replace the standardized methods to represent individual bus fault currents.

Chapter 6 discusses the implications of operating economics imposed by increased fault current due to the addition of DGs and/or merchant plans to a power system. The UC problem with the fault level constraints is solved by applying dynamic programming. The general conclusion can be drawn from the illustrative case in Chapter 6 that the generation of the merchant plants under the fault current level constraint may result in higher cost of operation than the operation without this constraint.

Chapter 7 proposes the artificial ant colony optimization technique to determine the optimal setting for coordinating the protective relays. In general, the ACO can be applied to solve the discrete optimization problem with large dimensionality. The main advantage of applying the ACO technique is the ability to solve the mixed scheme problem with large dimension (number of relays in the system) compare to the linear programming technique. Numerical results presented in Sections 7.5 and 7.6 show that installation of DG results in larger objective function. That is, the system with DG is not well coordinated as the previous design. The adjustment of protective relays in the system may be required.

The main subjects of this thesis and "claim of originality" are tabulated in Table 8.1.

Table 8.1 Summary of the topics in this thesis

Topic	Innovative concept	Classical concept	Presented in
Model of the inverter based DGs	✓	✓	Chapter 2
Fault current calculation		✓	Section 3.2
Increasing of fault current due to installing DGs	✓		Chapter 3
Calculation of fault current with the present of DGs	✓	✓	Section 3.2
Simulation strategies for the system with DGs (i.e., inverter based, synchronous machine DGs)	✓		Chapter 3
Online assessment of fault current with the presence of DGs	✓	✓	Chapter 4
Average Change of Fault (ACF) index	✓		Section 5.2
Application of the least squares method to approximate the ACF	✓		Section 5.3
Allocation of cost of upgrades	✓		Section 5.4
Implication of fault current increase on UC problem	✓		Chapter 6
Optimal coordination of protective relays by the ACO technique	✓		Chapter 7

8.2 Potential new research areas

The following sections are the potential research areas related to power system fault current due to DGs:

Dollar cost of upgrading

For specific applications of DG, the cost of upgrading protection and interruption devices should be considered. This dollar cost should be allocated properly. Minimizing the upgrade cost is one possibility. Sharing the cost is another alternative. The applications of the ACF concept in this thesis together with other new indices are a further alternative. The economic issues need to be analyzed in detail. The nonlinear relationship between $|I_f|$ and CB cost should be considered. Also, issues of the sequencing of DG installations should be considered. For example, if DGs are installed at A, B, and C and cost is allocated; then DGs are installed at D, E, and F, the final stage installation is different from if the installation sequence were {A, E, F} then {B, C, D} (for example). In this regard, the highest recommendation is that the costing techniques in this thesis be done with *actual* cost data (i.e., real distribution expansion cost data). And results of the methods shown in the thesis should be compared to actual historical cost data.

Simplified model of inverter based DG

The model of the inverter based DG requires a large amount computation effort and memory. There might be some techniques to simplify this model. This is an impor-

tant issue for analyzing a larger system without loosing accuracy. An alternative to be considered includes integration of PSpice analysis with Matlab models.

Optimal siting of DGs

Many governments in the industrial countries, especially in the Group of Eight (G8), have a target to substantially reduce the emission of greenhouse gas. This results in the gradually increase of the investment in the electricity from renewable sources and CHP plants. According to [35], the British government expects that 10 percent of electric energy consumed in 2010 will be provided by renewable sources and CHP. As a consequence, approximately three thousand installations of renewable sources and one thousand CHP are expected to be installed in distribution networks. This is probably a trend of the world energy market in the next decade. For this reason, it is necessary to develop a technique to locate the optimal siting of DRs. The objective of this optimization is to minimize the cost of system operation and the system upgrades. The possible technical approaches are Lagrangian relaxation and evolutionary algorithms (i.e., genetic algorithms, ant colony and tabu search). References [86, 87] document some of the issues for greenhouse gasses and DG use.

REFERENCES

[1] President G. W. Bush, *State of the union, Available: http://www.whitehouse.gov/stateoftheunion/2006/.*

[2] *The U.S. Department of Energy (DOE), Office of Distributed Energy Resources, Available: http://www.eere.energy.gov/der/.*

[3] *IEEE Standard for Interconnecting Distributed Resources with Electric Power Systems*, IEEE Standard 1547-2003, pp. 0_1-16, 2003.

[4] N. Miller, Z. Ye, "Distributed generation penetration study," National Renewable Energy Laboratory, Department of Energy, Tech. rep. NREL/SR-560-34715, Aug. 2003.

[5] *The Electric Power Research Institute (EPRI), Distributed Generation, Available: http://www.epri.com/target.asp.*

[6] T. Ackerman, G. Anderson, L. Soder, "Distributed generation: a definition," in *Proc*. *IEEE Electric Power System Research*, vol. 57, pp. 195–204, 2001.

[7] N. Jenkins, "Impact of increasing contribution of dispersed generation on the power system," CIGRE study Committee no. 37, Final Rep., 2003.

[8] *Distributed Coalition Power of America (DCPA), Distributed generation, Available: http://www.distributed-generation.com.*

[9] *Arizona Public Service (APS), Arizona PV cost, Available: http://www.solarelectricpower.org.*

[10] A. Chambers, S. Hamilton, B. Schnoor, *Distributed generation: a nontechnical guide*, Tulsa, Oklahoma: PennWell Corporation, 2001.

[11] H. Zareipour, K. Bhattacharya, "Distributed generation: current status and challenges," in *Proc*. *IEEE North American Power Symposium (NAPS)*, pp. 392-399, Moscow, Idaho, 2004.

[12] H. B. Püttgen, P. R. Macgregor, F. C. Lambert, "Distributed generation semantic hype or the dawn of a new era," *IEEE Power & Energy Magazine,* vol. 1, pp. 22-29, Jan. / Feb. 2003.

[13] J. C. Gomez, M. M. Morcos, "Coordination of voltage sag and overcurrent protection in DG systems," *IEEE Trans. Power Delivery,* vol. 20, no. 1, Jan. 2005.

[14] J. G. Slootweg, W. L. Kling, "Impacts of distributed generation on power system transient stability," in *Proc*. *IEEE Power Engineering Society Summer Meeting*, vol. 2, pp. 862-867, 2002.

[15] R. C. Dugan, T. E. McDermott, "Operating conflicts for distributed generation on distribution systems," in *Proc*. *IEEE Rural Electric Power Conf.*, pp. A3/1-A3/6, 2001.

[16] A. Girgis, S. Brahma, "Effect of Distributed generation on protective device coordination in distribution system," in *Proc*. *Large Engineering Systems Conf. (LESCOPE)*, pp. 115-119, Halifax NS, Jul. 2001.

[17] K. H. LaCommare, J. L. E. E. Gumerman, C. Marnay, "Distributed Generation Potential of the U.S. Commercial Sector," Environmental Energy Technologies Division, Tech. rep. DE-AC03-76SF00098, May 2005.

[18] National Energy Policy Development Work group, "National Energy Policies," Tech. rep. 0-16-050814-2, May 2001.

[19] N. Rader, S. Hempling, "The Renewables Portfolio Standard: A Practical Guide," National Association of Regulatory Utility Commissioners, 2001.

[20] Anonymous, *California's Energy Crisis: The NRDC Blackouts, Available: http://www.quivis.com/caenergy01.html.*

[21] "State of California Energy Resources Conservations and Development Commission," California Energy Commission, April 2004.

[22] *IEEE Standard rating structure for AC high-voltage circuit breakers*, IEEE Standard C37.04-1999, Jun. 1999.

[23] *ANSI Standard Electric Power Systems and Equipment - Voltage Ratings (60 Hz)*, ANSI Standard C84.1-1995, Jan. 1995.

[24] *IEEE Application guide for AC high voltage circuit breakers rated on a symetrical current basis*, IEEE/ANSI Standard C37.010-1999, May 1999.

[25] N. Nimpitiwan, G. T. Heydt, "Fault current issues for market driven power systems with distributed generation," in *Proc*. *North American Power Symposium (NAPS)*, pp. 400-406, Moscow, Idaho, 2004.

[26] M. P. Kazmierkowski, R. Krishnan, F. Blaabjerg, *Control in power electronics: selected problems*, San Diego, California: Academic Press, 2002.

[27] M. Prodanovic, T. C. Green, "Control of power quality in inverter based distributed generation," in *Proc*. *IEEE Industrial Electronics Society*, vol. 2, pp. 1185-1189, 2002.

[28] M. Prodanovic, T. C. Green, "Control and filter design of three-phase inverters for high power quality grid connection," *IEEE Trans. Power Electronics,* vol. 18, pp. 373-380, no. 1, Jan. 2003.

[29] T. Takeshita, T. Masuda, N. Matsui, "Current waveform control of distributed generation system for harmonic voltage suppression," in *Proc. IEEE Power Electronics Specialists Conf.*, vol. vol. 2, pp. 516-521, Jun. 2001.

[30] M. Marwali, A. Keyhani, "Control of distributed generation systems Part I: Voltages and currents control," *IEEE Trans. on Power Electronics,* vol. 19, pp. 1541-1550, no. 6, 2004.

[31] M. Marwali, A. Keyhani, "Control of distributed generation systems Part II: Load sharing control," *IEEE Trans. Power Electronics,* vol. 19, pp. 1551-1561, no. 6, 2004.

[32] M. E. Baran, I. El-Markaby, "Fault analysis on distribution feeders with distributed generators," *IEEE Trans. Power Systems,* vol. 20, pp. 1757-1764, no. 4, 2005.

[33] M. Huneault, F. D. Galiana, "A survey of the optimal power flow literature," *IEEE Tran. Power Systems,* vol. 6, pp. 762-770, no. 2, May 1991.

[34] B. H. Chowdury, S. Rahman, "A review of recent advances in economic dispatch," *IEEE Trans. Power Systems,* vol. 5, pp. 1248-1259, no. 4, Nov. 1990.

[35] C. Mortley, " The contribution to distribution network fault levels from the connection of distributed generation," KEMA, London, 2005.

[36] G. W. Stagg, A. H. El-Abiad, *Computer methods in power systems analysis*, New York: McGraw-Hill, 1994.

[37] A. Wood, B. Wollenberg, *Power generation operation and control*, 2nd ed., New York: Wiley Interscience Publication, 1996.

[38] K. C. Almeida, F. D. Galiana, "Critical cases in the optimal power flow," *IEEE Trans. Power Systems,* vol. 11, pp. 1509-1518, no. 3, Aug. 1994.

[39] W. F. Tinney, J. M. Bright, K. D. Demaree, B. A. Hughes, "Some deficiencies in optimal power flow," *IEEE Trans. Power Systems,* vol. 3, pp. 676-683, no. 2, May 1988.

[40] D. Gan, R. J. Thomas, R. D. Zimmerman, "Stability constrained optimal power flow," *IEEE Trans. Power Systems,* vol. 15, pp. 535-539, no. 2, May 2000.

[41] U.S. environmental Protection Agency, "Clean air act amendment," 1990.

[42] A. A. El-Keib, H. Ma, J. L. Hart, "Environmentally constrained economic dispatch using lagrangian relaxation method," *IEEE Trans. Power Systems,* vol. 9, pp. 1723-1729, no. 4, Nov. 1994.

[43] R. Ramanathan, "Emission constrained economic dispatch," *IEEE Trans. Power Systems,* vol. 9, pp. 1994-2000, no. 4, Nov. 1994.

[44] K. Deb, *Multi objective optimization using evolutionary algorithms*, New York: Wiley Inter science Series in Systems and Optimization, 2001.

[45] H. Ma, A. A. El-Keib, R. E. Smith, "A genetic algorithm based approach economic dispatch of power systems," in *Proc*. *IEEE International Conf. on Power Industry Computer Applications*, pp. 207-212, May 2001.

[46] K. P. Wong, J. Yuryevich, "Evolutionary programming based algorithm for environmentally constrained economic dispatch," *IEEE Trans. Power Systems,* vol. 13, pp. 301-306, no. 2, May 1998.

[47] T. Yalcinoz, H. Altun, "Environmentally constrained economic dispatch via a genetic algorithm with arithmetic crossover," in *Proc. IEEE Africon*, pp. 923-928, 2002.

[48] N. P. Padhy, "Unit commitment – a bibliographical survey," *IEEE Trans. Power Systems,* vol. 19, pp. 1196-1205, no. 2, May 2004.

[49] T. Siu, G. Nash, Z. Shawash, "A practical hydro, dynamic unit commitment and loading model," *IEEE Trans. Power Systems,* vol. 16, pp. 301-306, no. 2, May 2001.

[50] K. S. Kwarup, S. Yamashiro, "Unit commitment solution methodology using genetic algorithm," *IEEE Trans. Power Systems,* vol. 17, no. 1, Feb. 2002.

[51] A. Rudolf, R. Bayrleithner, "A genetic algorithm for solving the unit commitment problem of a hydro thermal power system," *IEEE Trans. Power Systems,* vol. 14, no. 4, Nov. 1999.

[52] T. Senjyu, H. Yamashiro, K. Shimabukuro, K. Uezato, T. Funabashi, "A fast solution technique for large scale unit commitment problem using genetic algorithm," in *Proc. IEEE Transmission and Distribution Conf. and Exhibition*, vol. 3, pp. 1611-1616, 2002.

[53] G. Liao, T. Tsao, "The use of genetic algoritm/ fuzzy system and tabu search for short term unit commitment," in *Proc*. *IEEE Power System Technology*, vol. 4, pp. 2302-2307, Oct. 2002.

[54] C. A. Rajan, M. R. Mohan, "An evolutionary programming based tabu search method for solving the unit commitment problem," *IEEE Trans. Power Systems,* vol. 19, no. 1, Feb. 2004.

[55] K. Srinivasan, C. Claude, "Short-circuit current estimation from measurements of voltage and current during disturbances," *IEEE Trans. Industrial Applications,* vol. 33, pp. 1061-1064, no. 4, Jul./Aug. 1997.

[56] P. M. Anderson, *Analysis of faulted power systems*, New York: IEEE PRESS Power Sys-tem Engineering Series, 1995.

[57] J. J. Grainger, W. D. Stevenson, *Power system analysis*, New York: McGraw-Hill, 1994.

[58] R. C. Dugan, "Issues for distributed generation in the U.S.," in *Proc*. *Power Engineering Society Winter Meeting*, vol. 1, pp. 121-126, Jan. 2002.

[59] C. W. So, K. K. Li, "Protection relay coordination on ring fed distribution network with distributed generations," in *Proc*. *IEEE Computers, Communications, Controls and Power Engineering*, vol. vol. 3, pp. 1885-1888, Oct. 2002.

[60] IEEE committee report, "Computer aided coordination of line protection schemes," *IEEE Trans. Power Delivery,* vol. 6, pp. 575-583, no. 2, April 1991.

[61] G. Benmouyal, M. Meisinger, J. Burnworth, W. A. Elmore, K. Freirich, P. A. Kotos, P. R. Leblanc, P. J. Lerley, J. E. McConnell, J. Mizener, J. Pinto de Sa, R.

Ramaswami, M. S. Sachdev, W. M. Strang, J. E. Waldron, S. Watansiriroch,S. E. Zocholl, "IEEE standard inverse-time characteristic equations for overcurrent relays," *IEEE Trans. Power Delivery,* vol. 14, pp. 868-872, no. 3, 1999.

[62] A. J. Urdaneta, H. Restrepo, S. Márquez, J. Sánchez, "Coordination of directional overcurrent relay timing using linear programming," *IEEE Trans. Power Delivery,* vol. 11, pp. 122-129, no. 1, 1996.

[63] L. G. Pérez, A. J. Urdaneta, "Optimal computation of distance relays second zone timing in a mixed protection scheme with directional overcurrent relays," *IEEE Trans. Power Delivery,* vol. 16, pp. 385-388, no. 3, July 2001.

[64] C. W. So, K. K. Li, "Time coordination method for power system protection by evolutionary algorithm," *IEEE Trans. Industry Applications,* vol. 36, pp. 1235-1240, no. 5, Sep. 2000.

[65] M. Dorigo, L. M. Gambardella, "Ant colony system: a cooperative learning approach to the traveling salesman problem," *IEEE Trans. Evolutionary Computation,* vol. 1, pp. 53-66, no. 1, 1997.

[66] M. Dorigo, T. Stützle, *Ant colony optimization*, Cambridge, Mass.: MIT Press, 2004.

[67] H. Shyh-Jier, "Enhancement of hydroelectric generation scheduling using ant colony system based optimization approaches," *IEEE Trans. Energy Conversion,* vol. 16, pp. 296-301, no. 3, 2001.

[68] J. F. Gomez, H. M. Khodr, P. M. De Oliveira, L. Ocque, J. M. Yusta, R. Villasana,A. J. Urdaneta, "Ant colony system algorithm for the planning of primary distribution circuits," *IEEE Trans. Power Systems,* vol. 19, pp. 996-1004, no. 2, 2004.

[69] C. Ji-Pyng, C. Chung-Fu, S. Ching-Tzong, "Ant direction hybrid differential evolution for solving large capacitor placement problems," *IEEE Trans. Power Systems,* vol. 19, pp. 1794-1800, no. 4, 2004.

[70] N. Nimpitiwan, G. Heydt, "Coordination of protective relays by artificial ant colony optimization," *IEEE Tran. Power Systems,* Submitted for publication 2006.

[71] N. Mohan, T. M. Underland, W. P. Robbins, *Power electronics: converters, applications and design*, 3rd ed., Hoboken, New Jersey: John Wiley and Sons, 2003.

[72] N. Nimpitiwan, G. T. Heydt, R. Ayyanar, S. Suryanarayanan, "Fault Current Contribution from Synchronous Machine and Inverter Based Distributed Generators " *IEEE Trans. Power Delivery,* vol. accepted to be published, 2006.

[73] M. Dorigo, *Ant colony optimization and swarm intelligence: 4th international workshop, ANTS 2004, Brussels, Belgium, September 5-8, 2004: proceedings*, Berlin ; New York: Springer, 2004.

[74] J. D. Glover, M. Sarma, *Power system analysis and design*, 2nd ed., Boston: PWS Publishing, 1994.

[75] G. T. Heydt, *Computer analysis methods for power systems*, Scottsdale, Arizona: Stars in a Circle Publications, 1996.

[76] A. S. Bozin, "Electrical power systems modeling and simulation using Simulink," in *Proc*. *IEE Colloquium on the Use of Systems Analysis and Modeling Tools: Experiences and Applications*, pp. 10/1-10/8, Mar. 1998.

[77] D. C. Montgomery, E. A. Peck, G. G. Vining, *Introduction to linear regression analysis*, 3 ed., New York: Wiley-Interscience, 2001.

[78] N. Nimpitiwan, G. T. Heydt, "Fault current allocation by the least-squares method," *IEEE Trans. Power Systems,* vol. 20, pp. 2148-2150, no. 4, Nov. 2005.

[79] S. Haykin, *Neural networks: a comprehensive foundation*, 2 ed., New York: Prentice Hall, 1999.

[80] J. Deneubourg, S. Gross, N. Franks, A. Sedova-Franks, C. Detrain,L. Chretien, "The dynamics of collective sorting: robot-like ants and ant-like robots," in *Proc*. *Simulation of adaptive behavior: From animals to animats*, pp. 356-363, Cambridge, MA, 1991.

[81] H. Yun-He, W. Yao-Wu, L. Li-Juan, X. Xin-Yin, "Generalized ant colony optimization for economic dispatch of power systems," in *Proc*. *Power System Technology (PowerCon)*, vol. 1, pp. 225-229, 2002.

[82] P. M. Anderson, *Power system protection*, New York: McGraw-Hill: IEEE Press, 1999.

[83] Y. H. Song, M. R. Irving, "An overview of heuristic optimization techniques for power system expansion planning and design," in *Proc*. *Power Engineering Society General Meeting*, vol. 1, pp. 933, Denver, 2004.

[84] S. H. Horowitz, A. G. Phadke, *Power system relaying*, New York: John Wiley and sons, 1992.

[85] L. G. Perez, A. J. Urdaneta, "Optimal coordination of directional overcurrent relays considering definite time backup relaying," *IEEE Trans. Power Delivery,* vol. 14, pp. 1276-1284, no. 4, Oct. 1999.

[86] D. Batten, *Australia's national electricity market, Available: http://www.cmit.csiro.au/research/special/green/nemp.cfm.*

[87] S. Zinga, "Distributed generation's role in green power programs," South Face Energy Institute, Jan. 2003.

[88] P. C. Krause, O. Wasynczuk, S. F. Sudhoff, *Analysis of electric machinery and drive systems*, 2nd ed., Piscataway, New Jersey: Wiley Inter science, 2002.

[89] P. Kundur, *Power system stability and control*, New York: McGraw-Hill, 1994.

APPENDIX A

SYSTEM PARAMETERS OF THE THUNDERSTONE SYSTEM

This appendix shows the detail of system parameters of the Thunderstone system, such as line parameters, transformer impedance, loads and impedance of DGs. All parameters are used in the experiments in Chapter 3 and Chapter 4.

Table A.1 Transmission line parameter for Thunderstone system

69 kV Line			Line parameters in p.u. @100°C (100 MVA Base)					
	FROM	TO	R1	X1	G1	B1	G2	B2
1	Cluff	Thundrst	0.00232	0.01552	0	0.0004		
2	Cluff	Cameron	0.00253	0.01636	0	0.00044	0	0.00046
3	Superst3	Cameron	0.01245	0.07996	0	0.00223	0	0.00223
4	Noak	Thundrst	0.00235	0.01295	0	0.00035	0	0.00034
5	Noak	SignalBu	0.00439	0.024	0	0.00064	0	0.00065
6	Shannon	SignalBu	0.00756	0.03097	0	0.00038	0	0.00038
7	Shannon	Superst4	0.00861	0.03572	0	0.00045	0	0.00045
8	SignalBu	Thundrst	0.01562	0.05749	0	0.00076		
9	Seaton	SignalBu	0.00868	0.03194	0	0.00042		
10	Sage	Thundrst	0.00436	0.02435	0	0.00064	0	0.00063
11	McCoy	Sage	0.00691	0.02809	0	0.00035		
12	McCoy	Seaton	0.00649	0.02638	0	0.00033		
13	Ealy	Seaton	0.00869	0.03517	0	0.00043	0	0.00043
14	Ealy	Superst1	0.01113	0.04134	0	0.00054		

Table A.2 Load bus data

Bus	MW	MVAR
Cluff	22	0.5
Cameron	27.1	0.5
Noack	21.6	0.8
SignalBU Bay 3	22.3	0.3
SignalBU Bay 4	21.5	1.8
Shanon	23.3	2.3
Superstition Bay 2	16	3.2
Superstition Bay 3	23.6	0.2
Sage	56.4	6.5
Seaton	23.2	2.6
Ealy Bay 2	21.4	0.4
Ealy Bay 4	8.6	2
McCoy	0	0

Table A.3 Substation transformer (230/69 kV) at Thunderstone substation

p.u. on a 100 MVA base		
R	*X*	*Bmag*
0.002	0.06	0
0.001	0.06	0
0.001	0.07	0
0.001	0.06	0

Table A.4 Distribution transformers

FROM	Bus kV	To	Bus kV	Rated MVA	p.u. at Rated MVA		*Bmag*
					R	*X*	
Cluff	69	Cluff LD1	12	12	0.024	0.0742	0
Cameron	69	Cameron LD1	12	15	0.02	0.078	0
Ealy LD1	69	Ealy LD2	12	15	0.0198	0.0779	0
Ealy LD2	69	Ealy LD4	12	10	0.0388	0.074	0
Mccoy	69	Mccoy LD2	12	15	0.0197	0.0758	0
Noack	69	Noack LD2	12	12	0.0232	0.076	0
Sage	69	Sage LD2	12	12.5	0.0422	0.0725	0
Sage	69	Sage LD3	12	12.5	0.0228	0.0744	0
Sage	69	Sage LD4	12	12.5	0.0228	0.0741	0
Seaton	69	Seaton LD1	12	12	0.0238	0.0733	0
Shanon	69	Shannon LD2	12	15	0.0198	0.0763	0
SignalBU	69	Signal LD3	12	12	0.037	0.069	0
SignalBU	69	Signal LD4	12	12	0.0243	0.073	0
Superstition	69	Superstition LD2	12	12	0.0233	0.083	0
Superstition	69	Superstition LD3	12	12	0.0239	0.1028	0

APPENDIX B

THE *dq0* TRANSFORMATION

B.1 Introduction

This appendix provides the basic concepts and interpretation of the reference frame theory. The reference frame theory is commonly applied in analysis of three phase rotating electrical machine models. Voltage equations and inductances of induction machines and synchronous machines are functions of rotor speed. In other words, the inductances and voltages of these machines are time varying variables. R. H. Park, H. C. Stanley, G. Kron and D. S. Brereton [88] introduce changes of variables in the analysis of electric machines. A change of variables, so called "real transformations or *dq0* transformation", are employed in the analysis of electric machines to eliminate the complexity of the differential equations with time varying variables.

The real transformation refers the machines variables to a frame of reference that can be chosen to rotate at an arbitrary angular velocity. The appropriate speed of rotation, ω, should be assigned to a particular application. For example, in the analysis of synchronous machine, the reference frame is set to fixed with the speed of rotor ($\omega = \omega_r$) to eliminate the time varying inductances in the voltage equations. The transformation with the velocity of reference frame at $\omega = \omega_r$ is first introduced by R. H. Park and is called "Park's transformation". In this work, the *dq0* transformation is used for a non-rotational application, namely AC analysis and control. The objective is nonetheless the same as in the rotational analysis case: to render the control signals independent (or nearly so) of time.

B.2. The *dq0* transform equation

A change of variables to an arbitrary reference frame can be expressed as [88, 89],

$$f_{dq0} = T_{dq0} f_{abc} \tag{B.1}$$

where f in (B.1) represents variables, such as voltage, current, and flux linkage, f_d ,f_q and f_0 are the variables in direct-axis, quadrature-axis, and zero sequence respectively,

$$f_{dq0}{}^{T} = \begin{bmatrix} f_d & f_q & f_0 \end{bmatrix},$$

$$f_{abc}{}^{T} = \begin{bmatrix} f_a & f_b & f_c \end{bmatrix},$$

$$T_{dq0} = \frac{2}{3}\begin{bmatrix} \cos\theta & \cos(\theta - \frac{2\pi}{3}) & \cos(\theta + \frac{2\pi}{3}) \\ \sin\theta & \sin(\theta - \frac{2\pi}{3}) & \sin(\theta + \frac{2\pi}{3}) \\ \frac{1}{2} & \frac{1}{2} & \frac{1}{2} \end{bmatrix},$$

$$\omega_e = \frac{d\theta}{dt}.$$

In this development, the d and q axis rotation is taken from rotating machine theory, but in this case there is no rotational element. The angular displacement, θ, can be expressed as

$$\theta = \int_0^t \omega_e dt$$

where ω_e is the radian frequency and this depends on the purpose of a particular analysis. It is assumed that ω_e is constant and therefore $\theta = \omega_e t$.

The inverse transformation can be expressed as

$$T_{dq0}^{-1} = \begin{bmatrix} \cos\theta & -\sin(\theta) & 1 \\ \cos(\theta - \frac{2\pi}{3}) & -\sin(\theta - \frac{2\pi}{3}) & 1 \\ \cos(\theta + \frac{2\pi}{3}) & -\sin(\theta + \frac{2\pi}{3}) & 1 \end{bmatrix}.$$

Note that the *dq0* transformation is applied to the instantaneous values (i.e., *v(t)* and *i(t)*), not the *rms* values. Also note from (B.1) that the direct axis and quadrature axis are orthogonal to each other.

One of the important properties of the *dq0* transformation is the energy and power conservation. That is, the energy and power in time domain representation of a signal is equal to the energy and power in the *dq0* domain. The total instantaneous power can be written in *abc* variables as

$$P_{abc} = v_{an} i_a + v_{an} i_a + v_{cn} i_c .$$

The total instantaneous power written in the *dq0* domain is

$$P_{dq0} = P_{abc} = \frac{3}{2}\left(v_d i_d + v_q i_d + 2 v_0 i_0\right).$$

The 3/2 factor is required due to the constant used in the transformation. Illustrative examples in the following sections are used to demonstrate the properties of the transformation. Two types of signal are demonstrated: balanced three phase voltage with harmonics in Case B.1 and unbalanced three phase voltage with harmonics in Case B.2.

B.3 Transformation of a balanced three phase signal (Case B.1)

To demonstrate the application of the *dq0* transformation to a balanced three phase signal, a three phase sinusoidal voltage, $v_{abc}(t)$, with power frequency ($\omega = 120\pi$ rad/s) is used as illustrative case denominated as Case B.1. Case B.1 illustrates the sinusoidal steady state with voltage harmonics h = 1, 2, 3, … in the sequences +, -, 0, +, … . Simplified notation of phase –neutral voltages $\{v_{an}(t), v_{bn}(t), v_{cn}(t)\}$ as $\{v_a(t), v_b(t), v_c(t)\}$, the waveform in Case B.1 is defined as

$$v_a(t) = 50\cos\omega t + 15\cos 5\omega t + 5\cos 9\omega t \tag{B.2}$$

$$v_b(t) = 50\cos(\omega t - \frac{2\pi}{3}) + 15\cos 5(\omega t - \frac{2\pi}{3}) + 5\cos 9(\omega t - \frac{2\pi}{3}) \tag{B.3}$$

$$v_b(t) = 50\cos(\omega t + \frac{2\pi}{3}) + 15\cos 5(\omega t + \frac{2\pi}{3}) + 5\cos 9(\omega t + \frac{2\pi}{3}). \tag{B.4}$$

Note that in (B.2) – (B4), the $\{v_a(t), v_b(t), v_c(t)\}$ are represented in zero-peak instantaneous volts. Assume that, in the transform matrix, the initial condition of angular displacement, $\theta(t=0)$, is set to zero and the angular velocity of the reference frame, ω_e, is fixed at the power frequency. The waveform and frequency spectrum of the balanced three phase voltage are shown in Fig. B.1. Note that in Fig. B.1, the amplitude spectrum of $v_a(t)$ is $|V_a(h\omega_e)|$ and this is shown in volts zero-peak. The amplitude spectra $|V_b(h\omega_e)|$ and $|V_c(h\omega_e)|$ are identical to $|V_a(h\omega_e)|$. The phase spectra, however, are not identical. Note that the illustrative waveform has fifth and ninth harmonics. By applying (B.1), the three phase voltage can be written in *dq0* variables as

$$\begin{bmatrix} v_d(t) \\ v_q(t) \\ v_0(t) \end{bmatrix} = \frac{2}{3}\begin{bmatrix} \cos\theta & \cos(\theta - \frac{2\pi}{3}) & \cos(\theta + \frac{2\pi}{3}) \\ \sin\theta & \sin(\theta - \frac{2\pi}{3}) & \sin(\theta + \frac{2\pi}{3}) \\ \frac{1}{2} & \frac{1}{2} & \frac{1}{2} \end{bmatrix}\begin{bmatrix} v_a(t) \\ v_b(t) \\ v_c(t) \end{bmatrix}$$

or

$$\begin{bmatrix} v_d \\ v_q \\ v_0 \end{bmatrix} = \begin{bmatrix} 50 + 15\cos 6\omega t \\ 15\sin 6\omega t \\ 5\cos 9\omega t \end{bmatrix}. \tag{B.6}$$

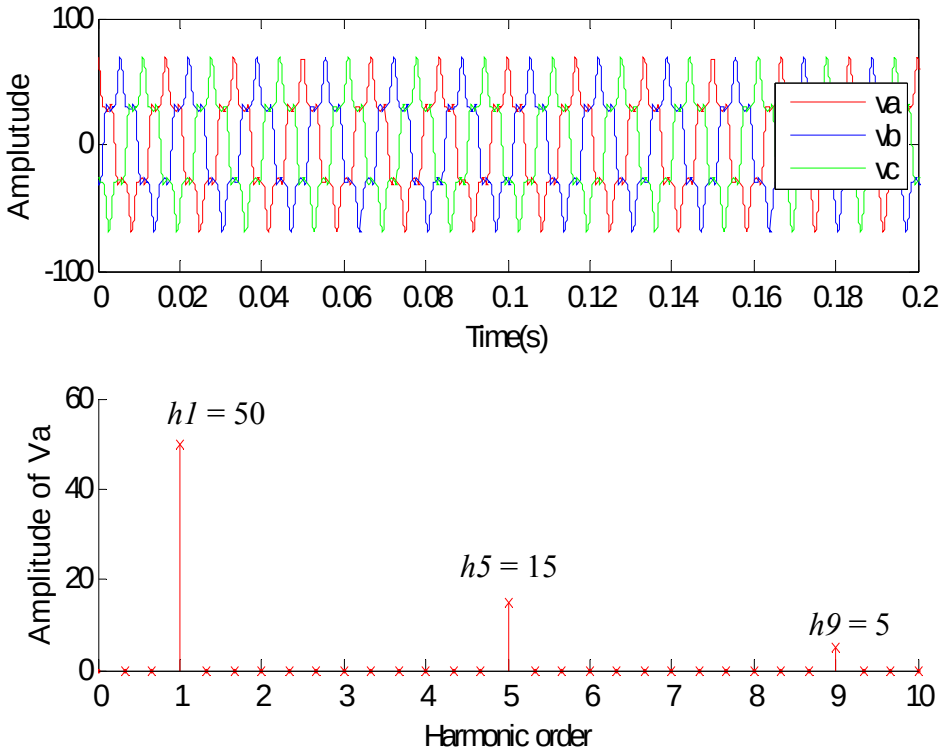

Figure B.1 Line to neutral voltage waveform (*a, b, c* variables) and amplitude of harmonic content, Case B.1

The results of *dq0* transformation in time domain and frequency domain are depicted in Figs. B.2 and B.3, respectively. Note that, from (B.2)-(B.4) and Fig. B.3, the amplitude of the fundamental frequency given in (B.2-B.4) becomes the DC component in the direct axis after transforming associated $\omega_e = 120\pi$ rad/s. The fifth harmonic in (B.2)-(B.4) is converted to the sixth harmonics in both direct and quadrature axes. Also note that the DC component and the triple harmonics (ninth harmonics in this case) appear in the zero sequence. This conclusion as well as other generalizations will be discussed later.

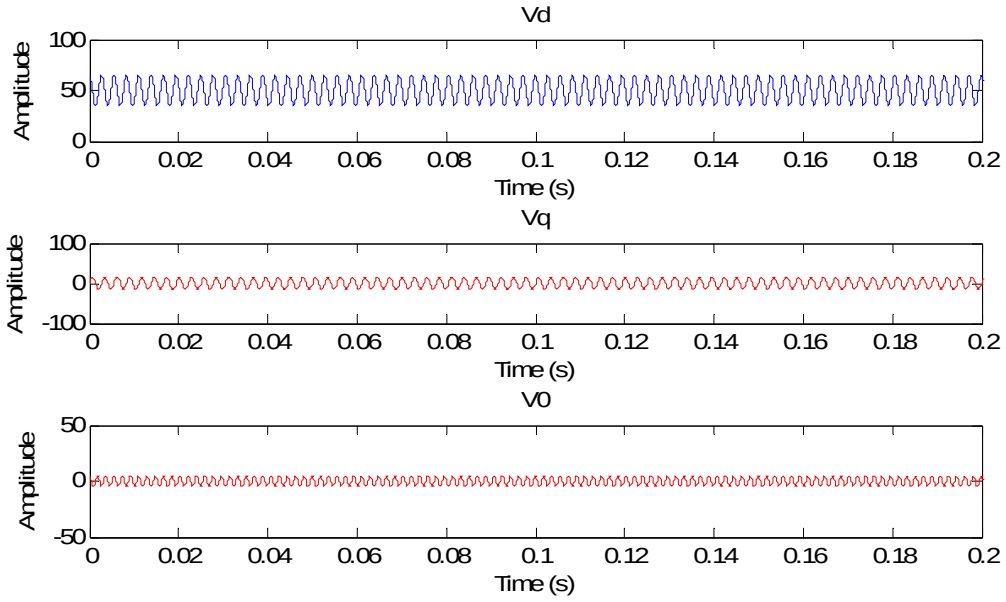

Figure B.2 Three phase waveform in the *dq0* variables for $\omega = 120\pi$ rad/s, Case B.1

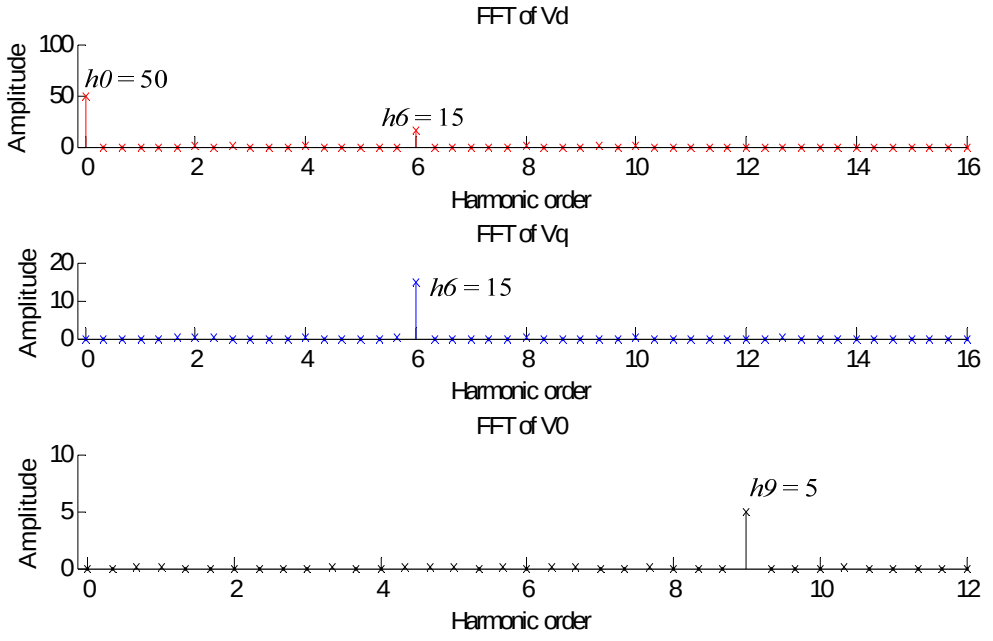

Figure B.3 Amplitude frequency spectra of a balanced three phase signal in the *dq0* variables, Case B.1

B.4 Transformation of an unbalanced signal with harmonics (Case B.2)

This case demonstrates the transformation of an unbalanced three phase signal which can be expressed as

$$v_a(t) = 100\cos\omega t + 10\cos 5\omega t + 5\cos 9\omega t \tag{B.5}$$

$$v_b(t) = 90\cos(\omega t - \frac{2\pi}{3}) + 8\cos 5(\omega t - \frac{2\pi}{3}) + 4\cos 9(\omega t - \frac{2\pi}{3}) \tag{B.6}$$

$$v_b(t) = 80\cos(\omega t + \frac{2\pi}{3}) + 6\cos 5(\omega t + \frac{2\pi}{3}) + 3\cos 9(\omega t + \frac{2\pi}{3}). \tag{B.7}$$

Note that the signal composed, unbalanced power frequency components (unbalanced harmonic contents 5th and 9th harmonics). Plots of the signal in time domain and frequency domain for Case B.2 are shown in Fig. B.4. As in Case B.1, the units depicted are all instantaneous (i.e., zero-peak) voltages.

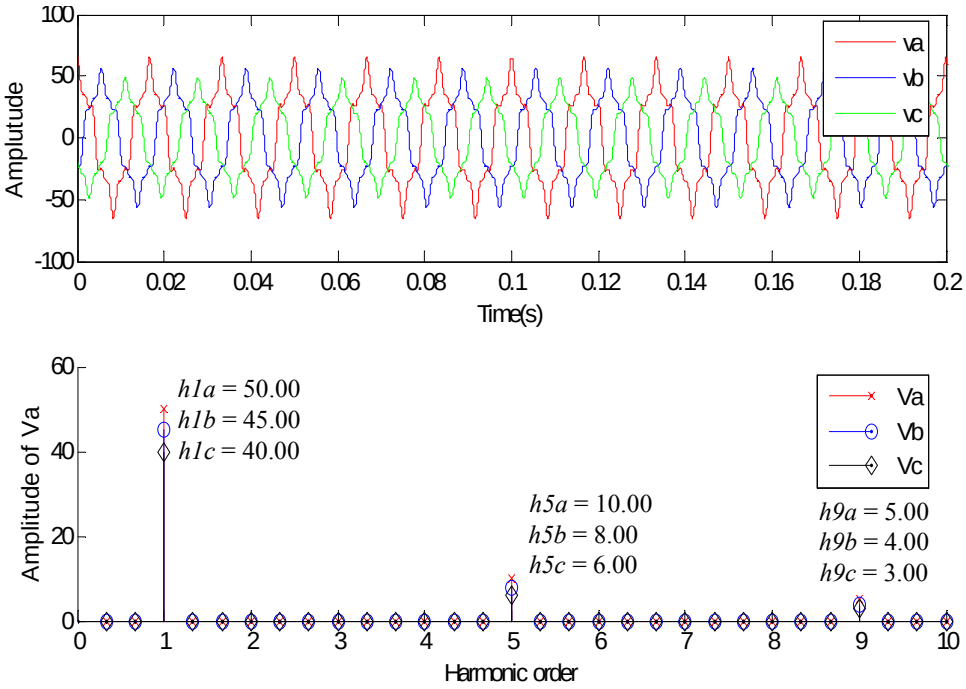

Figure B.4 Line to neutral voltage waveform (*a, b, c* variables) and amplitude of harmonic content, Case B.2

Transformation of the signal in Case B.2 associated with the velocity of reference frame is done by applying (B.1). Assume that, ω_e, is 120π rad/s. The transformed signal in time domain and frequency domain are shown in Figs. B.5 and B.6, respectively. From the results of transformation in Figs. B.5 and B.6, note that:

- Due to the unbalanced component in the fundamental component, there exists a DC component and second harmonic in the direct axis, $v_d(t)$. In the quadrature axis, $v_q(t)$, there exists a second harmonic component. In the zero sequence, there is a fundamental frequency component.
- The unbalanced non-triple harmonic signal, the fifth harmonic in Case B.2, creates a sixth harmonic with the same amplitude in both direct and quadrature axes. There exists a fifth harmonic in the zero sequence component.
- The unbalanced triple harmonic signal, the ninth harmonic in this case, creates the eighth and tenth harmonics in the direct and quadrature axes. There also exists the ninth harmonic in the zero sequence component.

The analysis of the *dq0* transformation is accomplished analytically by using the Symbolic toolbox provided in Matlab (not shown here). Properties of the synchronous rotational reference frame transformation can be drawn as shown in Table B.1

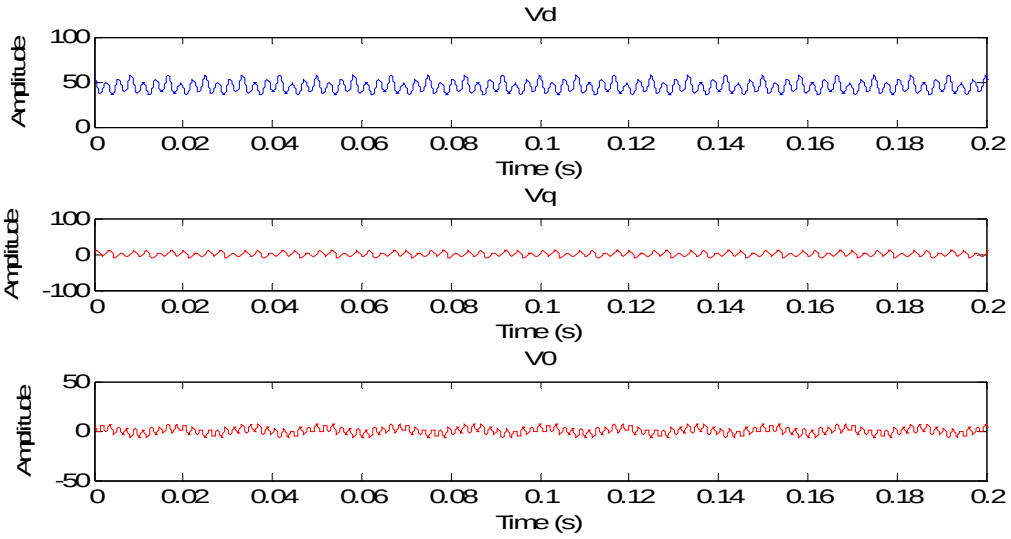

Figure B.5 Three phase waveform in *dq0* variables for $\omega_e = 120\pi$ rad/s, Case B.2

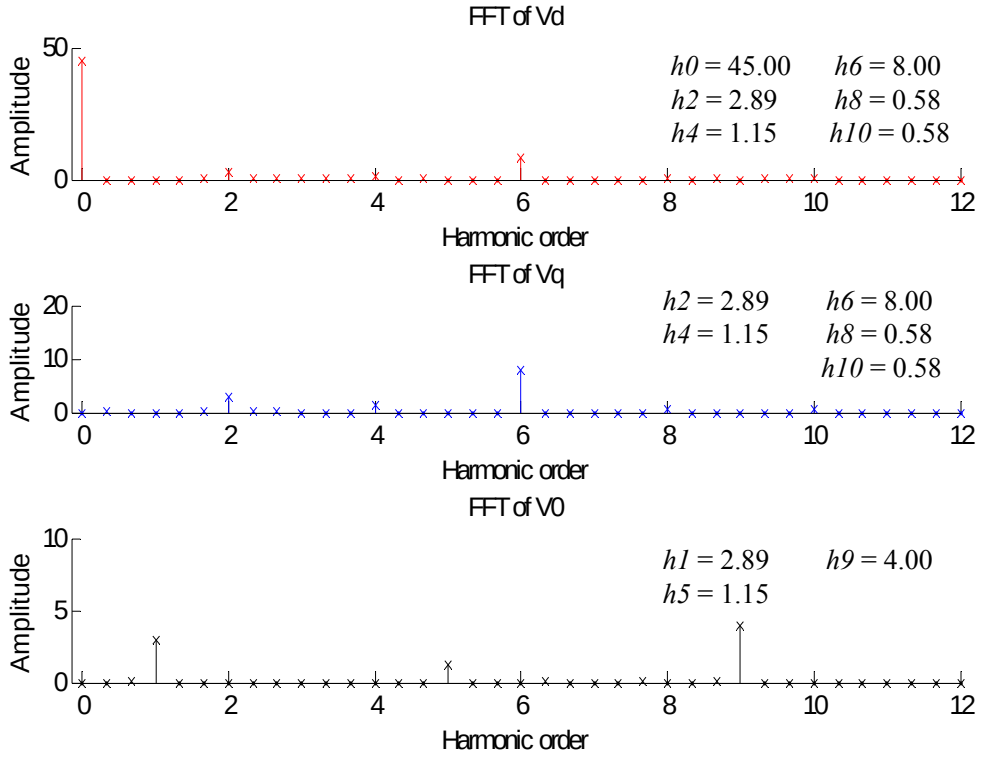

Figure B.6 Frequency spectra of the balanced three phase signal in the *dq0* variables, Case B.2

Table B.1 Properties of the *dq0* transformation for sinusoidal steady state signals

abc	*dq0*	
Frequency component	Balanced signal(2)	Unbalanced signal(3)
DC component (1)	• DC component in f_0	• Fundamental component in f_d and f_q. • DC component in f_0
Fundamental frequency	• DC component in f_d	• DC component and second harmonic in f_d • DC component and Second harmonic in f_q • Fundamental component in f_0
Non triple harmonics, $3k\pm1^{th}$ order (k = 1, 2, 3,…)	• $3k^{th}$ harmonic in f_d and f_q • f_0 is zero.	• $3k^{th}$ harmonic in f_d and f_q • $3k\pm1^{th}$ harmonic in f_0
Triple harmonics, $3k^{th}$ order (k = 1, 2, 3,…)	• f_d and f_q is zero. • $3k^{th}$ harmonic in f_0	• $3k\pm1^{th}$ harmonic in f_d and f_q • $3k^{th}$ harmonic in f_0

(1) Not shown in example cases

(2) Illustrated as Case B.1

(3) Illustrated as Case B.2

B.5 Transformation of a low pass filtered unbalanced signal with harmonics

With reference to Table B.1, considers the case of a low pass filtered signal obtained from the *dq0* variables (See Fig. B.7). If the $f > f_0$ components are rejected by the low pass filter, Table B.2 results. For this illustration, the cutoff frequency of the low pass filter is 60 Hz.

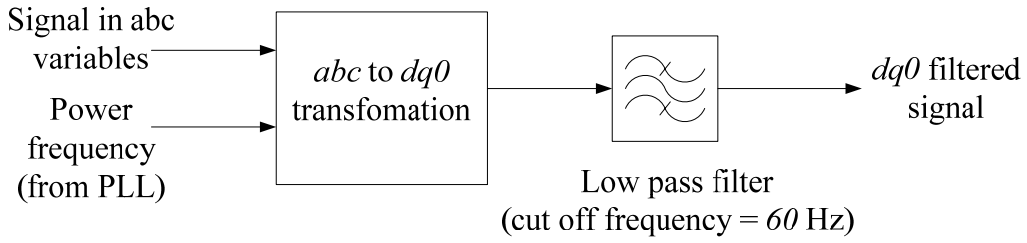

Figure B.7 Signal in *dq0* variables with low pass filter

Table B.2 Properties of the *dq0* transformation with low pass filter for sinusoidal steady state

abc	*dq0*	
Frequency component	Balanced signal	Unbalanced signal
DC component(1)	• DC component in f_0	• Fundamental component in f_d and f_q. • DC component in f_0.
Fundamental frequency	• DC component in f_d	• DC component in f_d. • DC component in f_q. • Fundamental component in f_0.
Non triple harmonics, $3k\pm1^{th}$ order (k = 1, 2, 3,…)	• $3k^{th}$ harmonic in f_d and f_q is zero • f_0 is zero.	• $3k^{th}$ harmonic in f_d and f_q is zero • $3k\pm1^{th}$ harmonic in f_0 is zero
Triple harmonics, $3k^{th}$ order (k = 1, 2, 3,…)	• f_d and f_q is zero. • $3k^{th}$ harmonic in f_0 is zero	• $3k\pm1^{th}$ harmonic in f_d and f_q is zero • $3k^{th}$ harmonic in f_0 is zero

(1) Usually does not occur in AC systems

B.6 The case of arbitrary time domain signals

Consider the three phase voltage $\{v_{an}(t), v_{bn}(t), v_{cn}(t)\}$ where the voltages are not in the sinusoidal steady state. That is, the voltages are arbitrary signals. As an example, Fig. B.8 shows a three phase PWM inverter connected to a three phase source with source inductance and resistance (where R, L of the source are unequal). This is Case B.3 offered as an example of a generalized case. Let S be closed at $t = 0$. Figure B.9 shows the time domain representation of the inverter supply voltages. The amplitude spectra of $\{V_{an}(h\omega_e), V_{bn}(h\omega_e), V_{cn}(h\omega_e)\}$ are shown in Fig. B.10. Note that the amplitude spectra are only part of the FFT: the phase spectra are not shown here. In Fig. B.10, the amplitude spectra are shown versus harmonics of 60 Hz, labeled h. The actual Fourier spectrum of these voltages are continuous in ω, and only for convenience depicted as an FFT with resolution $\Delta\Omega = 1.129$ rad/s in Fig. B.10. The actual resolution in the calculation shown in Fig. B.10 is

$$\Delta\Omega = \frac{2\pi}{N\Delta T}$$

$$= \frac{2\pi}{(334)(1/60)} = 1.129 \text{ rad/s.}$$

Also, the FFT shown in Fig. B.10 depicts only a part of the FFT calculated to avoid the mirror image effect

$$V(k\Delta\Omega) = [V((N-k-1)\Delta\Omega)], \qquad k = 0, 1, 2, ..., N/2.$$

The *dq0* voltages are shown in Fig. B.11. The corresponding amplitude frequency spectra depend on which time window is used. For example, the time window $[\frac{12}{60}, \frac{13}{60}]$ second and $[\frac{13}{60}, \frac{14}{60}]$ second results are shown in Fig. B.12.

Note that in Fig. B.12, the predominant *dq0* signals are in the *d* and *q* components for the time windows depicted. This agrees qualitatively with Table B.1.

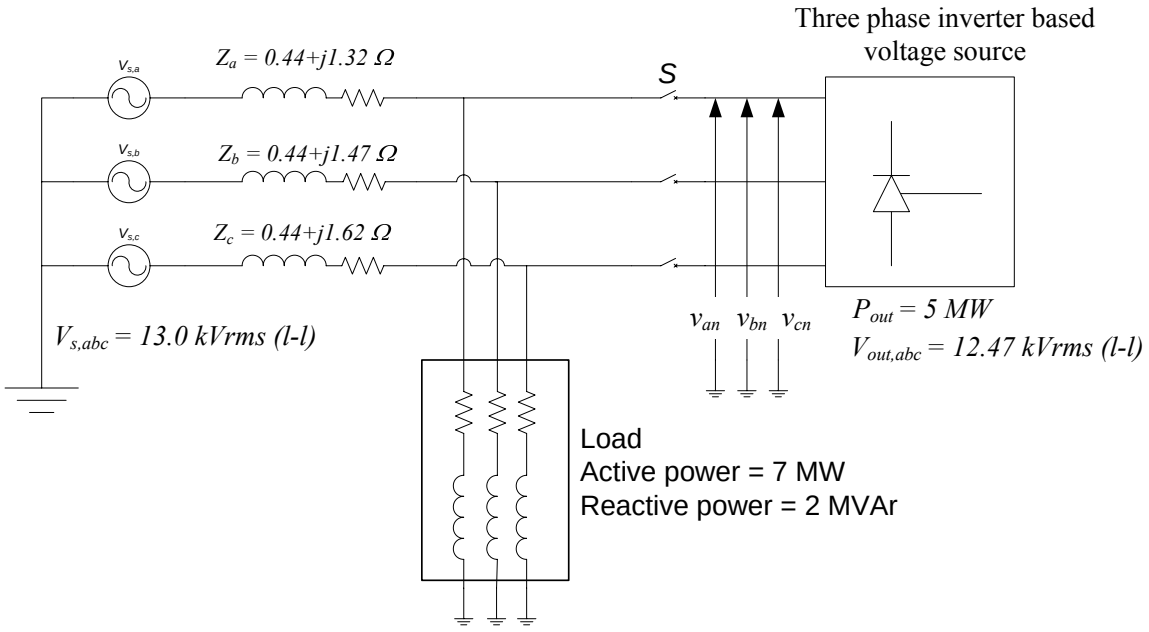

Figure B.8 Three phase PWM inverter connected to a three phase sinusoidal voltage through unbalanced impedances, Case B.3

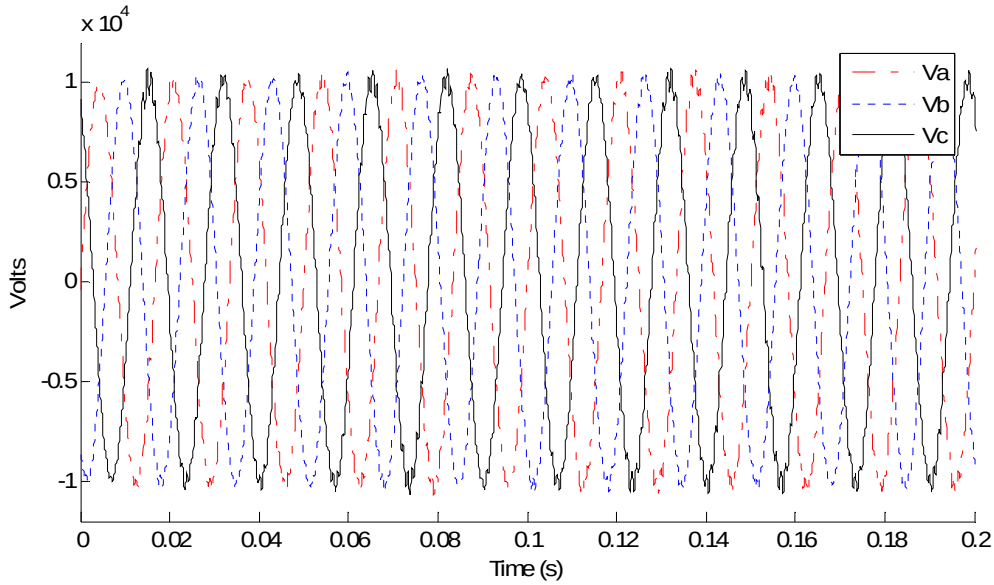

Figure B.9 Time domain representation (*abc* variables) of the inverter supply voltages $\{v_{an}, v_{bn}, v_{cn}\}$, Case B.3

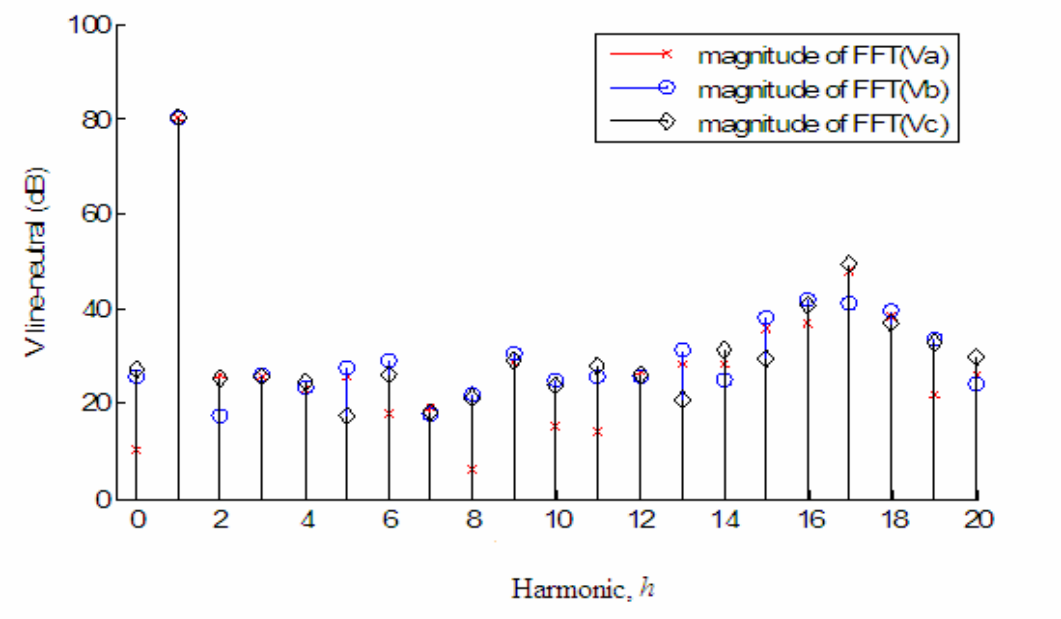

Figure B.10 Amplitude spectra of $V_{an}(h\omega_e)$, $V_{bn}(h\omega_e)$, and $V_{cn}(h\omega_e)$ calculated over time window, t_w = [0.2, 0.21667] s, Case B.3

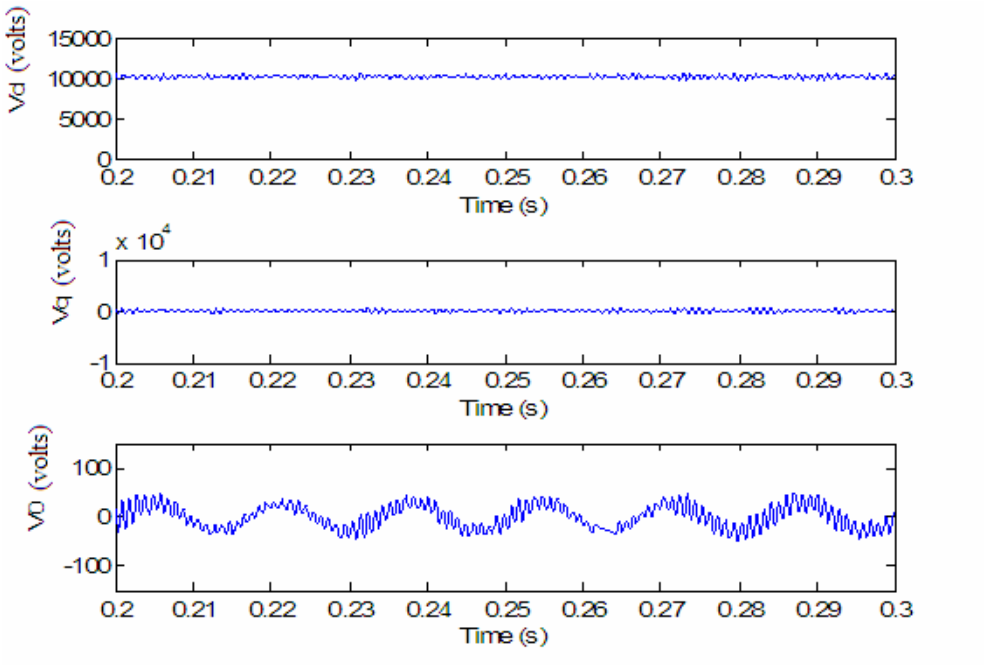

Figure B.11 Time domain representation (*dq0* variables) of the inverter supply voltages, Case B.3

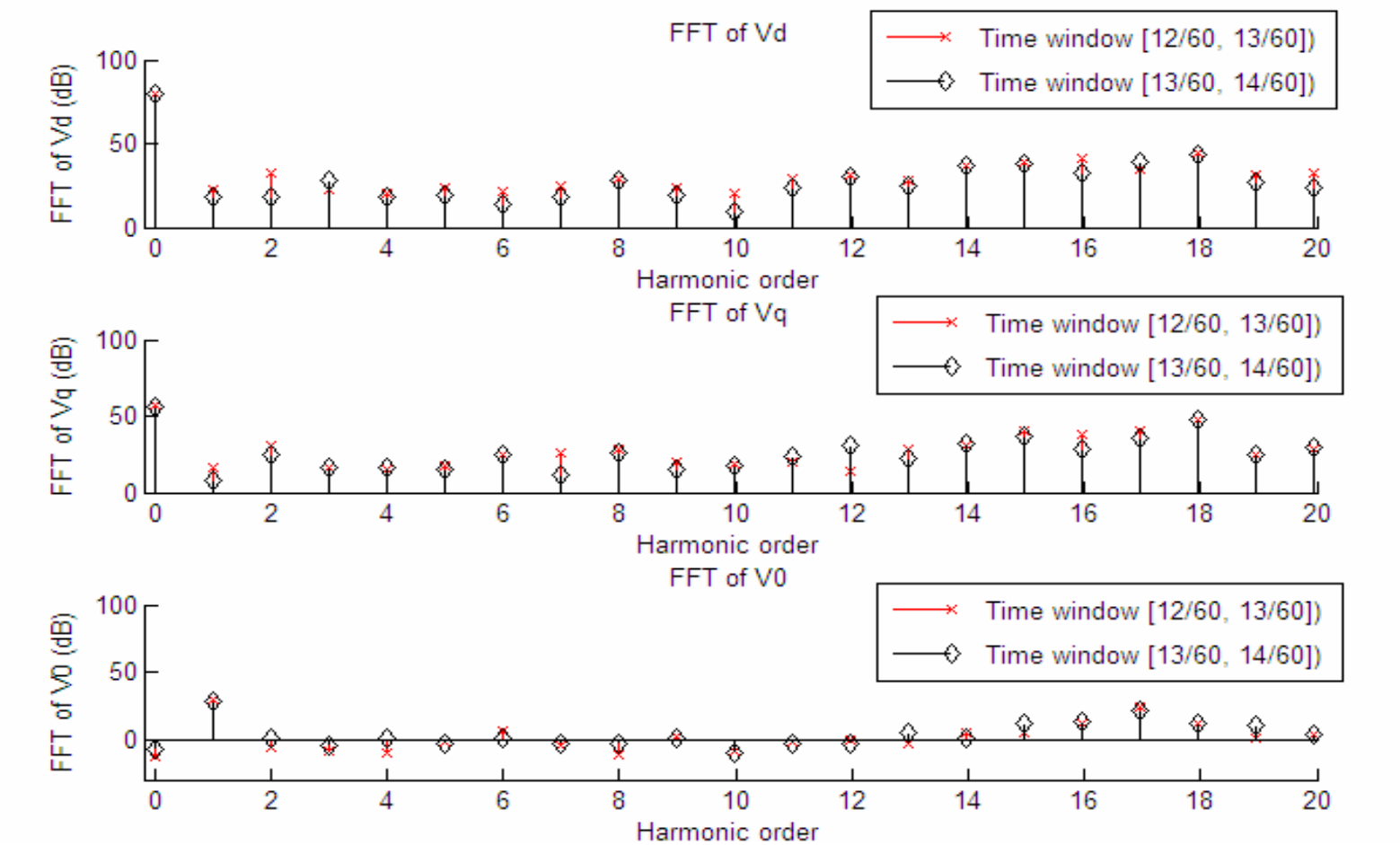

Figure B.12 Amplitude frequency spectra of the voltages in *dq0* variables with the time window [12/60, 13/60] and [13/60, 14/60] second Case B.3

APPENDIX C

LIST OF CONDITIONS FOR ALL THE EXPERIMENTS

This appendix shows the summary of the experiment in this thesis. All experiments in Chapters 3 - 6 are simulated based on the Thunderstone system.

Table C.1 Summary of the case studies in Chapters 2 - 4

Case	Locations of DG	Varied parameters	Target of experiments	Test bed
2.1	stand alone operation (disconnected from the grid)	MW power output	Illustrates the operation of inverter	-
2.2	DG connected to the grid	MW power output	Illustrates the operation of inverter	-
3.1	Cameron2, Signal3, Sage3, Seaton2	Number and locations of DGs in the system	Severity of the change of fault current	Thunderstone
3.2	Seaton, Cameron2, Signal3, Sage3	AVR turn on/off	Severity of the change of fault current	Thunderstone
3.3	Cameron2, Signal3 Sage3, Seaton2	Impedance of DGs	Severity of the change of fault current	Thunderstone
4.1	Cameron2, Signal3, Seaton2, Ealy3, Ealy4, Sage3.	Impedance of DGs, location of new DGs	Illustrates application of the online assessment of fault current (without DG)	Thunderstone
4.2	Cameron2, Signal3, Seaton2, Ealy3, Ealy4, Sage3.	Impedance of DGs, location of new DGs	Illustrates application of the online assessment of fault current (with DG)	Thunderstone

Table C.2 (cont.) Summary of the case studies in Chapters 5 – 7 and Appendix B

Case	Locations of DG	Varied parameters	Target of experiments	Test bed
5.1	Cameron2, Signal3, Seaton2, Ealy3, Ealy4 and Sage3	Impedance of DGs, location of new DGs	Demonstrate the estimation of ACF	Thunderstone
6.1	Cameron2, Signal13, Super14, Super15, Seaton2, Early3, Early4, Sage3	Impedance of DGs, location of new DGs	Application of dynamic programming for solving the UC protblem with FLC	Thunderstone
7.1	-	Settings of ITDOC relays	Illustrate the application of ACO optimization technique	Test bed Case 7.1
7.2	Bus 6	Settings of ITDOC and distance relays	Illustrate the application of ACO optimization technique	Test bed Case 7.2

APPENDIX D

MATLAB CODES FOR THE ANT COLONY ALGORITHM

D.1 Main program

```
% MAIN PROGRAM ==> ACO for RELAY COORDINATION with DGs
% INTERNAL VARIABLES
%   phero1    -  Dense matrix nAllTD x nAllTP contains pheromone
%                from line(1) to line (2).
%    ...
%   phero13   -  Sparse matrix nAllTD x nAllTP contains pheromone
%                from line(13) to line (14).
%   PathData  -  Dense matrix Nants x Nbus contains information (i.e., Ants
%                visited locations)
%   AntsChoiceTD
%             -  Dense matrix contains the choice of TD of each ant
%   AntsChoiceTP
%             -  Dense matrix contains the choice of TP of each ant
%
%   Example of phero1 from line(1) to line (2)
%
%  --------------------   TP  -----------------------
% TD            1   2    ...   nAllTP
% 1
% 2
% ...
% nAllTD
% ------------------------------------------------
% Structure of PathData
%                    Visited Line
% Ant1    2  3  4  5  6  ... 14
% Ant2    7  8  9 10  11 ... 6
% ...
% Antn

%-------------------------------------------------------------------------
% Standard Current transformer turn ratios
% 20:1, 40:1, 60:1, 80:1, 100:1, 120:1,160:1,180:1,200:1, 240:1
%-------------------------------------------------------------------------
% Standard Tap settings
% 1.0, 1.2, 1.5, 2.0, 2.5, 3.0, 3.5, 4.0, 5.0, 6.0, 7.0, 8.0, 10.0, 12.0
%-------------------------------------------------------------------------
% Standard Time dial settings
% 1/2, 1, 2, 3, 4, 5, 6, 7, 8, 9, 10, 11
%-------------------------------------------------------------------------
clc; clear;
global AdjB AdjIf RelayData BusIf A B p CTchoice TDChoice TapChoice

load data6bus.mat

fprintf('Base current = ');
fprintf('%5.2f',baseI)
fprintf(' A \n')
nline = 8;                    % number of distribution line
%-------------------------------------------------------------------------
% Ant colony system characteristics
ncount = 10;

Nants = 25;                                     % number of ants
round = 10;                                     % Number of travel
% Tf = 10;
alpha = 2.0; beta = 2.2;
rho = 0.2;                                      %Pheromone discount factor
q0 = 0.8;
CI = 0.3;                                       % Coordination time (s)

%-------------------------------------------------------------------------

nAllTap = length(TapChoice);
nAllTD  = length(TDChoice);
```

```
nAllCT  = length(CTchoice);

%-------------------------------------------------------------------------
% Pheromone initialization
% Note that the Phero matrices related to the RelayData
% Example
% Phero1 --> belong to RelayData(1,1) and RelayData(1,2) Consider the same
% set in each line protection (temporary)

%-------------------------------------------------------------------------
% Pheromone initialization
% Note that the Phero matrices related to the RelayData
% Example
% Phero1 --> belong to RelayData(1,1) and RelayData(1,2) Consider the same
% set in each line protection (temporary)
tic
BestObj = 10^6;     count = 0;
% % while BestObj > 4.0 & count < ncount;
% %     count = count + 1;
for n = 1 : length(RelayData)
    eval(['phero',num2str(n),' = 0.0002*ones(nAllTap,nAllCT,nAllTD);']);
end

%-------------------------------------------------------------------------

    for rnd = 1 : round
        PathData = zeros(Nants,length(RelayData));

        for n =1 : Nants
            %     PathData(n,:) = randperm(length(RelayData)/2);
            PathData(n,:) = randperm(length(RelayData));  % Create path data (not include
       the line to slack bus
        end

        % Initialize ant's options
        AntChoiceTD = zeros(Nants,nline*2);
        AntChoiceTP = zeros(Nants,nline*2);
        AntChoiceCT = zeros(Nants,nline*2);

        %-------------------------------------------------------------------------
        % Tour Construction
        TourconsRC;
        %-------------------------------------------------------------------------
        % Update statistics
        [Obj,BestChoice]= ObjFunc(AntChoiceTP,AntChoiceCT,AntChoiceTD);

        if BestObj > Obj
            BestTP =  AntChoiceTP(BestChoice(1),:);
            BestCT =  AntChoiceCT(BestChoice(1),:);
            BestTD =  AntChoiceTD(BestChoice(1),:);
            BestObj = Obj;
%             beep
        end
         LocalSearch;

        %-------------------------------------------------------------------------
        % Evaporate
        evaporate;
        UpdatePhe;
    end
    BestObj
%     BestRec(count) = Obj;
%     count
% end
if count == ncount
    fprintf('Stop --> ncount')
end
```

```
[BusPrim,CIout,BestObj] = CIs(BestTP,BestCT,BestTD);
BestTP
BestCT
BestTD
CIout
toc
t= toc
BestObj
RelayData(:,4) = BestCT;
RelayData(:,6) = BestTP;
RelayData(:,7) = BestTD;

% save testset14.mat BestTP BestCT BestTD RelayData Nants round alpha  beta rho q0 CI

% zone2;
% Rzone2
```

D.2 Data preparation

```
% +++ ACO algorithm for relays coordination -- 6 bus example +++
% This module calculate the fault current (SLG) as the input of ACO
% algorith for relays coordination  (by NN. Jan. 2006)
clc; clear;
%------------------------------------------------------------------------
% INTERNAL VARIABLES
%   RL    -    Line resistance (assumming pos. and neg sequence impedace are
%              the same) ohm/mile
%   RL0   -    zero sequence resistance of the line (ohm/mile)
%   XL    -    Line inductance (assumming pos. and neg sequence impedace are
%              the same) (ohm/mile)
%   XL0   -    zero sequence of the line inductance  (ohm/mile)

%------------------------------------------------------------------------
basemva = 15;  accuracy = 0.0001;  maxiter = 10;
a = cos(2*pi/3)+j*sin(2*pi/3);
At = [1   1  1;
      1 a^2  a;
      1 a   a^2];
% ========================================================================
% The following variables define system parameter of 6-bus system.
% Configuration of this system can be found in overview.visio
%
%    Bus code definition Slackbus==1  Load bus==0 GenBus==2
%        Bus  Bus   |V|  Ang   ---Load---      ---Gen---   Gen Mvar Injected
%        No.  code p.u.  Deg   MW     Mvar    MW   Mvar   Min   Max    Mvar
%    ------------------------------------------------------------------------
busdata=[1    1    1.03  0    00.0    0.0    0.0   0.0    0     0      0
         2    0    1.00  0    1.79   0.35    0.0   0.0    0     0      0
         3    0    1.00  0    0.98   0.32    0.0   0.0    0     0      0
         4    0    1.00  0   1.275   0.42    1.0   0.0    0     0.3    0
         5    0    1.00  0     1.1   0.244   0.0   0.0    0     0      0
         6    2    1.00  0    1.26   0.414   3.0   0.0    0     2      0 ];

%          Gen.      Ra         Xd'
gendata =[ 1         0.00      0.08*15/100+0.0786
%            4         0.00      1.5
           6         0.00      0.9*15/5 ];
gendata0=[ 1         0.00      0.02*15/100+0.0786
%            4         0.00      0.5
           6         0.00      0.3*15/5 ];

RL = 0.141 / (12^2/basemva);
XL = 0.332 / (12^2/basemva);
RL0 = 0.32 / (12^2/basemva);
XL0 = 0.934 / (12^2/basemva);
RL0 = RL0/3;
XL0 = XL0/3;
% include transformer reactance
%            Bus   Bus     R        X     1/2B     a
%            No.  No.   p.u.    p.u.  p.u.
linedata = [ 1     2    5.2*RL  5.2*XL    0.0000   1
             1     3    4.4*RL  4.4*XL    0.0000   1
             2     4    3.4*RL  3.4*XL    0.0000   1
             3     4    4.4*RL  4.4*XL    0.0000   1
             3     5      3*RL    3*XL    0.0000   1
             4     5    3.8*RL  3.8*XL    0.0000   1
             4     6    1.1*RL  1.1*XL    0.0000   1
             5     6    2.8*RL  2.8*XL    0.0000   1  ];
linedata0= [ 1     2    5.2*RL0  5.2*XL0   0.0000   1
             1     3    4.4*RL0  4.4*XL0   0.0000   1
             2     4    3.4*RL0  3.4*XL0   0.0000   1
             3     4    4.4*RL0  4.4*XL0   0.0000   1
             3     5      3*RL0    3*XL0   0.0000   1
             4     5    3.8*RL0  3.8*XL0   0.0000   1
```

```
            4     6    1.1*RL0  1.1*XL0    0.0000   1
            5     6    2.8*RL0  2.8*XL0    0.0000   1  ];
%-------------------------------------------------------------------------
AdjB  =  [1   2   3   0   0   0;
          2   1   4   0   0   0;
          3   1   4   5   0   0;
          4   2   3   5   6   0;
          5   3   4   6   0   0;
          6   4   5   0   0   0];
LinAdj =  [1000   inv(linedata(1,3)+j*linedata(1,4))
       inv(linedata(2,3)+j*linedata(2,4))   0     0    0;
           1000   inv(linedata(1,3)+j*linedata(1,4))
       inv(linedata(3,3)+j*linedata(3,4))   0     0    0;
           1000   inv(linedata(2,3)+j*linedata(2,4))
       inv(linedata(4,3)+j*linedata(4,4))  inv(linedata(5,3)+j*linedata(5,4)) 0    0;
           1000   inv(linedata(3,3)+j*linedata(3,4))
       inv(linedata(4,3)+j*linedata(4,4))  inv(linedata(6,3)+j*linedata(6,4))
       inv(linedata(7,3)+j*linedata(7,4))     0;
           1000   inv(linedata(5,3)+j*linedata(5,4))
       inv(linedata(6,3)+j*linedata(6,4))  inv(linedata(8,3)+j*linedata(8,4)) 0  0;
           1000   inv(linedata(7,3)+j*linedata(7,4))
       inv(linedata(8,3)+j*linedata(8,4))     0 0 0];


%-------------------------------------------------------------------------
Lfybus; % Calculate Ybus matrix for load flow calculation
Lfnewton % Power flow solution by Newton-Raphson method
Vf = V;
Zbus=Zbuildpi(linedata,gendata,yload);
Zbus0=Zbuildpi(linedata0,gendata0,yload);

for n=1:size(Zbus,1)
    BusIf(n)=  3*Vf(n)/(2*Zbus(n,n)+Zbus0(n,n)); % SLG Fault current of orig system
end

for n = 1 : length(AdjB)      % Fault at bus n
    AdjIfSLG(n,1) = n;        % Current flow from bus k
    for k = 1: length(AdjB)
        temp = [0;Vf(n);0] - [Zbus0(k,n) 0 0;0 Zbus(k,n) 0; 0 0 Zbus(k,n)]*...
               [BusIf(n);BusIf(n);BusIf(n)]/3;
        vp(n,k,:) = At*temp ;
    end
end
%-------------------------------------------------------------------------
% This module create SLG fault current
AdjIf = zeros(length(AdjB),length(AdjB));
for n = 1: length(AdjB)
    indx = find(AdjB(n,:)~=0);
    for k = 2 : length(indx)
        AdjIf(n,indx(k)) = (vp(n,AdjB(n,indx(k)),1)-vp(n,n,1))* LinAdj(n,indx(k));
    end
end
%-------------------------------------------------------------------------
% fprintf('-----------------------------------------------------------\n')
% fprintf('  Fault point     Bus#       A         B         C    \n')
% fprintf('-----------------------------------------------------------\n')
% for n = 1 : length(AdjB)
%     fprintf('%5.0f',n)
%     for k = 1: length(AdjB)
%         if k == 1
%             fprintf('%15.0f', k)
%         else
%             fprintf('%20.0f', k)
%         end
%         fprintf('%12.2f',abs(vp(n,k,1)));
%         fprintf('%10.2f',abs(vp(n,k,2)));
%         fprintf('%10.2f\n',abs(vp(n,k,3)));
%     end
```

```
% end
% fprintf('-----------------------------------------------------\n')
% -------------------------------------------------------------------------
% This module create RelayData 2 relays/line
indx2 =1;  indx3 = 1;
for n = 1:length(AdjB)
    line = length(find(AdjB(n,:) >= AdjB(n,1)));            % find number of line to the
       considering bus
    if line > 1
        indx = 2;
        for k = 2 : line
            while AdjB(n,1) > AdjB(n,indx)
                indx = indx+1;
            end
              RelayData(indx2,1) = AdjB(n,1);
              RelayData(indx2,2) = AdjB(n,indx);
              RelayData(indx2,3) = indx3;
              RelayData(indx2+1,1) = AdjB(n,indx);
              RelayData(indx2+1,2) = AdjB(n,1);
              RelayData(indx2+1,3) = indx3;

              indx = indx+1;
              indx2 = indx2+2;
              indx3 = indx3+1;
        end
    end
end
% -------------------------------------------------------------------------
baseI = 25*10^6/1.732/(12*10^3);
AdjIf(:,2:size(AdjIf,2)) = abs(AdjIf(:,2:size(AdjIf,2)))*baseI;
BusIf = abs(BusIf)*baseI;
%-------------------------------------------------------------------------
% Relay characteristics
% Model A CO:
% Moderately inverse  Very inverse  Extremely inverse
A = [0.047;              18.92;         28.08];
B = [0.183;              0.492;         0.130];
p = [0.02;               2;             2    ];
%              1   2   3   4    5    6    7    8    9   10
CT  =         [20; 20; 20; 20;  20;  20;  20;  20;  20;  20;...
               20; 20; 20; 20;  20;  20                    ];% CT ratio is 100:1

% CTchoice =    [20; 40; 60; 80; 100; 120; 160; 180; 200; 240];
CTchoice =    [20; 40; 60; 80; 100; 120; 160; 180; 200; 240];
% Tap setting of relays
%              1   2   3   4    5    6    7    8    9   10
tap =  1.0/10*[10; 10; 10; 10;  10;  10;  10;  10;  10;  10;...
               10; 10; 10; 10;  10;  10                    ];    % Tap setting of relays
TapChoice =   [1.0, 3.5, 4.0, 5.0, 8.0, 10.0, 12.0]';
% Type of relays
Type=  2*     [  1;  1;  1;  1;  1;   1;   1;   1;   1;  1;...
                 1;  1;  1;  1;  1;   1];

TD  = 2* ones(length(CT),1);
% TDChoice = [1/2, 1, 2, 3, 4, 5, 6, 7, 8, 9, 10, 11]';
TDChoice =   [1/2, 1, 2, 3, 4, 5, 6, 7, 8, 9, 11]';

%-------------------------------------------------------------------------
%-------------------------------------------------------------------------
% This module create RelayData 2 relays/line
%   ----------------------RelayData-------------------------
%      (1)       (2)    (3)    (4)     (5)    (6)     (7)
%   LineFrom    LineTo  Line#   CT    Type    Tap   TimeDial
%   -------------------------------------------------------
indx2 =1;  indx3 = 1;
for n = 1:length(AdjB)
    line = length(find(AdjB(n,:) >= AdjB(n,1)));            % find number of line to the
       considering bus
```

```
    if line > 1
        indx = 2;
        for k = 2 : line
            while AdjB(n,1) > AdjB(n,indx)
                indx = indx+1;
            end
              RelayData(indx2,1) = AdjB(n,1);
              RelayData(indx2,2) = AdjB(n,indx);
              RelayData(indx2,3) = indx3;
              RelayData(indx2+1,1) = AdjB(n,indx);
              RelayData(indx2+1,2) = AdjB(n,1);
              RelayData(indx2+1,3) = indx3;

              indx = indx+1;
              indx2 = indx2+2;
              indx3 = indx3+1;
        end
    end
end
% Create RelayData matrix.
RelayData(:,4) = CT;
RelayData(:,5) = Type;
RelayData(:,6) = tap;
RelayData(:,7) = TD;
%-------------------------------------------------------------------------
save data6bus.mat AdjB AdjIf RelayData BusIf A B p CTchoice TDChoice TapChoice...
     linedata baseI
fprintf('-------------------------------------------------------\n')
fprintf('  From     To       R         X         R0        X0  \n')
fprintf('-------------------------------------------------------\n')
for n = 1:length(linedata)
    fprintf('%5.0f',linedata(n,1));
    fprintf('%8.0f',linedata(n,2));
    fprintf('%10.3f',linedata(n,3));
    fprintf('%10.3f',linedata(n,4));
    fprintf('%10.3f',linedata0(n,3));
    fprintf('%10.3f\n',linedata0(n,4));
end
fprintf('-------------------------------------------------------\n')
```

D.3 Local search

```
% LOCAL SEARCH (Apply heuristic)
%-------------------------------------------------------------------------
% This module provide Local search in the Ants colony optimization.  The
% process will be executed after Tourconstruction.
%-------------------------------------------------------------------------
% Standard Tap settings
% 1.0, 1.2, 1.5, 2.0, 2.5, 3.0, 3.5, 4.0, 5.0, 6.0, 7.0, 8.0, 10.0, 12.0
%-------------------------------------------------------------------------
global CTchoice TDChoice TapChoice
BCh = BestChoice(1);
[BusPrim1,CIout1,ObjAnt1] = CIs(BestTP,BestCT,BestTD);
TPtemp = BestTP;
CTtemp = BestCT;
TDtemp = BestTD;
CIout2 = CIout1;
Objstart = ObjAnt1;
for relay = 1 : length(RelayData)

    [BusPrim1,CIout1,ObjAnt1] = CIs(TPtemp,CTtemp,TDtemp);

    indxLC = 0; indxLCTP = 0;
    end1 = RelayData(relay,1);   % end 1 is the fault location
    end2 = RelayData(relay,2);   % end 2 is another end of the line
    indx1 = find(AdjB(:,1) == end1);  % finding the index of the line in RelayData
    Adj1 = nonzeros(AdjB(indx1,2:size(AdjB,2)));  % adjacent bus of end1
    indx2 = find(AdjB(:,1) == end2);
    Adj2 = nonzeros(AdjB(indx2,2:size(AdjB,2)));  % adjacent bus of end2
    %
    Adj1 =  Adj1(find(Adj1~=end2));
    Adj2 =  Adj2(find(Adj2~=end1));
    % UpgradeLine tells the rows in RelayData that needed to be change
    % in this visit
    UpgradeLine = [];
    for kk = 1: length(Adj1)
        if end1 ~= 1   % ignore the relay on swing bus
            UpgradeLine =  [UpgradeLine,find(RelayData(:,1) == Adj1(kk) & RelayData(:,2)
       == end1)];
        end
    end

    if CIout2(relay) > 0.3    % if it's longer than 0.3
        for u = 1: length(UpgradeLine)  % Do for all Upgradeline
            CIout2(relay) = 0.31;
            countLC = 0;
            ObjAnt2 = ObjAnt1-0.1;
            while ObjAnt2 < ObjAnt1 & CIout2(relay) > 0.3 & countLC<10
                countLC = countLC +1;
                ObjAnt1 = ObjAnt2;
                if TDtemp(UpgradeLine(u))~= min(TDChoice)  % if BestTD is not at the
       boundary of TD
                    indxLC = find(TDChoice == TDtemp(UpgradeLine(u)));
                    TDtemp(UpgradeLine(u))= TDChoice(indxLC-1);
                    % if BestTD is at the boundary of TD --> step down CT --> faster
                elseif TDtemp(UpgradeLine(u))== min(TDChoice) & TPtemp(UpgradeLine(u))~=
       min(TapChoice)
                    indxLC = find(TDChoice == TDtemp(UpgradeLine(u)));
                    indxLCTP = find(TapChoice == TPtemp(UpgradeLine(u)));
                    TPtemp(UpgradeLine(u))= TapChoice(indxLCTP-1);
                    TDtemp(UpgradeLine(u)) = TDChoice(length(TDChoice)-5);
                elseif TDtemp(UpgradeLine(u))== min(TDChoice) & TPtemp(UpgradeLine(u))==
       min(TapChoice)...
                        & CTtemp(UpgradeLine(u))~= min(CTchoice)
                   TDtemp(UpgradeLine(u)) = TDChoice(length(TDChoice)-5);
                   TPtemp(UpgradeLine(u))= TapChoice(length(TapChoice)-5);
                   indxLCCT = find(CTchoice==CTtemp(UpgradeLine(u)));
```

```
                   CTtemp(UpgradeLine(u))= CTchoice(indxLCCT-1);
               end
               [BusPrim2,CIout2,ObjAnt2] = CIs(TPtemp,CTtemp,TDtemp);

           end
           if indxLC ~= 0
               TDtemp(UpgradeLine(u)) = TDChoice(indxLC);

               if indxLCTP ~=0 & TPtemp(UpgradeLine(u))~= max(TDChoice)
                   TPtemp(UpgradeLine(u)) = TapChoice(indxLCTP-1);
               elseif indxLCTP ~=0 & TPtemp(UpgradeLine(u)) == max(TDChoice)
                   TPtemp(UpgradeLine(u)) = TapChoice(indxLCTP);
                   TDtemp(UpgradeLine(u))= max(TDChoice);
               end
           end
               [BusPrim2,CIout2,ObjAnt2] = CIs(TPtemp,CTtemp,TDtemp);
       end                             % End Do for all Upgradeline > 0.3
   elseif CIout2(relay) < 0.0    % if it's longer than 0.3
% ------------------------------------------------------------------------
       for u = 1: length(UpgradeLine)  % Do for all Upgradeline
           CIout2(relay) = 0.29;
           countLC = 0;
           ObjAnt2 = ObjAnt1-0.1;
           while ObjAnt2 < ObjAnt1 %& CIout2(relay) < 0.29 & countLC<10
               countLC = countLC +1;
               ObjAnt1 = ObjAnt2;
               if TDtemp(UpgradeLine(u))~= max(TDChoice)  % if BestTD is not at the
       boundary of TD
                   indxLC = find(TDChoice == TDtemp(UpgradeLine(u)));
                   TDtemp(UpgradeLine(u))= TDChoice(indxLC+1);
                   % if BestTD is at the boundary of TD --> step down CT --> faster
               elseif TDtemp(UpgradeLine(u))== max(TDChoice) & TPtemp(UpgradeLine(u))~=
       max(TapChoice)
                   indxLC = find(TDChoice == TDtemp(UpgradeLine(u)));
                   indxLCTP = find(TapChoice == TPtemp(UpgradeLine(u)));
                   TPtemp(UpgradeLine(u))= TapChoice(indxLCTP+1);
                   TDtemp(UpgradeLine(u)) = TDChoice(length(TDChoice)-5);
               elseif TDtemp(UpgradeLine(u))== max(TDChoice) & TPtemp(UpgradeLine(u))==
       max(TapChoice)...
                      & CTtemp(UpgradeLine(u))~= max(CTchoice)
                  TDtemp(UpgradeLine(u)) = TDChoice(length(TDChoice)-5);
                  TPtemp(UpgradeLine(u))= TapChoice(length(TapChoice)-5);
                  indxLCCT = find(CTchoice==CTtemp(UpgradeLine(u)));
                  CTtemp(UpgradeLine(u))= CTchoice(indxLCCT+1);
               end
               [BusPrim2,CIout2,ObjAnt2] = CIs(TPtemp,CTtemp,TDtemp);

           end

               TDtemp(UpgradeLine(u)) = TDChoice(indxLC);

               if indxLCTP ~=0 & TPtemp(UpgradeLine(u))~= min(TDChoice)
                   TPtemp(UpgradeLine(u)) = TapChoice(indxLCTP+1);
               elseif indxLCTP ~=0 & TPtemp(UpgradeLine(u)) == min(TDChoice)
                   TPtemp(UpgradeLine(u)) = TapChoice(indxLCTP);
                   TDtemp(UpgradeLine(u))= min(TDChoice);
               end
               [BusPrim2,CIout2,ObjAnt2] = CIs(TPtemp,CTtemp,TDtemp);
       end                             % End Do for all Upgradeline > 0.3
% ------------------------------------------------------------------------
    end                        % endif local search
    [BusPrim1,CIout1,ObjAnt1] = CIs(TPtemp,CTtemp,TDtemp);
end
[BusPrim1,CIout1,ObjAnt1] = CIs(TPtemp,CTtemp,TDtemp);
if ObjAnt1 < Objstart
    BestTP= TPtemp;
    BestCT = CTtemp;
    BestTD = TDtemp;
```

```
end

[BusPrimLC,CIoutLC,BestObj] = CIs(BestTP,BestCT,BestTD);
if Objstart>BestObj
    fprintf(['Local search success!!!  BestBobj = ', num2str(BestObj),'\n'])
end
```

D.4 Tour construction

```
% TOUR CONSTRUCTION  (ACO_RC)
%-------------------------------------------------------------------------
%  This code provide the tour constuction of each ants.  The probability of
%  the neighborhood depends on the tour factor and amount of pheormone Pher(i,j).
%  The next TP and TD to be visited is choosen by the roullete wheel.
%-------------------------------------------------------------------------
% INTERNAL VARIABLES
% UpgradeLine -  Vector contains the relay that need to be upgraded.  This
%                vector in terms of row in RelayDATA
%
%-------------------------------------------------------------------------
% STEPS
% 1) Each agent move from the first Bus to the last Bus depending on the ;
% 2)
%
%-------------------------------------------------------------------------
%
TotalPheN = 0;
% set up the Relay data of the first line to the last line
for n = 1:size(PathData,2)
    for a = 1: Nants                            % Same procedure for all ants
            if rand(1) < q0
                % argmax(Til[nil]^beta)  --> choose hightest pheromone path
                dist = 1./DistMatrix(RelayData(PathData(a,n),:));
                eval(['Cphero = phero',num2str(PathData(a,n)),';']); % Draw data from
        current path

                arg = dist.^beta.*Cphero;
                maxarg=[0;0;0]; argmax=0;
                for TDarg = 1: length(TDChoice)
                    [Tapstep,CTstep] = find(arg(:,:,TDarg) == max(max(arg(:,:,TDarg))));
                    if argmax<arg(Tapstep(1),CTstep(1),TDarg)
                        argmax = arg(Tapstep(1),CTstep(1),TDarg);  % find the max arg
                        maxarg = [Tapstep(1);CTstep(1);TDarg(1)];
                    end
                end

                % update TD in RelayData (column 7)
                AntChoiceTD(a,PathData(a,n)) = TDChoice(TDarg(1));

                % update TP in RelayData (column 6)
                AntChoiceTP(a,PathData(a,n)) = TapChoice(Tapstep(1));

                % update CT in RelayData (column 4)
                AntChoiceCT(a,PathData(a,n)) = CTchoice(CTstep(1));
            else
                % Roulette wheel
                dist = 1./DistMatrix(RelayData(PathData(a,n),:));
                eval(['Cphero = phero',num2str(PathData(a,n)),';']); % Draw data from
        current path

                PheN = (dist.^beta.*Cphero.^alpha);   % Pheromone^beta * dist^alpha
                sumt = 0;

                % This part do the cumulative sumation of the PheN matrix
                % move from (1,1,1) --> (1,2,1) --> (1,3,1) --> (1,n,1)
                %           (2,1,1) --> ...
                %           (n,1,1) ...
                %           (1,1,2)...

                for pp = 1:nAllTD
                    for k = 1: nAllTap
                        cumPheN(k,:,pp)= sumt+ cumsum(PheN(k,:,pp));
                        sumt = sum(PheN(k,:,pp))+sumt;
                    end
```

```
                end

                TotalPheN = sum(sum(sum(PheN)));
%                 Cprob_TD = cumsum(dist.^beta.*Cphero.^alpha)./...
%                     (ones(nAllTD,1)*sum(dist.^beta.*Cphero.^alpha));
                Cprob  = cumPheN/TotalPheN;
                ran = rand(1);
                pp = 1;
                while isempty(find(Cprob(:,:,pp) > ran)) == 1
                    pp=pp+1;
                end
                [TPstep,CTstep] = find(Cprob(:,:,pp) < ran);
                CTstep = find(Cprob(max(TPstep),:,pp) > ran);
                if isempty(CTstep) == 1 & isempty(TPstep) == 1 & pp == 1
                    CTstep = 1;
                    TPstep = 1;
                elseif isempty(CTstep) == 1 & isempty(TPstep) == 1 & pp ~= 1
                    pp = pp - 1;
                    CTstep = nAllCT;
                    TPstep = nAllTap;
                elseif isempty(CTstep) == 1 & isempty(TPstep) == 0
                    TPstep = max(TPstep);
                    CTstep = nAllCT;
                else
                    CTstep = min(CTstep) -1;
                    TPstep = max(TPstep);
                end
                TDstep = pp;
%                 Cprob(TPstep,CTstep,TDstep)

                % update TD in RelayData (column 7)
                AntChoiceTD(a,PathData(a,n)) = TDChoice(TDstep);

                % update TP in RelayData (column 6)
                AntChoiceTP(a,PathData(a,n)) = TapChoice(TPstep);

                % update CT in RelayData (column 4)
                AntChoiceCT(a,PathData(a,n)) = CTchoice(CTstep);
            end
    end
end
```

D.5 Objective function

```
% Objective function
function [Obj,BestChoice] = ObjFunc(AntTP,AntCT,AntTD)
global AdjB AdjIf RelayData BusIf A B p CTchoice TDChoice TapChoice
BusPrim = zeros(size(AntTD)); vio =0;
SecT = zeros(length(AntTD),1);
for Ant = 1: length(AntTD)
    for relay = 1: length(RelayData)
        % Bus primary protection
        Mpri = BusIf(RelayData(relay,1))/(AntTP(Ant,relay)*AntCT(Ant,relay));
        Typ  = RelayData(relay,5);
        BusPrim(Ant,relay) = AntTD(Ant,relay)*A(Typ)/(Mpri^p(Typ)-1)+B(Typ);

        % ------------------ Find UpgradeLine -----------------------------
        end1 = RelayData(relay,1);   % end 1 is the fault location
        end2 = RelayData(relay,2);   % end 2 is another end of the line
        indx1 = find(AdjB(:,1) == end1);  % finding the index of the line in RelayData
        Adj1 = nonzeros(AdjB(indx1,2:size(AdjB,2)));  % adjacent bus of end1
        indx2 = find(AdjB(:,1) == end2);
        Adj2 = nonzeros(AdjB(indx2,2:size(AdjB,2)));  % adjacent bus of end2
        %
        Adj1 =  Adj1(find(Adj1~=end2));
        Adj2 =  Adj2(find(Adj2~=end1));
        % UpgradeLine tells the rows in RelayData that needed to be change
        % in this visit
        UpgradeLine = [];
        for kk = 1: length(Adj1)
            if Adj1(kk) ~= 1
                UpgradeLine =  [UpgradeLine,find(RelayData(:,1) == Adj1(kk) & Relay-
       Data(:,2) == end1)];
            end
        end
        if end1 ~=1  %***  Ignore fault at bus 1  --> Whole system collapse if fault oc-
       curs at bus 1
            for n = 1:length(UpgradeLine)
                if RelayData(UpgradeLine(n),1) ~= end1 & RelayData(UpgradeLine(n),1) ~=
       end2
                    indx = find(AdjB(end1,:) == RelayData(UpgradeLine(n),1));
                    Ifsec = AdjIf(end1,indx);
                else
                    indx = find(AdjB(end1,:) == RelayData(UpgradeLine(n),2));
                    Ifsec = AdjIf(end1,indx);
                end
                Msec = Ifsec/(AntTP(Ant,UpgradeLine(n))*AntCT(Ant,UpgradeLine(n)));
                Typ  = RelayData(UpgradeLine(n),5);
                SecTnew = AntTD(Ant,UpgradeLine(n))*A(Typ)/((Msec^p(Typ)-1))+B(Typ);
                newCI = SecTnew - BusPrim(Ant,relay);       % CI of adjacent line
                % Penalize SecTnew
                if newCI < 0   % sec. operates before pri.  (unacceptable)
                    SecTnew = 10000;
                    vio = vio + 1;
                elseif newCI - 0.3 < 0 % CI less than 0.3
                    SecTnew = ((0.3- newCI)*20)^2;
                elseif newCI - 0.3 > 0 % CI more than 0.3
                    SecTnew = ((0.3- newCI)*10)^2;
                end
                SecT(Ant) = SecT(Ant)+ SecTnew;     % record the secondary protection
       with penalty
            end
        end  %***End Ignore fault at bus 1  --> Whole system collapse if fault occurs at
       bus 1
    end
end
ObjAnt = sum(BusPrim')' + 0.8*SecT; BestChoice = find(ObjAnt == min(ObjAnt));
Obj = min(sum(BusPrim')'+ 0.8*SecT);
% BestChoice = find(BusPrim==Obj);
```

D.6 Consideration of distance relays

```
% CONSIDERATION OF DISTANCE RELAYS (SLG)
%    This module contains the code to include the back up relays in the
%    process of computing the time dial setting of IDMTL

% STEPs
% 1) Calculate the fault current at the associate location of the setting
%    relays
% 2) Set the relay with 2 major constaints
% 3) repeat until finnishing all of the relays\

% Branch data

% Transformer/short ckt impedance / loads
%
function  [F20,F80] = DistanceRelays(LinedataOrg,LinedataOrg0,TFM,BusA,BusB)
basemva = 15;  accuracy = 0.0001;  maxiter = 10;
busdata=  [1    1    1.03  0    00.0    0.0    0.0   0.0    0     0      0
           2    0    1.00  0    1.79   0.35    0.0   0.0    0     0      0
           3    0    1.00  0    0.98   0.059   0.0   0.0    0     0      0
           4    0    1.00  0   1.275   0.205   0.0   0.0    0     0      0
           5    0    1.00  0     1.1   0.244   0.0   0.0    0     0      0
           6    0    1.00  0    1.26    0.28   0.0   0.0    0     0      0 ];
busdata = [busdata;
           7    0    1.00  0       0       0   0.0   0.0    0     0      0
           8    0    1.00  0       0       0   0.0   0.0    0     0      0 ];

%          Gen.      Ra         Xd'
gendata =[ 1         0.00      0.08*15/100+0.0786 ];
gendata0=[ 1         0.00      0.02*15/100+0.0786 ];

% Modified Linedata --> add 2 buses in to the system (fault points) that
% also means add 3 lines in to the Linedata
indxAB = find((LinedataOrg(:,1) == BusA & LinedataOrg(:,2) == BusB) |...
            (LinedataOrg(:,1) == BusB & LinedataOrg(:,2) == BusA));
nlineOrg = size(LinedataOrg,1);
nbusOrg = max(max(LinedataOrg(:,1)),max(LinedataOrg(:,2)));
Linedata = LinedataOrg;
Linedata0 = LinedataOrg0;

% Create the fault bus at 20% from BusA
Linedata(nlineOrg+1,1) = LinedataOrg(indxAB,1);
Linedata(nlineOrg+1,2) = nbusOrg+1;
Linedata(nlineOrg+1,3) = LinedataOrg(indxAB,3)*0.2;
Linedata(nlineOrg+1,4) = LinedataOrg(indxAB,4)*0.2;
Linedata(nlineOrg+1,6) = 1;

Linedata0(nlineOrg+1,1) = LinedataOrg0(indxAB,1);
Linedata0(nlineOrg+1,2) = nbusOrg+1;
Linedata0(nlineOrg+1,3) = LinedataOrg0(indxAB,3)*0.2;
Linedata0(nlineOrg+1,4) = LinedataOrg0(indxAB,4)*0.2;
Linedata0(nlineOrg+1,6) = 1;
% Create the fault bus at 80% from BusA
Linedata(nlineOrg+2,1) = LinedataOrg(indxAB,2);   % From bus
Linedata(nlineOrg+2,2) = nbusOrg+2;               % To bus
Linedata(nlineOrg+2,3) = LinedataOrg(indxAB,3)*0.8;  % Resistance
Linedata(nlineOrg+2,4) = LinedataOrg(indxAB,4)*0.8;  % inductance
Linedata(nlineOrg+2,6) = 1;                          % turn ratio

Linedata0(nlineOrg+2,1) = LinedataOrg0(indxAB,2);   % From bus
Linedata0(nlineOrg+2,2) = nbusOrg+2;                % To bus
Linedata0(nlineOrg+2,3) = LinedataOrg0(indxAB,3)*0.8;  % Resistance
Linedata0(nlineOrg+2,4) = LinedataOrg0(indxAB,4)*0.8;  % inductance
Linedata0(nlineOrg+2,6) = 1;                           % turn ratio
% Create the line between fault bus
Linedata(nlineOrg+3,1) = nbusOrg+1;
Linedata(nlineOrg+3,2) = nbusOrg+2;
```

```
Linedata(nlineOrg+3,3) = LinedataOrg(indxAB,3)*0.6;
Linedata(nlineOrg+3,4) = LinedataOrg(indxAB,4)*0.6;
Linedata(nlineOrg+3,6) = 1;

Linedata0(nlineOrg+3,1) = nbusOrg+1;
Linedata0(nlineOrg+3,2) = nbusOrg+2;
Linedata0(nlineOrg+3,3) = LinedataOrg0(indxAB,3)*0.6;
Linedata0(nlineOrg+3,4) = LinedataOrg0(indxAB,4)*0.6;
Linedata0(nlineOrg+3,6) = 1;

% Remove the linedata which is the location of fault point -- We already
% inserted two point in the middle of the considered line.
if indxAB ~= 1
   LinedataNew(1:indxAB-1,:) = Linedata(1:indxAB-1,:) ;
   LinedataNew(indxAB:size(Linedata,1)-1,:) = Linedata(indxAB+1:size(Linedata,1),:);

   LinedataNew0(1:indxAB-1,:) = Linedata0(1:indxAB-1,:) ;
   LinedataNew0(indxAB:size(Linedata0,1)-1,:) = Linedata0(indxAB+1:size(Linedata0,1),:);
elseif indxAB == 1
    LinedataNew(1:size(Linedata,1)-1,:) = Linedata(2:size(Linedata,1),:);
    LinedataNew0(1:size(Linedata0,1)-1,:) = Linedata0(2:size(Linedata0,1),:);
end


nbus = max(max(LinedataNew(:,1)),max(LinedataNew(:,2)));
linedata = Linedata;
linedata0 = Linedata0;

Lfybus; % Calculate Ybus matrix for load flow calculation
Lfnewton % Power flow solution by Newton-Raphson method
Vf = V;
Zbus = Zbuildpi(linedata,gendata,yload);
Zbus0 = Zbuildpi(linedata0,gendata0,yload);

F20 =  3*Vf(7)/(2*Zbus(7,7)+Zbus0(7,7)); % SLG Fault current of orig system
F80 =  3*Vf(8)/(2*Zbus(8,8)+Zbus0(8,8)); % SLG Fault current of orig system
%
%
% F20 = 1/zbus(nbusOrg+1,nbusOrg+1);
% F80 = 1/zbus(nbusOrg+2,nbusOrg+2);
```